

Signals and Communication Technology

Amit Kumar Mishra
Ryno Strauss Verster

Compressive Sensing Based Algorithms for Electronic Defence

Signals and Communication Technology

More information about this series at <http://www.springer.com/series/4748>

Amit Kumar Mishra · Ryno Strauss Verster

Compressive Sensing Based Algorithms for Electronic Defence



Springer

Amit Kumar Mishra
Department of Electrical Engineering
University of Cape Town
Rondebosch, Cape Town
South Africa

Ryno Strauss Verster
Department of Electrical Engineering
University of Cape Town
Rondebosch, Cape Town
South Africa

ISSN 1860-4862 ISSN 1860-4870 (electronic)
Signals and Communication Technology
ISBN 978-3-319-46698-9 ISBN 978-3-319-46700-9 (eBook)
DOI 10.1007/978-3-319-46700-9

Library of Congress Control Number: 2016956629

© Springer International Publishing AG 2017

This work is subject to copyright. All rights are reserved by the Publisher, whether the whole or part of the material is concerned, specifically the rights of translation, reprinting, reuse of illustrations, recitation, broadcasting, reproduction on microfilms or in any other physical way, and transmission or information storage and retrieval, electronic adaptation, computer software, or by similar or dissimilar methodology now known or hereafter developed.

The use of general descriptive names, registered names, trademarks, service marks, etc. in this publication does not imply, even in the absence of a specific statement, that such names are exempt from the relevant protective laws and regulations and therefore free for general use.

The publisher, the authors and the editors are safe to assume that the advice and information in this book are believed to be true and accurate at the date of publication. Neither the publisher nor the authors or the editors give a warranty, express or implied, with respect to the material contained herein or for any errors or omissions that may have been made.

Printed on acid-free paper

This Springer imprint is published by Springer Nature
The registered company is Springer International Publishing AG
The registered company address is: Gewerbestrasse 11, 6330 Cham, Switzerland

To our loving families and colleagues.

Contents

Part I Electronic Defence and Compressive Sensing

1	Introduction	3
1.1	Motivation and Problem Statement	4
1.2	Outline and Contribution	5
2	Electronic Defence Systems	7
2.1	Introduction	7
2.1.1	Electronic Defence Overview	8
2.1.2	Electronic Support	10
2.1.3	Electronic Attack	11
2.1.4	Electronic Protect	11
2.2	Electronic Support Communication Applications	13
2.2.1	Communication Electronic Support—CES	13
2.2.2	Communication Intelligence—COMINT	16
2.2.3	Signal Processing Techniques	16
2.2.4	Signal Classification	17
2.2.5	Signal Feature Extraction	21
2.2.6	Emitter Identification	22
2.3	Direction of Arrival Methods Used for Electronic Support Tasks	23
2.4	DOA Methods	24
2.4.1	Phase Interferometry	25
2.4.2	DOA Estimation Algorithms	29
2.5	Existing Compressive Based Direction-of-Arrival Methods	31
3	Compressive Sensing: Acquisition and Recovery	33
3.1	Introduction	33
3.2	Compressive Sensing Formulation	34
3.2.1	Compressible Signal and Sensing Matrices	35
3.2.2	Implementation for 1-Dimensional Signals	37

3.3	Compressive Sampling	39
3.3.1	Random Demodulator (RD) Analog-to-Information Sampler	41
3.3.2	Non-uniform Sampler (NUS)	42
3.3.3	Compressive Multiplexing (CMUX) Sampler	44
3.3.4	Summary of CS Sampling Methods	44
3.4	CS Recovery Algorithms	45
3.4.1	Convex Optimization-Based Algorithms	47
3.4.2	Fast ℓ_1 -Algorithms	48
3.4.3	Greedy Algorithms	55
3.4.4	Summary of CS Recovery Algorithms	58
Part II Simulations of Compressive Sensing Used for Electronic Support Applications		
4	Design of CS Based DOA Estimation for Modulated Shift-Keying Signal	63
4.1	Overview	63
4.1.1	Shift-Keying CS Sensing Matrix Development	66
4.1.2	CS Recovery Method	71
4.1.3	Implementing CS DOA Estimation	72
5	CS Based Shift-Keying Modulation	75
5.1	Simulation Outline	75
5.1.1	General Simulation Setup	76
5.1.2	Performance Indicators	76
5.1.3	Simulation Parameters	78
5.2	Simulation 1.1.1—Phase CS Recovery for 2FSK	80
5.3	Simulation 1.1.2—Phase CS Recovery for 2PSK	81
5.4	Simulation 1.2.1—CS Recovery of BIE for 2FSK	82
5.5	Simulation 1.2.2—CS Recovery of BIE for 2PSK	83
5.6	Assessment of System Parameters for Shift-Keying CS Recovery	84
5.7	Demodulation Capability	86
5.8	Simulation 1.3.1—Computational Performance of CS Recovery for 2FSK Signal	88
5.9	Simulation 1.3.2—Computational Performance of CS Recovery for 2PSK Signal	88
5.10	Computational Performance of CS Recovery	89
6	Modulation Specific CS DOA	93
6.1	Chapter Outline	93
6.1.1	General Simulation Setup	94
6.1.2	Performance Indicators	94
6.1.3	Simulation Parameters	95
6.2	Simulation 2.1—CS DOA for 2FSK Signals	96

6.3	Simulation 2.2—CS DOA for 2PSK Signals	98
6.4	Assessment of CS DOA Estimation Algorithm for Shift Keying Modulated Signals	100
6.4.1	Performance Assessment for ULA ₁₀	100
6.4.2	Performance Assessment for ULA ₃	102
6.4.3	Comparison of ULA ₁₀ and ULA ₃	102
7	CS Based Spectrum Sensing for ES	105
7.1	Problem Statement	106
7.2	Selective Spectrum Weighted CS Approach	107
7.3	Simulation Results	109
7.3.1	Case 1: Wide Band Spectrum Recovery	109
7.3.2	Case 2: Selective Spectrum Sensing	111
Part III Concluding Statements and Appendices		
8	Concluding Remarks	117
8.1	CS Based DOA	117
8.1.1	Accurate Phase Recovery Achievable Using Orthogonal Matching Pursuit (OMP)	117
8.1.2	Demodulation Capability via CS Recovery for 2FSK Signals	117
8.1.3	Equivalent Computational Performance of CS DOA as for Conventional DOA	118
8.1.4	Higher Accuracy of DOA Estimates for CS DOA Than Conventional DOA for Low SNRs	118
8.1.5	Reduction of Memory Required Using CS DOA Estimation	118
8.1.6	Scalability of CS DOA Estimation for Electronic Support	119
8.2	CS Based Spectrum Sensing	119
8.3	Final Remarks	120
9	Appendix: Some Useful Theoretical Background	121
9.1	Electromagnetic Waves	121
9.2	Receiver Components: Background	122
9.2.1	Antennas	122
9.2.2	RF Front-End Systems	124
9.2.3	Radio Frequency Propagation Operations	131
9.3	Typical ED System Configuration	138
9.4	Electronic Support Receiver Systems	141
9.4.1	ES Receiver Characteristics	142
9.4.2	Sensitivity Conversion	146
9.4.3	Types of ES Receivers	150

9.5	Compressive Sensing Mathematical Fundamentals	158
9.5.1	Vector Space	158
9.5.2	Sets, Bases and Frames	160
9.5.3	Matrix Construction for CS Sensing	162
9.5.4	Null Space Property	162
9.5.5	Restricted Isometry Property	164
9.5.6	Compliant RIP Matrices	165
9.5.7	Incoherence	166
9.6	Sampling Techniques	167
9.6.1	Sampling Theory	167
9.6.2	Conventional Sampling Mixing-Acquisition	169
9.6.3	Under Sampling Techniques	170
9.6.4	Direct Sampling	171
9.7	Wideband CS Sampling Techniques	172
9.7.1	Multi-rate Asynchronous Sub-nyquist Sampling (MASS)	172
9.7.2	Xampling-ADC and Modulated Wideband Converter (MWC)	174
References	177

Part I

**Electronic Defence and Compressive
Sensing**

Chapter 1

Introduction

In this book we describe applications of Compressive Sensing (CS) based algorithms for Electronic Support (ES) tasks such as direction-of-arrival (DOA) estimation of modulated communication signals and spectrum sensing. We also provide the reader with an overview of Electronic Defence and Compressive Sensing. The objective of applying CS to ES tasks¹ is to reduce the computation and memory requirements and improve system performance.

The majority of modern ES systems are developed to function as receivers that perform detection, classification, DOA estimation, and identification of radio frequency (RF) signal simultaneously, these are performed in an environment rife with high noise, interference, and frequency agile signal. Even in low intensive conflict scenario ES systems have a requirement for computational performance [42]. As a consequence, to match the computational load, modern ES receivers use field programmable gate array (FPGA) technologies [147] and digital signal processing (DSP) cores for processing.

The adoption of FPGAs and DSP cores as part of the ES hardware has lead to improved processing power. However, the problem of dealing with the memory requirements has not necessarily improved. In fact, modern DOA estimation techniques require additional memory than conventional techniques. CS methods provide an alternative solution, as it deals with the memory requirement by means of sub-Nyquist sampling, resulting in a reduction of input data required.

CS research has rapidly developed, since its inception [28, 44] for real world deployment on modern DSP platforms. In most cases, depending on the CS technique,

¹Electronic support is a sub-category of electronic defence (ED). ES equipment is developed to collect, intercept, identify and locate enemy signals [3] in order to execute a specific task relative to the threat level that received signal holds. Received signals can also be used for situational awareness [1] or in other words, determine the type and location of enemy weapons or electronic capabilities. ES systems need to optimize data throughput whilst gathering a considerable amount of real time data. The objectives of ES systems are to determine the type of electromagnetic emitters present, and where they can be located.

deployment is possible without requiring additional hardware. In other words, CS can be implemented, in principle, by simply altering the signal processing software used for ES tasks, with only a slight increase in cost on hardware. However, a marginal cost on computation is required [173].

In the remainder of this section we outline the problem statement, scope, and limitation of CS methods applied to DOA estimation techniques with specific application to modulated communication signals. We then discuss our design objectives, and lastly, present a summary of each of the chapters in this monograph.

1.1 Motivation and Problem Statement

The abundance of communication signal encountered in ES scenario presents a challenging environment for ES operations [42]. Moreover, modern communication signal comprises of several modulation techniques, which include conventional analog type modulation (FM, AM, SSB, etc.) as well as digital modulation (FSK, MSK, QPSK, BPSK, etc.). This abundance of communication signal creates a greater need to optimize data throughput, whilst gathering considerable amounts of real time data which results in higher memory requirements.

Most modern ES system processing is computed on digital processing platforms (i.e. FPGAs and DSP cores), as opposed to prior analog sub-systems [175]. Even with the computational core development, which has been tracking Moore's law [155], cost effective DSP platforms have not been realized. Hence, there is the incentive in the ES domain to develop low-cost systems that are readily replaceable [34].

CS methods tackle the problem of memory load by sub-Nyquist sampling resulting in optimized data throughput. Moreover, newly developed CS techniques can be implemented using existing signal processing platforms, by adapting the software and fine-tuning the method of signal acquisition. Thus, the unique attributes CS methods hold, make it an ideal candidate to reduce the amount of data required.

We aim to show specific electronic defence (ED²) applications that CS techniques could be applied to and produce comparable computational performance by CS dependant methods, as opposed to conventional Nyquist dependent methods. However, it shall be noted that we do not aim at showing the efficacy of CS for all ED systems and hence it remains an open question whether CS techniques can be developed for the complete ES/ED system.

²Electronic defence and the term electronic warfare are interchangeably used in the open literature and refer to the same objective—that is to protect and ensure the use of the electromagnetic spectrum for friendly and hostile scenarios for the purpose of tactical military tasks which enable the safety of assets (i.e. equipment and people) in the field. In this body of work we will use the term electronic defence.

1.2 Outline and Contribution

Throughout the remainder of this work we develop, design, test, and report on findings of implementing CS based methods for ES tasks. We detail existing CS methods used for ES type applications in the open literature and provide insights on several unique techniques of using CS based recovery to determine the DOA of communication signals and CS based spectrum sensing.

The framework of the book is detailed below in terms of its content, per chapter.

Chapter 2: Electronic Defence Systems

In this chapter we discuss and review conventional and modern Electronic Defence systems with particular focus on Electronic Support Tasks such as detection and estimation methods, and their associated computation and memory requirements.

Chapter 3: Compressive Sensing Acquisition and Recovery

In Chap. 3 we review the general CS framework. Thereafter the CS acquisition scheme in the current literature is reviewed to determine the best method for CS based recovery and acquisition to be used for ES tasks.

Chapter 4: Design of Modulation Specific Compressive Sensing Based Direction-of-Arrival

Based on the literature reviewed, we describe a CS based approach to recover the phase of digitally modulated input signal where the carrier frequency is known. Thereafter, we outline how such phase estimates can be used to determine the direction of arrival of digitally modulated signal which is incident on a uniform linear array (ULA).

Chapter 5: CS Based Shift-Key Modulation

In this chapter we show, by means of simulation, the capability of retrieving CS phase for amplitude shift keying (ASK), phase shift keying (PSK), and frequency shift keying (FSK) digitally modulated input signal for low SNR situations. Based on the findings from the simulations, retrieval performance is discussed to form coherent arguments and concluding remarks.

Chapter 6: Modulation Specific CS-DOA

In Chap. 6 we show, by means of simulation, the capability of accurate CS based DOA estimation given ASK, PSK, and FSK input signals for low SNR environments. Based on the findings from the simulations, various performance parameters relating to computation and memory requirements are discussed to form coherent arguments and concluding statements.

Chapter 7: Spectrum Sensing for ES

In this chapter we show the benefit of the recently proposed CS schemes on reducing the load on acquisition for ED spectrum monitoring. Further, we describe a modified CS scheme, which we denote as selective spectrum sensing, to further improve signal estimation performance for spectrum sensing. The proposed scheme leverages on a-priori knowledge of the frequency bands of interest and is shown to perform efficiently under severe signal to noise ratio (SNR) conditions.

Chapter 8: Concluding Remarks

In this chapter we conclude the monograph with some discussion on the future directions CS based EW system design may take.

Chapter 9: Appendix on Some Useful Theoretical Background

In the appendix we give some useful theoretical background. In case the reader is new to the domain it is strongly suggested that she goes through this chapter before starting the monograph.

Chapter 2

Electronic Defence Systems

2.1 Introduction

Electronic Defence (ED) is defined as the art and science of preserving the use of the Electro-Magnetic (EM) spectrum for friendly use while denying its use to the enemy [157]. The inherent value that the EM spectrum has as a natural resource, which is utilized and/or abused, is a pivotal reason why ED has such a vested interest in preserving its use. ED protects the spectrum by utilizing task specific passive ED receiver systems and ED transmitter systems (i.e. Jammers). ED receiver systems (falling within the sub-category of electronic support (ES)) are designed to detect, monitor and locate EM radiation sources (Friend or Foe), whereas ED countermeasures are designed to reduce the effectiveness of threats (i.e. Enemy EM radiation sources).¹

Concerning communication operations, the EM spectrum that is utilized commercially and for exclusive military use, occupies large sections/bands of the Electromagnetic spectrum (i.e. FM, AM, GSM, UMTS, LTE, WiFi, WiMax, etc.). As is the case with supportive measures, monitoring/sensing certain bands of interest is a typical technique to ensure that the spectrum usage is preserved. As a consequence other operative tasks become available, allowing for tracking capability and intercepting communications for intelligence gathering.

In this chapter we develop a critical literature review, detailing the context of ES in the domain of ED and its application as well as implementation for communication systems. We deal with a wide range of topics starting from ED passive communication systems (namely Electronic Support (ES) receivers), operations for detection, communication techniques, RF propagation theory to direction finding.

¹Both ED receiver and transmitter systems are designed by sourcing from multi-disciplinary fields such as radar, communications, digital signal processing, antenna theory, radio frequency systems, high performance computing and computer networks to preserve the EM spectrum with high effectiveness for the user.

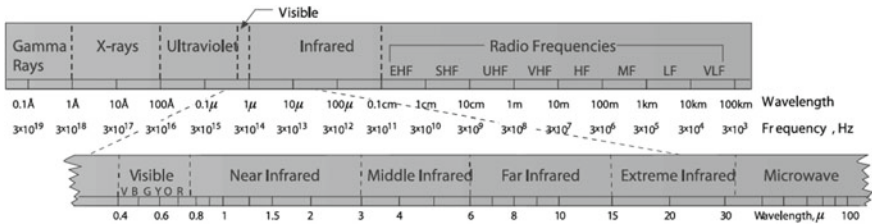


Fig. 2.1 Illustrates the electromagnetic spectrum usage in terms of frequency and wavelength, sourced and adapted from [99]

2.1.1 Electronic Defence Overview

ED systems sense and monitor the EM spectrum. The frequencies that comprise the EM spectrum range from Alternating Current (AC) to Gamma rays, which from a governing and/or controlling entity's (i.e. ED systems) point of view, is an enormous band to sense and determine the usage thereof.

ED domain utilizes full extent of this usable electromagnetic (EM) spectrum namely the radio frequency, infra-red, optical and ultraviolet spectrum [2]. Usability of the EM spectrum is detailed in Fig. 2.1.

Classically, ED has been divided into following three domains.

- Electronic Support Measures (ESM),
- Electromagnetic countermeasures (ECM).
- Electromagnetic counter-countermeasures (ECCM).

However, in recent years these subdivisions were renamed and redefined under the guidance of NATO [2]—now widely accepted in many countries, but not all.

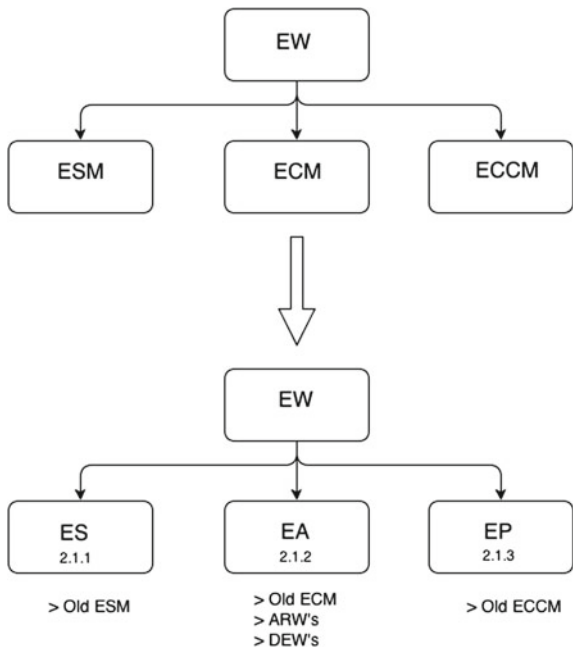
Under the previous definition² the ED subdivisions were understood as follows (see Fig. 2.2 for detail).

- **ESM**—Receiver systems, mainly used for intercept purposes in ED.
- **ECM**—Jamming, chaff, flares used for the sole purpose to counter systems such as radars, military communication and weapon systems.
- **ECCM**—Design or operational measures taken to counter radar and communication systems against the effectiveness of ECM.

Under the newly redefined view of NATO, ED subsystems/divisions are now defined as Electronic Support (ES), Electronic Attack (EA) and Electronic Protect (EP) subsystems. These three divisions are detailed below. In Sects. 2.1.2–2.1.4 we shall describe how these divisions include classical definitions which can be correlated to Fig. 2.2.

²Definitions sourced and modified from [1, 2].

Fig. 2.2 Illustrates the classical definition subdivision of the ED domains for operational tasks



- **ES**—This is the same as the classical definition of ESM.
- **EA**—This is same as the previous ECM including jamming, chaff, and flares. Also including anti-radiation weapons and direct energy weapons.
- **EP**—This is identical to the classical ECCM definition.

For clarity, it is important to distinguish ESM (or ES) from signal intelligence (SIGINT) which contains two streams of intelligent systems, namely communication intelligence (COMINT) and electronic intelligence (ELINT) [2]. Differentiation between these types of signal has become increasingly vague—as signal complexity develops—for the purpose of transmissions received [1].

Purpose of the respective subdivisions:

- **COMINT**—The operational tasks involve receiving communication signals for the purpose of extracting intelligence from the data/information carried by the signals of interest.
- **ELINT**—These operations are interested in non-communication signals (i.e. radar signals) to determine the type of electromagnetic system in use by an enemy, in order to develop a counter measure. ELINT systems typically collect a large amount of data over an extended period of time.
- **ES/ESM**—The modus operandi of ES is to collect, intercept, identify and locate enemy signals [3] in order to execute a specific task relative to the threat level that the received signal holds. The signal can also be employed for situational awareness [1]. In other words, the signal can be used to determine the types and

locations of enemy weapons or electronic capabilities. ES systems typically need to optimize data throughput whilst gathering a considerable amount of real time data. The main objective of such systems is to determine which emitter types are present and where they can be located.

The majority of the objectives, and hence the operational tasks for this monograph, will be focused within the domain of ES. However, due to the nature of exclusively dealing with communication signals, certain aspects of COMINT will be included for a holistic approach of the topic.

2.1.2 *Electronic Support*

In combat or passive scenarios where assets are in the field, it is a high operational priority to gather as much information about the physical environment and communications in the immediate vicinity in order to assess the threat level. This information gathering ensures the safety of people and equipment [3]. ES undertakes this task via electronic interception of communication and other RF signals (i.e. Radar). A typical topology of this is shown in Fig. 2.3.

The objective of ES is to provide other electronic defence (ED) systems with accurate combat information in order to alert and react appropriately to threats. We refer the reader to the appendix for further information on ED theory and the application of ES systems therein.

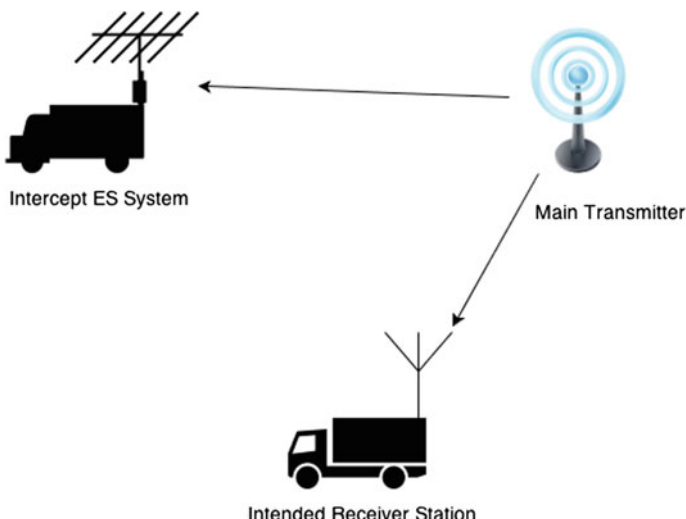


Fig. 2.3 The operation of a possible Electronic Support deployed in the field. This is a typical application of an intercept layout of an ES system, intercepting communication from an adversary's transmissions from a communication node. Adopted from [3] and modified by the authors

ES systems deliver the capability to search, intercept, identify and locate intentional and unintentional sources of electromagnetic (EM) radiation [157]. These tasks involve real-time signal acquisition and processing of combat or friendly information gathered to generate intelligence and pass onto sub-systems. Intercepting communication signals comprise of several steps; namely receiving the signal, identifying the type of signal, and finally locating the source of the radiation which is done by DOA estimation methods. Information gained from a signal to infer the location of the emitter source, namely DOA estimation, is regarded as a pivotal task for ES systems [126].

2.1.3 Electronic Attack

Electronic Attack (EA) has at its core, the objective to restrict enemy signals access in using the EM spectrum for communication, information exchange and/or other illicit activities (i.e. infrared and optical detection and tracking). This denial of information can be categorized into two schemes; firstly, in terms of information protection (protecting your own communication link via deception or encryption), and secondly as information attack (denying the user the use of their own communication link) [3]. For most of the situations in ED, the attack of an adversary's communication systems to deny information exchange is one of the most important task in ensuring a successful control strategy for information dominance.

Typically the denial of an adversary in exchanging information via RF communication is done via jamming. In brief, a communication jammer emits an excess (large amounts) of RF energy in the RF link of the enemy [3, 157]. This in no way reflects the entire scope of EA techniques and technologies. The sophistication of such jammer technology in literature and industry [3, 34, 157] serves as a remainder of how involved this aspect of ED is.

However, as far as the scope of the current work is concerned, more diverse EA systems will not be critically analysed herein. Further investigation of EA systems are left up to the reader (Fig. 2.4).

2.1.4 Electronic Protect

EP Systems are designed to restrict penetration and susceptibility of friendly systems being interfered with by enemy ES and EA systems [1, 157]. This is an involved process. A range of approaches must be adopted in achieving the intended task of protecting friendly forces. EP systems have a focal objective to protect friendly information, usually telecommunication, from being manipulated by an adversary.

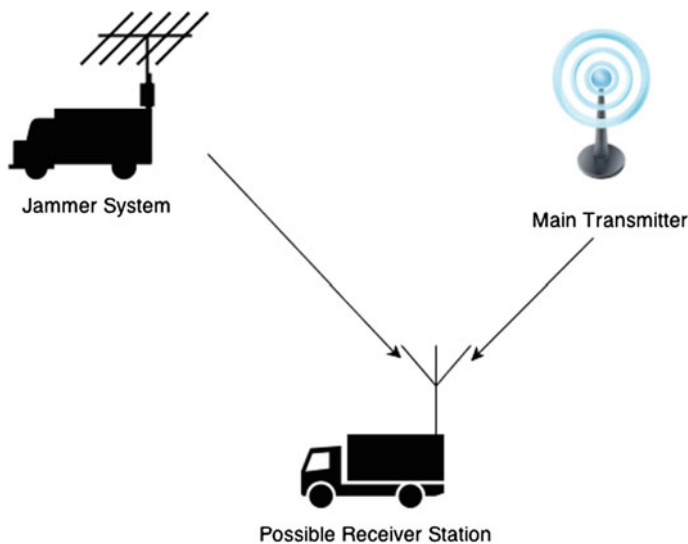


Fig. 2.4 Illustrates the operation of a possible Electronic Attack deployed in the field. This is a typical application of an EA system, whereby a Jammer is used to reduce the efficacy of an adversary's transmissions from a communication node. Adopted from [3] and modified by author

Some of the major kinds of EP measures are detailed below.

- Emission Control (EMCON) is the intelligent control that coordinates friendly transmissions for a period of time. In particular, it limits access of certain transmission sources at critical junctures as to not risk exposure for detection by enemy ES and EA systems [3].
- Low Probability Intercept *LPI* (spread spectrum) signals is the use of deliberate spreading of the transmitted data over frequency, and hence bandwidth. This is intentional, so as to prevent any attempt of adversary ES and EA systems to intercept, locate and jam signals [2].
- Screen Jamming is a clever, yet simple, technique to introduce RF energy between friendly communication networks and the SIGINT systems of enemies to impede the interception of transmission [3]. This is done by user specific jammer systems, much the same as the EA jammer systems, but with a different objective.
- Encryption is the classical technique to ensure the fidelity of data transmission, in cases where transmissions are intercepted and extracted for intelligence gains.

All these techniques are utilized to protect friendly communications being intercepted or susceptible to adversary electronic tactics.

The discussion of EP serves as part of the overview for the ED domain, whereas our focus will be restricted to ES systems and hence little more will be detailed on EP herein this work.

2.2 Electronic Support Communication Applications

The application of our work incorporates both ES and COMINT (a sub section of SIGINT) tasks, as detailed in Sect. 2.1.2, with a focus on implementing the new signal processing techniques using compressive sensing. As a result, the question of which equipment platforms such techniques can be implemented on (i.e. digital or analog), becomes a focal point.

In fact the typical equipment platforms that are used to perform ES and COMINT tasks are communication electronic support (CES) and communication intelligence (COMINT) equipments. The distinction between the two systems varies in terms of both equipment architecture and purpose.

In this section we highlight the equipments needed for both systems, their applications and purpose. We also include common signal processing techniques used as part of the processor unit. Then, we review how certain techniques such as emitter identification, feature extraction, and classification are typically implemented for communication ES purposes. Lastly, we discuss the implementation of spectrum monitoring and direction finding techniques that are pertinent to our work.

2.2.1 *Communication Electronic Support—CES*

Communication Electronic Support systems provide immediate emitter signal information to troops and other operators in order to make informed decisions in the battlefield [139]. The functions that are tasked to CES equipment include:

- Search,
- Interception,
- Classification,
- Identification, and
- Direction Finding.

As pointed out earlier, the large frequency coverage as well as the congestion of the RF spectrum requires a receiver system that can cope with the demand of complete coverage of the intended spectrum. In the case of CES equipment, this is either implemented by a wide-band channelized receiver or with a number of wide-band Super-Heterodyne (SH) channelized receivers, coupled with the number of receiving antennas, that rapidly scan over the RF bands [107]. These bands are known as the instantaneous bandwidth (IBW) corresponding to the SH receiver channel width, typically 40 MHz wide [139]. This receiver architecture is the most commonly used one in practice for CES equipment [107] and serve as motivation for its review. We refer the reader to the work done in [1, 8, 139] for further study on the working details of different available architectures.

CES equipment typically comprise of the following sub systems (sourced from [8, 107]). See Fig. 2.5 for the CES system block diagram.

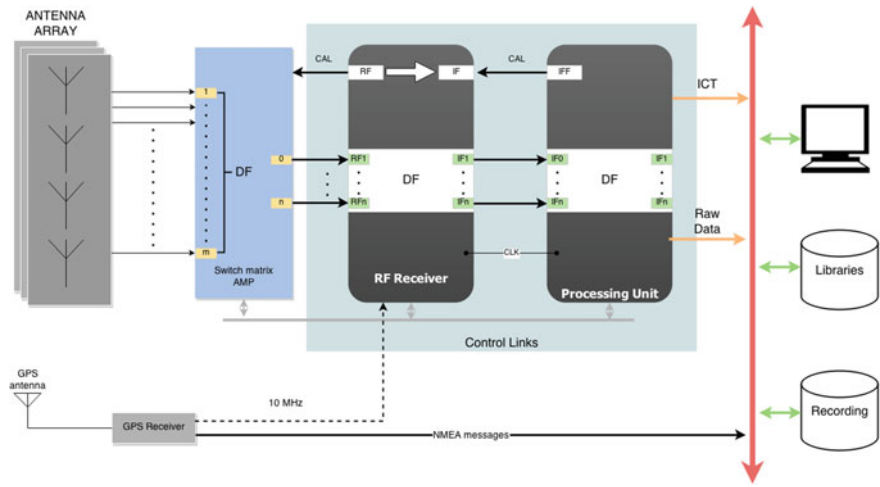


Fig. 2.5 System block diagram for a typical CES system and equipment requirement. Sourced from [107] and modified by the authors

1. Antenna array, composed of different sub-band antennas typically covering the VHF, UHF and SHF bands

- These arrays typically form a sub-band circular array (UCA) useful for DF methods [156], especially correlative methods. Further discussion of these methods are detailed in Sect. 2.4.
- The UCAs are made up of an odd number of vertical poles to reduce the phase ambiguities.
- An additional antenna used as a GPS antenna and receiver which provides information about its global position, necessary for ground deployment, as well as synchronizing a CES receiver with other systems in a CES sensor network.

2. Antenna front-end (AFE) and sub-band array switching matrix

- Provides pre-selector filtering and low noise amplification of the received RF signal before being passed to the RF receiver
- The switch matrix selects between the different sub-array of antennas in order to perform DF measurement as the number of UCA channels are limited.

3. RF receiver

- The CES monitoring equipment exploits the SH architecture and channel nature to do stepwise sweeping over the entire frequency spectrum. The IBW is usually 40 MHz (as previously suggested).
- The sweeping speed is determined by the tuning time, typically in the order of 10s of microseconds.

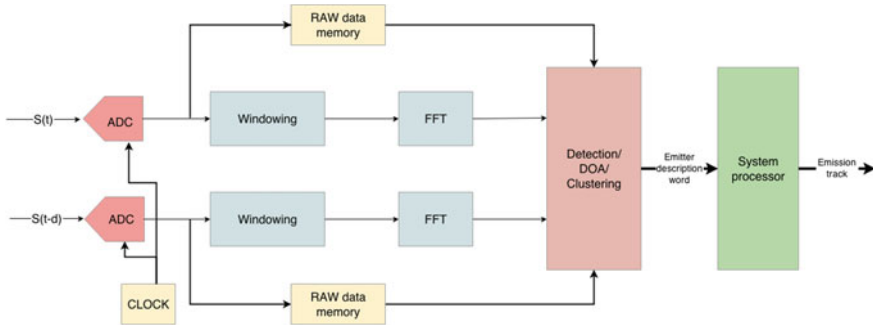


Fig. 2.6 A two channel DRx shown performing detection and differential phase measurement using two antenna channels from the IBW equipment. Sourced from [107]

- Adjusting the IBW tuning speed can be used to either increase/reduce the frequency resolution for a specific purpose, such as detecting and locating frequency agile signals, better known as frequency hopping (FH) signals.
- The required instantaneous dynamic range (IDR) is usually IDR > 60 dB, with a signal-to-noise (SNR) ratio between 8 and 10 dB.

4. Processing Unit

- The IF signal from each channel of the RF receiver is then converted via a 12–14 bit ADC (providing the needed 60 dB IDR). All the channel data then gets processed via FPGAs, which provide the DSP capability such that detection using a filter bank implementation and phase measurement algorithms can be accomplished.
- The processing of these channels is shown in terms of processing blocks in Fig. 2.6, which shows two channels from the UCA. The processing tasks, shown as system blocks (i.e. Windowing, FFT, Detection etc.), are executed by the FPGA. The blocks are merely system descriptions describing the processing steps.
- Windowing applied to the data stream reduces the sidelobe response of frequencies for Fast Fourier Transform (FFT) detection.

5. Axillary Units i.e. Human Machine Interface (HMI), computer, databases, libraries and storage

- After preliminary detection, direction of arrival (DOA) and clustering are performed. The auxiliary units use this information to perform classification and feature extraction.
- Classification and feature extraction techniques are discussed in Sect. 2.2.4.

2.2.2 *Communication Intelligence—COMINT*

Communication Intelligence systems are used to analyse signal over an extended period of time giving sufficient processing time to provide accurate intelligence about signal characteristics and content [139]. Signal intelligence includes emitter location, signal structure and the level of electronic counter counter measures (ECCM) employed by an enemy to evade detection. These characteristics are then used to compile and support mission control plans and provide insight to generate the appropriate waveforms used in jamming enemy signals [40]. In this respect COMINT is vital for jamming and protecting RF supremacy. The main functions ascribed to COMINT are as follows.

- Signal Acquisition and feature extraction;
- Signal Classification;
- Signal demodulation;
- Voice signal demodulation, decryption and listening;
- Signal Recording; and
- Decoding, transmission standard recognition and speech recognition.

Furthermore, use for COMINT equipment extends to civilian application for spectrum monitoring, whereby surveillance of the spectrum use is monitored to determine if users are broadcasting within the legal specified bands [12]. Any RF emitter broadcasting in a defined civilian area must comply with the regulatory body licensing agreement that defines the broadcasting standards within a specific geographical location. The Independent Communications Authority of South Africa (ICASA) is an example of such a body. However, as far as DF tasks are concerned, COMINT equipment typically does not include omnidirectional antennas and sub-systems needed to perform DF. The DF (360°) antennas are substituted for high gain directional antennas in order to improve sensitivity and provide higher SNR for signal parameter estimation [1].

It is worth mentioning that the architecture for COMINT equipment share similarities with CES equipment including similar AFE, UCA, RF receiver, DRx (Dual Receiver) channels, and processing units. However, as mentioned before, the DF antennas are replaced by high-gain directional antennas and as a consequence the DOA processing steps are omitted and additional number of processors, recording systems (i.e. storage devices), and software tools are added.

2.2.3 *Signal Processing Techniques*

Any intelligent receiver system requiring classification and/or identification of signal are highly dependent on some form of signal processing unit, and/or HMI (i.e. computer) [68, 167]. Moreover, signal processing techniques—specific to transforms—play a pivotal role in generating a representative base that allows different digital

methods to classify, identify, and extract features from RF signals in ES communication systems [42]. Some transforms that are integral to ES equipment include the Fast Fourier Transform (FFT), Wavelet Transform (WT), Walsh Hadamard Transform (WHT), and the Hilbert Transform (HT). A few of these tasks are described below.

1. **Filtering Methods** based on cyclostationary signal properties [63] using an FFT accumulation technique. A lower level implementation that does not involve feature detection, as cyclostationary techniques do, involve FIR filters that are quite commonly seen as part of digital receiver systems to perform digital filtering of signals.
2. **Time-Frequency Analysis** which is either implemented via a Wavelet Transform or else, in some systems, via the Wigner-Ville distribution coupled with a quadrature mirror filter (QMF) method. Time-frequency analysis of signals, especially for ES systems, are vital to determine if a signal is frequency agile.
3. **Signal Detection** using a strip spectral correlation analysis (SSCA) [138] that comprises of FFT blocks to achieve detection. Detection is ubiquitous with signal processing of RF signals within ED. However, elementary detection techniques such as *threshold detection* simply do not suffice for some kinds of signal. Hence is the need for more probabilistic detection methods such as the SSCA and cyclostationary signal processing that provide improved detection performance with more deterministic parameters [7, 138].

2.2.3.1 Transforms

A transform, for the discrete case, is the process where an input signal is mapped from one domain represented as real discrete values to another vector space. This mapping process is the basis on which any transform is based. Transforms are ubiquitous in signal processing. Herein we have selected the most frequently used and prominent transforms used as part of the ES signal processing block. However many more transforms exist and can be applied to ED, but such a discussion merits a study on its own (Tables 2.1, 2.2 and Fig. 2.7).³

2.2.4 Signal Classification

Classification techniques in the equipment mentioned earlier serve to recognize specific characteristics about a received communication signal [139]. These are known as classifiers of the system, whereby the output parameters from the receiver unit of a CES or COMINT system (i.e. DF, frequency carrier and detection) are used as

³See the following literature on the advances [165] and implementation of different transforms for the uses in ES [32, 73, 110].

Table 2.1 A table detailing the expressions for the transforms and the associated complexity

Transforms	Definition	Fast algorithm		Complexity
		Name	Complexity	
Discrete Cosine Transform (DCT)	DCT-II: $X_k = \sum_{n=0}^{N-1} x_n \cos \left[\frac{\pi}{N} (n + 1/2)k \right]$	(FCT)	$O(N \log_2(N))$	$O(N)$
Discrete Fourier Transform (DFT)	$X_k = \sum_{n=0}^{N-1} x_n e^{-j2\pi n k / N}$	(FFT)	$O(N \log_2(N))$	$O(N)$
Discrete Short Time Fourier Transform (DSTFT)	$X(m, u) = \sum_{n=-\infty}^{\infty} x[n]w[n-m]e^{-ju n}$	(WFFT)	$O(N \log_2(N))$	$O(N)$
Walsh Hadamard Transform (WHT)	$(H_m)_{k,n} = \frac{1}{2^{m/2}} (-1)^{\sum_j k_j n_j}$ where $k = \sum_0^{i < m} k_i 2^i$ and $n = \sum_0^{i < m} n_i 2^i$	(FWHT)	$O(N \log_2(N))$	$O(N)$
Wavelet Transform (WT)	$[W_\psi, f](a, b) = \frac{1}{\sqrt{ a }} \int_{-\infty}^{\infty} \psi \left(\frac{x-b}{a} \right) f(x) dx$	(FWT)	$O(N) - O(N \log_2(N))$ per scale	$O(N)$ per scale

Table 2.2 A table detailing the advantages and disadvantages associated with different signal processing transforms used to facilitate electronic support processing tasks

Transforms	Application	Advantage	Disadvantages
(FCT)	<ul style="list-style-type: none"> • Spectral methods • Lossy compression (i.e. MP3, Image processing) 	<ul style="list-style-type: none"> • Efficient representation of signals • Smaller data length • Multiple DCT variants (i.e. I-VII-DCT) 	<ul style="list-style-type: none"> • Single basis to represent signals • No phase information
(FFT)	<ul style="list-style-type: none"> • Spectral methods (i.e. Filter banks) • Demodulation • Broad application to RF detection, identification, and classification 	<ul style="list-style-type: none"> • Magnitude & Phase information • Efficient representation of frequencies 	<ul style="list-style-type: none"> • Assumption of periodicity causes spectral leakage • No time information (exclusive to frequency domain) • Only two representative basis (sin & cos)
(WFFT)	<ul style="list-style-type: none"> • Non-periodic signal analysis • Sidelobe reduction 	<ul style="list-style-type: none"> • Provides time-frequency information • Major reduction in spectral leakage 	<ul style="list-style-type: none"> • Computationally intensive (Let time slots be M then complexity is $O(MN \log_2(N))$) • Equal resolution for time and frequency transformations
(FWHT)	<ul style="list-style-type: none"> • Frequency signal processing • Digital signal detection/estimation • Used when signals are choppy 	<ul style="list-style-type: none"> • Less computationally expensive than FFT, as only 2 discrete states exist (i.e. 2 bits) for addition and subtractions • Reduction in Bit depth needed 	<ul style="list-style-type: none"> • Reduction in true frequency representation • Representative basis leads to different frequency interpretation
(FWT)	<ul style="list-style-type: none"> • Time-Frequency signal processing analysis • Signal detection, estimation, and classification 	<ul style="list-style-type: none"> • Varying resolution for time-frequency transformations • Numerous wavelet basis (i.e. Haar, Daubechies, Coifman, Symmlet) [37] • Provides adequate signal approximations that have sharp discontinuities 	<ul style="list-style-type: none"> • Prior knowledge of the signal must generally be known • Computationally more expensive

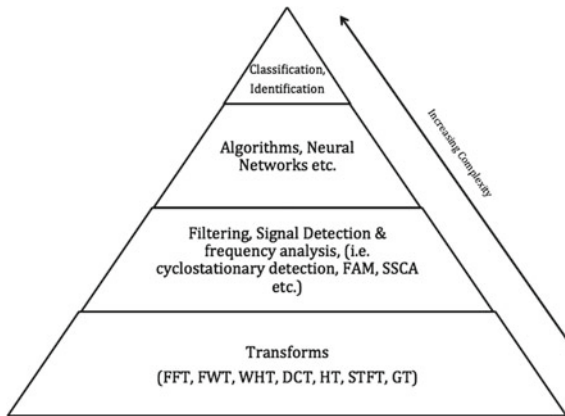


Fig. 2.7 Illustrates how signal processing in the context of ES maintains a hierarchy, in that the lower level signal processing techniques all add up and aid the upper, more complex levels, in order to accomplish the ultimate task of classification and identification of emitters

input to another system processor to classify the signal. Signal classification of the signals include one or more of the following.

- Signal type recognition (i.e. Analog or Digital),
- Analog modulation recognition (i.e. AM, FM, PM),
- Digital Modulation recognition (i.e. FSK, PSK, ASK), and
- Type of multiplexing recognition (i.e. FDM, PPM).

Classifiers above are vital for emitter identification tasks.

In practice there are two major perspectives on classification for communication signals that have been adopted in military applications [139]. These are based on two algorithmic approaches, namely pattern recognition processing and decision theoretic approach, sourced from [107, 139]:

- **Pattern Recognition Processing**—uses signal feature knowledge processed by an artificial neural network type of algorithm [121]. Two major works that have contributed to classification processing using neural networks include:
 1. the **Nandi-Azzouz** classifier [121], that proved to be successful in distinguishing between 13 analog and digital modulation types, namely AM, FM, FSK2-4, ASK2-4, DSB, LSB, VSB, USB, PSK2-4, and combined (amplitude and phase) modulation, and
 2. the **Assaleh-Farrell-Mammone** classifier used to discriminate between different digitally modulated signals [10] (The modulation types include CW, BPSK, QPSK, BFSK, and QFSK.).
- **Decision Theoretic Approach**—depends on likelihood or probability to determine the modulation of a signal. Two of these decision-based methods include:

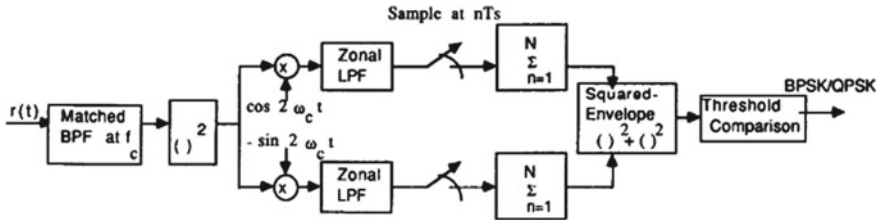


Fig. 2.8 Functional system block diagram describing the qLLR classifier used in the work by Kim and Polydoros, taken from [135]

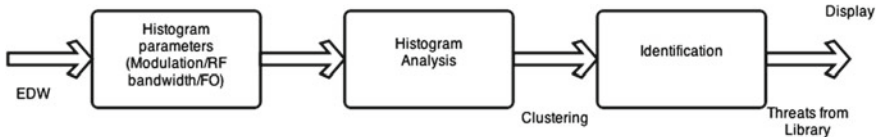


Fig. 2.9 System block describing the processing steps involved for emitter sorting process. Compiled by author, but sourced from [107]

1. the **Sills** classifier [161], which can discriminate between the three different types of PSK (BPSK, QPSK, PSK-6) and three types of Quadrature Amplitude Modulation (QAM) signals (i.e. 2^4 QAM, 2^5 QAM, 2^6 QAM) (The classifier implements a maximum-likelihood (ML) algorithm for coherent classification and validate the findings using a noncoherent ML version of the algorithm.); and
2. the **Kim-Polydoros** classifier [141] which is an efficient means to discriminate between modulation, relying on a quasi-log-likelihood ratio (qLLR) rule to base decisions (Fig. 2.8).

2.2.5 Signal Feature Extraction

Signal feature extraction is a critical step, used after a signal has been classified, to extract and catalogue the features that are assigned to the signal in order to identify the emitter type [2], see Fig. 2.9. The process for feature extraction is similar to the process used for emitter deinterleaving⁴ and sorting of radar warning receiver (RWR) systems within ES [113].

Although the tasks are similar, to deinterleave and to sort the features based on classifiers, the fundamental difference depends upon the emission description of the signals [156]. In communication scenarios, emission descriptor words (EDW) that are

⁴“Deinterleaving is a kind of clustering analysis, which clusters inter-weaved pulses—intercepted by a scout or by other means—into distinct groups belonging to respective emitters, according to the pulses’ features.” [88].

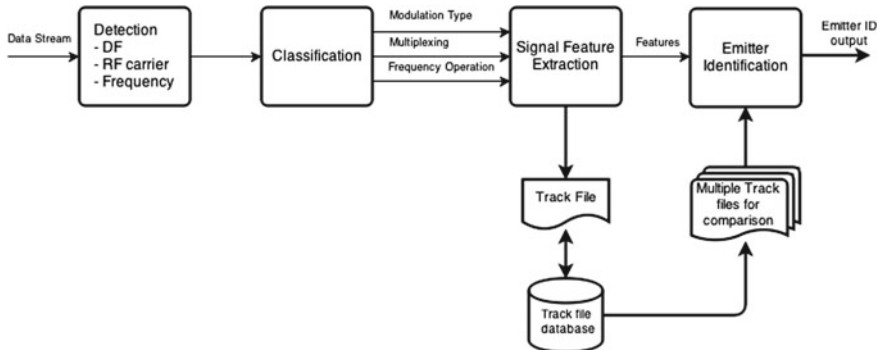


Fig. 2.10 System block diagram describing the processing steps involved to identify a RF emitter

assigned to communication signals are different in nature to that of radar signals (i.e. RWR systems), as they are primarily pulsed [88]. Nevertheless, the process remains similar, although the features assigned to signals differ. Typical features associated with communication signals [139] which serve as an input to the clustering analysis process (i.e. deinterleaving) are:

- Signal classification
- Frequency of operation
- RF bandwidth
- Modulation type
- Power Levels.

The features assigned to a particular signal are transformed into a digital word, which is then passed onto the clustering analysis process based on a knowledge-based algorithm which is mostly a histogram analysis method [88] (see Fig. 2.10 for the sorting process). A key component of the feature extraction is to sort the EDW into a subspace based on the parameters of the feature in order to generate a track file of the emitters that are catalogued. This track file is then used as an input to identify the emitter. The process of generating the track file is discussed in the following section. Furthermore Fig. 2.10 adeptly contextualizes how the processing of an RF communication signal, by means of detection, classification, and feature extraction, enables an emitter to be identified. We refer the reader to the following literature [13, 145, 163] for further discussion.

2.2.6 Emitter Identification

Once the features of the signal emitter has been sorted and the accompanying track file generated as depicted in Fig. 2.10, the following process takes over in identifying

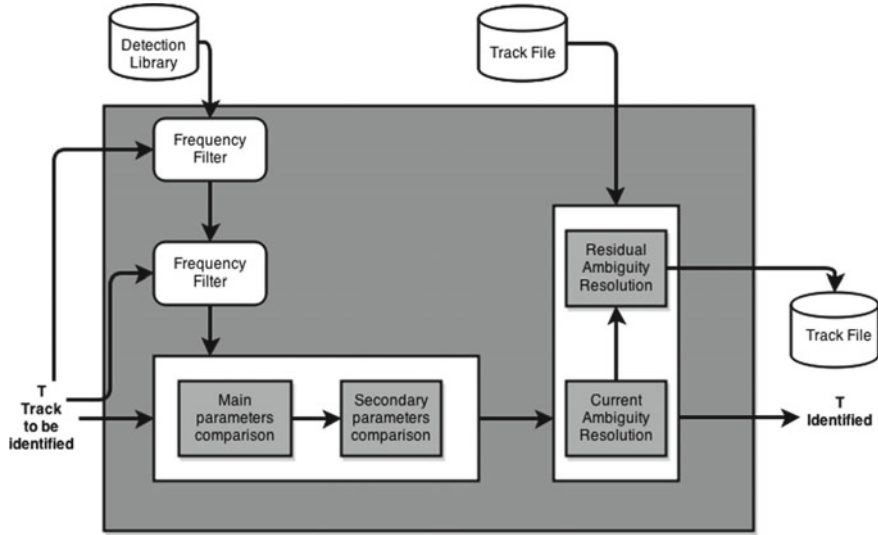


Fig. 2.11 System block diagram describing the flow process for emitter identification. Compiled by author, but sourced from [107]

the most likely emitter based on a history of emitters as well as the database that stores relevant parameters that comprise the details of a specific emitter [107].

Every parameter that is defined in the track file based on the EDW from the signal features are used as a comparison to the measured values of an incoming track. As depicted in Fig. 2.11 the process of identifying an emitter is based on scoring the specific parameters based on the correlation from past emitters in the database. Consider an emitter signal that has been received with a specific frequency operation (FO) modulation type and signal power. The input signal is assigned with a score based on the correlation measured of each of the values against emitters in the database [108]. Then, the sum total score is calculated and if the total score exceeds a selected threshold, the received signal can be identified with a probability relative to the score, which is known as the confidence level [109].

2.3 Direction of Arrival Methods Used for Electronic Support Tasks

DOA systems determine accurate estimates, within probabilistic bounds, of the direction from where a signal of interest (SOI) is received—also known as the line of bearing (LOB). Once an accurate estimate of the signal DOA is determined a second DOA must be acquired from a different geographical location, which can either be done from a second receiver or a mobile intercept receiver. When two estimates

from varying locations are acquired the location of a communication signal can be accurately determined, which is known as direction finding (DF).

It is important to distinguish between the signal processing task which constitute DOA estimation methods and the operational task of DF. As explained, DF is the operational objective in ES to use DOA estimates from multiple receivers to find the direction of an EM source with high accuracy. In other words, DOA forms a part of DF.

Main requirements of a DOA system are:

- High accuracy i.e. resolution less than 1° ;
- High sensitivity;
- Real time data capturing and processing;
- Short minimum requirement signal duration;
- Immunity to field distortion and polarization errors.

Both azimuth and elevation characteristics can be considered to provide a three-dimensional estimate of a signal DOA. However, as elevation DOA is common in air-to-ground scenarios, we do not continue the 3D discussion herein,⁵ we only consider the case for azimuth DOA methods as we are interested in ground-to-ground scenarios.

In this section we review conventional and modern DOA techniques used in ES, and discuss why only phase interferometry is considered for our ES application, especially communication DOA estimation. We then discuss modern DOA algorithms used for ES systems and their associated performance to estimate the DOA of a signal. Thereafter, we review the scalability of existing DOA estimation using compressive sensing in the open literature.

2.4 DOA Methods

The two main DOA methods used in ES are amplitude comparison and phase interferometry [37]. Table 2.3 details the comparison of the two DOA measurement methods and their associated benefits and drawbacks.

Amplitude comparison methods, as the name suggests, compare the amplitude of a measured signal from multiple antennas [126] or in some instances a single rotating antenna [107], in order to determine the DOA of a signal. Although amplitude comparison DOA is widely used, with adequate directional resolution and bandwidth coverage, it is generally designed for pulsed transmissions. That is why they are predominantly used for radar warning receivers. Subsequently, the use of amplitude comparison DOA in ES equipment is almost non-existent, except for some electronic intelligent (ELINT) equipment where rotating antennas are used [107]. As a consequence, we do not develop amplitude comparison methods further in this work.

⁵We refer the reader to the following literature for further reading on the subject of DOA and elevation direction finding techniques [61, 21, 107, 126].

Table 2.3 DOA measurement method comparison, sourced from [37]

	Amplitude comparison	Phase interferometer
Sensor configuration	Typically 4–6 equispaced antenna elements for 360° coverage	2 or more RHC or LHC spirals in fixed array
DF accuracy	$DF_{ACC} \approx \frac{\theta_{BW}^2 \Delta C_{dB}}{24S}$ (Gaussian Shape)	$DF_{ACC} = \frac{\lambda}{2\pi d \cos \theta} \Delta \theta$
DF accuracy improvement	Decrease antenna BW; Decrease amplitude mistrack; Increase squint angle	Increase spacing of outer antennas; Decrease phase mistrack
Typical DF accuracy	3°–10° rms	0.1°–3° rms
Sensitivity to multipath/Reflections	High sensitivity; Mistrack of several dB can cause large DF errors	Relatively insensitive; Interferometer can be made to tolerate large phase errors
Platform constraints	Locate in reflection free area	Reflection free area; Real estate for array; Prefers flat radome
Applicable receivers	Crystal video; Channelizer; Acousto-optic; Compressive	Superheterodyne

ΔC_{dB} = Amplitude monoipulse ratio in dB; S = Squint angle in degrees; θ_{BW} = Antenna beamwidth in degrees

Phase interferometry on the other hand, is widely used in ES equipment [37]. Phase interferometry is dependent on using multiple antennas, typically an array of uniform spacing. The received signal's phase between the individual receiving antennas, is correlated to provide an estimate of the DOA based on the phase difference [176]. Due to the breadth of implementation of this DOA method for ES, a review of phase interferometry follows.

2.4.1 Phase Interferometry

Phase interferometry is considered as one of the best suited technique for communication signal DOA estimation [126]. If a scenario demands higher accuracy, in the order of 0.1°–1°, the antenna spacing distance $d = \lambda/2$ (referred to as the baseline width) can be decreased as it is relatively insensitive to phase errors [139]. Moreover, one can reduce phase mistrack by increasing the spacing of the outer antennas in the array. Phase interferometry is relatively responsive, but requires complex RF circuitry and processing when compared to other methods.

DOA phase interferometry system consists of the following components:

- an array of equidistant antennas which take various configuration—linear, circular or lattice;

- front end channelized receiver circuitry, including mixers and analog-to-digital converters (ADC); and
- digital signal processing back-end.

A typical configuration of this architecture is shown in Fig. 2.13.

Phase interferometry works on the following principle. Consider a plane wave incident on a linear antenna array at an angle Φ , as shown in Fig. 2.12. Then based on the geometry of the configuration the time difference of the signal being received at every antenna can be expressed as phase difference. The phase difference can then be expressed in terms of the angle of arrival as shown in Eq. 2.1. Following the notation in Fig. 2.12 gives:

$$\Phi = \omega \frac{d}{dt} = 2\pi f \left(\frac{\Delta s}{c} \right) = 2\pi(d \sin \theta)/\lambda, \quad (2.1)$$

where

Φ phase of the signal,

ω angular frequency of the signal,

s vector component of the antenna separation distance,

f frequency of the signal,

θ angle of arrival,

d the antenna separation,

λ the wavelength of the RF signal,

c speed of light (3×10^8).

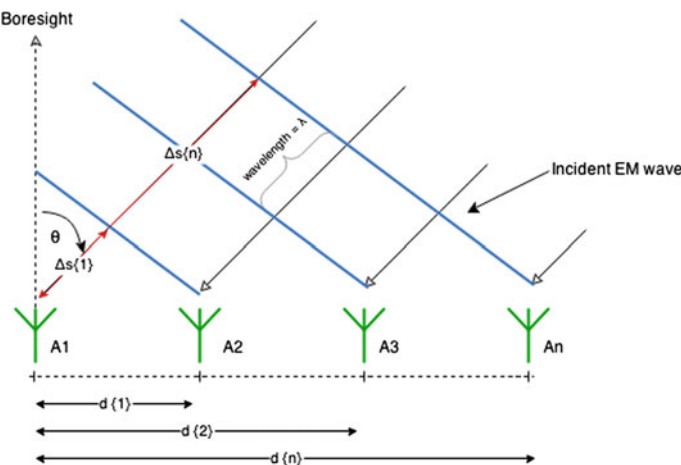


Fig. 2.12 An n length linear antenna array showing the 2 dimensional dynamics of phase interferometry, using phase representation of the time difference to solve the angle θ of an incident RF wave. (Compiled by the authors.)

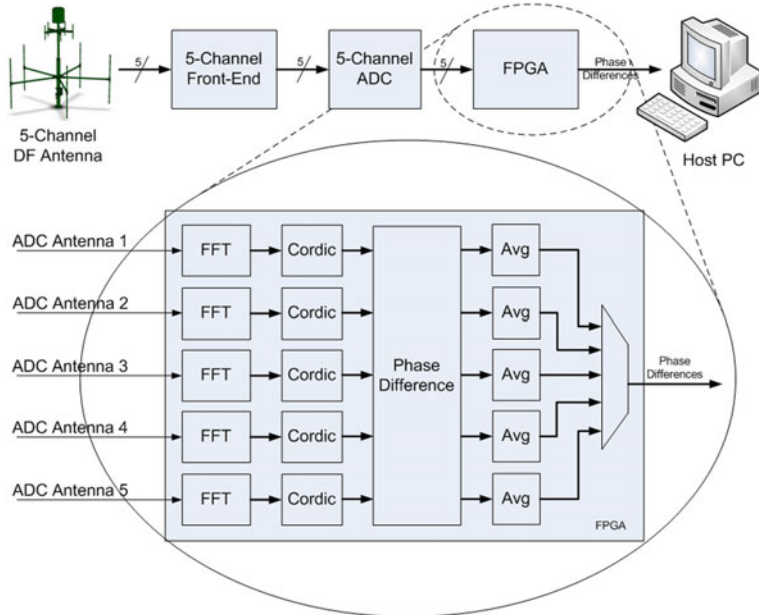


Fig. 2.13 5-channel DF antenna processing architecture, taken from [144]

The phase information of the signal received at every branch of the receiver is used by estimation algorithms to resolve the DOA. Before we review estimation algorithms it is important to mention system considerations of phase interferometry systems deployed in the field. Some of the system considerations restrict accurate DOA estimation, and an awareness of them provide insight to which estimation algorithm to choose.

A typical phase interferometric system using a uniform circular array (UCA) dipole antennas is shown in Fig. 2.14. The processing back-end is shown in Fig. 2.13 implementing an FPGA back-end processing unit to perform correlative interferometric estimation. This architecture and processing implementation in most cases is considered as the standard approach for DOA tasks on modern ES equipments [176].

2.4.1.1 System Considerations

To deploy phase interferometry techniques in the field, there are several considerations that have to be made, namely antenna spacing, coning error, system noise, and signal-to-noise ratio (SNR).

Phase interferometric systems require minimal phase ambiguities as they distort the accuracy of the field of view. When the antenna spacing is less than $\lambda/2$ the field of view is 180° wide, which results from solving $\theta = 2 \sin^{-1}(\pi/2d)$ [37]. Therefore, the spacing must match the highest frequency (i.e. smallest wavelength)

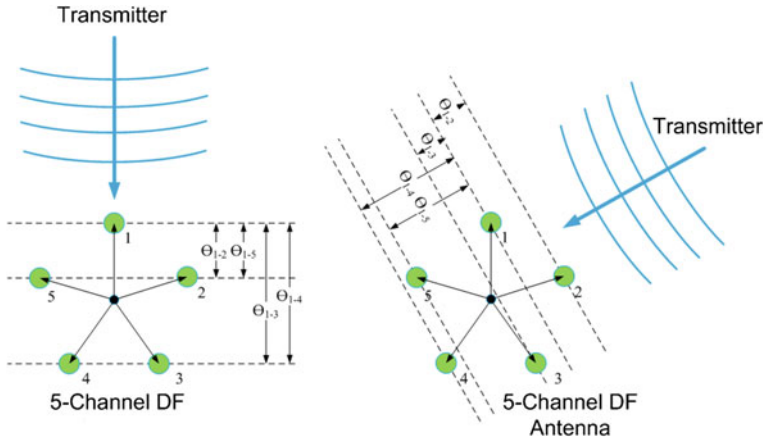


Fig. 2.14 Phase differences shown for two different incident waves for a 5-channel DF antenna system, taken from [144]

of the received signal in the bandwidth of interest [149]. The restriction on the antenna array for higher frequency cases (i.e. UHF/VHF communication) results in ES DOA systems adopting multiple antenna arrays for various bandwidths of interest, or resolving phase ambiguities with correlative algorithms; the latter solution being more computationally expensive than the former.

When an EM source is elevated, for example an air-to-ground scenario, the elevation of the incoming signal in relation to the receiver on the ground introduces discrepancies in azimuth estimation for 2-Dimensional DOA task, which is known as the coning error function [37]; adequately named because of the shape the locus points create, which share the same phase delay.

Coning error adds to phase ambiguities when a signal is incident on the receiver array at an elevated position, which in some cases can be large. Coning error can be calculated by equating the ideal 2-D case $\phi = 2\pi(d \sin \theta)/\lambda$ with the 3D case $\phi = 2\pi(d \sin \theta \cos \varphi)/\lambda$ (with azimuth θ and elevation φ) which gives:

$$\theta^* = \sin^{-1}(\sin \theta \cos \varphi). \quad (2.2)$$

For cases when the emitter location is either on the horizon and/or restricted to ground-to-ground application, the coning error is almost negligible [139] as elevation increases. Fortunately for our application these effects are negligible.

The noise effects due to sensitivity and thermal noise contribute to the accuracy in determining the DOA. The relationship for standard deviation of phase θ_ϕ relative to noise is given as

$$\sigma_\phi = \frac{1}{\sqrt{2SNR}}, \quad (2.3)$$

which is then used to determine the common expression for angle accuracy using interferometric techniques:

$$\sigma_\theta = \frac{c \sigma_\phi}{2\pi d_i f \cos \theta} = \frac{c}{2\pi d_i f \cos \theta \sqrt{2SNR}}. \quad (2.4)$$

The restriction in the width between antenna elements in the array d_i , in order to mitigate incorrect DOA estimation, requires a higher SNR of the system to process and estimate the DOA of a SOI accurately. In some cases the required SNR could be up to, and above 50 dB, which is unrealistic as interception systems operate in low sensitivity environments [8].

Given such a high SNR demand, for certain tasks phase interferometry cannot be used for ES. However, to overcome SNR demand, phase interferometric methods in ES systems make use of circular harmonic (base-lengths are $d_i = 2^{i-1}d_1$) and non-harmonic (prime number multiples of base-length) antenna array with wider baselines, which result in a lower SNR level requirement [37].

There are a variety of DOA estimation algorithms in the literature that are capable of performing accurate DOA estimation given phase interferometric data. Several estimation algorithms have seen successful implementation for ES systems, namely the correlative interferometer algorithm (most widely used method) [15], multiple signal classification (MUSIC) algorithm [158] and the estimation of signal parameters via rotational invariance techniques (ESPRIT) algorithm [153].

2.4.2 DOA Estimation Algorithms

2.4.2.1 Correlative Interferometer [15]

The correlative interferometric method is based on a two step process. Firstly, the respective phase differences between the antenna's, respective to a primary antenna (e.g. θ_1 as shown in Fig. 2.14), are measured according to a known predefined bearing.

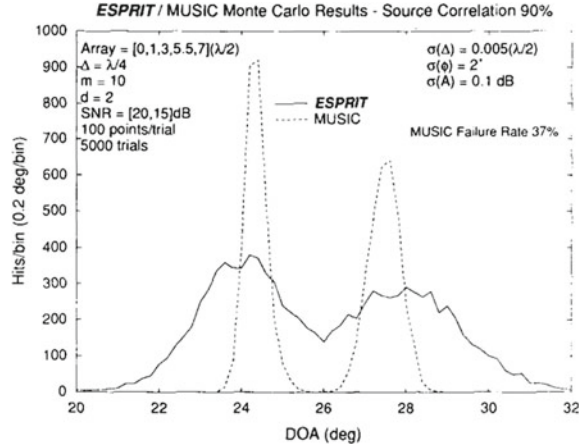
Then, based on a phase-history acquired during the system calibration of known transmitter angles, the method performs a correlation between the different phase measurements of the n -channel antennas and the stored phase history. The best corresponding phase set is chosen for the phase of the received signal which results in the correlative interferometric estimate of a incoming signal DOA.

The reliance on calibration history of some parameters make it susceptible to elevation ambiguities and lower SNR, as well as lower resolution compared to MUSIC and ESPRIT.

2.4.2.2 MUSIC [158] and Root-MUSIC [148]

The method of MUSIC as it applies to DOA was first formalized in [158] with beam-forming [159] and maximum likelihood [191] DOA methods as seminal components preceding its development. The algorithm is based on a probabilistic spectral search method over all the angles in the subspace, using eigen decomposition methods to

Fig. 2.15 Histogram of MUSIC and ESPRIT results-random IO-element linear array, source correlation 90 %, small array aperture ($\Delta = \lambda/4$), taken from [153]



resolve the DOA estimate. The search technique is computationally demanding and therefore can be very expensive for some real-world applications. Developments such as the alternative root-MUSIC algorithm [148] has shown to reduce the computational complexity and improve estimation accuracy [137].

The conventional MUSIC algorithm, although computationally expensive works for any antenna array configuration and multiple simultaneous RF signals. But it remains vital for the algorithm to have knowledge—in terms of the spatial model—of the positions of the antennas relative to one another. Furthermore, it is sensitive to position, gain errors, and phase. Therefore careful consideration must be applied for calibration.

2.4.2.3 ESPRIT [153]

ESPRIT is another estimation algorithm used for DOA estimation closely following the MUSIC DOA method. The algorithm is based on a similar correlation matrix generation and steering vector method as in MUSIC. The main difference is that by using a non-singular matrix subject to the eigenvector noise subspace, a single execution approach can be taken to determine the DOA instead of a search method. This is sometimes referred to as a “one shot” approach.

Based on this single step process the computation for this algorithm is significantly less as compared to MUSIC. However, due to the constraints imposed on the signal model and matrix rank, the amount of antennas needed for ESPRIT is double that of MUSIC which increases system cost. Furthermore, the use of total least square instead of previous least square (LS) ESPRIT method reduces the error when SNR is low as well as reducing error. The resolution of ESPRIT is reduced as compared to MUSIC. Figure 2.15 shows the difference in DOA estimations for these two algorithms.

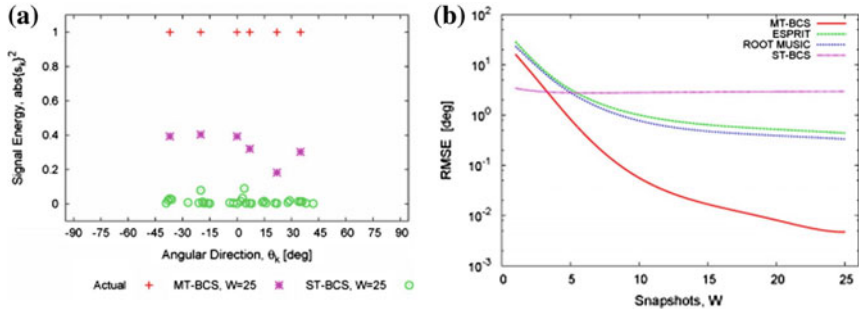


Fig. 2.16 In **a** showing the actual and estimated DOA using both BCS snapshot methods as well as the **b** error in terms of RMSE of the estimates with varying number of snapshots compared to other DOA estimation methods. Courtesy [31]

In summary, where sub-space DOA estimation algorithms are considered for our Compressive Sensing (CS) approach, MUSIC is the preferred DOA estimation algorithm due to the lower requirement on the number of antennas compared to ESPRIT, and higher resolution outcomes for DOA estimation.

2.5 Existing Compressive Based Direction-of-Arrival Methods

In many respects compressive sensing (CS) based techniques used for DOA methods are still in their infancy, which is interesting as CS theory is based on seminal works from beamforming and super resolution [62] techniques.

In the open literature there are several CS methods used for DOA estimations, which apply CS algorithms at various points in the processing chain. Majority of the literature do not include CS sampling techniques for DOA estimation, rather, only focus on applying CS recovery techniques. Such methods include the following major work.

Bayesian CS based DOA estimation [31] develops a single and multi snapshot approach using Bayesian compressive sensing (BCS) to estimate the DOA of a narrowband signal. Rather than relying on compressive sampling, BCS determines the estimates for DOA based on Nyquist-sampled voltage outputs directly from the antenna elements. It was shown that by adopting this method, computation of the covariance matrix for voltage outputs is not needed (as is the case with MUSIC [158] and ESPRIT [153]). Also, robust and accurate estimates were determined without the need for a-priori knowledge of the number of incident angles. However, the magnitude estimates were somewhat degraded due to estimation error, but no such effect to boresight-direction estimates were observed (see Fig. 2.16).

Radius	6.3λ
Search area	$\sqrt{u^2 + v^2} \leq 0.5$
Grid spacing in u, v -plane	0.02
Signal-to-noise ratio	30 dB
Number of elements	$M = 40$
Number of elements for $\lambda/2$ -array	500
Number of grid points	$N = 2000$

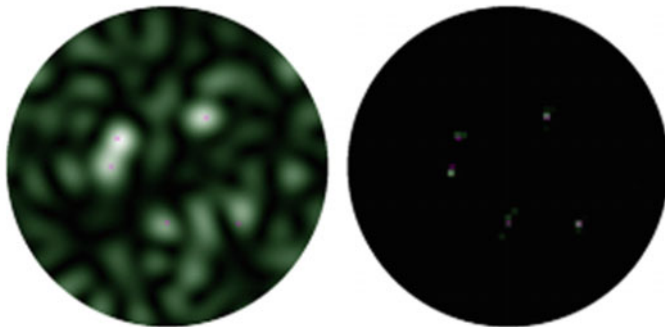


Fig. 2.17 DOA estimation of five simulated aeroplanes crossing the observation area. *Left* DOA estimates from beamforming methods. *Right* amplitude distribution estimates by means of CS methods. The true target position is highlighted by violet ‘x’ marker, whereas the estimates are shown in green intensity points. Sourced from [52]

CS based radar DOA estimation [55] is another attempt to investigate the application of CS for DOA estimation, specifically for radar (Fig. 2.17).

Even though this approach is successful in theory and has been shown to have favourable results, the application value for implementation lacks system benefits in terms of computational performance or sample reduction. In fact, it adds more complexity to the system and requires additional processing time.

In summary, based on the open literature, there have been minimal investigations as to how CS acquisition and recovery can be developed and applied to DOA estimation tasks in ES resulting in optimized memory and computational use. This puts the work of this monograph well in context.

Chapter 3

Compressive Sensing: Acquisition and Recovery

3.1 Introduction

The pioneering steps taken toward digitization of signals can be attributed to the theoretical work done by Kotelnikov, Nyquist, Shannon and Whittaker on sampling continuous-time band-limited signals [87, 128, 160, 187]. Their work resolved the issue of consistently recovering band-limited signals conditioned on the rate at which the input signal is sampled, which later became known as the Nyquist Rate. This rate empirically proved that a continuous band-limited signal can be accurately represented in the digital domain, if sampled at twice the highest frequency present [128].

The Nyquist rate remains the current convention for digital acquisition by means of an analog-to-digital converter (ADC), whereas CS approaches the task of acquisition in a completely different way. Instead of restricting digital acquisition to twice the highest frequency of the signal, CS acquires it by means of random sampling. Thereafter, the randomized-sampled signal is used to recover the original signal by means of linear optimization algorithms using sub-space modelling, which results in acquisition at a lower rate than the Nyquist criteria under certain conditions. Hence, CS is called a sub-Nyquist acquisition technique [53].

In this section we provide an overview of CS techniques as presented in the current literature with respect to RF signal recovery and acquisition techniques. We discuss the method of acquiring RF communication signal by CS techniques. Then, we shall discuss the current CS acquisition schemes developed for RF signal acquisition and propose the best suited scheme for DOA estimation. Thereafter, we shall review new CS recovery algorithms that reduce memory and computation for applications in DOA ES tasks.

The mathematical formulation of CS is extensive but vital in order to apply the theory correctly. Therefore, we refer the reader to our theoretical review of CS mathematical formulation in the appendix 9.5, which describes signal requirements in mapping to appropriate subspaces and the criteria on signal which result in a high probability of recovery.

3.2 Compressive Sensing Formulation

Compressive sensing (CS) attempts to address the task of compression as it relates to acquisition, storage and communication by means of randomization to reduce the input data set [18]. Since its seminal work in [28, 44] CS has been applied to various fields with varying success, viz. in signal processing [28], radar imaging [16, 69, 169], telecommunications [72, 140], data compression [174], image processing [101, 152], and optical sensor applications [52].

CS theory provides the necessary conditions that a signal—being sparse in some basis i.e. DFT, DCT, WHT—can be exactly recovered using a reduced set of samples dependent on a sensing matrix satisfying the restricted isometry property (RIP) [44] (refer Sect. 9.5.1 for further detail).

Taking an input signal $F(t)$ with finite length N , which we represent as a vector $X[n] \in (N, 1)$ after sampling with its coefficients $K \ll N$ in some sparse basis. Then as CS theory dictates, we choose an independent and identically distributed (iid) Gaussian sampling matrix, $\Phi \in [M, N]$, which when applied to the input vector $X[n]$ provides an output vector $Y \in (M, 1)$. Once the vector Y is acquired—which is the CS sampled signal—CS recovery algorithms solve the condition in Eq. 3.5, allowing for the original input vector to be recovered with high probability, represented as a vector \hat{s} .

The notations regarding CS acquisition and recovery, with respect to Fig. 3.1, are shown below.

$$Y = \Phi X \quad (3.1)$$

The Fourier transform coefficients, denoted as s , are given for X based on the basis Ψ comprising of the DFT matrix. Subsequently, the sensing matrix (see Sect. 9.5.3) is composed of the DFT matrix and the randomized acquisition method for sampling.

$$X = \Psi \times s \quad (3.2)$$

$$\text{then } Y = \Phi \Psi s \quad \text{letting} \quad \Phi \Psi = A \quad (3.3)$$

$$\text{gives } Y = A \times s. \quad (3.4)$$

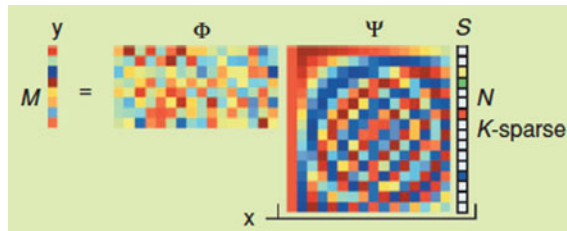


Fig. 3.1 CS measurement takes place for a vector x that is K-sparse in some other orthonormal basis Ψ and sensed via a randomized sub-Gaussian matrix Φ where the number of measurements $M \ll N$. (Sourced from [18].)

A typical method to recover the signal coefficients, which represent the signal, involves solving the mathematical program:

$$\hat{s} = \operatorname{argmin} \|v\|_1 \text{ s.t. } Y = Av. \quad (3.5)$$

Here v represents the solving vector being minimized in order to represent the final estimated vector \hat{s} by means of iterative optimization. The equation above is a convex optimization problem that can be solved via linear programming algorithms [150] and several other algorithms, reviewed later in Sect. 3.4.

3.2.1 Compressible Signal and Sensing Matrices

A discrete signal is said to be sparse in a domain, if there exists a basis and/or frame (Ψ) that produce coefficients (α) that mostly comprise of zero coefficients [53]. If this condition holds true, the sparsity of the signal can be exploited to compress the signal for other applications. If we have a-priori knowledge that a signal is sparse in some domain such as the Fourier domain for RF signal; we can use the knowledge of that basis or frame to recover the input signal with reduced number of measurements.

In mathematical terms we describe a signal x as K -sparse when it has at most K non-zero values, denoted as $\|x\|_0 \leq K$. It is common to refer to a signal as K -sparse, when in fact the signal x is actually K -sparse in terms of the representative coefficients produced as a product of the basis and/or frame Ψ , i.e. $x = \Psi\alpha$ with $\|\alpha\|_0 \leq K$.

Most signal that we will be dealing with, in the RF domain, are rarely entirely sparse for all applications. Thus, a better definition of compressibility is adopted in describing a signal's sparsity. The definition of compressibility of a signal x , requires the sorted magnitude coefficients α —derived from the basis (or frame) Ψ —to decay at a rate similar to that of the power law decay [150]. Importantly, if this definition holds for x , it is compressible in the basis Ψ . The power law decay rate can be expressed as:

$$|\alpha_s| \leq K \frac{1}{s^q}, \quad s = 1, 2, \dots, N, \quad (3.6)$$

where K is an arbitrary constant, s is the sorted index, and q is the given rate of decay.

One such compressible basis (i.e. Ψ), which will be used extensively throughout, is the Fourier transform, mapping time domain signal to a frequency-dependent subspace with magnitude and phase coefficients [131]. However, the rate of decay is not the only criteria to guarantee successful recovery by CS methods. For a basis to be used for CS recovery it must also comply with the following criteria:

- an orthonormal basis;
- obey the null space property (NSP);
- obey the restricted isometry property (RIP); and
- have a lower bound for coherence.

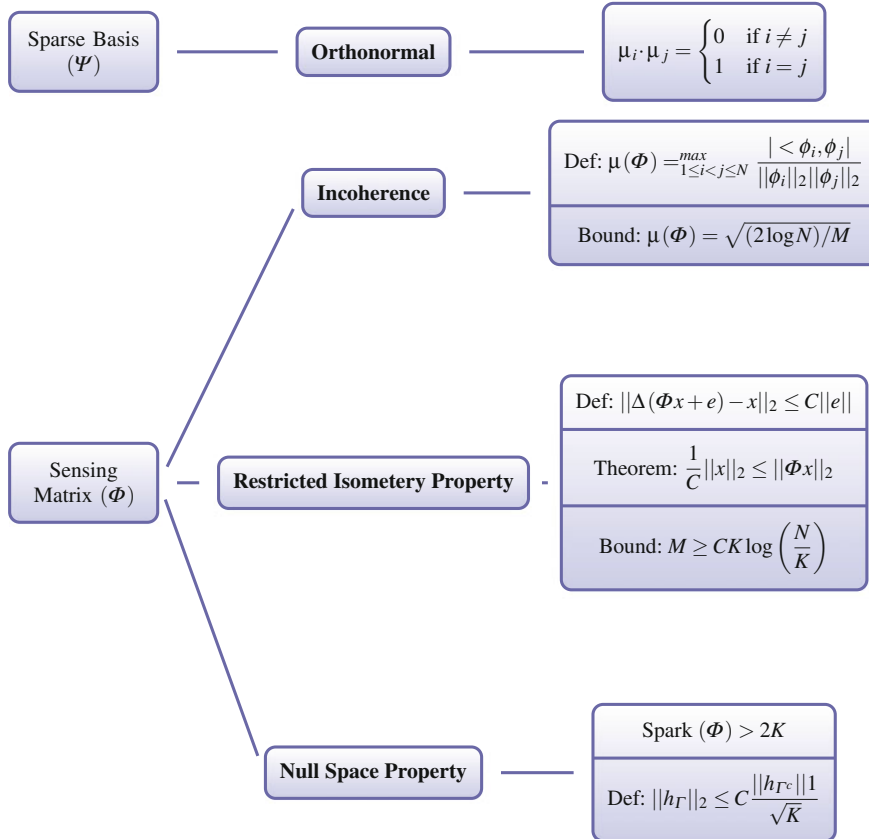


Fig. 3.2 Illustrates the condition of a given basis Φ and the conditional requirements (i.e. Coherence, NSP, RIP) for use in CS recovery, as well as the related sparse basis Ψ that has to be orthonormal

The representation in Fig. 3.2 diagrammatically relates the relationship of the basis to the respective properties. We refer the reader to Sect. 9.5.3 where we detail the theory for CS basis criteria.

If a matrix operates on an input vector $X \in \mathbb{R}^N$, producing a suitable vector $Y \in \mathbb{R}^M$ that allows for an unambiguous recovery of the input signal X [43] via CS recovery algorithm then it is a suitable basis. This, as has been described above, is possible only if it complies with the CS basis criteria.

Existing transform bases such as the discrete Fourier transform (DFT) does not comply with the CS basis criteria, which is a problem for our investigation as the DFT is pivotal to our digital processing goals. However, when a DFT is operated on by an iid Gaussian matrix it results in an overall matrix that does comply with the CS basis criteria. This result is further discussed in a later section, but it is important to note that other discrete transforms such as DCT, WHT, etc. use the same operation with an iid Gaussian matrix to achieve CS basis compliance.

3.2.2 Implementation for 1-Dimensional Signals

The CS acquisition and recovery steps for a 1-dimensional input signal, using a conventional RF receiver as the sensing system, in order to implement CS techniques are entirely different from 2-dimensional signals typical with imaging equipment.

For the 1-dimensional case the operation of the matrix multiplication of the DFT and iid Gaussian matrix is implemented by randomly sampling the input signal at a sub-Nyquist rate where the total number of samples $M = O(K \log(N/K))$ [35] must be taken in order to guarantee successful CS recovery, with:

- M = number of CS samples required;
- K = the total number of sparse coefficients represented in the sparse basis i.e. DFT; and
- N = the total number of samples of the input signal.

Once the input signal has been randomly sampled, a DFT matrix is applied to the input signal to complete the CS sampled vector used for CS recovery of the original N length vector X from the M length vector Y .

Figure 3.3 illustrates the system block proposed in order to apply CS for this work in achieving compressive sampling with $y[n]$ denoting the CS signal (Fig. 3.4).

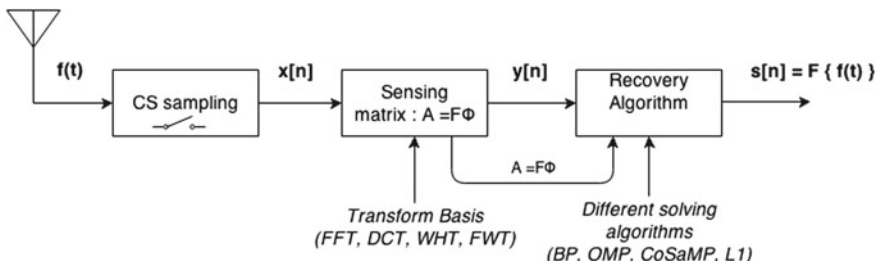


Fig. 3.3 A basic block diagram of a CS RF receiver channel used to compressively sample and recover a time domain RF input signal. Compiled by the authors

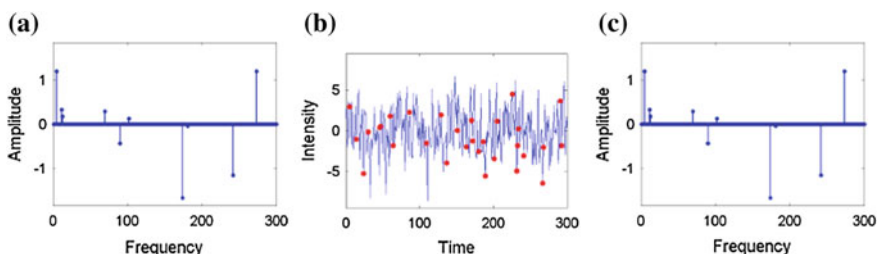


Fig. 3.4 **a** Is shows the frequency plot of the input time-domain signal $f(t)$. In **b** the input signal $f(t)$ (in blue) corresponding to Fig. 3.3 and the CS random sampled signal (red) with **c** as the recovered CS output estimate of the frequency spectrum of input signal $f(t)$

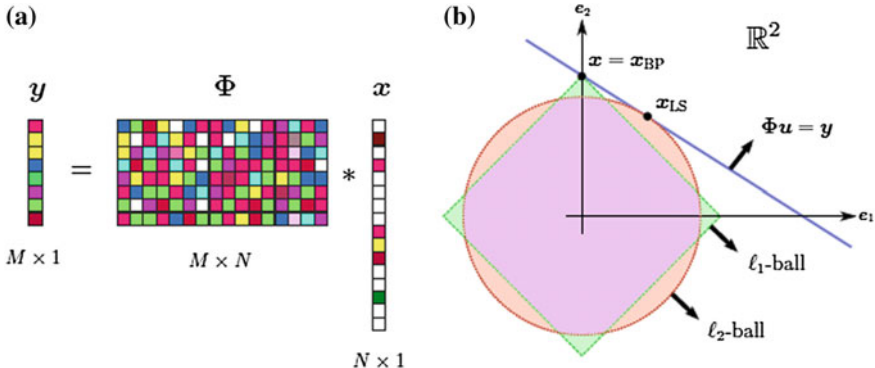


Fig. 3.5 **a** Illustrates the visual representation of compressed sensing via a matrix operation with Φ the randomized sensing matrix operating on the input signal x . In **(b)** the approximation error for two recovery techniques using different ℓ_p strategies, namely Least squares (i.e. ℓ_2) and Basis Pursuit (BP) (i.e. ℓ_1) are shown. (Courtesy of [78].)

As an aid to Fig. 3.3, the process that gets applied to the input signal $x[n]$ can be summarized by the matrix multiplication shown in Fig. 3.5 with the approximation error denoted by ℓ_p norm with $0 < p < \infty$.

Based on the discussion of the previous section, several conclusive conditions apply to practical implementation of 1-dimensional signal processing. Given, that a finite discrete signal x is K -sparse in some orthonormal basis, the sensing matrix satisfies the RIP of order $2K$, and has a low coherence of order $K = O(\sqrt{K})$. Then its exact recovery, by some arbitrary recovery algorithm, is made possible by taking $M = O(K \log(N/K))$ [35] measurements. These conditions are depicted in both Figs. 3.1 and 3.2.

It is worth mentioning here that the arbitrary recovery algorithm is based on the proof and guarantee of l_1 norm minimization [45]. The proof and guarantee predicts that solving the optimization problem of the form below, will yield a solution that optimally matches the K-sparse input signal.

$$\hat{x} = \operatorname{argmin} \|s\|_1 \text{ subject to } y = As, \quad (3.7)$$

where A is the product of $\Phi\Psi$ and s the K-sparse vector. Note that $x = \Psi s$. Thus, given the CS measurements y , x can be exactly recovered either with noise-free $y = \Phi x$ measurements (Theorem 4.1 in [150]) or measurements subject to noise $y = \Phi x + e$ (Theorems 4.3–4.4 of in [150]), bounded or Gaussian.

3.3 Compressive Sampling

Before reviewing the techniques for CS recovery it is pivotal to determine which CS sampling technique in the open literature serves as the best method for DOA estimation of modulated communication signals assuming a conventional ES RF receiver channel. In order to determine such a sampling technique we discuss conventional sampling technologies used in modern RF receivers to determine a baseline for comparison. Thereafter we review several CS sampling techniques and determine the best algorithm which is able to reduce memory and computational requirements.

Analog-to-digital converter (ADC)¹ development lags behind the conventional processing core (i.e. CPU) development by a large margin (i.e. Moore's law [155]), with sampling rates not doubling every year but every 2–4 years [173]. Slower development of ADC technology is a major motivation to develop techniques that trade processing power for sampling speed, in order to recover wider bandwidths. A variety of techniques exist that exploit processing power and Nyquist theory to increase use of bandwidth, reduce sampling rates, and remove the need for mixing and filtering stages to reduce system costs. Such techniques comprise conventional mixing-filter Nyquist sampling, bandpass sampling, direct sampling, and compressive sampling.

Although there exists several sub-Nyquist sampling techniques, which are mature in their development; they only remain effective for special cases in relation to low noise environments (bandpass), and limitations on ADC technology (direct). Refer Table 3.1 for a quantitative comparison between such sampling techniques. For our application CS sampling methods have a distinct advantage as they are custom developed for CS recovery algorithms, and thus used in our investigation. Moreover, CS has the capability of using lower rated ADCs to recover higher frequency sparse signals with ever more bit depth resulting in improved dynamic range [18]. Perhaps this is the most potential sub-Nyquist technique to break the barrier (i.e. red line in b) of Fig. 3.6) which serves as the rate of innovation for current ADC technology.

In the open literature CS sampling techniques can be categorised into two groups. The first consists of compression by modifying the input signal before sampling in order to use a low rate ADC. The second, samples at rates equivalent to the Nyquist frequency and then applies several techniques for compression.

Although both methods are applicable in theory, for practical purposes discussing techniques that align with the former method, not the latter, are relevant to this work. After all, the purpose for CS RF signal acquisition is to reduce the number of samples needed before processing, in order to reduce memory and computational

¹Sampling a signal, in order to represent analog information (i.e. electromagnetic RF) in a digital form, is done by means of an analog-to-digital converter (ADC) [185]. Many variations of these electrical components exists, all sharing the same principle for acquisition but with varying techniques. Additionally, some exhibit benefits over others in terms of bit depth and/or sampling rate. The ADC types that exist and are widely used, include *flash*, *sigma-delta*, *successive-approximation*, *ramp-compare*, and *pipeline* [183]. Current ADCs are capable of a conversion rate of up to 3.6 GSPS and a bit depth of 12 bits. However these ADCs, although fast, do come at a price that for conventional use in RF systems is exorbitantly high—in the range of > \$4 000 per ADC, as of 2013 [76].

Table 3.1 Comparative table of different sampling techniques available for use in receiver systems, compiled by the authors

Features	Conventional	Bandpass	Direct	CS
Number of samples (Memory load)	M	M	H	L
Bandwidth	L-M	L-M	H	H
Sparsity of frequency in spectrum	L	L-M	L	H
Resolution	M-H	M-H	M-H	L-M
Complexity	L	M	H	M
Computational load	L	M	H	M
Cost	L	L-M	H	L-M
KEY:	H = High	M = Medium	L = Low	

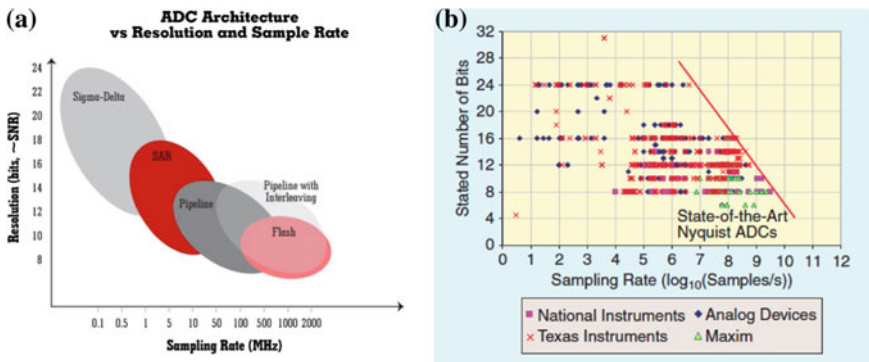


Fig. 3.6 **a** Shows the sampling rate versus bit depth for different variations of ADCs, and **b** the rate of innovation for ADC technologies for different manufacturers. (Sourced from [116, 133].)

requirements. Therefore the requirements of CS sampling techniques that can be applied for our application for DOA estimation of modulating communication signals are:

- bandlimited CS sampling technique;
- able to simulate in software;
- practical implementation capability;
- able to utilize conventional CS recovery techniques; and
- minimized memory and computational requirements.

We refer the reader to Sect. 9.7 which deals with wideband CS sampling techniques used for spectrum sensing tasks—as wideband CS sampling falls outside the scope for our application.

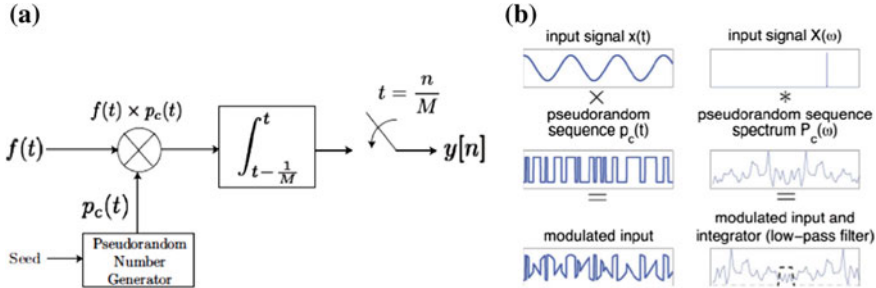


Fig. 3.7 In **a** a system block is shown for the random demodulator analog-to-information sampler method and in **b** the corresponding outputs with respect to time and frequency spectrum is shown. The input signal is effectively mixed with random noise which shifts the spectrum by a relative amount from the original; this is filtered and the original signal inferred by the CS recovery by determining the shift of the spectrum. Sourced from [85, 173]

3.3.1 Random Demodulator (RD) Analog-to-Information Sampler

The RD analog-to-information sampler utilizes a wideband pseudo-random demodulator (i.e. a ± 1 generator clocked at the Nyquist frequency) to mix with the input signal $f(t)$, apply a sample and hold (S/H) circuit that acts as a discrete low pass filter, and finally sample the output from the S/H with a low-rate ADC (see Fig. 3.7).

The RD sampler has the effect of imposing randomization on the signal which mimics an iid Gaussian RIP compliant matrix multiplication with the signal [85], such that the recovery via CS is viable. The sampled signal $y[n]$ can then be used to recover the input signal $f(t)$ via CS recovery algorithms, provided that frequency support for $f(t)$ is sparse. In Fig. 3.7 the distinct time and frequency signal spectrum is shown at different stages of the RD process chain.

Work done in [85] suggested the feasibility of the RD sampler, and developed further in [173] wherein it was shown to be an efficient CS sampling method for band-limited sparse signals. Moreover, a practical prototype of an analog-to-digital conversion method, referred to as the compressive analog-to-digital converter (CADC), based on the RD method was realized. Their work resulted in practical compressive sampling and recovery using a 160 MHz DSP board of RF frequency sparse signal up to 900 KHz with low-rate ADC sampling at 100 KHz.

A more recent practical implementation of the RD method was developed in [190], known as the random demodulator pre-integrator (RDPI), shown in Fig. 3.8. By adopting an eight channel RD architecture with a sub-channel correlated pre-integrator design, high frequency sparse signal recovery was proven; with an effective dynamic range of 54 dB, bandwidth coverage of 2.2 GHz and a sampling reduction by a factor of 12.5 using a 90nm CMOS chip design (refer [190]). However, this technique is primarily used for radar applications, conditioned to short pulse transmissions, and has low applicability at ED bandwidths.

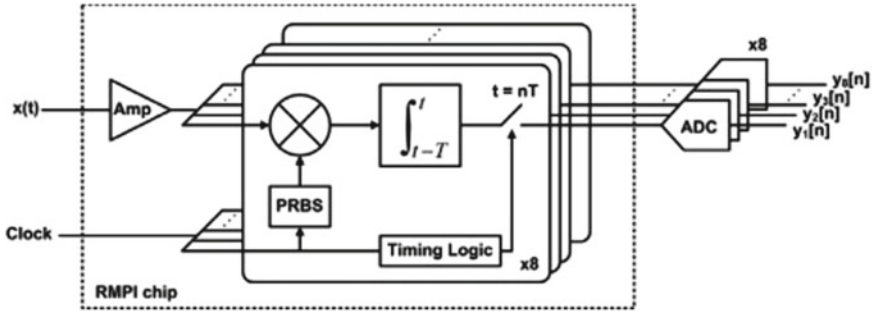


Fig. 3.8 System block of the RDPI, sourced from [190]

The RD method and its implemented RDPI extension is an effective CS sampling method in reducing the sample size during acquisition. However, the inherent reliance of the method on a large matrix inversion places a computational load on processing. For example, taking a wideband frequency sparse bandlimited signal, requiring a sampling rate of $f_{NQ} = 10\text{ GHz}$, would need a matrix of dimension 2.6×10^8 by 1×10^7 for CS recovery—a large memory and computational requirement not practical for real-time processing at the current technology.

The constraint of bandwidth on the input signal impedes the RD method as a real-time technique for use in wide bandwidths and high RF frequency cases, but feasible for lower frequency operations. For scenarios where only a single bandlimited signal is of interest, a pre-mixing stage can be added before the ADC to down convert the input signal to an intermediary frequency (IF). Digitizing the IF signal requires less memory and computation, making it feasible for real-time CS recovery.

3.3.2 Non-uniform Sampler (NUS)

The NUS attempts to randomly sample a signal at the level of the ADC, applying innovative techniques to control the flow of data by means of S/H circuits before quantization. In [182] a seminal prototype of an NUS IC device was developed, using commercially off-the shelf components (COTS) for quantization and recovery of signal from 800 MHz to 2 GHz sub-Nyquist sampling, using a 14 bit 400 MHz ADC.

NUS relies on selecting, at random, integer multiples of the underlying Nyquist rate allowing for corrective calibration, comparatively different to the random unrelated Nyquist sampling technique used by [91]. Nonetheless, using a S/H hold circuit controlled by a pseudo-random bit-sequence (PRBS) clocked at the Nyquist frequency (i.e. 4.4 GHz), allows the NUS architecture to select and hold samples at random, conditioned on the PRBS. The specifications for the NUS sampler, are a bandwidth of 2 GHz, an occupied spectrum of 100 MHz, 5.8W power consumption,

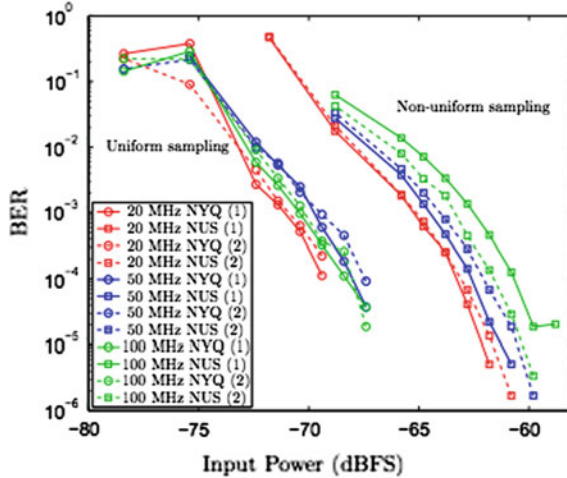


Fig. 3.9 BER of the decoded GSM signal as a function of input power. Circular markers indicate the performance of the uniform ADC for each of two randomly generated signals (denoted (1) or (2)) at each of three levels of clutter (20, 50 and 100 MHz). Square markers indicate the performance of the NUS on the same signals. The *solid* and *dashed lines* correspond to separate trials. (Taken from [182].)

and a sample resolution of 8.8 ENOB with 55 dB of SNDR.² The samples “held” by the S/H circuits are then digitized by the under-sampling ADC and controlled by the ADC sampling speed. Of every 8192 Nyquist rate samples only 440 are taken. Thereafter, the samples are reconstructed and recovered on a desktop personal computer with GPU hardware using a block algorithm.

The recovery method employed in [182] is non trivial as it requires multiple interpolations, stitching, and windowing functions being applied before recovery of the original signal is made possible. To some extent this complexity could serve as a deterrent for practical implementation. However, the experimental evidence in [182] suggests that real-time implementation is possible for high frequency bandlimited signal with conditions on the spectral support and effective instantaneous bandwidth (EIBW) dependent on the clocking frequency.

The experimental data indicate similar results for the bit-error rate (BER) of a GSM input signal (see Fig. 3.9) when using the sub-sampling NUS architecture versus a conventional 4.4 GHz ADC. Moreover, the NUS technique allows for higher bandwidth recovery than the RD and RDPI with significant improvements on recovery of sparse signals.

A similar approach, following the same logic as the NUS sampler, known as the random-ADC (RADC), was developed in [91]. It used a multiplexer and demultiplexer stage controlled via a PRBS, similar to [182]. The RADC method showed

²ENOB refers to the effective number of bits and the SNDR denotes the signal to noise ratio + distortion ratio.

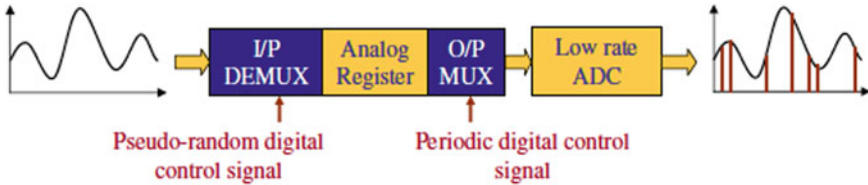


Fig. 3.10 Showing the implementation of the RADC. (Taken from [91].)

promise for application in sparsogram and time-frequency applications. However, practical implementation of the system has not yet been realized for high frequency RF scenarios. Figure 3.10 shows the RADC implementation.

3.3.3 *Compressive Multiplexing (CMUX) Sampler*

CMUX, by definition, is a multi-channel architecture conceptualized in [162] whereby a single ADC is used to sample the output of multiple channels. CMUX has a dual approach to sub-sampling. The first approach relies on RF mixers to down convert each channel to an IF. It then applies a psuedo-random chipping sequence (PRCS), equivalent to [146], to each channel that has the effect of randomizing the IF signal. Secondly, a bandpass sampling approach is taken, by first digitizing the signal according to the respective Nyquist zones (see [4]), which is then mixed with the PRCS.

Development of the CMUX draws from the RD and RDPI design with significant differences in terms of parallel architecture and recovery. The recovery method differs with other typical CS recovery methods, in that a condition known as joint sparsity [51] must be used relating the sensing matrix to each branch in the CMUX scheme for accurate recovery. The parallel architecture imposes a larger computational load on recovery when compared with other common CS techniques.

A conceptual practical prototype is suggested in [182] with the remainder of their work proven by simulation for low RF frequency signal applications (i.e. 10–20 MHz). However, using this method for wideband applications is possible but not yet practically implemented.

3.3.4 *Summary of CS Sampling Methods*

For practical application of a CS sampling method, NUS and RDPI are the most developed schemes scalable to the current DSP architectures. The RDPI implementation is preferable over the NUS sampling scheme for our application, due to less complex software and sampling requirements, and the use of conventional CS recov-

Table 3.2 Comparison of the different CS sampling techniques reviewed for bandlimited signal acquisition, compiled by the authors

Features	RD	RDPI	NUS	RADC	CMUX
Software complexity	L	L	H	M	H
Conventional CS recovery	Y	Y	N	Y	N
Sampling complexity	L	L-M	H	M	H
Computational requirements	L-M	M	M	M	H
Reduction of samples	M	H	H	H	H
Hardware implementation	N	Y	Y	Y	N
KEY:	H = High	M = Medium	L = Low		
	Y = Yes	N = No			

ery methods (detailed in a later section). See Table 3.2 for comparison of CS sampling methods.

For simulation purposes RD, RDPI and RADC are adequate candidates as they have similar computational requirements, sampling and software complexity, and can use conventional CS recovery techniques. CMUX and NUS are effective CS sampling techniques for simulation as well. However, their software complexity and reliance on non-conventional CS recovery methods do not meet the requirements for our application which depend on conventional CS recovery.

3.4 CS Recovery Algorithms

Once CS based sampling occurs, producing a sub-sampled signal y , it becomes the responsibility of the CS recovery algorithm to produce an estimate of the input signal x . There are numerous algorithms developed specifically for CS recovery, and can be categorised into one of three classes; convex-optimization techniques, greedy methods, and combinatorial methods.³ For adoption into the CS camp of recovery algorithms, all sparse recovery methods must optimize the following.

- Minimal number of measurements.
- Robustness to noise and mismatch errors.
- Speed of computation.
- Performance guarantee on recovery.

³Combinatorial techniques —developed by the theoretical computer science community [38]—utilize the *count-min*, *count-median* or *Bayesian* methods. Combinatorial algorithms assume that the origin of a signal of interest comes from a probability distribution, which imposes a belief of propagation on the recovery [20]; or modelled for data network [72] and probabilistic learning applications [79]. Thus, the relevance to our work—with exception to Fourier sampling in [64]—is minimal, and we leave it to the reader to explore further.

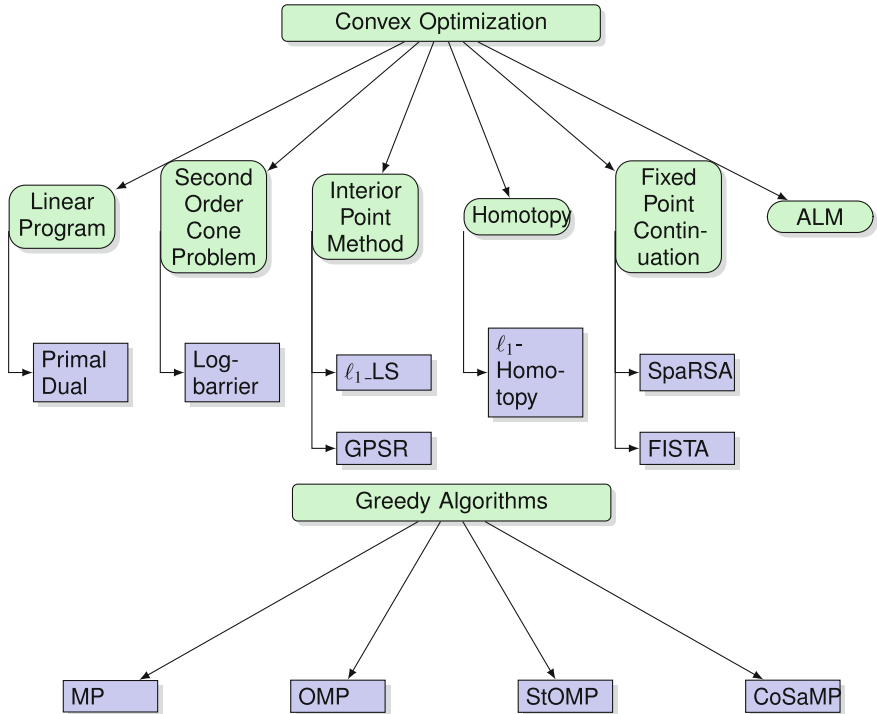


Fig. 3.11 A work breakdown structure of the algorithms to be discussed; categorized according to the two algorithmic groups, convex optimization and greedy algorithms, respectively. (Compiled by the author.)

The type of CS recovery algorithm to use is dictated by the input signal considered. For example, where the sparsity of the signal is known with high probability—greedy algorithms are preferred. However, when the sparsity is unknown but the signal is still sparse—convex-optimization algorithms are preferred. We discuss the reason for the constraint of sparsity on the CS algorithm in the section to follow, by detailing the CS recovery algorithms which constitute each category. Also, the advantages and disadvantages of each algorithms are reviewed.

The objective of reviewing current CS recovery algorithms are to determine which CS algorithm can be applied to our task of CS DOA estimation for modulated signals. Specifically, we want to investigate which CS recovery algorithm can optimize speed, memory, and computational requirements can match conventional DOA estimation performance.

A work breakdown structure is provided in Fig. 3.11 revealing the relevant algorithms reviewed for this work.

3.4.1 Convex Optimization-Based Algorithms

Convex optimization based algorithms adopt the definition of a convex problem, where it is the objective to minimize a convex function $f(x)$, for an unknown sparse vector x , over a convex subset where $f : x \rightarrow \mathbb{R}^N$ [23]. Thus, based on the guarantees of Eq. (3.7) the minimized output will result in the K -sparse input vector x . Although, convex optimization algorithms employed by CS methods are categorically solved by linear programs or iterative approaches, both adopt a similar set-up for solving the convex problem.

Conventional convex optimization techniques do not provide adequate results [150] when applied to CS recovery on their own. Therefore, CS specific sparse recovery algorithms have been developed.

Recently developed CS recovery algorithms, based on convex optimization, take the following approach. To recover an estimate \hat{x} given the measurements via $y = \Phi x$: $\Phi \in \mathbb{R}^{M \times N}$ a cost function $J(x) = ||x||_1$ and a noisy cost function⁴ $F(\Phi x, y) = \frac{1}{2} ||\Phi x - y||_2^2$ are used. Based on basis pursuit de-noising (BPDN) [33, 100] an adequate estimate of the K -sparse input vector x can be determined by solving the following expressions.

Noise free case:

$$\min_x \{J(x) : y = \Phi x\} \quad (3.8)$$

Noisy case:

$$\min_x \{J(x) : F(\Phi x, y) \leq \varepsilon\}. \quad (3.9)$$

where choosing a penalty parameter γ resolves this into an unconstrained case with $\min_x \{J(x)\} + \gamma F(\Phi x, y)$ with $\gamma > 0$ and determined by statistical trial [105].

3.4.1.1 Linear Programming

Linear programming (LP) is used to tackle the noise free implementation of the ℓ_1 – minimization problem, where a standard interior-point method [127] can be used to solve the linear program in time complexity of order $O(N^3)$ [150]. Although exact recovery is guaranteed, the exponential growth in computational requirement is undesirable for larger signal. Moreover, for practical purposes dealing with measured signal, this approach is impractical for cases which include noise. Therefore more robust algorithms have been developed in literature to solve problems with noisy measurements. These, more robust convex optimization methods, are detailed in the sections to follow.

⁴ F cost function penalizes the difference in terms of Euclidean distance between the Φx and y in vector form [150].

3.4.2 Fast ℓ_1 -Algorithms

For the case when noisy CS measurements are considered for recovery, a different approach based on BPDN is adopted taking the form shown in Eq. (3.9) based on the work in [30, 33]. More importantly, the results in [30] restructures the convex optimization as a second order cone program (SOCP) [23] that can be solved by the interior point method. Subsequently, this result has aided the development of *fast* ℓ_1 -norm algorithms.

A collection of the most relevant and widely reviewed algorithms in the open literature, fitting the criteria of convex optimization, follows.

3.4.2.1 L1 Magic [26]

ℓ_1 -magic comes as an algorithm package⁵ used for CS research that comprise two fundamental solving algorithms, both able to robustly recover noisy CS measurements using the interior point method described in Chap. 11 of [23]. However, as one of the first CS recovery algorithms, and with the advent of newer algorithms, these algorithms are comparatively slower, yet robust and accurate for CS recovery. Nonetheless, they provide a solid theoretical introduction for other algorithms wherein similar techniques are used, and therefore, mentioned herein.

The first, is a **primal-dual algorithm for linear programming** based on basis pursuit and Newton's iterative algorithm. This can, briefly, be described in terms of a standard-form LP as in [26]:

$$\min_z \langle c_0, z \rangle \text{ subject to } A_0 z = b, \quad (3.10)$$

$$f_i(z) \leq 0, \quad (3.11)$$

where the search vector $z \in \mathbb{R}^N$, $b \in \mathbb{R}^M$, A_0 is a $M \times N$ matrix with $f_i, i = 1, \dots, m$ as a linear function

$$f_i(z) = \langle c_i, z \rangle + d_i, \quad (3.12)$$

for $c_i \in \mathbb{R}^N$, $d_i \in \mathbb{R}$. At the optimal point of the LP, there exists a dual vector $v^* \in \mathbb{R}^M$, $\lambda^* \in \mathbb{R}^M$, $\lambda^* \geq 0$ such that the Karush-Kuhn-Tucker (KKT) conditions are satisfied.

$$(KKT) \quad c_0 + A_0^T v^* + \sum_i \lambda_i^* c_i = 0 \quad (3.13)$$

Thus, in summary the primal dual algorithm finds the optimal z^* based on the optimal dual vectors v^* and λ^* by solving the above-mentioned non-linear equations. A solution can be found by following the pseudo-code.

⁵Distributed as open source code, written in Matlab and it can be accessed at [27].

Algorithm 1 Primal-Dual interior-point method [23]

Require: x that satisfies $f_1(x) < 0, \dots, f_m(x) < 0, \lambda > 0, \mu > 1, \varepsilon_{feas} > 0, \varepsilon > 0,$
repeat

1. Determine $t, t \leftarrow \mu m / \hat{\eta}$
2. Compute primal dual search direction Δy_{pd}
3. Line search and update

until $\|r_{pi}\|_2 \leq \varepsilon_{feas}, \|r_{dual}\|_2 \leq \varepsilon_{feas}$ and $\hat{\eta} \leq \varepsilon$

The primal, dual and central residuals provide a condition for the proximity of (z, v, λ) which satisfies (3.13) in light of the slackness condition⁶:

$$r_{dual} = c_0 + A_0^T v + \sum_i \lambda_i c_i \quad (3.14)$$

$$r_{cent} = -\Lambda f - (1/\tau) \quad (3.15)$$

$$r_{pri} = A_0 z - b, \quad (3.16)$$

where Λ is the diagonal matrix where $\Lambda_{ii} = \lambda_i$, and $f = (f_1(z) \dots f_m(z))^T$.

The second approach, known as the **log-barrier algorithm for SOCPs**, is similarly based on the work in [23] and, although SOCPs are more involved than LP, the algorithm implementation is less involved than the primal-dual method mentioned above. However, it is still founded on solving iterative Newton steps, much like the LP problem. This can be written as follows (based on work in [26]).

$$\min z \langle c_0, z \rangle \text{ subject to} \quad A_0 z = b, \quad (3.17)$$

$$f_i(z) \leq 0, \quad i = 1, \dots, m \quad (3.18)$$

where f_i denotes the constraint (i.e. cost) taking the form of a second-order conic

$$f_i(z) = \frac{1}{2} (\|A_i z\|_2^2 - (\langle c_i, z \rangle + d_i)^2). \quad (3.19)$$

The log-barrier method modifies Eq. (3.17) into logarithmic form constituting a series of linearly constrained programs, which can be expressed as:

$$\min z \langle c_0, z \rangle + \frac{1}{\tau^k} \sum_i -\log(-f_i z) \text{ subject to } A_0 z = b. \quad (3.20)$$

It is important to mention that at log-barrier iteration k , by minimizing the series of quadratic approximations generated by means of Newtons method, the algorithmic approach begins to solve the system of equations. The quadratic approximations are

⁶ $\lambda_i f_i = 0$, which converges subject to $\lambda_i^k f_i(z^k) = -1/\tau^k$ where the parameter τ^k is increased progressively in accordance to the Newton iterations [26].

initialized around a point z based on Eq. (3.20) and expressed as

$$f_0(z + \Delta z) \approx z + \langle g_z, \Delta z \rangle + \frac{1}{2} \langle H_z \Delta z, \Delta z \rangle := q(z + \Delta z), \quad (3.21)$$

where g_z is the gradient given as $g_z = c_0 + \frac{1}{\tau} \sum_i \frac{1}{-f_i(z)} \nabla^2 f_i(z)$, and H_z the Hessian matrix (see [26]).

Based on the above expressions the log-barrier algorithm pseudo code, to follow, can be used as an outline to solve the SOCPs for CS noisy measurements.

3.4.2.2 ℓ_1 -Least Squares (L1-LS) Regularization Algorithm [84]

L1-LS undertakes a different approach for solving CS measurements. This is also known as a *Gradient Projection* method [189] and preceded by the *Gradient Projection Sparse Reconstruction* method in [59] on which the L1-LS is founded. Consequently, the novelty of this approach stems from defining the convex optimi-

Algorithm 2 Log-barrier algorithm for SOCPs [26]

Require: Feasible starting point z^0 , tolerance η , parameter μ and initial τ^1 with $k = 1$

```

repeat
  if  $m/\tau^k < \eta$  then
     $\alpha \leftarrow z^k$ 
  else
     $\tau^{k+1} \leftarrow \mu\tau^k, k \leftarrow k + 1$ 
  end if
until Solved (3.20) using Newton's method subject to (3.21), using  $z^{k-1}$  as initial point. return
 $z^k \leftarrow \alpha$ 

```

mization problem as a ℓ_1 -regularized least squares (LS) problem. By substituting the sum of absolute values for the sum of squares used in Tikhonov regularization [65] gives a general form,

$$\min ||Ax - y||_2^2 + \lambda ||x||_1 \quad (3.22)$$

where λ is given as the Lagrange regularization parameter. Then, based on statistical linear regression methods, a custom interior point-method similar to that of Eq. (3.20) results, known as the Truncated Newton Interior-Point Methods (TNIPM). However, the performance advantage depends on a preconditioned conjugate gradient (PCG) step for initialization, whereas in [33] a LSQR [132] is used. The TNIPM therefore transforms the ℓ_1 -regularized LS problem into a quadratic convex problem to be solved, based on the following constraints:

$$\min ||Ax - y||_2^2 + \lambda \sum_{i=1}^n u_i \text{ s.t. } u_i \leq x_i \leq u_i, i = 1, \dots, n. \quad (3.23)$$

where TNIPM aims to solve a custom interior-point problem, given in [84] with respect to the *log-barrier method* for bound constraints (3.23).

$$\Phi(x, u) = - \sum_{i=1}^n \log(u_i + x_i) - \sum_{i=1}^n \log(u_i - x_i) \quad (3.24)$$

$$\phi_t(x, u) = t\|Ax - y\|_2^2 + t \sum_{i=1}^n \lambda u_i + \Phi(x, u) \quad (3.25)$$

An important result from [84] is based on defining a Lagrangian dual that places a bound on an arbitrary x that produces a suboptimal x by constructing a dual feasible point v , so that $G(v)$ is the lower bound for the optimal value in Eq. (3.23) [84]. The point v is given as:

$$v = 2s(Ax - y) \quad (3.26)$$

$$s = \min\{\lambda/|2((A^T Ax)_i - 2y_i)|\} , i = 1, \dots, m \quad (3.27)$$

and the duality gap, known as $G(v)$, is used to determine the distance between the objective value of x and the gap, which is denoted by η .

$$\eta = \|Ax - y\|_2^2 + \lambda\|x\|_1 - G(v) \quad (3.28)$$

The Newton solution system is given as

$$H \begin{bmatrix} \Delta x \\ \Delta u \end{bmatrix} = -g \quad (3.29)$$

with the Hessian $H = \nabla^2\phi_t(x, u)$ and the gradient at a given iteration denoted as $g = \nabla\phi_t(x, u)$. All this, results in constructing the TNIPM Algorithm 3 as detailed below.

Algorithm 3 Truncated Newton IPM for ℓ_1 -regularized LSPs. Courtesy of [84]

Require: Relative tolerance $\varepsilon_{rel} > 0$

Initialize : $t := 1/\lambda$, $x := 0$, $u := 1$

repeat

1. Compute the search direction $(\Delta x, \Delta u)$ as an approximate solution to the Newton system (3.29)
2. Compute the step size s by backtracking line search as in (3.26)
3. Update the iterate by $(x, u) := (x, u) + s(\Delta x, \Delta u)$
4. Construct dual feasible point v from (3.26)
5. Evaluate the gap η from Eq.(3.28)
6. Update t

until $\eta/G(v) \leq \varepsilon_{rel}$

Finally, the development of the ℓ_1 -regularized LS algorithm⁷ proved to be an improvement over the previous convex optimization algorithms (i.e. ℓ_1 -magic), in that the recovery time could be reduced due to the initializing PCG step, prior to solving the optimal estimate for x . This was shown in [84] by means of the problem of MRI image recovery being investigated using a host of recovery algorithms.

3.4.2.3 L1-Homotopy [9]

One of the more recent algorithms, that have shown promising results for Frequency Modulated Continuous Wave (FMCW) application using CS (see [9]), is the ℓ_1 -homotopy algorithm.⁸ This method exploits the homotopy transformation of the objective function (see Eq. (3.30)) from a ℓ_2 constraint to the ℓ_1 function. Put differently, this method starts with an initial solution and finds a homotopy path to the final solution. The progression along the homotopy path is governed by the homotopy parameter, which corresponds to the two endpoints of the path given as $\varepsilon \in [0, 1)$ [9].

Given a CS measurement vector $y = A\tilde{x} + e$, the ℓ_1 -homotopy algorithm solves the ℓ_1 -norm minimization, by including a homotopy parameter and recasts the ℓ_1 -norm minimization as the following optimization problem:

$$\min_x ||Wx||_1 + \frac{1}{2} ||Ax - y||_2^2 + (1 - \varepsilon)u^T x \quad (3.30)$$

where, by changing ε from 0 to 1 u can be defined as:

$$u = -W\hat{z} - A^T(A\hat{x} - y), \quad (3.31)$$

with W a diagonal matrix that has as its diagonals the positive weights w , and the warm-start vector \hat{x} chosen arbitrarily given the corresponding matrix $A_{\hat{f}}^T A_{\hat{f}}$. It is important to realize that as ε changes from 0 to 1, the optimization problem in Eq.(3.30) transforms into the standard ℓ_1 -norm, and therefore the solution follows a piece-wise linear homotopy path towards the solution of

$$\min_x ||Wx||_1 + \frac{1}{2} ||Ax - y||_2^2. \quad (3.32)$$

For optimal conditions the sub-differential of its objective function must be set to zero [9]. The results in [9] and the homotopy optimization definition above leads to the ℓ_1 -homotopy algorithm as shown in Algorithm 4.

The computational costs associated with this approach are significantly less, in terms of time and iterative operations, than other state-of-the-art ℓ_1 solvers, namely SpaRSA[188] and YALL1[9, 102]. Most of the cost relates to the update matrix

⁷L1_LS source code (written in Matlab[®]) and can be accessed in [129].

⁸ ℓ_1 -homotopy code can be accessed at [129].

Algorithm 4 ℓ_1 - homotopy algorithm. Courtesy of [9]

Require: A , y , W , \hat{x} , and u (optional: inverse or decomposition factors of $A_{\hat{F}}^T A_{\hat{F}}$)
Ensure: x^*
Initialize: $t := 1/\lambda$, $x := 0$, $u := 1$
repeatCompute ∂x (28) in [9]Compute p and d (27b) of [9]Compute $\delta^* = \min(\delta^+, \delta^-)$ (29) of [9]
if $\varepsilon + \delta^* > 1$ **then** $\delta^* \leftarrow 1 - \varepsilon$ $x^* \leftarrow +\delta^* \partial x$ **break**
end if $x^* \leftarrow +\delta^* \partial x$ $\varepsilon \leftarrow \varepsilon + \delta^*$
if $\delta^* = \delta^-$ **then** $\Gamma \leftarrow \Gamma / \gamma^-$
else $\Gamma \leftarrow \Gamma \cup \gamma^+$
end if
until $\varepsilon = 1$

inverse operation and the update matrix factorization for A ; with the complexity cost in the order of $MS + 2S^2$ and $MN + MS + 3S^2 + O(N)$, respectively [9].

3.4.2.4 Fixed Point Continuation (FPC) Methods [70]

Another approach that falls within the domain of fast ℓ_1 -algorithms, is the fixed-point continuation method, which deviates from the previous notion of the interior point method by applying a shrinkage method (a method applied to wavelet-based denoising [150]). The FPC solves the ℓ_1 -minimization problem by defining a convex-differentiable function H and employs an iterative shrinkage procedure. Consequently, the ℓ_1 -minimization problem then takes the form of

$$\min_x \mu ||x||_1 + H(x), \quad (3.33)$$

where the coefficient of x for the $(k+1)^{th}$ time step is denoted as

$$x_i^{k+1} = \text{shrink}((x^k - \tau \nabla H(x^k))_i, \mu \tau) \quad (3.34)$$

with $\tau > 0$ the step-length for gradient descent and μ is defined by the user [70]. Moreover, specifying the typical convex cost function according to the residual squared norm gives $H(x) = ||y - \Phi x||_2^2$ and its corresponding gradient $\nabla H(x) = 2\Phi^T(y - \Phi x)$. Based on the selection of cost function, the program

is run until it converges to a fixed point and thus yields the sparse estimate vector \hat{x} . The generic algorithm of FPC form is given below, in Algorithm 5, with the respective penalty parameter used in Eq. (3.34).

Algorithm 5 Fixed point continuation algorithm. Courtesy of [70] & [150]

Require: CS matrix Φ , measurement y , parameter sequence μ_n

Ensure: Signal estimate \hat{x}

Initialize : $\hat{x}_0 = 0, r = y, k = 0$

while alting criterion false **do**

1. $k \leftarrow k + 1$
2. $x \leftarrow \hat{x} - \tau \Phi^T r$ {take a gradient step}
3. $\hat{x} \leftarrow \text{shrink}(x, \mu_k \tau)$ {perform soft thresholding}
4. $r \leftarrow y - \Phi \hat{x}$ {update measurement residual}

end while

return $\hat{x} \leftarrow \hat{x}$

In previous studies it has been shown that FPC is a favourable candidate as opposed to other recovery techniques based in the same category as ℓ_1 -minimization. It was shown that algorithms based on FPC methods such as SpaRSA⁹ [188] and Fast Iterative Shrinkage-Thresholding Algorithm (FISTA)¹⁰ [22] are able to out perform algorithms such as ℓ_1 -LS in terms of computational time taken for recovery [98]. Moreover, in terms of direct comparison between the two best placed algorithms using FPC techniques, FISTA outperforms SpaRSA by a computational factor of 4, for Fourier based signal recovery [189] (a problem which is of importance for this monograph).

3.4.2.5 Augmented Lagrange Methods [102]

Augmented Lagrange Multiplier (ALM)¹¹ methods form a subclass of algorithms included as part of convex programming. Instead of employing a cost function to determine the optimal solution, concurrent estimates of the optimal solution and Lagrangian multipliers are calculated at every step, to adjust for the solution outcome [189]. By doing this the following ℓ_1 -minimization problems is recast as an augmented Lagrangian function:

$$L_\mu(x, \lambda) = \|x\|_1 + (\lambda, b - Ax) + \frac{\mu}{2} \|b - Ax\|_2^2 \quad (3.35)$$

⁹Software package for SpaRSA algorithm can be accessed in [129].

¹⁰Software package for FISTA algorithm can be accessed in [129].

¹¹Software package for ALM algorithm can be accessed in [129].

with $\mu > 0$ used as a penalty parameter and λ given as the Lagrangian multiplier vector. By increasing the penalty parameter μ the function can be written as the norm of the residual, as in [23]. Therefore, the optimal solution \hat{x} can be expressed as:

$$\hat{x} = \arg \min_x L_\mu(x, \hat{\lambda}). \quad (3.36)$$

For an optimal solution to be reached efficiently, the chosen $\hat{\lambda}$ must closely approximate λ . Otherwise the iterative process can be exhaustive. Therefore an approach, as discussed in [102], is adopted to compute an approximate estimate for both $\hat{\lambda}$ and \hat{x} for use in minimizing Eq. (3.35) rapidly. This process is expressed as:

$$x_{k+1} = \arg \min_x L_{\mu_k}(x, \lambda_k) \quad (3.37)$$

$$\lambda_{k+1} = \lambda_k + \mu_k(b - Ax_{k+1}) \quad \text{where } \lambda_{k+1} \leftarrow \hat{\lambda}. \quad (3.38)$$

It is important to note that this only becomes computationally feasible if the above iterative process is less expensive iteratively than the minimization tasks of Eq. (3.35).

The algorithm known as YALL1,¹² described in [102], is one of the seminal works that applies ALM methods for use in CS recovery; and has shown success over predecessor algorithms such as the ℓ_1 -LS.

3.4.2.6 Summary of CS Convex Optimization Algorithms

In summary, the ℓ_1 -homotopy algorithm provide the best performance for K -sparse input signal when minimal CS measurements are available. However, when more CS measurements are taken the FPC algorithm, namely FISTA, provide improved recovery performance for computational time than ℓ_1 -homotopy. Therefore, depending on the amount of CS measurements acquired, either of the two convex optimization algorithms can produce optimized computational time. Work done in [22] support the previous statement—wherein several above-mentioned algorithms (ℓ_1 -LS, ℓ_1 -Homotopy, SpaRSA, FISTA, ALM) were compared for computational recovery time required for Fourier based CS measurements (see Table 3.3).

3.4.3 Greedy Algorithms

Greedy algorithms takes an entirely different approach to the problem of sparse recovery via random CS measurements, by solving the non-convex program, expressed as:

$$\min_{\zeta} \{|\zeta| : y = \sum_{i \in \zeta} \phi_i x_i\}, \quad (3.39)$$

¹²Software package for YALL1 algorithm can be accessed in [129].

Table 3.3 Average run time for recovery for different ℓ_1 -fast algorithms. Courtesy of [189]

Corruption	0 %	20 %	40 %	60 %	80 %
L1-LS	19.48	18.44	17.47	16.99	14.37
Homotopy	0.33	2.01	4.99	12.26	20.68
SpaRSA	6.64	10.86	16.45	22.66	23.23
FISTA	8.78	8.77	8.77	8.88	8.66
ALM	18.91	18.85	18.91	12.21	11.21

where ζ is given as the subset of indices $i = 1, \dots, N$, and ϕ_i is the i_{th} column of the sensing matrix Φ . Thus, based on Eq. (3.39) the recovery technique applies a sparse approximation to the actual signal, which is solved by greedily selecting columns from Φ and forming a better fit approximation iteratively [150].

As discussed earlier in this chapter, for a recovery algorithm to be used in CS certain objectives need to be met namely. speed, robustness, performance guarantee, and minimal measurements. Greedy algorithms, with the aid of a user defined estimate for sparsity, significantly increase the recovery speed compared to ℓ_1 -minimization algorithms at the cost of performance guarantee. Here the estimated output signal approximates the input signal with less accuracy than its ℓ_1 -minimization algorithms. However, greedy algorithms are still robust with regards to noisy measurements, and require similar number of measurements.

In following section we detail the computational requirements, constraints, speed and guarantee on performance of several Greedy algorithms. Thereafter we discuss the constrains of applying Greedy algorithms for DOA estimation and comment on the best algorithm to be used. Lastly, we compare Greedy algorithms with convex optimization algorithms for use in our application which is CS DOA estimation.

3.4.3.1 Matching Pursuit [103]

Matching pursuit (MP) algorithm, first shown as a feasible solution to the sparsity approximation problem in [103], is arguably the foundation on which most greedy algorithms are based (in the field of CS) [105]. MP uses a given sampling matrix $\Phi \in \mathbb{R}^{M \times N}$ (otherwise referred to as a dictionary or basis) to construct a coefficient index λ_k and residual $r \in \mathbb{R}^M$, where r is an iterative portion of the approximated measurement, and λ_k selected from the basis [150].

The algorithm selects a vector, indexed by λ_k , from the basis that has a high correlation with the residual r expressed similar to that in [103] as:

$$\lambda_k = \arg \max_{\lambda} \frac{\langle r_k, \phi_{\lambda} \rangle \phi_{\lambda}}{\|\phi_{\lambda}\|^2}. \quad (3.40)$$

For each iteration of the algorithm, the following update for the approximation is given.

$$r_k = r_{k-1} - \frac{\langle r_k, \phi_\lambda \rangle \phi_\lambda}{\|\phi_\lambda\|^2} \quad (3.41)$$

$$\hat{x}_{\lambda_k} = \hat{x}_{\lambda_{k-1}} + \langle r_k, \phi_\lambda \rangle \phi_\lambda \quad (3.42)$$

The update is repeated until a threshold is met, dependent on the norm r being sufficiently smaller than a specified quantity (i.e. $\|r\|_2 < \varepsilon$). The MP algorithm is provided in pseudo-code below in Algorithm 6. We refer the reader to [103] for further implementation details.

Algorithm 6 Matching Pursuit Algorithm. Courtesy of [103] & [150]

Require: CS matrix Φ , measurement y , stopping criteria ε

Ensure: Signal estimate \hat{x}

Initialize : $\hat{x}_0 = 0, r = y, i = 0$

while alting criterion false **do**

1. $i \leftarrow i + 1$
2. $b \leftarrow \Phi^T r$ {form residual signal estimate}
3. $\hat{x}_i \leftarrow \hat{x}_i - 1 + T(1)$ {update largest magnitude coefficient}
4. $r \leftarrow r - \Phi \hat{x}_i$ {update measurement residual}

end while

return $\hat{x} \leftarrow \hat{x}_i$

Based on the insight of [105] the MP algorithm cannot provide any guarantee on recovery error for the estimate, and the requirement on iterations needed can become computationally expensive. The complexity time of MP, given as $O(MNT)$ and T denotes the number of MP iterations. Nonetheless, the approach of MP, given a high sparsity signal, does provide favourable recovery time and can provide accurate approximations for the signal x .

3.4.3.2 OMP [135]

Orthogonal Matching Pursuit (OMP) is an improvement on MP, due to the computational linear relationship on iterations T , that in special instances, has the potential to grow excessively large. The proof of implementation using CS measurements and sparse recovery was shown in [171] and founded on work in [135].

The novelty of the approach taken by OMP depends on modifying the residual r in such a way as to remove unwanted portions of the residual to produce an improved replica, at every iteration [171]. The residual modification is done by projecting r onto a orthogonal subspace, based on the span of the sensing matrix Φ . The process can be expressed according to the following sets of operations (based on [135]),

$$x_k = \arg \min_x ||y - \Phi_{\Omega} x||_2 \quad (3.43)$$

$$\hat{\beta}_t = \Phi_{\Omega} x_t \quad (3.44)$$

$$r_t = y - \hat{\beta}_t. \quad (3.45)$$

The steps for r are repeated until the process converges. The pseudo-code steps are shown in Algorithm 7.

In [171] it was shown that, convergence based on this approach for sparse recovery, takes the form of $O(MNK)$ for computational complexity time. Consequently, it proves that OMP is faster than MP and independent of the iteration. However, guarantees on recovery are weaker than most convex optimization techniques, and the robustness against noise is not clear. Moreover, the impact of large or small noise additions can result in ambiguous recovery. Yet, if the sparsity K is small then robustness can be insured.

3.4.3.3 CoSaMP

The adaptation of matching pursuit algorithms for CS based recovery (i.e. OMP, MP etc.) forms a crucial base on which compressive sampling matching pursuit (CoSaMP) is built, especially the precursory work based on regularized-OMP [124]. Interestingly, the approach of CoSaMP operates on an assumption that the RIP of a given sensing matrix Φ of every subset K columns are roughly orthonormal [150]. This assumption results in a strong convergence with the added benefit of adding and removing unwanted indices of the atoms chosen from the sensing basis. See Algorithm 8 for further detail on implementation, represented by means of pseudo-code. Currently, CoSaMP is arguably one of the fastest greedy algorithms for sparse signal recovery using CS measurements [150]. It has been shown to require, under specific sparsity conditions, a time complexity of $O(MN)$ for which it converges independent of the sparsity level of the input signal. However, a priori knowledge of the sparsity or at least a high probability of sparsity, denoted as K , of the signal is required. Otherwise, convergence and recovery guarantees are increasingly ambiguous.

3.4.4 Summary of CS Recovery Algorithms

Having considered both classes of CS algorithms used for 1-dimensional signal recovery, for the ideal case where sparsity levels can be accurately approximated before signal acquisition, greedy algorithms out perform convex optimization algorithms in terms of recovery time and computational load.

If a scenario exists where the sparsity of a signal is known for a desired sensing basis, CoSaMP would be preferred over other greedy algorithms as it requires the lowest complexity $O(MN)$ and is complete with the guarantee for recovery.

Algorithm 7 Orthogonal Matching Pursuit Algorithm. Courtesy of [135] & [171]

Require: CS matrix Φ , measurement y , the sparsity level m of the ideal signal

Ensure: Signal estimate \hat{s} in \mathbb{R}^d , a set $A_m \in \mathbb{R}^{m \times d}$, residual $r_m = v - a_m$

Initialize : $r_0 = v$, $A = \emptyset$, $t = 1$

repeat

1. Find index λ_t that solves

$$\lambda_k \leftarrow \arg \max_{j=1, \dots, d} |\langle r_{t-1}, \varphi_j \rangle|$$

If maximum occurs, break.

2. Augment the index set and the matrix of chosen atoms:

$$A_t = A_{t-1} \cup \{\lambda_t\}$$

$$\Phi_t = [\Phi_{t-1}, \varphi_j]$$

3. Solve least square problem to obtain new signal estimate

$$x_t \leftarrow \arg \min_x \|v - \Phi_t x\|_2$$

4. $a_t \leftarrow \Phi_t x_t$, $r \leftarrow v - a_t$ {update measurement residual}

5. $t \leftarrow t + 1$

until $t \geq m$

return $\hat{s} \leftarrow x_t^j$

If a sparse input signal is considered with unknown sparsity, convex optimization are able to provide sufficient guarantees for accurate recovery,

Algorithm 8 Compressive Sampling Matching Pursuit Algorithm. Courtesy of [123].

Require: CS matrix Φ , measurement u , the sparsity level s of the ideal signal

Ensure: Signal estimate \hat{s} of the target signal

Initialize : $a_0 \leftarrow 0$ { Trivial initial approximation}

$v \leftarrow u$ {Current samples = input samples }

$k \leftarrow 0$

repeat

1. $k \leftarrow k + 1$
2. $y \leftarrow \Phi^T v$ { Form signal proxy }
3. $\Omega \leftarrow \text{supp}(y_{2s})$ {Identify large components}
4. $T \leftarrow \Omega \cup \text{supp}(a_{k-1})$ {Merge supports}
5. $b|_T \leftarrow \Omega_T^\dagger u$ {Signal estimation by least-squares}
6. $b|_{T^c} \leftarrow 0$
7. $a_k \leftarrow b_s$ {Prune to obtain next approximation}
8. $v \leftarrow u - \Phi a_k$ {Update current samples}

until Halting criterion *true*

return $\hat{s} \leftarrow x_t^j$

whereas greedy algorithms cannot. Thus, for cases where input signal sparsity is unknown, convex optimization algorithms are preferred, namely FISTA and

ℓ_1 -homotopy (see Sect. 3.4.2.6). It is, however, important to mention that convex optimization algorithms have a higher requirement on memory, computation, and time complexity than greedy algorithms. Therefore, real-time application of convex optimization algorithms are preferably processed off-line.

Part LXII

**Simulations of Compressive Sensing Used
for Electronic Support Applications**

Chapter 4

Design of CS Based DOA Estimation for Modulated Shift-Keying Signal

4.1 Overview

In light of the data acquisition and recovery benefits that CS provides, as discussed in the previous chapters, it remains a non-trivial task to adopt CS techniques in the signal processing chain—from sampling to recovery—for DOA estimation. In order to match the conventional DOA estimation performance there are several problems that need to be considered when applying CS techniques. These problems include phase recovery, choice of the sensing matrix, and choice of the recovery algorithm. These problems are discussed below.

1. Phase recovery: From an RF signal processing perspective phase recovery seems trivial, as one simply calculates the arctan of the complex components from the DFT of an input time domain signal is expressed as

$$\angle X_k = \tan^{-1} \left(\frac{Im(X_k)}{Re(X_k)} \right)$$

where $X_k = \sum_{n=0}^{N-1} [x_n e^{-2\pi j (kn/N)}]$ is the complex representation of the Fourier transform of x_n .

This results in a phase spectrum which, in general, is non-sparse when multi-band signals are considered, with the exception of highly sparse frequency input signals (see Fig. 4.1). Nevertheless, the correlation between magnitude and phase coefficients remains non-trivial to determine under most circumstances for CS phase recovery.¹ In other words, the allocation of phase coefficients to their

¹To the best of our knowledge, based on the open literature, minimal avenues in terms of CS based phase recovery have been investigated, with the exception of phase retrieval, which selectively uses CS methods as part of recovering phase information given the Fourier magnitude data of a signal [57]. Phase retrieval, traditionally, has a long-standing application in image processing problems, particularly optics and x-ray crystallography [130]. Regardless of the success of CS as a

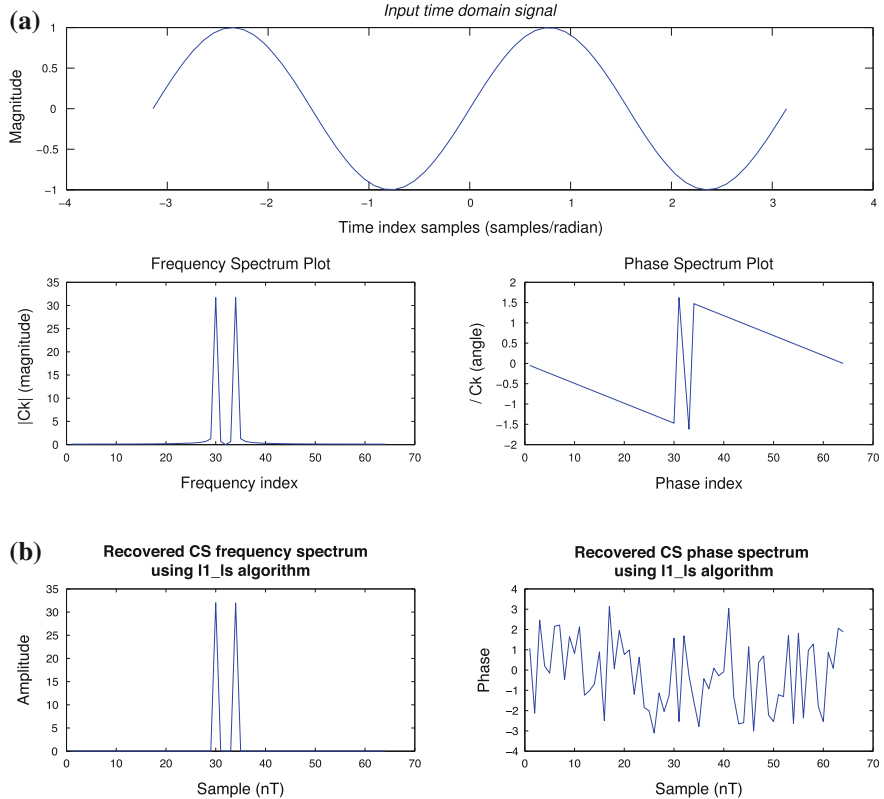


Fig. 4.1 A simple illustration of **a** the frequency and phase spectrum of a trivial input signal of a frequency sparsity $K = 1$ determined using conventional methods. In **b** is shown the CS recovered magnitude and phase spectrum using the l_1 _ls algorithm. Observe that the phase spectrum is non-sparse and ambiguous for the case of CS phase recovery

corresponding frequency magnitude coefficients is difficult to determine, unless the signal has frequency sparsity of $k = 1$.

Although CS recovery is well established for frequency-magnitude recovery of sparse DFT based signals, due to the non sparse nature of the signal phase, most CS recovered estimates of the phase spectrum are either poor or highly ambiguous (see Fig. 4.1). Thus, an entirely different approach must be considered to enable CS phase recovery by taking the signal structure into account, as DOA estimation techniques require accurate phase information of the input signal.

(Footnote 1 continued)

candidate for phase retrieval [57, 104, 120, 130], and the similarities it shares with CS phase recovery (due to only using Fourier magnitude data), its use in phase recovery is not trivial where sparsity is conditional. This leaves the problem of phase recovery, by means of CS techniques as an open problem according to the current literature.

2. Sensing matrix—For conventional RF communication signal processing the input signal will be transformed by a DFT to the Fourier domain for further processing. CS techniques employ the same technique by using a DFT sensing matrix during the recovery process for similar RF communication signal. However, in order to match conventional processing performance for large input signal requires a large DFT sensing matrix for recovery which is computationally expensive and therefore not viable in achieving similar performance (see Sect. 3.4). Thus, an alternative CS sensing matrix and/or method must be found or developed to match conventional processing performance.
3. Recovery algorithm usage—As mentioned in Sect. 3.4.4, the only viable algorithms to use for CS recovery which match conventional DFT processing time complexity are greedy algorithms. However, greedy algorithms require a-priori information of the signal sparsity in some basis (i.e. sensing matrix) to guarantee non-ambiguous recovery, which limits its application for communication signal DOA estimation. The constraint on prior knowledge of sparsity for a communication signal can be addressed by limiting DOA estimation to scenarios for narrow band signal and using a sensing basis where the input signal is highly sparse, in the order of $K = 1$.

To address all three problems mentioned above, we propose using a generated shift keying modulated sensing matrix (for amplitude—ASK, frequency—FSK and phase—PSK) as the sensing matrix instead of the conventional DFT sensing matrix used in similar RF communication CS recovery techniques.

By using a sensing matrix that consists of digitally modulated linear combinations of finite length input vectors results in an orthonormal basis which complies to the CS sensing matrix criteria (see Sect. 3.2.1); with sparsity of an input signal known a-priori allowing the use of greedy algorithms, and recovery where sparsity is $K = 1$ allowing unambiguous recovery of phase.

Shift-keying modulated signals form the foundation for most digitally modulated communication signal and has the potential to be scaled to more complex digital modulated signal applications if our proposed method is successful. Thus, for simulation purposes we only consider the case of 2-ary digital modulated signal. Higher order digitally modulated signal is deemed out of scope for simulation purposes within this work.

To summarize, our objectives as it relates to the problems outlined earlier include:

- Producing accurate phase recovered estimates of shift keying modulated signal for DOA estimation;
- Frequency specific, narrowband application for digitally modulated communication signal in order to produce highly sparse input vectors for CS recovery;
- Optimize CS recovery by using greedy algorithms to match conventional processing time complexity; and
- Reduce memory and computational requirements for DOA estimation whilst matching processing performance with conventional DOA estimation techniques.

In the section to follow we detail the construction of the shift keying modulation specific CS sensing matrices for our proposed method. We then detail the required

system parameters for use in CS based DOA estimation. Thereafter, we discuss our simulation based implementation using an altered conventional DOA acquisition and processing architecture.

4.1.1 Shift-Keying CS Sensing Matrix Development

To simulate a 2-ary shift keying modulated signal in discrete form, a finite length input bit sequence is applied to a specific shift-keying expression—either frequency, amplitude, or phase—to produce a discrete output vector. If this process is followed iteratively spanning all m linear combinations of the binary bit stream $a[n]$, one can generate a modulation specific matrix.

The goal is to generate a square subset matrix, which replaces the DFT matrix typically used for frequency CS recovery (see Sect. 9.5.3). Thus, we adopt the same CS criteria for the shift-keying modulation specific subset matrices to ensure guarantees for CS recovery as well as phase recovery capability. These criteria are listed below.

- Matrix must be square— $M \times M$;
- Composed of complex sinusoidal elements; and
- The subset must be orthonormal.

We then denote this matrix as $\psi_{2\text{-ary}}[m, n]$, with $m = n$ where the generation of $\psi_{2\text{-ary}}[m, n]$ is done by calculating each successive row, based on the complex forms of Eqs. 4.2, 4.5 and 4.9, for all binary combinations spanning $0 \rightarrow 2^{N_b} - 1$ and each row of the matrix corresponding to a specific binary sequence. In other words, $\Psi_{2\text{-ary}}$ can be defined as a linear independent orthonormal subset sampled from complex sinusoids, determined by the form of shift keying modulation scheme (i.e. 2ASK, 2FSK, 2PSK) and spanning the binary combinations of n_b . Thus, we have the following vector and sensing matrix notation for each shift-keying type.

2-Amplitude-Shift Keying (2ASK)

The discrete vector notation for 2ASK typically involves assigning two amplitude values to a carrier sinusoidal waveform at a fixed frequency f_c . In practice the amplitude values are represented as voltages v and span a limited range β , where each voltage value can be denoted by

$$v_j = \frac{\beta}{L-1} j - \beta \quad \text{with } j = 0, 1, \dots, L-1. \quad (4.1)$$

For our case the steps considered is limited to 2. For the discrete case, we have the following expression for generating a 2ASK signal.

$$S_{ask}[n] = (1 + v_i[n]) \left(\frac{A}{2} \cos \left[\frac{2\pi k}{N} n \right] \right) \quad (4.2)$$

where

$S_{\text{ask}}[n]$ = amplitude-shift keying output signal

$v_i[n]$ = amplitude related to binary input stream $a[n]$, with

$v_i[n]$ taking on values of $(-1; 1)$

$\frac{A}{2}$ = carrier frequency sinusoidal amplitude

$\frac{2\pi k_c}{N}$ = carrier angular frequency

$k_c = f_c N$

To generate an ASK output signal given an input bit stream $a[i]$ of length N_b , where i represents the bit at a given sample time T_b , one can express the output in terms of the input bit stream sampling rate. In other words, we want to obtain samples of the bit stream $a[i]$ for each given sample point of the digitally generated 2ASK signal, also known as upsampling [131]. This results in a re-sampled bit stream written in discrete form as

$$a[n] = a[i/L] = a(iT_b/L), \quad i = 0, L, 2L, \dots, \quad (4.3)$$

with $L = N/N_b$, which represents the samples per bit of the 2ASK output signal reducing the period for sampling, denoted above as T_b . As a result, the number of samples per bit are restricted to an integer multiple of the bit stream length, expressed as $L = \frac{2^{N_b}}{N_b}$ (refer Fig. 4.2).

The matrix expansion of Eq. 4.2 for all linear combinations of 2ASK modulated signal given a finite length bit sequence results in the sensing matrix, denoted herein as $\Psi_{\text{2-ASK}}[m, n]$.

Given an input binary selection matrix $A[m, n]$ where $m = n$ and the rows of A corresponds to the bit stream $a[n]$ for a given binary range $(2^0)_{\text{base}2} - (2^{(N_b-1)})_{\text{base}2}$, we can describe the 2ASK subset matrix as follows.

$$\Psi_{\text{2ASK}}[m, n] = (1 + A[m, n])(\beta e^{-j(2\pi k_c n / N)}) \quad (4.4)$$

where $\{0 \leq m \leq 2^{N_b} \text{ } m \in K; 0 \leq n \leq 2^{N_b} \text{ } n \in K\}$

and β is the amplitude of the carrier frequency

$k_c = f_c N$ - where f_c denotes the carrier frequency

2-Frequency Shift Keying (2FSK)

The discrete vector notation for 2FSK involves transmission of binary information (i.e. a bit stream) in terms of discrete sinusoidal frequencies, which can be represented as:

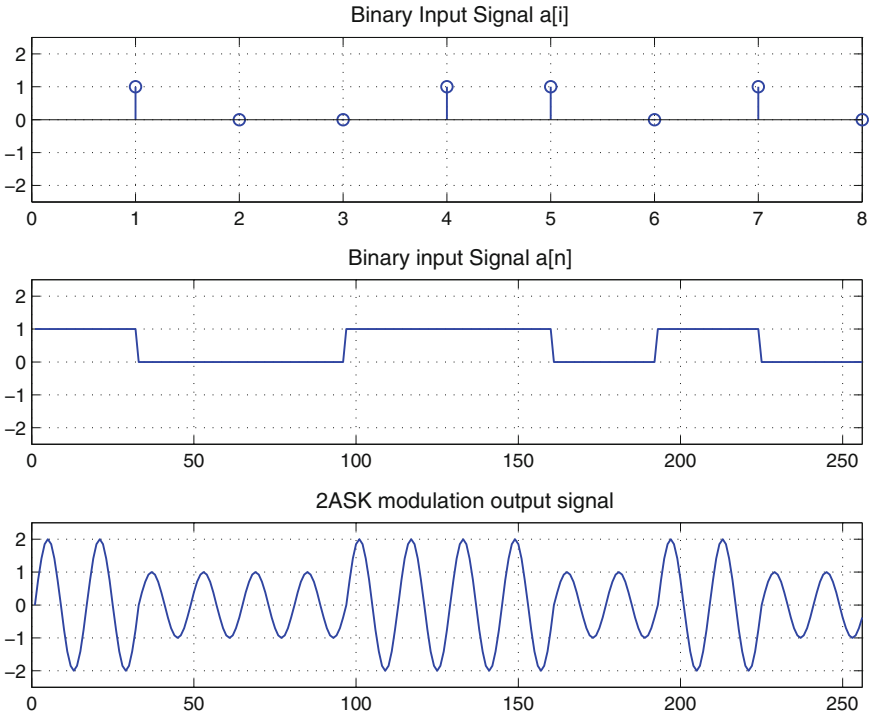


Fig. 4.2 A simple illustration for generating a 2ASK signal given a binary input stream. The input bit stream $a[i]$ is of length $N_b = 10$ whereas $S_{ASK}[n]$ is of length 2^{N_b}

$$S_{FSK}[n] = A \cos[2\pi(k_c + k_0)n/N], \quad 0 \leq n \leq N - 1, \quad \text{for } 1 \quad (4.5)$$

$$S_{FSK}[n] = -A \cos[2\pi(k_c + k_1)n/N], \quad 0 \leq n \leq N - 1, \quad \text{for } 0 \quad (4.6)$$

$$k_c = f_c N. \quad (4.7)$$

A is the amplitude expressed in terms of $A = \sqrt{\frac{2E_b}{T_b}}$ with E_b defined as the energy per bit² and f_c denotes the carrier frequency.

The frequencies chosen to represent the binary information (i.e. k_0 and k_1) are integer multiples of the sampling frequency $1/N$ (i.e. $k_0 = q/N$ and $k_1 = 2q/N$ with $q \in \mathbb{Z}$). This ensures the output 2FSK signal is synchronized in phase and periodic.

An example of this approach is shown in Fig. 4.3. For further reference to generation of higher order FSK signals, we refer the reader to [131].

²It must be noted that for ED application purpose the signal amplitude is less relevant, as the final joint matrix will be normalized for CS recovery. The amplitude is more relevant for specification relating to Bit Error Rate.

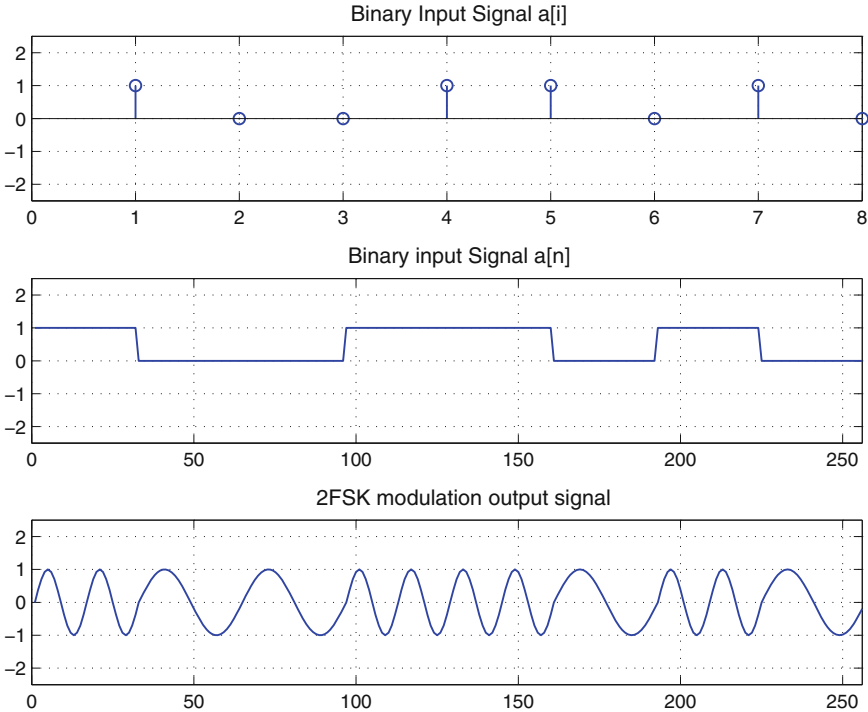


Fig. 4.3 A simple illustration for generating a 2FSK signal given a binary input stream. The input bit stream $a[i]$ is of length $N_b = 10$ whereas $S_{FSK}[n]$ is of length 2^{N_b} . (Simulated by the authors.)

The matrix expansion of Eq. 4.5 for all linear combinations of 2FSK modulated signal given a finite length bit sequence, results in the sensing matrix denoted herein as $\Psi_{2-FSK}[m, n]$.

We assume the same input binary selection matrix as for $\Psi_{2-ASK}[m, n]$ which results in a 2FSK subset matrix and expressed as follows.

$$\Psi_{2FSK}[m, n] = (2 - (A[m, n] - 1))(\beta e^{-j(2\pi(k_c + k_0)n/N)}) + ((A[m, n] + 1) - 1)(\beta e^{-j(2\pi(k_c + k_1)n/N)}) \quad (4.8)$$

where $\{0 \leq m \leq 2^{N_b} \text{ } m \in K; 0 \leq n \leq 2^{N_b} \text{ } n \in K\}$

and β is the amplitude of the carrier frequency

$k_c = f_c N$ - where f_c denotes the carrier frequency

2-Phase Shift Keying (2PSK)

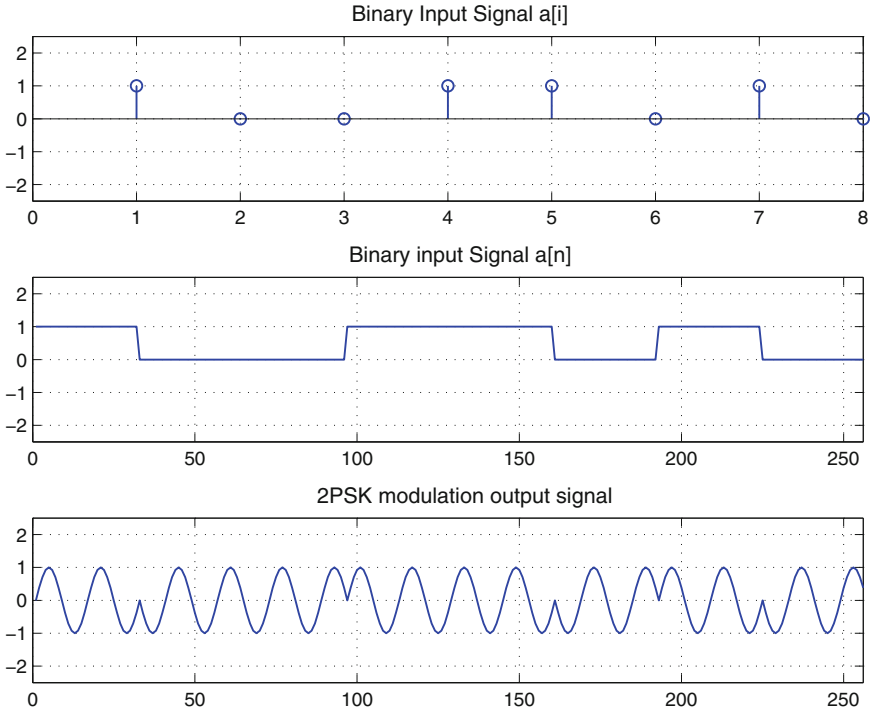


Fig. 4.4 A simple illustration for generating a 2PSK signal given a binary input stream. The input bit stream $a[i]$ is of length $N_b = 10$ whereas $S_{PSK}[n]$ is of length 2^{N_b} . (Simulated by the authors.)

The discrete vector notation for 2PSK involves transmission of binary information using two phase states, where we use 0 and π respectively,³ which can be represented as follows.

$$S_{2PSK}[n] = A \cos\left(\frac{2\pi k_c n}{N} + q\pi\right), \quad q = 0, 1 \quad (4.9)$$

$$k_c = f_c N, \quad (4.10)$$

where q corresponds to the bit stream $a[n]$ of length N_b . For the carrier frequency we denote $f_c = m/T$, $m \in \mathbb{Z}$ which is an integer multiple of the sampling time. This ensures the output signal is synchronized and is void of phase discontinuities other than $0 - \pi$.

An example of this approach is shown in Fig. 4.4. For further reference on the generation of higher order PSK signals, we refer the reader to [131].

³Phase modulation states can be chosen as $-\pi/2$ and $\pi/2$. The choice of phase states can be interchanged.

The matrix expansion of Eq. 4.9 for all linear combinations of 2PSK modulated signal given a finite length bit sequence, results in the sensing matrix denoted herein as $\Psi_{2-PSK}[m, n]$.

Given an input binary selection matrix $A[m, n]$ where $m = n$ and the rows of A corresponds to the bit stream $a[n]$ for a given binary range $(2^0)_{base2} - (2^{(N_b-1)})_{base2}$, we can describe the 2PSK subset matrix as follows.

$$\Psi_{2PSK}[m, n] = (2 - (A[m, n] + 1))(\beta e^{-j(2\pi k_c n/N)}) + ((A[m, n] + 1) - 1)(\beta e^{-j(2\pi(k_c + k_1)n/N)}), \quad (4.11)$$

where $\{0 \leq m \leq 2^{N_b} \text{ } m \in K; 0 \leq n \leq 2^{N_b} \text{ } n \in K\}$

and β is the amplitude of the carrier frequency

$k_c = f_c N$ - where f_c denotes the carrier frequency

When tested against the criteria for CS recovery—as outlined in Sect. 3.2.1—requiring a sensing matrix to be orthonormal, we observe that matrix Ψ_{2ASK} does not comply with the CS recovery criteria. Specifically, the columns of Ψ_{2ASK} are not linearly independent from one another creating a non-orthonormal basis. Therefore, we cannot pursuit the CS-DOA estimation for 2ASK digital modulation scheme, further in this work. However, Ψ_{2FSK} and Ψ_{2PSK} conforms to the CS recovery criteria and is used for DOA estimation simulations.

4.1.2 CS Recovery Method

The notation regarding CS acquisition and recovery for the general case, given a shift-keying modulated signal as the input signal X , can be expressed as the sampled CS signal

$$Y = \Phi X, \quad (4.12)$$

where Φ represents the randomized sampling matrix in the form as the notational expansion of the sampling method described in Sect. 3.3. Furthermore, we can represent the shift-keying input vector X in terms of Ψ_{2ary} and the coefficient output vector with sparsity $K = 1$, denoted as s , which corresponds to a single binary vector from a column of Ψ_{2ary} ; expressed as,

$$X = \Psi_{2ary} \times s \quad (4.13)$$

$$\text{then } Y = \Phi \Psi_{2ary} s \quad \text{letting } \Phi \Psi = A \quad (4.14)$$

$$\text{gives } Y = A \times s. \quad (4.15)$$

The CS recovery mathematical program which must then be solved to determine the coefficients of the shift-keying input vector is

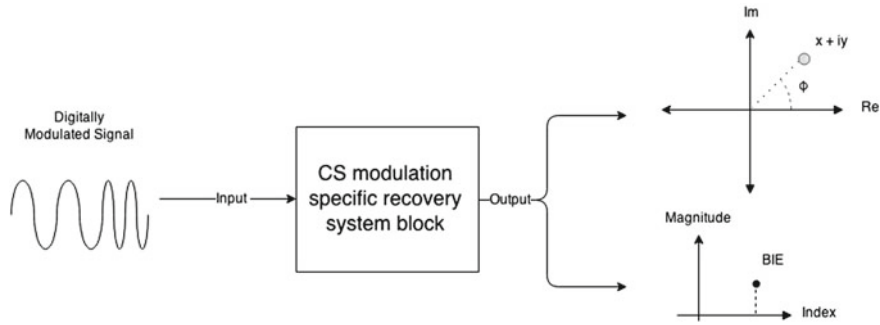


Fig. 4.5 A simplified illustration of the CS modulation specific recovery method utilized for our approach of CS based DOA and phase recovery

$$\hat{s} = \operatorname{argmin} \|v\|_1 \text{ s.t. } Y = Av. \quad (4.16)$$

Here v is the update solving vector being minimized to represent the final estimated vector \hat{s} .

Solving the mathematical program in Eq. 4.16 results in a CS recovered vector output \hat{s} with sparsity $K = 1$ which contains the complex valued phase, magnitude and binary index estimates of Ψ_{2ary} . The binary index corresponds to the row index of the sensing matrix Ψ_{2ary} which we denote as the Binary Index Estimate (BIE).

To illustrate this approach, let us assume a bit stream of length 3, then we have $N_b = 3$ and the sample length $N = 2^3 = 8$. We then choose the bit stream $a[i] = [1 \ 1 \ 0]$, and based on the CS recovery described above we should receive a vector output for $\hat{s}[n] = [0 \ 0 \ 0 \ 0 \ a + ib \ 0 \ 0 \ 0]$ where the non-zero element of \hat{s} constitutes the BIE, and the complex value element corresponding to magnitude and phase components of the sampled signal. A simplified diagram of this method is illustrated in Fig. 4.5.

The BIE serves as an elementary means of demodulation. Knowing the input vector sparsity a-priori allows optimal use of greedy algorithms for CS recovery simulations. However, in order for successful CS recovery to occur using either Ψ_{2FSK} or Ψ_{2PSK} , requires the carrier frequency and modulation type to be identified or known in advance so as to select and/or generate the corresponding shift-keying sensing matrix. This places a limitation on application and scalability.

4.1.3 Implementing CS DOA Estimation

Our proposal to reduce cost on memory and computation, involves replacing the conventional receiver-comparator architecture shown in Fig. 4.6 with that of a sub-Nyquist CS acquisition receiver block (using the simulated CS acquisition RDPI [190]) coupled with the CS recovery block, conditioned on the modulation specific

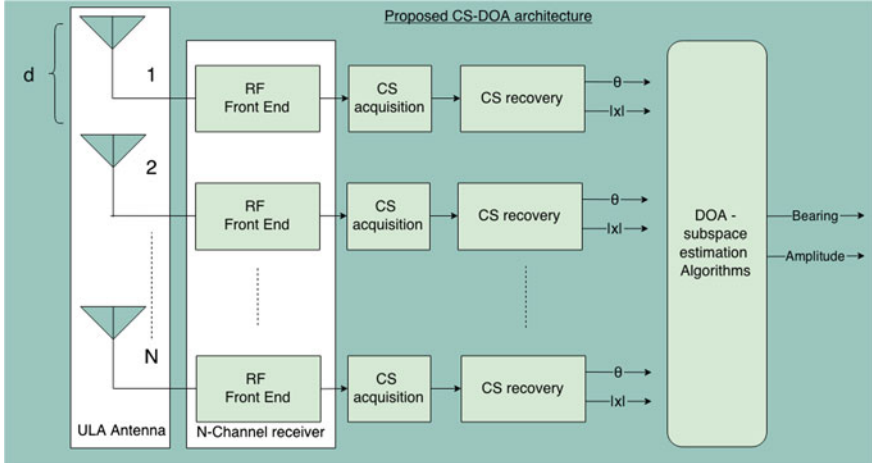


Fig. 4.6 A simplified block diagram of our approach in applying CS methods for modulation specific DOA estimation. It should be noted that $d \leq \lambda/2$ and input signals are still down converted to baseband (i.e. IF) as for a conventional digital receiver. (Illustration compiled by the authors.)

sensing matrix. This results in CS resolved magnitude and phase estimates of respective signal of each channel. In conjunction with the steering vector this provides the DOA estimates via sub-space algorithms.

The design of our proposed CS based DOA simulation is two-fold: first designing accurate CS phase estimates for shift-keying modulated received signals; and second investigating performance of sub-space DOA estimation algorithms given recovered CS data. As shown in the previous section, phase recovery by CS means for a RF signal is non-trivial and conventional CS recovery fails to produce non-ambiguous results. Moreover, the DOA estimation algorithms that are able to integrate to the system architecture proposed in Fig. 4.6 are limited.

We therefore adopt an approach which has the following assumptions to enable modulation specific CS-DOA estimation:

1. Carrier frequency can be identified or is known in advance.
2. The signal is narrowband digitally modulated shift keyed.
3. DOA estimates are frequency specific.
4. DOA is dependant on digital modulation type.

Ultimately, our method must use signal data via an N -channel antenna array receiver through a DOA estimator algorithm which outputs a bearing estimation for an incoming shift-keyed modulating signal. We assume a system architecture⁴ as shown in Fig. 4.6 and simulate the CS recovered scalar quantities per channel for phase, magnitude, and BIE which are processed via sub-space DOA algorithms for DOA estimation.

⁴The system blocks are simulated-only in MATLAB® and have not been taken further for actual implementation; this is deemed out of scope for this work.

Our implementation method follows on from the results in the previous section, reliant on retrieving accurate phase estimates.⁵ On this basis our CS-DOA proceeds, where the following steps describe the CS-DOA process corresponding to the system blocks denoted in Fig. 4.6.

4.1.3.1 CS-DOA Steps

1. Input signal incident on a uniform linear array (ULA) antenna which is down converted to base band (i.e. IF signal) for all channels via the N-channel receiver.
2. The IF signal is then randomly sampled by means of a simulated RDPI sampler.
3. The CS sampled signal is recovered via both greedy algorithms, viz. OMP and CoSaMP. These algorithms are used for performance comparison purposes, their time complexity being equal when an input signal has sparsity of 1.
4. The CS resolved signal output i.e. BIE, magnitude and phase estimates, are recorded.
5. The CS phase and magnitude estimates become the input parameters for the sub-space DOA estimation MUSIC algorithms to calculate the DOA estimates.

For the sub-space DOA estimation algorithm, namely MUSIC, we assume a signal model with M signals incident on a ULA, given Gaussian noise associated with the signals, which can be expressed in matrix form as:

$$\mathbf{x} = \mathbf{S}\mathbf{A} + \mathbf{w} \quad (4.17)$$

$$\mathbf{A} = [\alpha_1, \alpha_2, \dots, \alpha_M]^T \quad (4.18)$$

$$\mathbf{S} = [s(\phi_1), s(\phi_2), \dots, s(\phi_M)], \quad (4.19)$$

where α is the input signals incident on the ULA of length N which results in A as a $N \times M$ matrix. Also, S is the steering vector of size $N \times M$. The goal is for the sub-space algorithms (i.e. MUSIC) to produce orthogonal solutions for the steering vector bearings (refer to Sect. 2.4 for further detail) which become the input signal bearing estimates of the incidence angle.

Our method deviates from conventional estimation scheme, in describing the input signal A in terms of CS recovered phase and magnitude estimates instead of time domain input vectors.

⁵Phase recovery for sub-space DOA estimation is much more critical for accurate bearing estimation as oppose to magnitude estimates, (See Sect. 2.4).

Chapter 5

CS Based Shift-Keying Modulation

5.1 Simulation Outline

Shift-keying specific CS DOA estimation requires accuracy guarantees of CS recovered phase and magnitude estimates before being used as input information for the sub-space DOA estimation algorithms. Otherwise, if accuracy of phase and magnitude estimates cannot be guaranteed, the use of CS sampled and recovered information for DOA estimation will fail. Only when the accuracy guarantees are determined for shift-keying specific CS recovery, can we proceed to utilize CS recovered phase, magnitude, and BIE estimates as scalar inputs to sub-space DOA estimation algorithms.

In this section the performance and accuracy of the modulation specific shift-keying CS recovery method (see Sect. 4.1.2) is investigated by means of simulation to estimate the signal parameters (i.e. phase, and BIE) of a CS sampled modulated signal (i.e. 2FSK and 2PSK) in a narrow bandwidth. The objectives of the investigation are to determine the following:

1. Accuracy of phase recovery;
2. Accuracy of Binary Index Estimate;
3. Estimation performance in high noise environments (i.e. low SNR);
4. Most suitable CS recovery algorithm strategy;
5. Sampling compression ratio requirements for adequate CS recovery; and
6. Computational performance of CS recovery.

The input signal variables considered for simulations are SNR and the compression ratio (CR) of sampling. These variables are varied over a pre-defined range typical for an ES receiver in a low SNR environment.

The performance indicators used for testing simulation outcomes are mean squared error (MSE), Cramer Rao lower bound (CRLB), and probability of detection (PD), which provide a statistical base for CS recovery estimate performance analysis. In addition, we test the time of computation for CS recovery estimates and

derive the number of floating point operations per second (FLOPS) for the respective modulated signals considered.¹

5.1.1 General Simulation Setup

The CS recovery block assumes that the respective basis matrix Ψ_{2FSK} or Ψ_{2PSK} for recovery are generated given the carrier frequency of the input signals. The input signal comes from a bit stream $a[n]$ of length $M = 256$ (derived from the bit length $N = \log_2 M = 8$ equal to a byte.), which can be denoted as a vector k of the sensing basis $\Psi[k, m] + w$ corrupted with Gaussian noise, denoted as $w \sim \mathcal{N}(0, \sigma^2)$.

The bit sequences are considered as input signals with varied noise to represent different SNR conditions. Also, for CS recovery the compression ratio (CR) for signal sampling is varied over a selected range to determine its effect on the performance of recovery. CR is ratio of CS sub-sampled vector length to that of the equivalent Nyquist sampled vector length for the same input signal.

The output for all possible combinations of SNR and CR are measured against performance indicators, namely MSE for phase and magnitude recovery, and probability of detection (PD) for the BIE. In addition, we use the Cramer Rao lower bound (CRLB) as the ideal minimum variance of unbiased estimator (MVUE) to compare with the MSE of our simulations. It can be noted here that the CRLB dictates the lower bound of the best performing estimation achievable given an estimator MSE [136].

5.1.2 Performance Indicators

5.1.2.1 MSE of Phase Estimates

Mean Squared Error (MSE) provides insights into estimation accuracy by measuring the error of the actual signal parameter Y (i.e. phase) and the estimated parameter \hat{Y} . MSE is calculated for each signal input length $a[n]$, with iteration over the subset of variables SNR and CR—their variable range is denoted as i, j respectively. Thus, we can denote the MSE as follows:

$$MSE[i, j] = \frac{1}{N} \sum_{n=1}^N [Y[n] - \hat{Y}[n]]^2. \quad (5.1)$$

It is worthwhile noting that we can write MSE in terms of a variance of the estimator distribution with a bias factor, as follows:

¹All simulations herein are simulated using MATLAB®.

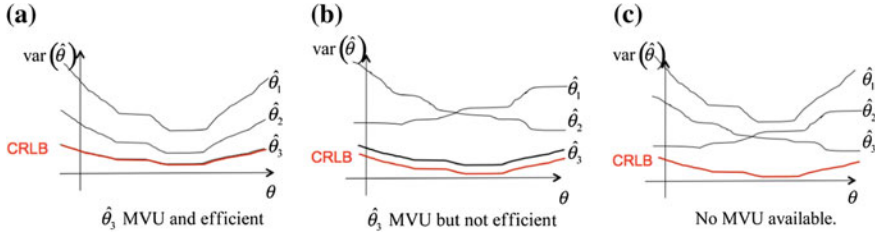


Fig. 5.1 A simplified diagram of the possible cases for various MVU estimators compared to the CRLB, with the estimation value denoted as θ rather than \hat{Y} as described in Eq. 5.2. (Sourced from [82].)

$$MSE(\hat{Y}) = Var(\hat{Y}) + (Bias(\hat{Y}, Y))^2. \quad (5.2)$$

Therefore we can express the MSE of the phase estimates in terms of variance, comparable with the CRLB, where the respective CRLB for each estimate are derived² as follows:

$$\text{Phase : } Var(\hat{Y}) \leq \frac{2}{SNR \times N}. \quad (5.3)$$

N represents the number of samples in the set and σ , the standard deviation of the estimation.

If we assign the estimates for each respective compression ratio as a potential MVUE, mapped over the range for SNRs, this provides a means of comparing the estimation error with the CRLB for the same range, as a statistical bench mark test for the estimation performance [83]. Figure 5.1 shows the various cases for a possible MVUE and more interestingly, which comparison yields the most adequate result for an estimator. Note that the closer the MVU estimate tends toward the CRLB the more efficient it becomes.

5.1.2.2 Probability of Detection (PD) of BIE

Determining the probability of detection (PD) is trivial, in that the condition of detection or correct recovery is measured as a summed boolean statement of the correct corresponding BIE with the actual binary index of the input signal $a[n]$. This can be expressed as

$$PD[i, j] = \sum_{n=1}^N \alpha \text{ where } \begin{cases} \alpha = 1 & \text{if } Y = \hat{Y} \\ \alpha = 0 & \text{if } Y \neq \hat{Y} \end{cases} \quad (5.4)$$

²For the derivation of both CRLBs we refer the reader to [83] wherein the details are provided, complete with worked examples.

5.1.2.3 Computational Performance

The computational performance is measured in terms of FLOPS which in theory, given a computational platform, can be calculated according to the following expression.

$$\text{No. Flops} = \text{Cores} \times \frac{\text{CPU frequency}}{\text{No. Cores}} \times \frac{\text{FLOPS}}{\text{Cycle}} \quad (5.5)$$

FLOPS are a standard measurement of computation in showing how a similar simulation or algorithm will fare, given a different computational platform, say for example an embedded system or DSP core.

However, from experimental knowledge the calculated number of FLOPS are typically much greater than the measured FLOP count during simulation [47]. Therefore we conduct a bench mark test to determine the number of FLOPS during the simulation and measure the time of computation for CS recovery as well,³ which provides another measure for FLOPS and computational performance of CS recovery.

Simulations were conducted on a 4 core, 2.9 GHz Intel® i7 platform.

5.1.3 Simulation Parameters

Figure 5.2 illustrates the typical output for a single iteration of the simulations to follow, where magnitude, phase and BIE estimates (shown in red) are measured against the actual signal parameters (in blue).

The simulation is based on taking a 2FSK signal, with the carrier frequency known a-priori, and varying the phase from $[-\frac{\pi}{2} : \frac{\pi}{2}]$ corresponding to a 180 degree azimuth range of a ULA receiver. The compression ratio is 15 % of the Nyquist sampling rate, the SNR 5 dB, and the input vector length of 256 for this particular iteration of the simulation. Several iterations of this simulation are carried out for 2FSK and 2PSK signal according to the following signal variable parameters.

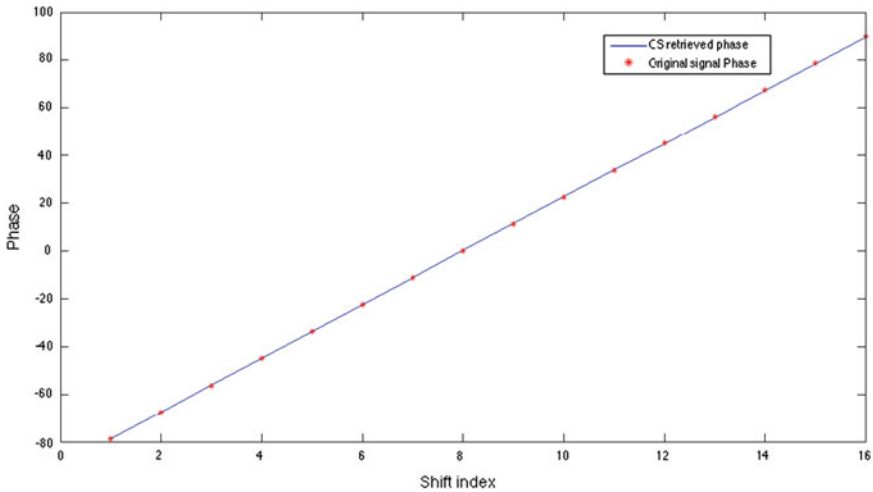
1. SNR [-5 dB : 20 dB]
2. CR of 3–36 %
3. The signal bit length $M = \log_2 N = 8$
4. Bit sequence varied in the range $[0 : 2^8]$

Only OMP and CoSaMP greedy algorithms are considered for CS recovery, due to their computational efficiency properties when the input signal considered has the sparsity of 1.

It should be noted that the phase estimates for Fig. 5.2 correspond to the actual phase values accurately, and the BIE as well. However, the magnitude estimates do not share the same accuracy levels of phase and BIE. Nonetheless, DOA estimation

³The bench mark tests for FLOPS/second are conducted using an open-source software, known as Xbench.

- (a)** Phase recovery plot of the retrieved BIE index with a 256×256 sensing matrix, for FSK modulated signals. The given compression ratio is 15% of the original sampling size, whereas phase shifts are from -90 to 90



- (b)** Magnitude plot of the retrieved BIE index with a 256×256 sensing matrix, for FSK modulated signals. The given compression ratio is 15% of the original sampling size.

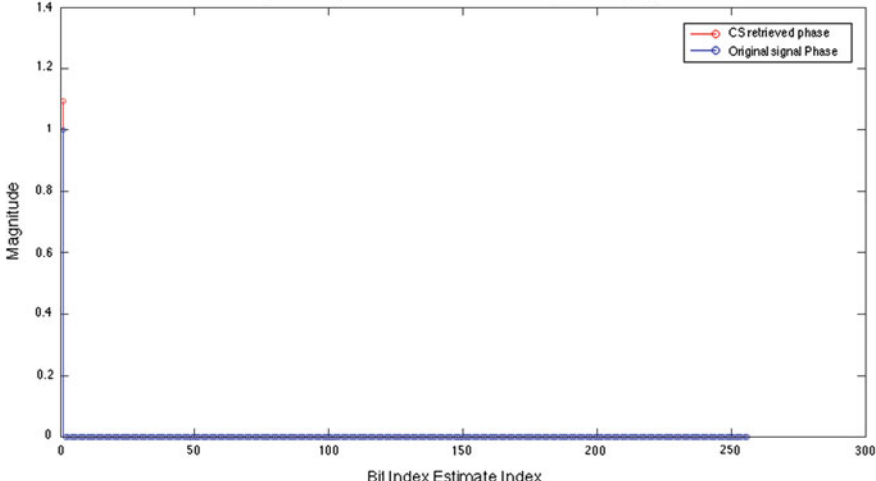


Fig. 5.2 a Illustrates the phase recovery estimates, in red, with the actual phase shown in blue. In b magnitude recovery estimates are shown in red, with the actual magnitude shown in blue. The BIE estimate corresponds to the non-zero element in b with relation to the $\Psi[m, n]$ sensing matrix used for CS recovery. The input signal is a 2FSK vector of length 256 with a binary stream input length 2^8 and modulated to equal a bit sequence equalling $2^8 = 1$

algorithms are not dependent on magnitude information for accurate performance, but require accuracy for phase for optimal performance. Therefore, we focus on phase estimation further in this work.

Once all the various iterations of the simulations are complete for both 2FSK and 2PSK signal, according to the signal variable ranges, the calculated MSEs, PDs, and FLOPs are analysed in line with the performance parameters. Thereafter, the results of the analysis are used to determine the feasibility of using shift keying CS recovered estimates for DOA estimation algorithms, which is covered in the next chapter.

5.2 Simulation 1.1.1—Phase CS Recovery for 2FSK

In this set of simulations CS phase recovery of 2FSK signal inputs were simulated and resultant graphs drawn for the parameters SNR and CR.

Figure 5.3 depicts the detail of estimation MSE and how those figures compare to the corresponding CRLB. Figure 5.4 serves as an aid to illustrate the relationship of estimation error mapped over the variable range, providing an indicative character of the estimates.

From Fig. 5.3a we observe CoSaMP producing MVU estimates for the various CR values that are unbiased but not efficient. In (b) OMP produces improved MVU estimates for the set of CR value that are unbiased and efficient for CR = 23 %, but for lower values the respective MVUs are non efficient. For higher SNR values both OMP and CoSaMP MSE tend towards the CRLB making them efficient regardless of the CR.

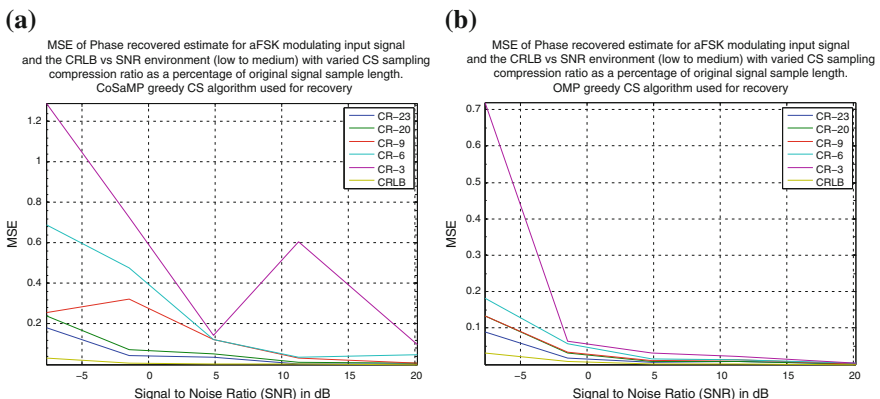


Fig. 5.3 The phase recovery Mean Squared Error (MSE) using greedy algorithms CoSaMP in **a** and OMP in **b**, given an input signal that has type 2-Ary FSK modulation. The CRLB representing the ideal MVUE and serves as the benchmark for recovery estimates. MSE scale of graphs are not similar

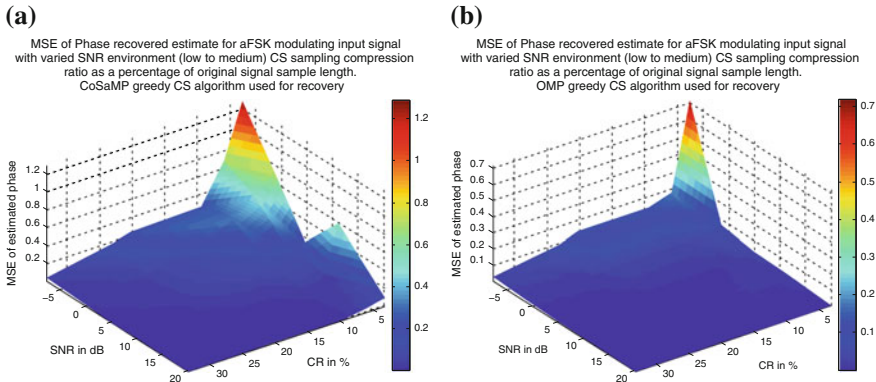


Fig. 5.4 Phase recovery MSE using greedy algorithms CoSaMP in **a** and OMP in **b**, given an input signal that has type 2-Ary FSK modulation. The 3D graph shows the relationship of varying SNR (y-axis) and CR (x-axis) on the accuracy of CS based phase recovery

The OMP algorithm outperforms the CoSaMP algorithm, in terms of MSE. As the scales are not similar for graphs Fig. 5.3a, b, graphical illustrations on first inspection might be misleading. However, notice that for all CR values, with SNR greater than -8 dB, the MSE OMP is lower than CoSaMP.

For phase estimation of 2-Ary FSK using CS recovery, OMP serves as a more efficient unbiased algorithm for DOA estimation. For higher SNR environments both CS recovery methods work equally well.

5.3 Simulation 1.1.2—Phase CS Recovery for 2PSK

In this set of simulations CS phase recovery of 2PSK signal inputs were simulated and resultant graphs drawn for the parameters SNR and CR.

Figure 5.5 depicts the estimation values compared to the corresponding CRLB, whereas Fig. 5.6 serves as an aid in illustrating the relationship of the estimation error mapped over the variable range of SNR, which provides an indicative character of the estimates.

In Fig. 5.5a we see CoSaMP producing MVU estimates for the various CR values that are unbiased but not efficient. In (b) OMP produces an improved MVU estimates, for the set of CR values, which are unbiased but not efficient.

The OMP estimates are lower than the corresponding CoSaMP values in terms of MSE. As the scales are not similar for graphs in Fig. 5.5a, b, graphical illustration on first inspection might be misleading. However, notice that for CR lower than 16 %, OMP MSE is lower than CoSaMP MSE, where CR is at its highest regardless of SNR.

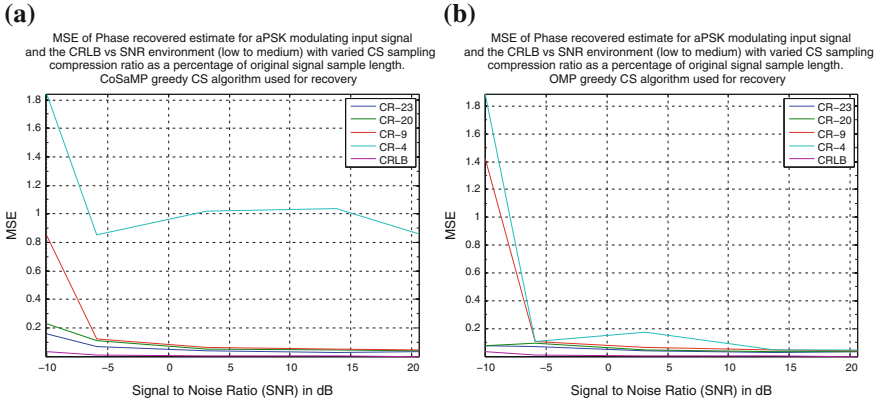


Fig. 5.5 Phase recovery MSE using greedy algorithms CoSaMP in **a** and OMP in **b**, given an input signal that has type 2-Ary PSK modulation. The CRLB representing the ideal MVUE and serves as the benchmark for recovery estimates

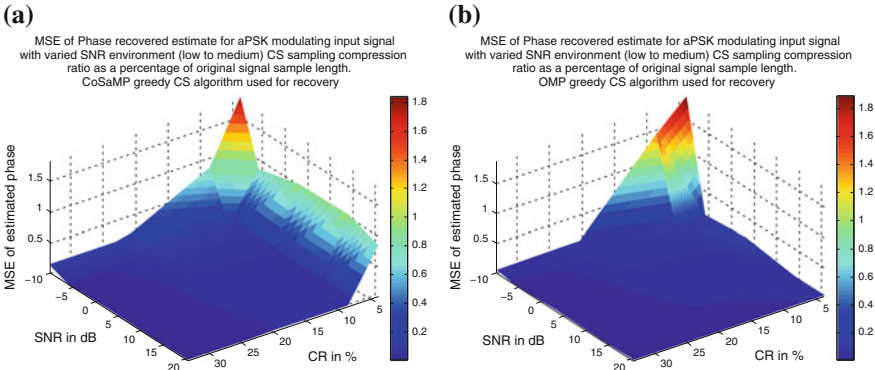


Fig. 5.6 Illustrates the phase recovery MSE using greedy algorithms CoSaMP in **a** and OMP in **b**, given an input signal that has type 2-Ary PSK modulation. The 3D graph shows the relationship of varying SNR (y-axis) and CR (x-axis) on the accuracy of CS recovery for phase

For phase estimation of 2-Ary PSK using CS recovery, OMP serves as a more efficient unbiased algorithm for DOA estimation deployment.

5.4 Simulation 1.2.1—CS Recovery of BIE for 2FSK

The BIE performance was simulated using CS recovery for all combinations of 2FSK signal parameters, for a finite length input vector. The resultant graphs were drawn for different SNR and CR, according to the simulation parameters (see Sect. 5.1.3). Figure 5.7 detail the results obtained.

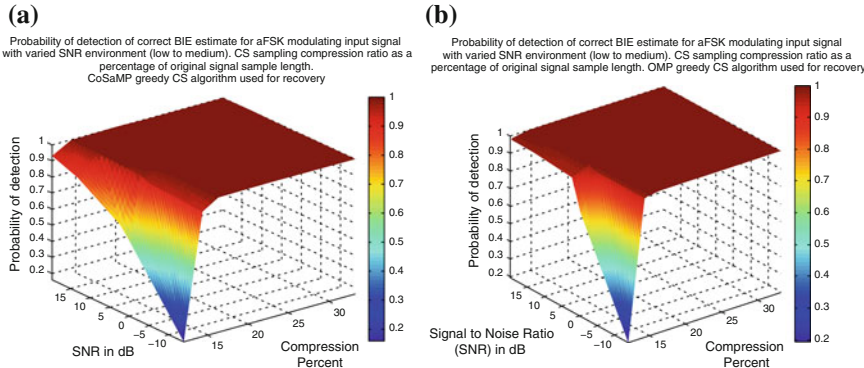


Fig. 5.7 Binary index estimate (BIE) recovery probability of detection (PD) using greedy algorithms CoSaMP in **a** and OMP in **b**, given an input signal that has type 2-Ary FSK modulation. The 3D graph shows the relationship of varying SNR (y-axis) and compression ratio (x-axis) on the PD by means of CS recovery

In Fig. 5.7a we observe that CoSaMP estimates of BIEs for FSK input signals are accurately estimated for $\text{CR} \geq 17\%$ attaining a probability of detection (PD) of 1 for the entire range of SNR. Virtually all BIEs will be correctly estimated when the SNR and CR values do not exceed a $\text{CR} \leq 17\%$ and $\text{SNR} \leq 0\text{ dB}$. Part b) in the same figure shows that OMP estimates of the BIE, given the same input signal, have marginally improved PD for $\text{CR} \geq 15$. Similarly, BIE will be correctly estimated if the CR and SNR values do not exceed a $\text{CR} \leq 15\%$ and $\text{SNR} \leq 0\text{ dB}$. As mentioned in the previous chapter, if the BIE of an input vector can be correlated to the correct sensing matrix row index, it would serve as a rudimentary form of demodulation using CS recovery. Therefore, given that BIE for 2FSK can be achieved with high probability, the use of shift-keying CS sensing matrix can provide additional signal information without additional computation. Use of both OMP and CoSaMP for CS recovery makes simultaneous demodulation capability of 2FSK plausible.

Notice that for both (a) and (b) (in Fig. 5.7) the PD remains high for $\text{SNR} \geq 5\text{ dB}$ with CR tending to 10 %. Nevertheless, OMP serves as the superior BIE CS estimator as it results in a wider operating range of SNR and CR whilst maintaining a PD of 1.

5.5 Simulation 1.2.2—CS Recovery of BIE for 2PSK

The BIE performance was simulated using CS recovery for all combinations of 2PSK signal-parameters, given a finite length input vector, and resultant graphs were drawn for given variable parameters SNR and CR, according to the simulation parameters (see Sect. 5.1.3). Figure 5.8 details the results obtained.

In Fig. 5.8a, b we observe that neither CoSaMP nor OMP estimate BIEs for 2PSK input signal accurately enough; PD of 1 is never attained for the entire SNR and CR

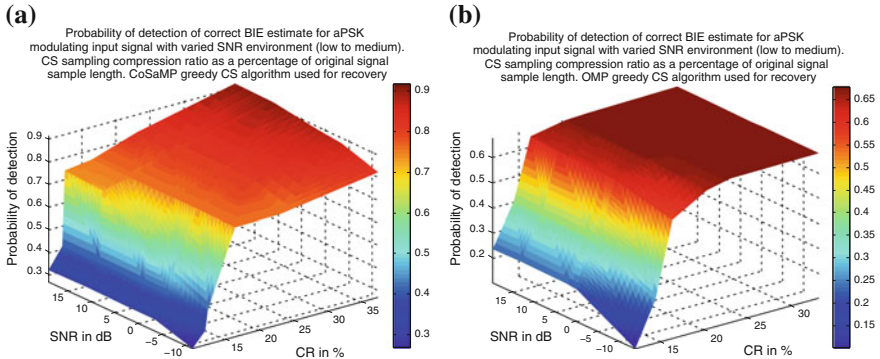


Fig. 5.8 Binary Index Estimate (BIE) recovery Probability of Detection using CoSaMP **(a)** and OMP **(b)** greedy algorithm given an input signal that has type 2-Ary PSK modulation. The 3D graph shows the relationship of varying SNR (y-axis) and Compression ratio (x-axis) on the probability of detection by means of CS recovery

range. The low PD of the BIE estimates can be attributed to the phase modulated structure of the sensing matrix vectors and row vector time delay similarities. The sudden changes of phase between modulation segments creates non-linearity, which introduces ambiguities for the greedy CS recovery algorithms as the sparsity is equal to 1. Additionally, some row vectors of the sensing matrix can be represented by other row vectors by adding a time shift to the original row vector, which is then confused with the correct row vector (i.e. BIE) during CS recovery—reducing the PD of the BIE estimates.

Even though a higher PD is achieved by CoSaMP than OMP, the condition for demodulation was a PD of 1 for all BIEs. Therefore, our approach of shift-keying sensing matrix CS recovery does not merit further development for BIE estimation for 2PSK signal, as PD is too low for unambiguous BIE estimation.

5.6 Assessment of System Parameters for Shift-Keying CS Recovery

Findings of CS recovery simulations for phase and BIE estimation performance are summarized in Table 5.1 and regularly referred to for this discussion. The summarized values provide insight for optimal system parameter choice for shift-keying specific CS-recovery, where low-SNR environments are concerned.

For both 2FSK and 2PSK input signal we have shown that the phase estimation performance of shift-keying sensing matrices using OMP and CoSaMP provides sufficient accuracy, in terms of the MVUE criteria which is dependent on the CR range. However, the more efficient algorithm to use, of the two greedy algorithms, is

Table 5.1 The summarized finding from the previous simulations and the operational range for modulation specific CS recovery for low to medium SNR and compression ratios as small as 3% of Nyquist sampling

Modulation type	CS algorithm	Phase	BIE			Mod-CS operational range					
			Sim No.	CR values with reliable MVUE (%)	MSE range	Sim No.	PD value 1	CR	SNR	CR (for BIE)	SNR (dB)
2FSK	OMP	1.1.1	>3	0.01–0.42	1.2.1	>15%	All	>15%	>−5	*	
	CoSaMP		>6	0.02–0.6		>17%	All	>17%	>−5	*	
2PSK	OMP	1.1.2	>4	0.01–0.2	1.2.2	NA	NA	NA	>−5	*	
	CoSaMP		>9	0.03–0.16		NA	NA	NA	>−5		

OMP as it provides superior performance for phase estimates in terms of MSE, and a lower requirement for CR.

Where 2FSK input signals are considered for DOA estimation using shift-keying sensing matrices for CS recovery, the simulation outcomes dictate the following operational variable range for accurate phase estimates:

1. $CR \geq 3\%$,
2. $SNR \geq -5\text{dB}$.

For the case where we need BIE estimates along with 2FSK phase estimates the operational range for CR will have to be increased to 15 %, the SNR range remaining the same.

Where 2PSK input signals are considered for DOA estimation using shift-keying sensing matrices for CS recovery, the simulation outcomes dictate the following operational variable range for accurate phase estimates:

1. $CR \geq 4\%$,
2. $SNR \geq -5\text{dB}$.

It is important to note that phase estimates are required for DOA estimation, not BIE estimates. BIE estimates are a like an extra parameter that can be estimated using shift-keying matrices, which provides a means of demodulation as the BIE represents the demodulated input signal in terms of its indexing.

Based on the simulations and the summary, as shown in Table 5.1, accurate phase estimates, given shift-keying modulated 2FSK & 2PSK signal, are realizable using CS techniques with the estimation performance margin (i.e. MSE and MVUE criteria) dependent on the CR and SNR. CS phase estimates for such signal are possible for low SNR environments, typical for ES receivers. However, for accurate BIE estimation the system performance deviates, requiring an increase in the CR from 3 % to 15 % and the guarantee of BIE estimates is only possible for 2FSK signals.

5.7 Demodulation Capability

Based on the values for BIEs from Table 5.1, we can assert that for $CR \geq 15\%$ using OMP and only for 2FSK, BIE can be achieved. In addition we observe that the computational performance requires 5 MFLOP for recovery (see Fig. 5.9).

The estimated BIE can be used as a rudimentary form of demodulation as it corresponds to the correct modulation sequence of the row vector in the sensing matrix. Therefore, to determine if the BIE can be used as such, it needs to be compared with a conventional yet similar demodulation scheme. For this reason, we assume a GSM input signal which uses GMSK for digital modulation equivalent to 2FSK modulation.

In a typical GMSK demodulation process the input signal is demodulated via a demodulator block done in real-time, which then immediately disqualifies our CS recovery demodulation as competitive. Nevertheless, we know that GSM uses time

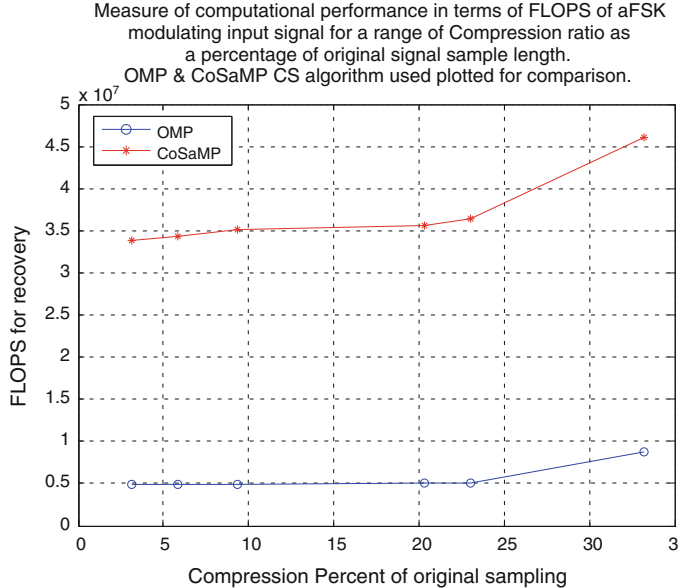


Fig. 5.9 Shows the computational performance in terms of FLOPS as it relates to compression ratio for CS recovery. The input signal is of type FSK

division multiple access (TDMA) allowing a multiple channel transmission at the same carrier frequency at 271 Kbits/s. Therefore, to demodulate the same input signal using CS means, results in a FLOP count that can be implemented on a DSP core. Considering that CS-recovery results in 5 MFLOPS for a bit length of 256, we develop the following expression to determine the FLOP count required:

$$\text{Required Flops} = \frac{\text{CS-FLOPS No.} \times \text{transmission speed } (k\text{B/s})}{\text{CS bit length}} \quad (5.6)$$

$$= \frac{5 \times 10^6 \times 271 \times 10^3}{256} \quad (5.7)$$

$$= 5.29 \times 10^9. \quad (5.8)$$

At present similar FFT based deployment on currently available FPGA platform yields 400 GFLOPS [6], whereas similar DSP deployment can achieve over 200 GFLOPS [75]. Therefore demodulation for modulation specific CS is achievable using a FPGA or DSP platform, which only requires 5.29 GFLOPS where a GSM signal is concerned. Thus, demodulation using the BIE of the CS recovered estimate can be achieved using digital processing platforms at a comparable cost as conventional demodulation algorithms.

5.8 Simulation 1.3.1—Computational Performance of CS Recovery for 2FSK Signal

To determine the computational performance for 2FSK signal, simulations were undertaken to find the number of FLOPS required given a 2FSK signal with varying CR. Resultant graphs were obtained based on the simulation outcomes for different values of CR. SNR is not considered for these simulations as computational performance is independent of SNR. Figure 5.9 details the results obtained. From Fig. 5.9 it is observed that the OMP algorithm (in blue), for this application, is computationally more efficient than CoSaMP as it requires less FLOPS. As expected, the FLOPS required increase with increasing CR. This is due to the increase in sample length requiring more FLOPS for CS recovery. The operational range of FLOPS required by OMP, given a 2FSK input signal of length $N = 256$, varies from 5 MegaFLOPS to 11 MegaFLOPS and is dependent on the CR.

We therefore observe that OMP provides improved computational performance for 2FSK signals. Thus, the use of OMP for CS based DOA estimation is further motivated and preferred for deployment in terms of computational performance and accuracy (see Simulation 1.1.1).

5.9 Simulation 1.3.2—Computational Performance of CS Recovery for 2PSK Signal

In order to determine the computational performance for 2PSK signal, simulations were undertaken to find the number of FLOPS required for CS recovery using OMP and CoSaMP, given a 2PSK signal with varying CR. Resultant graphs were obtained based on the simulations for different CR. SNR is not considered for these simulations as computational performance is independent of SNR. Figure 5.10 details the results obtained.

From Fig. 5.10 it is observed that the OMP algorithm (in blue), for this application, is computationally more efficient than CoSaMP. The computational operational range of FLOPS required by OMP, given a 2PSK input signal of length $N = 256$, varies from 5 MegaFLOPS to 10 MegaFLOPS which is dependent on CR.

We therefore observe that OMP provides improved computational performance for consideration in our CS recovery approach for 2PSK signals. Thus, the use of OMP for CS based DOA estimation is further motivated and preferred for deployment in terms of computational performance and accuracy (see Simulation 1.1.2).

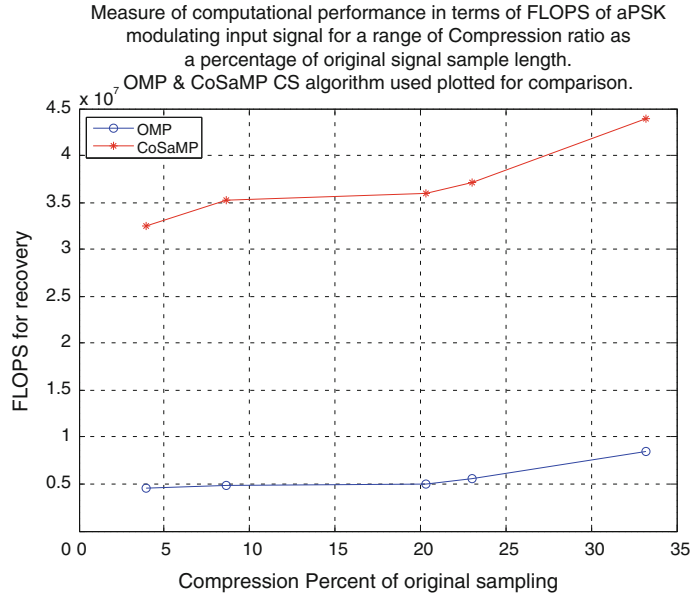


Fig. 5.10 Shows the computational performance in terms of FLOPS as it relates to compression ratio for CS recovery. The input signal is of type PSK

5.10 Computational Performance of CS Recovery

As CS-recovery is the only computational block that is additional to the conventional Nyquist scheme, we are interested in the comparison of this to the conventional schemes and whether the reduction in samples required (i.e. compression ratio/percentage) provides an adequate return on computational time to make our shift-keying specific CS method a competitive approach for deployment.

For both the OMP and CoSaMP algorithms the computational load (i.e. time complexity) grows linearly at $O(MNK)$ for OMP and $O(MN)$ for CoSaMP (refer to Sect. 3.4). However, it should be noted that due to the condition of sparsity $K = 1$ the computational loads of both OMP and CoSaMP are equal, in terms of time complexity $O(MN)$ where M is the size of the input vector and N the size of the square sensing matrix. Therefore, computational performance has to be determined by means of testing with regards to the specific application, which is depicted in Simulations 1.3.1–1.3.2 yielding a lower computational load for OMP—with a calculated range between 5 and 11 MFLOPS.

To evaluate the computational load of a similar Nyquist scheme, we consider a conventional FFT algorithm to produce phase estimates for comparison, which has an associated time complexity of $O(N \log_2 N)$ [164]. Therefore, our approach for CS-recovery would have to match a similar order of computation, which leads to the the condition of similar time complexity expression where:

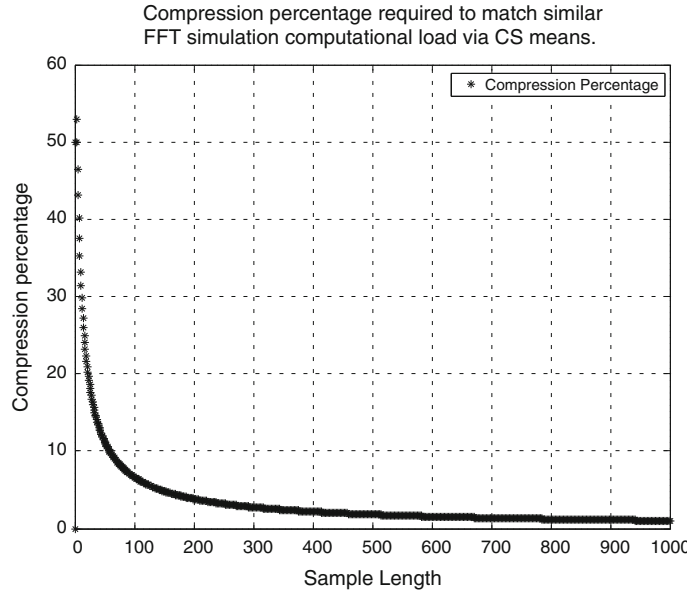


Fig. 5.11 Compression ration required to match the equivalent FFT implementation via CS means for phase recovery

$$MN = N \log_2 N \quad (5.9)$$

$$M = \log_2 N. \quad (5.10)$$

Thus, the CS sensing matrix size would have to comply with the above expression in order to match the conventional FFT time complexity, where the compression ratio, denoted as a percentile, is $CR = 100 \times M/N$. The condition where the conventional FFT approach matches our CS recovery approach follows the curve shown in Fig. 5.11.

Therefore, the criteria of compression ratio (expressed as a percentage) required to match the time complexity of the conventional FFT approach, given binary bit lengths of an input signal for both 2FSK and 2PSK, is as follows.

- $256 \simeq 3\%$
- $512 \simeq 1.7\%$
- $1024 \simeq 1\%$

If comparative computational time using our CS recovery technique is the goal, for sample lengths larger than 256, compression ratio smaller than 3 % is required. The only scenario where the constraint on CR can be matched is for 2FSK phase estimation using OMP for recovery (see Simulation 1.1.1). For scenarios where higher CRs are required, the cost of computational load (i.e. processing time) must be weighed against the reduction in sample size.

In summary the use of CS-recovery using shift-keying sensing matrices in conjunction with the OMP algorithm, for phase estimates, provide similar computational performance as compared to the conventional FFT scheme when small sample lengths are considered. For sample lengths ≤ 256 —with our current phase modulation CS scheme—comparative computational performance are realizable. Where larger sample lengths are concerned Fig. 5.11 should be referred to for computational performance comparison.

Chapter 6

Modulation Specific CS DOA

6.1 Chapter Outline

Based on the results of the foregoing chapter, wherein accurate phase estimations were achieved using shift-keying sensing matrices for 2FSK and 2PSK signal, we further our investigation by using CS recovered phase estimates for DOA estimation—referred to as CS DOA in this chapter.

In this chapter the performance of the proposed CS DOA method is investigated by means of simulations. The aim is to accurately estimate the DOA of modulated shift-keying signals in a narrow bandwidth given CS phase estimates. CS sensing matrices, developed in the previous chapter, are used to estimate the phase and thus the DOA of SOIs by means of sub-space algorithms (i.e. MUSIC). These simulations are structured to address the following tasks. The aims are to investigate

- the accuracy of CS DOA estimation compared to conventional Nyquist sampled DOA estimation using similar sub-space algorithms (i.e. MUSIC);
- the estimation performance in high noise environments (i.e. low SNR);
- the compression ratio required for adequate CS DOA estimations; and
- the scalability of CS DOA estimation for ES.

Simulations are based on the method described in Sect. 4.1.3, taking the CS recovered output data generated from simulation 1.1.1 (for 2FKS signals) and simulation 1.1.2 (for 2PSK signals) for N number of channels, assuming an ULA antenna as inputs. Then sub-space DOA estimation algorithm MUSIC is used to determine the CS DOA estimates. For comparison, we simulate a conventional Nyquist sampled 2FSK and 2PSK signal, via the same ULA antenna, and use MUSIC to determine the DOA estimates. Similar SNR and CR values are considered for these simulation as in Chap. 5.

All simulations herein are performed using MATLAB®.¹

¹The *Phased Array System Toolbox* is utilized for DOA estimation and CS outputs verified by means of a custom written DOA MUSIC estimation algorithm.

6.1.1 General Simulation Setup

The ULA antenna simulated comprise N elements spaced length $d \leq \lambda/2$ apart, where λ corresponds to the carrier frequency of the modulating signal input. Two scenarios are considered of the ULA antenna, where $N = 3$ (the minimum number required to estimate bearing) and $N = 10$ which represent a more typical deployment of a conventional ULA.

A digital modulated shift-keying signal (i.e. 2FSK and 2PSK) is generated for a specific bearing ranging from $-75 : 75$, which is then received at the simulated ULA. A corresponding delay on each channel dependent on the bearing of incidence is also imposed.

Each channel resolves the input signal by means of CS, as per Simulations 1.1.1 & 1.1.2, which provide the CS phase and magnitude recovery estimates for each channel. Thereafter CS recovered estimates become the input parameters to DOA estimation algorithm MUSIC. The DOA estimators use the CS DOA method. The simulation of the MUSIC based CS DOA estimation follows on as per Sect. 4.1.3.

The shift keying input signal, given an incident angle, can be denoted as $X[n] = S(\phi)a[n] + w[n]$ where the input modulating signal $a[n]$ of length M (derived from the bit length $N = \log_2 M = 8$ equal to a byte) can be denoted as a vector k of the sensing basis $\Psi[k, m]$. $S(\phi)$ is the steering vector which is used in MUSIC to determine the optimal DOA estimate and $w \sim \mathcal{N}(0, \sigma^2)$ white Gaussian noise corrupting the input signal. SNR is varied by changing the w and the CR by changing M .

The output DOA estimates for the range of SNR (0 dB – 20 dB) and the range of CR (1 % – 36 %) values are simulated and the results measured for the performance indicators, viz. the MSE of the CS DOA estimates as compared to the actual DOA. Figure 6.1 illustrates a single iteration of a simulation where SNR and CR are fixed, which produce the CS DOA estimates (in black) and conventional DOA estimates (in blue) compared to actual DOA (in red) of a 2FSK modulated input signal incident from a bearing ranging $[-80 : 80]$.

6.1.2 Performance Indicators

Mean Squared Error (MSE) is used to measure the difference between the actual signal parameter Y (i.e. DOA incident signal) and the estimated \hat{Y} (using CS-DOA). MSE is calculated for the set of signal angles $N = [-80 : 80]$ of the input shift keying modulated signal $a[n]$, and with iterations over the subset of variables SNR and CR with their variable range denoted as i and j respectively. Thus we can denote the MSE as follows.

$$MSE[i, j] = \frac{1}{N} \sum_{n=1}^N [Y[n] - \hat{Y}[n]]^2 \quad (6.1)$$

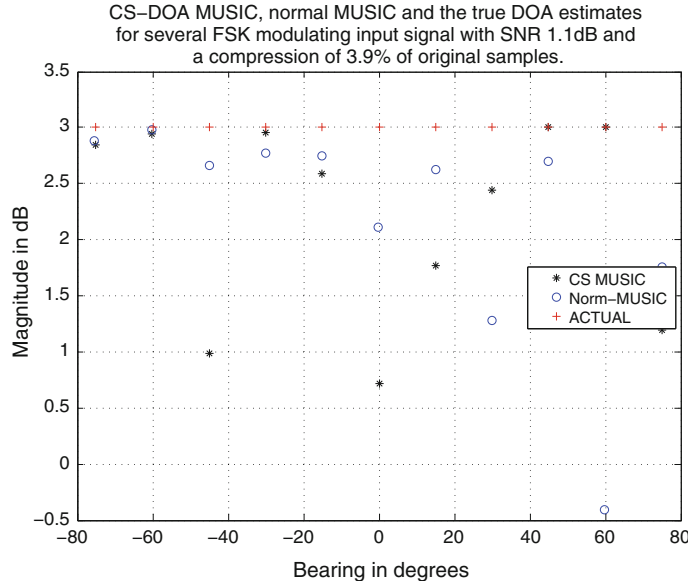


Fig. 6.1 This figure illustrates the estimated CS DOA using our CS method versus the normal Nyquist sampled DOA and the actual DOA for specified SNR and CR

MSE can also be written in terms of variance of the estimator distribution coupled with a bias factor, as follows.

$$MSE(\hat{Y}) = Var(\hat{Y}) + (Bias(\hat{Y}, Y))^2 \quad (6.2)$$

6.1.3 Simulation Parameters

The following simulation parameters are chosen for the set of CS DOA estimation simulations. The motivation for the choices are detailed as well.

1. Azimuth ranged in the limit $[-80 : 80]$. The range excludes the full 180° field of view because phase ambiguities are high for bearings higher than ± 80 .
2. Elevation kept at 0 because our scope only considers azimuth for this investigation.
3. Distance between antenna elements is kept at $d \leq \lambda/2$ which is required to mitigate phase ambiguities.
4. $SNR \in [0 \text{ dB} : 20 \text{ dB}]$ which is the typical SNR range for ES receivers.
5. CR is varied in the range of 1–36 % that of Nyquist sampling i.e. (ratio of: [0.02–0.3]). This is based on results CS recovery operational range from previous chapter (see Sect. 5.6).
6. Antenna ULA is of 3 and 10 elements. (Refer to Sect. 6.1.1.)

7. MUSIC sub-space DOA algorithm is considered. Although other sub-space DOA algorithms are available, such as ESPRIT, MUSIC has a lower requirement on the number of antennas and is more efficient and accurate.
8. The signal bit length $M = \log_2 256 = 8$. (Refer to Sect. 5.6.)
9. OMP algorithm is considered for CS recovery. (Refer to Sect. 5.6.)

6.2 Simulation 2.1—CS DOA for 2FSK Signals

CS DOA estimation of 2FSK signal was simulated using MUSIC estimation algorithm and the resultant graphs are drawn for given variable parameters SNR and CR. Separate simulations were done where the antenna elements in the ULA are 10 and 3. Figure 6.2 details the results obtained.

In Fig. 6.2a where 10 elements are simulated for the ULA it can be seen that for $\text{SNR} \leq 17 \text{ dB}$ the CS DOA method provides lower MSE values than the normal DOA estimation for all CR values. This translates into lower variances between the estimate and the actual DOA value using CS DOA for estimation, than the normal DOA estimation.

Where low SNR values are considered (i.e. $\leq 5 \text{ dB}$) the MSE of the CS DOA method ranges between $0.00132 : 0.0025$, dependent on the CR considered the normal DOA MSE, although not conspicuous in the graphs, varies from 0.026 to 0.0437. The method of determining these ranges are shown in Fig. 6.3.

Taking the minimum and maximum MSE at SNR values 1.1 dB and 5 dB for both normal and CS DOA in (a), we can describe the overall MSE improvement in terms of a factor expressed as

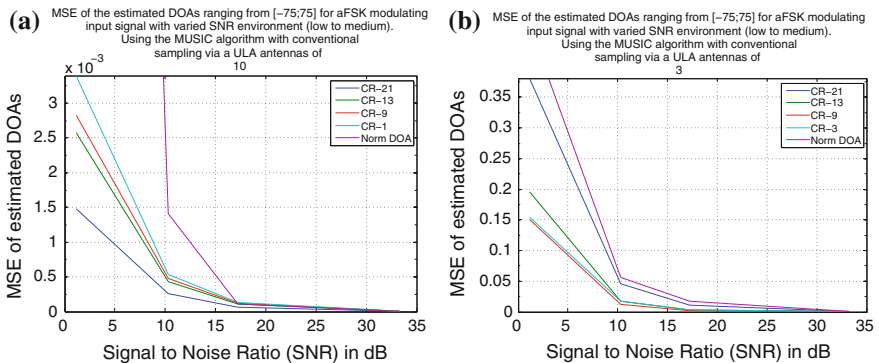


Fig. 6.2 Mean Squared Error (MSE) of the normal DOA method and the CS DOA method, compared to the true DOA for each compression ratio denoted as a separate line. The OMP greedy algorithm is used for CS recovery and the MUSIC algorithm for DOA estimation in both cases. The MSE is measured for an input signal of type 2FSK modulation incident on an ULA antenna where in **a** there are 10 antennas and **b** only 3. The DOA of the incident signal ranges from $-75^\circ : 75^\circ$

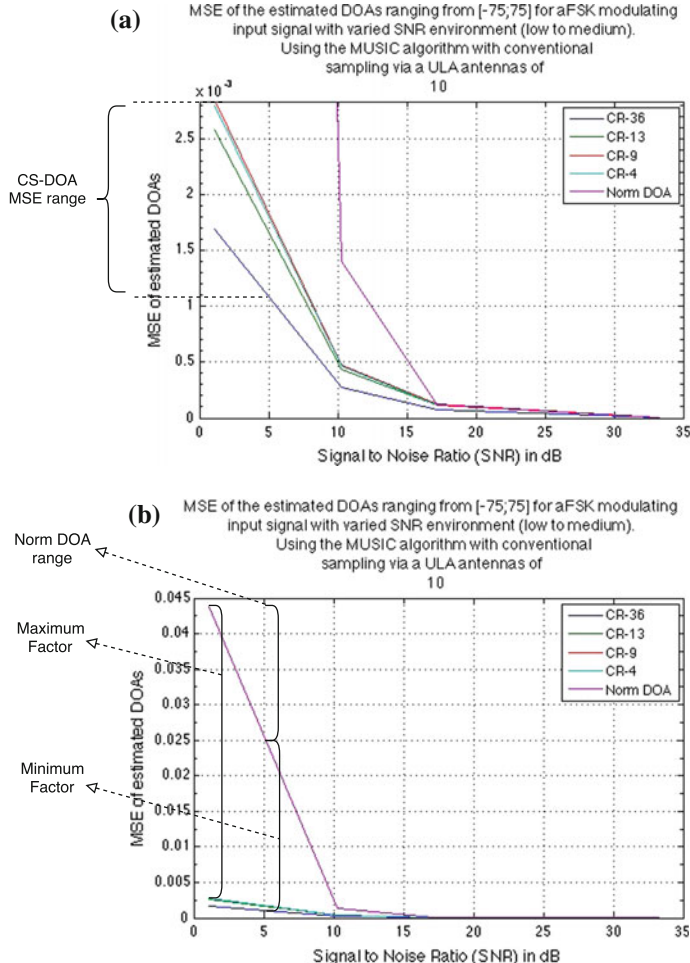


Fig. 6.3 A simplified illustration with **a** showing how to determine the CS DOA MSE range for low SNR, and **b** the MSE minimum and maximum factor as well as the conventional DOA MSE range. The same convention holds for calculating similar values in other simulations in this section

$$IF_{max} = \frac{\text{MSE Norm DOA at } 1.1 \text{ dB} - \text{MSE CS DOA at } 1.1 \text{ dB}}{\text{MSE Norm DOA at } 1.1 \text{ dB} - \text{MSE Norm DOA at } 5 \text{ dB}}, \quad (6.3)$$

$$IF_{min} = \frac{\text{MSE Norm DOA at } 5 \text{ dB} - \text{MSE CS DOA at } 5 \text{ dB}}{\text{MSE Norm DOA at } 1.1 \text{ dB} - \text{MSE Norm DOA at } 5 \text{ dB}}, \quad (6.4)$$

where the minimum improvement factor (IF_{min}) is 14 and maximum improvement factor (IF_{max}) is 16.2 compared with the conventional DOA scheme. The improvement factors depend on the CR chosen for CS recovery, and as expected the MSE improves when the CR is increased.

When 3 elements are simulated for the ULA, as shown in (b) of the same figure, a different result is observed. For all SNR values the CS DOA method provides lower MSE values than the normal DOA method. For low SNR values are considered (i.e. ≤ 5 dB) the MSE of the CS DOA method varies between 0.09 and 0.22 dependent on the CR whereas the normal DOA MSE varies in the range of 0.294–0.47.

Again, taking the average of the minimum and maximum MSE at SNR 1.1 dB and 5 dB for both normal and CS DOA in (b), we obtain the overall MSE improvement factors (IF) of

$$IF_{min} = 2.45$$

and

$$IF_{max} = 3.1$$

(as compared with the conventional DOA scheme). The improvement factor depends on the CR chosen for the CS recovery. However, the relationship of MSE to CR is not proportional as in (a). As CR decreases from 36 to 3 % the MSE improves, with CR = 9 % providing the lowest MSE. The non-proportional relationship that results, as opposed to the linear relationship in (a), can be attributed to the effect of reduced ULA elements.

In summary, the CS based algorithm results in improved DOA estimation accuracy described in terms of a IF_{min} and IF_{max} . The improved CS DOA estimation accuracy holds true when ULA elements are 3 or 10.

6.3 Simulation 2.2—CS DOA for 2PSK Signals

CS-DOA estimation of 2PSK signal was simulated using MUSIC estimation algorithm and resultant graphs were drawn for different SNR and CR. Separate simulations were done where the antenna elements in the ULA are 10 and 3. Figure 6.4 details the results obtained.

In Fig. 6.4a where the 10 elements are simulated in the ULA we observe that for $SNR \leq 16$ dB, the CS DOA method provides lower MSE values. This means when SNR is higher than 16 dB the conventional DOA scheme provides lower MSE values, and thus improved DOA estimates.

Where low SNR values are considered (i.e. ≤ 5 dB) the MSE of the CS DOA method ranges between 0.00132 and 0.0026, dependent on the CR, whereas the normal DOA MSE, although not visible on the graph, varies from 0.0156 to 0.0268. Following the convention for minimum and maximum improvement factor as detailed in Eq. 6.3 for MSE at 1.1 dB and 5 dB for both normal and CS DOA result in improvement factors of

$$IF_{min} = 9.1$$

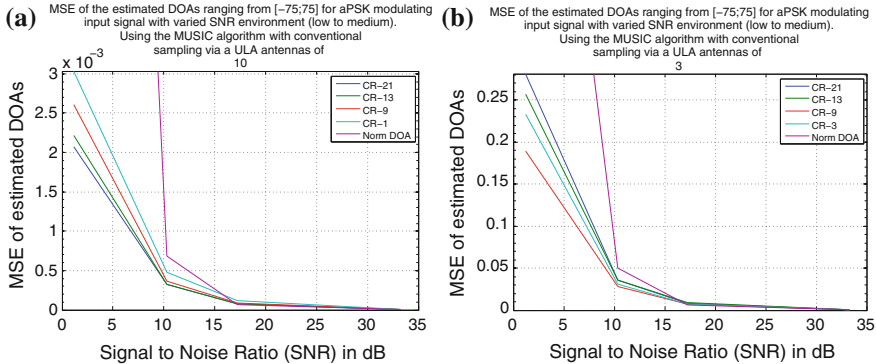


Fig. 6.4 Mean Squared Error (MSE) of the normal DOA method and the CS-DOA method, compared to the true DOA for each compression ratio. MSE is measured for an input signal of 2PSK modulation incident on an ULA antenna where in **a** there are 10 antenna and in **b** 3. DOA of the incident signal ranges from $-75^\circ : 75^\circ$

and

$$IF_{max} = 13$$

as compared with the conventional DOA scheme. The improvement factor depends on the CR chosen for CS recovery and as expected the MSE improves when the CR is increased.

When 3 elements are simulated for the ULA, as shown in b) of the same figure, for all SNR values ≤ 16 dB the CS DOA method provides lower MSE values. Where low SNR values are considered (i.e. ≤ 5 dB) the MSE of the CS-DOA method varies between 0.121 and 0.281, whereas the normal DOA MSE varies between 0.56 and 0.937.

The minimum and maximum MSE at 1.1 dB and 5 dB for both normal and CS DOA result in MSE improvement factors of

$$IF_{min} = 3.1$$

and

$$IF_{max} = 4.9$$

as compared with the conventional DOA scheme. The improvement factor depends on the CR chosen for CS recovery. However, the relationship between MSE and CR is not that of direct proportionality. As CR decreases from 21 to 3 %, CR = 9 % provides the lowest MSE. The non proportional relationship that results, as opposed to the linear relationship in a), can be attributed to the reduction of ULA elements.

In summary, using DOA estimation algorithm MUSIC for CS results in improved DOA estimation accuracy.

6.4 Assessment of CS DOA Estimation Algorithm for Shift Keying Modulated Signals

Findings of the previous CS DOA simulations are summarized in Table 6.1 and will regularly be referred to for the remainder of this discussion. The summarized values provide insight as to the optimal system parameters for CS DOA where low SNR environments are concerned and ULA equal to 10 and 3, which we denote as ULA₁₀ and ULA₃, respectively.

6.4.1 Performance Assessment for ULA₁₀

Considering Simulations 2.1–2.2 where the elements of the ULA are 10, CS DOA provides improved DOA estimates (in terms of MSE) as compared to the conventional scheme. This is true for both 2FSK and 2PSK input signals, at a compression ratio as low as 1 % and medium to low SNR environments (i.e. $0 \text{ dB} \leq \text{SNR} \leq 15 \text{ dB}$).

In reality the improvement factors IF_{min} & IF_{max} , although large for some simulation outcomes, do not result in large improvements on accuracy for DOA estimation. For example, consider Simulation 2.1 where a 2FSK signal is the input and MUSIC estimation algorithm is used for CS DOA estimation which yields the largest improvement factor for all the simulations which is $IF_{max} = 16.2$. Using IF_{max} applied to the CS DOA MSE at SNR 1.1 dB results in an MSE of $16.2 \times 0.0025 = 0.0405$ for normal DOA estimation. Then the maximum deviation from the actual DOA can be determined by calculating the statistical 95 % percentile of the deviation based on both the MSEs. The 95 % of deviation for CS DOA estimation for Simulation 2.1 results in

$$\sigma \times 1.64 = \sqrt{0.0025} \times 1.64 = \pm 0.082^\circ,$$

whereas the normal DOA is

$$\sigma \times 1.64 = \sqrt{0.0405} \times 1.64 = \pm 0.33^\circ.$$

Therefore, although the CS DOA method provides improved DOA estimates than that of the conventional DOA method, it only translates to a DOA accuracy improvement of $0.33^\circ - 0.082^\circ = 0.248^\circ$.

The real value of our CS DOA approach, when large antennas are used, is the reduction in the number of samples required. For example, consider an input signal of length 1000 for ULA₁₀ which requires 10 separate channels. If a digital receiver is considered and no beamforming is done this results in $1000 \times 10 = 10000$ samples. However, if CS DOA estimation method is implemented for the same scenario the total number of samples required will reduce to $10000 \times 1\% = 100$ samples, which is a significant reduction in memory with a small improvement for estimation accuracy of DOAs.

Table 6.1 Summary of the findings from Simulations 2.1–2.2 and the operational range for CS-DOA for low to medium SNR, compression ratios ranging from 1 to 36 % of Nyquist sampling, and ULA elements of 10 and 3 for 2FSK and 2PSK CS recovered input signals

Modulation type	DOA algorithm	Sim no.	ULA = 10; 1% ≤ CR ≤ 36 %		ULA = 3; 3% ≤ CR ≤ 21 %					
			MSE factor for SNR <5dB	MSE range CS-DOA	SNR range where MSE (CS-DOA) < MSE (Norm-DOA) (dB)	MSE factor for SNR <5dB	MSE range CS-DOA	SNR range where MSE(CS-DOA) < MSE (Norm-DOA) (dB)		
2FSK	MUSIC	2.1	14	16.2	0.001–0.0025	<17	2.45	3.1	0.09–0.35	<30
2PSK	MUSIC	2.2	9.1	13	0.0013–0.0026	<16	3.1	4.9	0.12–0.28	<16

6.4.2 Performance Assessment for ULA_3

Considering Simulations 2.1–2.2 where the elements of the ULA is 3, CS-DOA provides improved DOA estimates (in terms of MSE) as compared to the conventional DOA estimation scheme. The improved DOA estimates are true for both 2FSK and 2PSK input signal, at a compression ratio of as low as 3 % and for medium to low SNR environments (i.e. $0 \text{ dB} \leq \text{SNR} \leq 15 \text{ dB}$).

When ULA elements are restricted to ULA_3 , MSE values increase compared to the case where ULA_{10} for both CS DOA and conventional DOA estimates. Nonetheless, the increased in MSE for ULA_3 does not result in large deviations in terms of the 95 % percentile of deviation. As before, lets consider Simulation 2.1 where a 2FSK signal is an input. MUSIC estimation algorithm is used for CS DOA estimation which yields the largest improvement factor for all the simulations, i.e. $IF_{max} = 3.1$ where ULA_3 (see Table 6.1). Using IF_{max} applied to the CS DOA MSE at SNR 1.1 dB results in an MSE of $3.1 \times 0.35 = 1.0805$ for normal DOA estimation. Thus the 95 % of deviation for CS DOA estimation is

$$\sigma \times 1.64 = \sqrt{0.35} \times 1.64 = \pm 0.97^\circ,$$

whereas the normal DOA is

$$\sigma \times 1.64 = \sqrt{1.0805} \times 1.64 = \pm 1.7^\circ.$$

Therefore the CS DOA provides an improved DOA estimate, at a compression ratio of 3 %, than the conventional DOA method. However, in reality the difference in degrees for the conventional DOA and CS DOA estimate is less than 0.73° . Thus, the deployment of either approaches will depend on the type of ES application and the allowable tolerances for DOA deviation. For applications where large distances are involved the tolerance for DOA deviation might be more crucial.

Again, the real value of the CS DOA approach is the reduction of samples required to achieve equivalent, and in some cases, improved estimates. Consider an input signal of length 1000 for the ULA_3 which requires 3 separate channels. If a digital receiver is considered and no beamforming is done, this implies $1000 \times 3 = 3000$ samples. However, if CS DOA is implemented instead, the total memory required will reduce to $3000 \times 3 \% = 90$ samples in total, which is a significant reduction in memory.

6.4.3 Comparison of ULA_{10} and ULA_3

In terms of sample reduction we can express the comparison of both the ULA cases as per the following expression.

$$\text{ULA}_{10} = B \times N \times CR = 10 \times N \times 1\%, \quad (6.5)$$

$$\text{ULA}_3 = B \times N \times 3CR = 3 \times N \times 3(1\%), \quad (6.6)$$

$$\text{ULA}_3 = 0.9 \times \text{ULA}_{10}, \quad (6.7)$$

where B denotes the number of branches, N the number of samples.

Thus an interesting case can be made. Regardless of the number of antennas used in the ULA for our CS DOA method, a similar reduction in memory is attained. However, in terms of system cost, ULA_3 provides an overall monetary cost reduction due to less sampling branches.

Performance in terms of MSE and DOA accuracy is higher for the case where ULA is greater. Therefore the deployment of either ULA_{10} or ULA_3 has to then be justified in terms of the performance criteria of the system. Considering ULA of 10 yields a maximum statistical 95 % percentile deviation of 0.082° , whereas for ULA_3 the deviation is 0.97° .

For most DOA applications the operational performance where ULA is 3 (i.e. ULA_3), it is sufficient to determine accurate DOA estimation. Nevertheless, this will depend on the performance criteria required for deployment. Moreover, it should be noted that for ULA_3 a similar DOA estimation accuracy is achieved compared to the conventional DOA with ULA of 10, with CS DOA of ULA_3 having maximum 95 % percentile deviation of $\pm 0.97^\circ$ and the the conventional DOA using ULA_{10} a maximum with 95 % percentile deviation of $\pm 0.33^\circ$.

In summary, for both the ULA cases the CS DOA estimation method, considering 2FSK and 2PSK CS recovered input signals, outperforms the conventional DOA estimation method in terms of DOA accuracy. However, in some cases the improvement on actual DOA estimation accuracy is negligible. More importantly, both the ULA cases result in a large reduction of memory and according to Eq. 6.7 the memory reductions for ULA_{10} and ULA_3 are similar.

Chapter 7

CS Based Spectrum Sensing for ES

One of the major challenges of electronic defence (ED) systems is to sense a wide spectral band in real time. In this chapter we show the use of compressive sensing (CS) schemes to which have the potential of reducing the load on acquisition for ED spectrum monitoring. We also propose a modified CS scheme, which we denote as selective spectrum sensing, to further improve signal estimation for spectrum sensing. The proposed scheme is shown to perform efficiently under severe signal to noise ratio (SNR) conditions by leveraging a-priori knowledge of the frequency bands of interest.

Most wideband sensing scenarios, from an electronic support (ES) perspective, require high performance analog and digital systems to perform timely tasks such as detection and identification accurately [3]. In a competitive technological field such as ES, there is a continuous need to improve system management and performance in order to reduce the risk of hardware and software bottlenecks which result in system stagnation. Improved system performance is typically achieved by reducing acquisition time and memory load whilst improving computational performance. Our focus relates to the former—by reducing acquisition load using CS techniques.

Recent developments in making radio communication systems more intelligent, flexible, and efficient for RF spectrum usage in a cognitive way, has led to the inception of the field of Cognitive Radio (CR) [93]. One of the major system functional blocks of any CR system is the spectrum monitoring block. The functional block of CR is a mutual framework common to ES sensing schemes. The noteworthy-similarities are in sampling and detection requirements for a wide-band signal, which allows a unique opportunity to exploit current advances made in the domain of CR for use in ES spectrum detection and awareness.

Lately there have been attempts at using compressive sensing (CS) principles [170] for more efficient spectrum sensing in CR [11]. These works can be categorised into two types. The first type consist of attempts to reduce ADC rates of individual spectrum sensors using CS [119], and the second type consists of the use of distributed sensing employing multiple sensors to have an overall reduction in ADC and data

rates [168]. The use of CS based algorithms in the domain of electronic defence (ED) is sparse in the open literature.

In this chapter we address the current restrictions of using greedy algorithms in resolving a wide band spectrum and then utilize a recent model based approach to achieve selective spectrum sensing. Our work leverages a development made in the work [54] which deals with frequency scenarios where the spectrum is block sparse, and also, the model-based CoSaMP algorithm developed in [19] which allows for signal recovery based on modelling the spectrum as segments. The main feature of our work shows that by weighting the bands that are of interest in the wide band spectrum, during the recovery process, these bands are selectively recovered with better accuracy using the modified model based algorithm developed in [19]. It is an elegant solution to favour certain frequency bands for different modes of operation and can be thought of as a varied form of discrete filtering. An added benefit includes an increase of the spectral recovery in high SNR environments with lower computational requirements than other CS methods.

7.1 Problem Statement

When using CS as a sensing technique to perform spectrum sensing, most performance and optimization improvements are related to the recovery algorithms. As has been discussed in the previous chapters iterative methods, although more accurate [105], demands more computational time whereas greedy algorithms such as OMP [172] or CoSaMP [122] tend to be preferred for faster recovery of the signal. Subsequently these recovery algorithms require, as an input, the a-priori estimate of the active frequencies within the spectrum. From a detection perspective, this is not desirable but a necessity to obtain adequate recovery. This constraint causes the spectrum estimation to degrade significantly if the estimate and true value do not comply within a reasonable margin [172].

Fortunately when dealing with a wide frequency spectrum, such as in an ES scenario spanning 30 GHz, we have the benefit of knowing that most communication and radar signals operate within a specified operational bandwidth with unique signal characteristics which are typically, if not always, known. This a-priori knowledge of frequency band occupation provides an opportunity to model the signal offline, and supply the recovery algorithm with a pre-weighted sensing matrix to recover bands of interest. The CS recovery algorithm shown in [19] is used to investigate and formulate this method.

Rather than estimating the number of frequencies present, the estimated bandwidths of the signal are given as an input during the recovery step. This approach allows for more accurate estimation and faster computational time on signal recovery. Signal that can be modelled as part of this recovery technique[19] are referred to as block sparse signals. With most recovery techniques, recovering a signal within a low SNR environment i.e. ≤ 5 dB, remains a high priority task [71] as recovery algorithms are typically susceptible to high noise environments. Herein lies the inception of our

approach to selectively recover specific bands of interest during the recovery step, as detailed in Sect. 3.2. This is possible by, as discussed, using the a-priori knowledge of the bandwidth of the signal of interest; and weighting the sparse basis (i.e. IDFT) appropriately before recovery. This could potentially improve the spectral estimation error of the signal in a high SNR environment. Details of the scheme are explained in the following sections.

7.2 Selective Spectrum Weighted CS Approach

For a typical RF system the prioritising of bands would traditionally be achieved by means of analog mixing, filtering, differential amplification, quantisation and a wide band STFT-filter bank. For a detailed discussion on standard techniques associated with wide band RF receiver systems the readers are referred to [97]. It can be argued that our approach of selectively favouring/biasing a specific band, is similar to bandpass filtering which could achieve the same task by adding a notch filter in the RF receiver chain. However, this isn't entirely similar, in that the selection or biasing of a bandwidth of interest is done as part of the CS recovery step. This is where the novelty in our approach stems.

Implementation of this method as part of the digital signal processing (DSP) back-end, adds to the adept reconfigurability capability of a system. Subsequently, using the CS-based scheme, the biased recovery of a sub-band of interest can be configured in real-time without changes being made to either RF front end, analog or digital filters.

We model the input signal as block sparse, similar to the model in both [54] and [19], where the Fourier transform of the input signal can be modelled as follows.

$$X[k] = (X_1, X_2, X_3, \dots, X_N)$$

$$s[k] = \begin{cases} X[k] & \text{if } k \text{ within } (B_1, B_2, \dots, B_n) \\ 0 & \text{if } k \text{ is not within } (B_1, B_2, \dots, B_n) \end{cases}$$

Where:

$$\begin{aligned} X[k] &= \sum_{k=0}^N x[n] e^{-2\pi kn/N} \\ s[k] &= \text{approximation of the signal spectrum} \\ x[n] &= \text{time domain signal } \sim x(t) \\ B_n &= \text{bandwidths of the block sparse signal} \end{aligned}$$

Although in practice the signal $s[k]$ is identical to the spectrum of $X[k]$, for the sake of clarity, during the discussion it is appropriate to work with $s[k]$. Moreover, $s[k]$ now accurately resembles the spectrum in Fig. 7.1 which helps our cause. The proposed

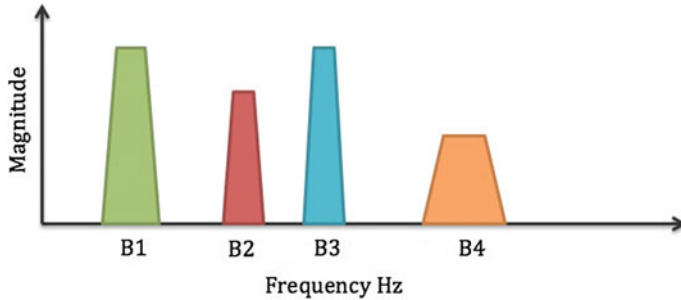


Fig. 7.1 Showing a representative frequency spectrum that is *block sparse*, denoted by B1–B4. Note that any frequencies outside of these bands are not of interest to the user

selective spectrum sensing scheme works in the following way. During the recovery stage, as mentioned in Sect. 3.2, the sub-nyquist signal is represented as $Y = As$. The CS based recovery algorithm needs the sensing matrix $A = \Phi F^{-1}$ as an input. We show that weighting/modifying the columns of the matrix F^{-1} appropriately before CS recovery, provides a viable means of favouring certain bands in the spectrum of a signal thereby achieving selective spectrum sensing. This is illustrated by means of a diagram in Fig. 7.2. This operation only modifies the matrix F^{-1} as the sampling matrix Φ remains unchanged within our sensing scheme. The weighting of the matrix F^{-1} is illustrated by matrix operations, as seen in Eq.(7.1) where $diag$ creates a diagonalized matrix from a vector.

$$\hat{F} = [(F^{-1})^T * diag(\delta(n))]^T \quad (7.1)$$

This gives a modified matrix denoted as \hat{F}^{-1} with $\delta(n) = (\alpha_1, \alpha_{-1}, \dots, \alpha_n)$ equating to the weighting vector that favours certain columns.

For our purposes δ_n can only occupy two values which are either a minimum or maximum value, dependant on the interest in a specified bandwidth. These two values are denoted as $\alpha_1 \rightarrow min$ and $\alpha_2 \rightarrow max$, which are pre-set. This set of extreme values was found to be working optimally when the elements differ by a factor ≥ 100 . More than two values can be assigned to δ . The result of assigning multiple values to δ on CS recovery will be addressed as part of our future work.

Imagine we have an $N \times 1$ coefficient vector $s[k]$ of a frequency spectrum that is block sparse. For the sake of simplicity we take N to be 8 which in matrix operation will lead to a \hat{F}^{-1} weighted DFT matrix subject to Eq.(7.1). In the recovery step, in light of Eq.(3.1), this becomes a condition of

$$Y = \Phi \hat{F}^{-1} s.$$

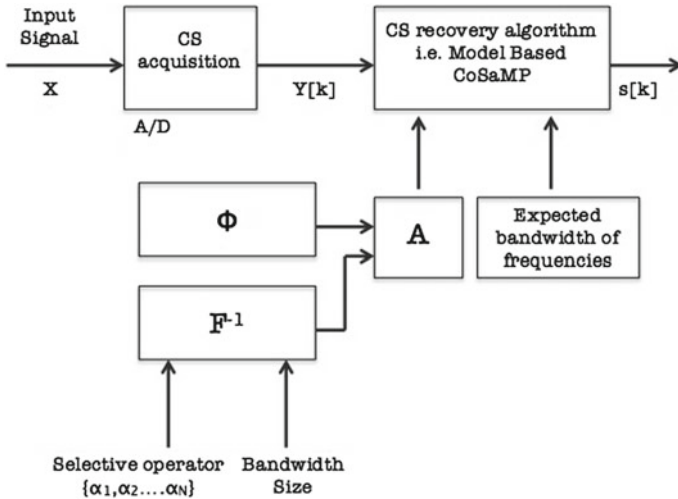


Fig. 7.2 The system block diagram of how selective spectrum sensing is implemented. The quantized signal $y[k]$ sampled by compressive means is recovered via a biased matrix, depicted by A . The recovery algorithm needs both the A and the expected bandwidth of the inverse Fourier matrix F^{-1} and is biased by the input parameters α which take on either a high value or low value, similar to a binary process. This combined with the bandwidth of interest as an input allows the construction of the biased Fourier matrix

7.3 Simulation Results

In our simulation we explore two key aspects. The first one involves the recovery of a signal spanning a wide band i.e. 0–20 GHz and the second is to show that we can selectively sense frequency bands of interest (i.e. GSM signal uplink band) within the wide band with improved mean square error (MSE) in a high noise environment.

In both the simulations we used four CS recovery algorithms, viz. Basis Pursuit (BP), Orthogonal Matching Pursuit (OMP), Compressive Sampling Matching Pursuit (CoSaMP) and Model Based CoSaMP (MB-CoSaMP). Those can be categorized as either iterative or greedy (see Sect. 3.2). In these simulations we show that using the MB-CoSaMP algorithm, provides improved spectral estimation capability compared to the other algorithms.

7.3.1 Case 1: Wide Band Spectrum Recovery

An input signal with a wide band support was considered throughout the simulation, consisting of $M = 9$ randomly located non-overlapping carrier frequencies f_n with bandwidths of $B_n = 0.50\text{ MHz}$ varying with different magnitudes. The received signal $x(t)$ is sampled via a random sampling scheme which is sub-Nyquist. Signal

generation scheme closely follows that of [168].

$$x(t) = \sum_{n=1}^M \sqrt{E_n} \cdot B_n \cdot \text{sinc}(B_n(t - \Delta)) \cdot \cos(2\pi f_n(t - \Delta)) + w(t)$$

The signal is modelled in such a way as to generate a signal in the frequency domain that replicates the convolution of M delta functions convolved with a rectangular function. The signal model contains a Sinc function which is defined as $\text{sinc}(t) = \frac{\sin(\pi t)}{\pi t}$. Δ denotes time delay of the signal which also introduces phase shift and E_n includes different receive powers. The term $w(t)$ represents additive white Gaussian noise (AWGN) to simulate instrumentation and channel noise. The magnitude of the received power E_n remains the same throughout the sampling period of T_s . Since the signal has a bandwidth of 20GHz the sampling time was chosen to be $2\mu\text{s}$. As is the case with the conventional Nyquist sampling scheme this equates to $2WT_s = 80\ 000$ number of samples (i.e. M). However, by using CS recovery techniques i.e. MB-CoSaMP [19] the number of samples (i.e. N) can be reduced to well below 8000 samples with adequate probability of recovery.

Figure 7.3 illustrates the estimation performance of the generated signal power spectral density (PSD) as well as the CS recovered PSD, using the recovery algorithm in [19]. The CS recovered signal, represented in red, shows that the spectral information of the input signal is well recovered for almost all active sub-bands in a high noise environment (i.e. SNR=2dB). This claim is substantiated by the normalized Mean Squared Error (nMSE) which was found to be lower than 8.9×10^{-2} . This is within acceptable range for most electronic defence applications. However,

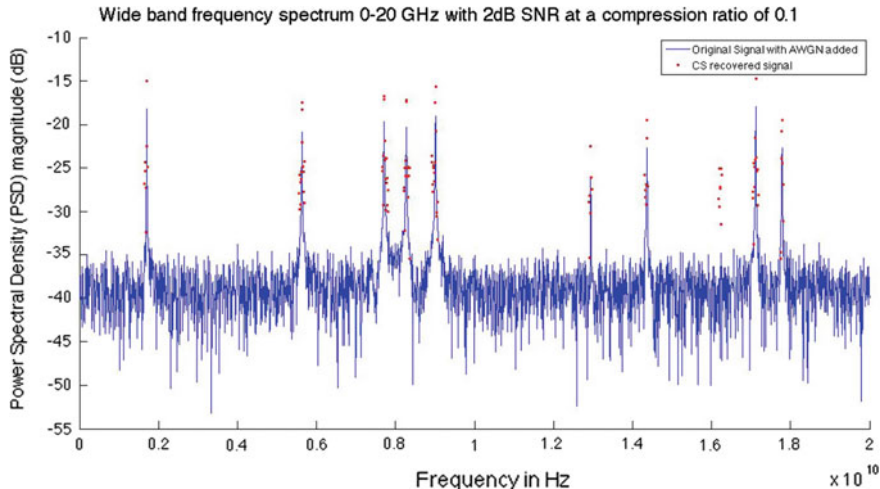


Fig. 7.3 Figure showing the power spectral density (PSD) of the CS recovered signal and the original signal

Table 7.1 nMSE for different CS recovery algorithms varying the compression ratio's for spectral estimation of the wide band input signal

Algorithm	Compression Ratio (M/N)		
	0.5	0.2	0.1
BP	0.0980	0.4195	0.4425
OMP	0.0949	0.1045	0.253
CoSaMP	0.0960	0.1186	0.251
MB-CoSaMP	0.0204	0.0458	0.0891

the spectral magnitudes of the recovered signal are offset by a small amount introducing error in the magnitude of the estimation, but not in the frequency estimation. Performance degradation of the CS recovery spectral estimation, in terms of frequency and magnitude, is observed with lower SNR environment i.e. ≤ 0 dB. The Comparative nMSE for the spectral estimation of all four CS recovery algorithms are shown in Table 7.1, highlighting the difference in error for different compression ratios. The compression ratio is given as M/N with M being the number of samples needed for CS recovery and N being to the number of samples needed as required by the Nyquist criteria for signal acquisition. For all the compression ratios the MB-CoSaMP recovery algorithm results in the lowest nMSE which motivates its use in selective spectrum sensing and holds the most promise for better recovery of a wide spectrum.

7.3.2 Case 2: Selective Spectrum Sensing

For the selective spectrum sensing case, we consider the same wide band signal, with an added GSM 900 uplink band that is at a carrier frequency of 898.5 MHz with a bandwidth of 25 MHz. We condition the matrix \hat{F} as in Eq. 7.1 according to the GSM band of interest as well as adjusting the recovery constant for the block sparsity in the MB-CoSaMP algorithm to the bandwidth of the signal of interest.

As mentioned in Sect. 3.2 there are numerous CS algorithms that can recover a sparsely populated spectrum. This being the case, four algorithms were chosen on the basis of the criteria defined in this Chapter and Sect. 3.2, namely BP, OMP, CoSaMP and model-based(MB) CoSaMP. We have shown that out of these four the best performing one for wide band application is the model-based CoSaMP. So we focus on improving the error in spectral recovery using this algorithm. The other algorithms, serve to provide comparative results and a measure for system performance statistics. The graphs detailed below, follow the same structure, whereby a pair of graphs are shown for either a high, medium or low SNR environment; with the first graph illustrating the nMSE of all the recovery algorithms using normal recovery and the second, with our approach of selective spectrum sensing applied to the recovery process.

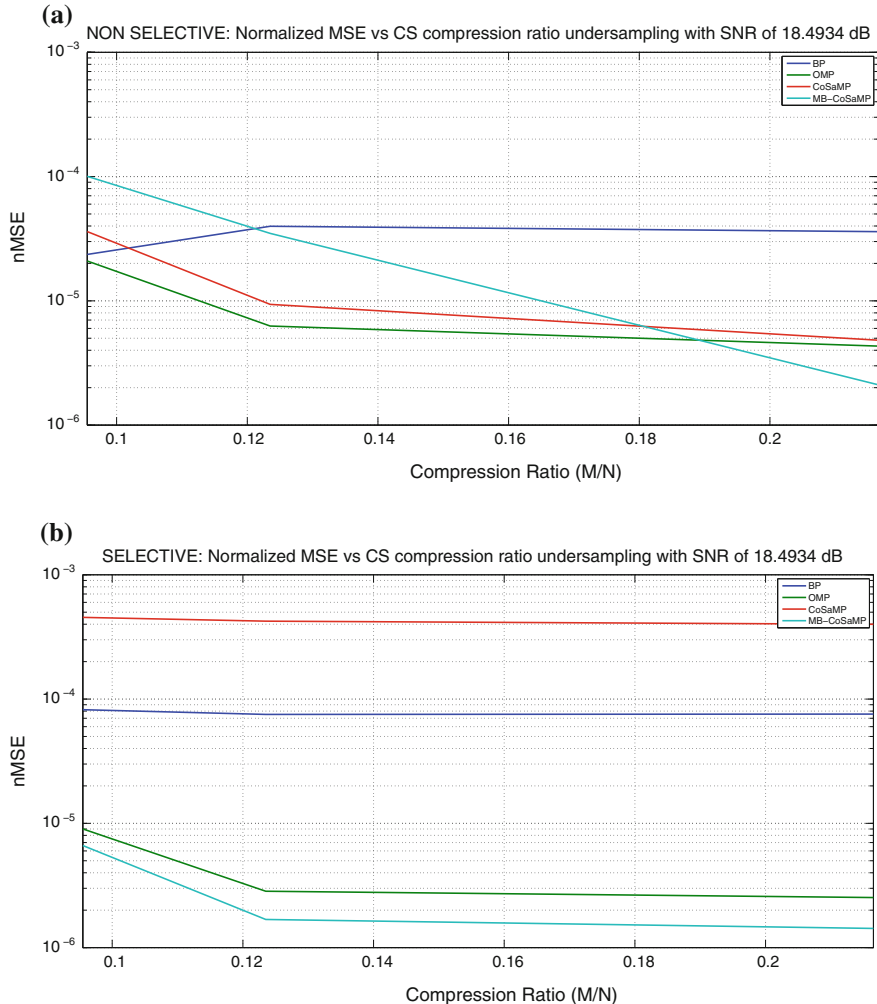


Fig. 7.4 Normalized mean squared error (nMSE) for sampling compression ratio less than 0.2. For non selective sensing **a** and selective sensing **b** as described in Sect. 7.2 for a high SNR environment, i.e. 18 dB

In these simulations we only consider the nMSE related to the recovered signal of the selected GSM band of interest that forms part of the wide band spectrum i.e. 0–20 GHz, such as in Sect. 7.3. In other words, any error of spectral recovery from other frequencies do not contribute to the final nMSE values associated with the recovered CS signals. Comparing the pairs of plots as shown in the figures above we observe that regardless of the SNR environment, when Selective Spectrum Sensing is applied the normalized mean squared error (nMSE), conditioned to the sampling

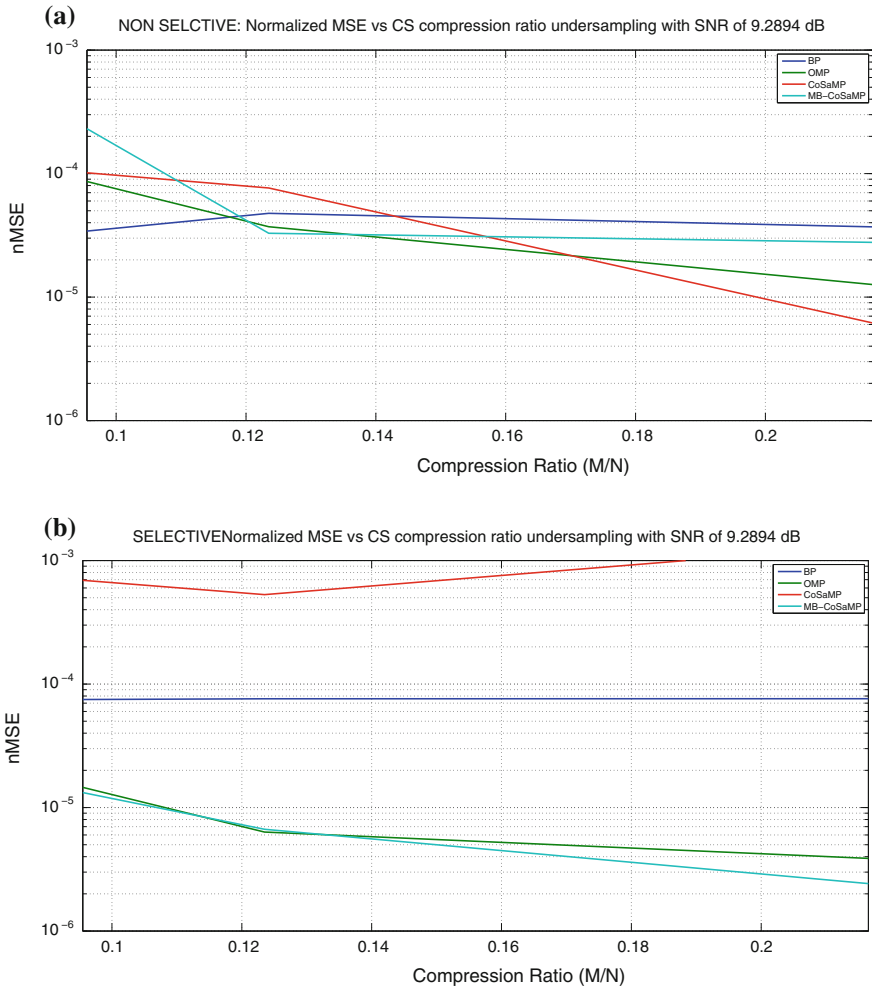


Fig. 7.5 Normalized mean squared error (nMSE) for sampling compression ratio less than 0.2. For non selective sensing **a** and selective sensing **b** as described in Sect. 7.2 for a medium SNR environment i.e. 9dB

compression ratio improves. This results in more accurate estimation as denoted in Sect. 7.2. Also, by applying selective spectrum sensing in the recovery stage provides robustness in higher SNR environments (Figs. 7.4b, 7.5b and 7.6b).

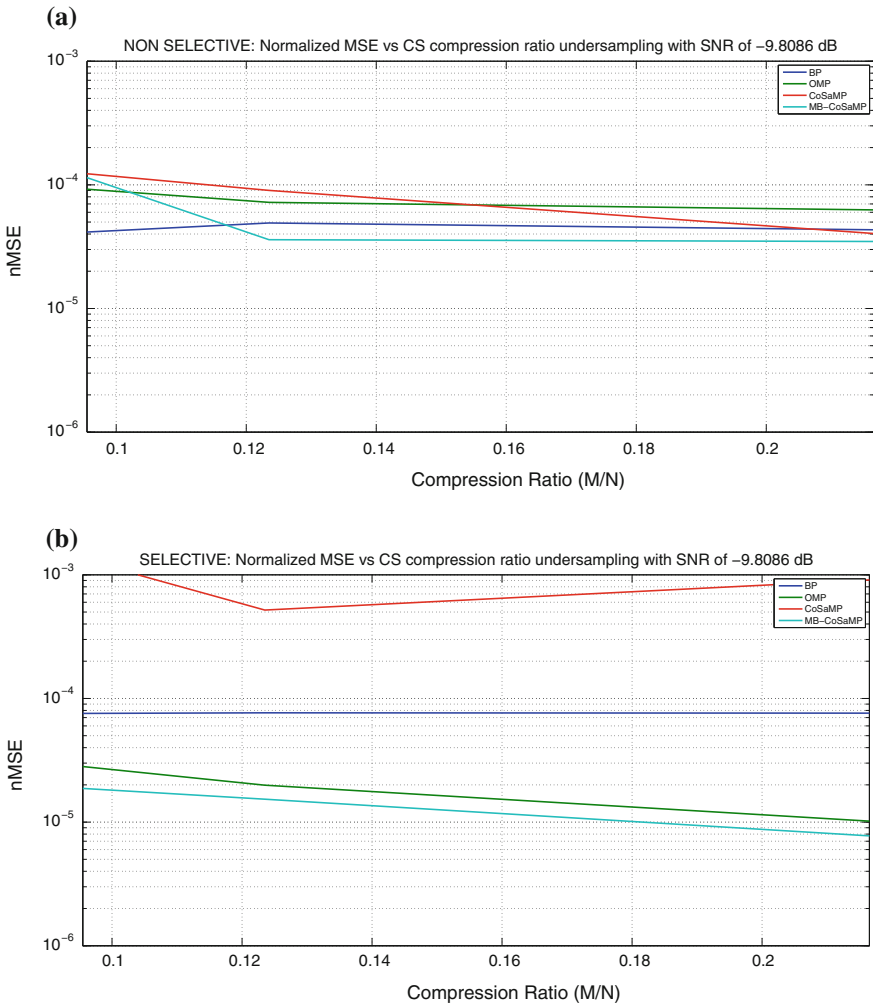


Fig. 7.6 Normalized mean squared error (nMSE) for sampling compression ratio less than 0.2. For non selective sensing **a** and selective sensing **b** as described in Sect. 7.2 for a low SNR environment i.e. -9 dB

Part CXVI

Concluding Statements and Appendices

Chapter 8

Concluding Remarks

In this work we have covered the framework for electronic defence (ED) operations and system requirements of current electronic support (ES) receivers, with specific focus on how to use existing receiver types/architectures to aid in a theoretical implementation of compressive sensing (CS) techniques. More specifically, we identified two main areas within the ES framework where CS can be implemented, namely communication based direction of arrival (DOA) estimation and spectrum sensing, and investigated the efficacy of both CS methods.

The efficacy of both the CS methods of implementation are summarized herein separately, followed by a brief discussion on scalability in the ED domain.

8.1 CS Based DOA

8.1.1 Accurate Phase Recovery Achievable Using Orthogonal Matching Pursuit (OMP)

Within the scope of greedy CS algorithms utilized for CS recovery, OMP yields an improved MVUE phase recovery performance for both 2FSK and 2PSK input signal for low SNR ranging 0–5 dB and CR as low as 3 %. We therefore assert that OMP is the optimal CS greedy algorithm to use for our CS DOA estimation method.

8.1.2 Demodulation Capability via CS Recovery for 2FSK Signals

Demodulation is possible using shift keying sensing matrix for CS recovery of 2FSK input signals, but not 2PSK. The demodulation corresponds to the probability of

detecting (PD) the correct binary index estimate (BIE), which requires a CR $\geq 15\%$ and OMP for successful CS recovery estimates. Demodulation using BIE can be performed in a low SNR environment (i.e. $SNR \geq -5$ dB).

8.1.3 Equivalent Computational Performance of CS DOA as for Conventional DOA

The use of CS-recovery on our uniform linear array (ULA) CS DOA architecture yields equivalent computational performance compared to a conventional FFT scheme for both 2FSK and 2PSK signals. The computational performance, in terms of time complexity, only remains equivalent if the sample size of input signals remain lower than 1024 samples, requiring CS sampling to have a CR = 1 % to the number of samples required by Nyquist sampling.

For larger sample lengths of 2PSK and 2FSK signals than 1024 samples, the conventional FFT based DOA estimation scheme requires less computation, resulting in faster processing. Thus for larger sample lengths the CS DOA estimation does not yield similar computational performance to conventional DOA estimation methods.

8.1.4 Higher Accuracy of DOA Estimates for CS DOA Than Conventional DOA for Low SNRs

For low SNR values (i.e. $SNR \leq 5$ dB) and CR $\geq 1\%$ the CS DOA ULA₁₀ provides the most accurate DOA estimation over the conventional DOA method by an improvement factor of $IF_{max} = 16.2$ for 2FSK signals and $IF_{max} = 13$ for 2PSK signals. For higher SNR values the CS DOA estimation and conventional DOA estimation scheme tend towards equivalent accuracy performance.

8.1.5 Reduction of Memory Required Using CS DOA Estimation

For all the various parameters considered to determine an operational range for CS DOA, a large memory reduction for adequate system operation can be obtained through out. The memory reduction for the best case using CS DOA ULA₁₀ only requires 1 % of the total number of samples required by a conventional Nyquist sampled DOA estimation method.

The large reduction of memory required by CS DOA does not result in degradation to DOA accuracy, in fact the accuracy is equivalent to conventional DOA for high SNR and improved for low SNR scenarios.

8.1.6 Scalability of CS DOA Estimation for Electronic Support

Both 2PSK and 2FSK are sufficiently representative as modulation types for application in our CS DOA method. However, direct application of 2FSK and 2PSK modulated signals in ES systems are rare, in current communications systems. The intent in choosing these digital modulation types were that they form the fundamental building blocks for more complex digital modulation schemes. Thus, if shown to perform sufficiently well for stand-alone CS application, it would merit further development for higher ordered of N -ary modulation.

The applications where 2FSK is currently used for electronic communication in ES comprise GSM, Bluetooth 1 and FMCW (Frequency Modulated Continuous Wave Radar), whereas for 2PSK the applications comprise wireless LAN standard (IEEE 802.11b.1999 basic rate) and Bluetooth 2.

For practical RF application of our CS DOA method for ES tasks can be achieved for GSM application as discussed in Sect. 6.4. Moreover, GSM uses GMSK for modulation which can be described as a spectrally efficient and coherent form of 2FSK which would require minimal development for CS DOA. However, for practical applications synchronization, multiple access and other signal characteristics will have to be considered for full operational deployment. If the TDMA bursts can be synchronized across the RF carriers for the entire GSM operational bandwidth of 25 MHz, it would allow our CS DOA estimation method to determine the direction of 992 channels spanning a DOA of 180° using a ULA.

8.2 CS Based Spectrum Sensing

CS selective spectrum sensing as a wide spectrum sensing method can improve spectral error recovery in severe signal to noise ratio (SNR) conditions as well as improve computational costs. It is important to highlight that this can only be achieved based on the a priori knowledge of the spectrum, which in most scenarios for ED systems are available. And as motivated earlier, the model based CoSaMP recovery algorithm, for our implementation, is well suited for spectrum sensing applications and result in an improved recovery of the wide band spectrum as compared to other CS algorithms.

8.3 Final Remarks

Both implementations of CS for ES tasks have yielded practical and system performance benefits for ES receiver systems which only realize for specific cases and are subject to special conditions. However, our modest addition to the literature, by successfully using CS methods for ED tasks shows the scalability of current CS theory, and we are confident that further investigation of CS, as a new signal processing method, can aid hardware and software performance for ED systems.

Chapter 9

Appendix: Some Useful Theoretical Background

9.1 Electromagnetic Waves

The operation of using electromagnetic radiating fields to transmit encoded energy (i.e. data) over a distance, for our purpose, can be expressed¹ in the following way, consider a source EM radiating element (i.e. antenna) located at an origin point in space. A signal generated from such a point using an *isotropic* omni directional antenna, radiates into free space as an ever-expanding sphere [39] which then is able to interact with another resonating elements (i.e. receiver antenna). This expansion of the field is called EM propagation and for illustration purposes detailed in Fig. 9.1.

At a significant distance from the transmit antenna the spherical wave-front starts to approximate a planar wave which is known as the far-field distance and calculated in meters by $R_{ff} = \frac{2D^2}{\lambda}$ m, where D is the antenna aperture and λ is the wavelength.

From this far-field distance, the radiated electrical field of an arbitrary field can be expressed in the following way

$$\bar{E}(r, \theta, \phi) = [\hat{\theta}F_\theta(\theta, \phi) + \hat{\phi}F_\phi(\theta, \phi)] \frac{e^{-jk_0r}}{r} \text{ V/m.} \quad (9.1)$$

$\bar{E} \rightarrow$ The electrical field

$\hat{\theta}, \hat{\phi} \rightarrow$ Are unit vectors according to the spherical coordinate system

$r \rightarrow$ The radial distance from the origin

$k_0 = 2\pi/\lambda \rightarrow$ The free space propagation constant

$\lambda = c/f = 3 \times 10^8/f \rightarrow$ The wavelength, dependant on the frequency (Hz)

$F_\theta(\theta, \phi), F_\phi(\theta, \phi) \rightarrow$ Are the pattern functions

¹Theoretical work was modified and sourced largely from the following sources, [3, 143, 181]. For further detail, we refer the reader to the literature listed.

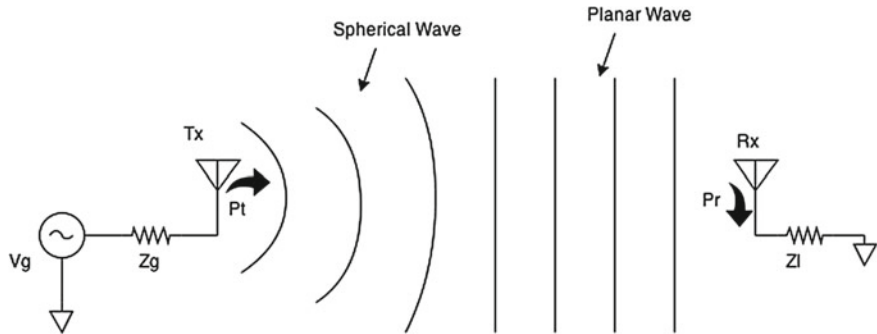


Fig. 9.1 Far field distance and the propagation dynamics needed from both, transmit and receive systems. (Modified by the authors from [143])

In other words, considering the transverse electromagnetic wave equation in (9.1), the electrical field propagates in the radial direction with a phase function of e^{-jk_0r} , an amplitude of $1/r$, and polarized in either ϕ or θ directions [143]. Also, according to Maxwell's equations, we know that any propagating electrical field has an associated magnetic field that can be formalized using (9.1) where H and E denote the respective magnetic and electrical fields.

$$H_\phi = \frac{E_\theta}{\eta_0}, \quad (9.2)$$

$$H_\theta = \frac{E_\phi}{\eta_0}, \quad (9.3)$$

where $\eta_0 = 377 \Omega$ and is also referred to as the wave impedance of free space. Furthermore, the poynting vector [80] which stipulates the directivity of the electromagnetic field is given by the cross product of the electric and magnetic field vectors, as shown below.

$$\bar{S} = \bar{E} \times \bar{H} \text{ W/m}^2 \quad (9.4)$$

9.2 Receiver Components: Background

9.2.1 Antennas

In all ES receiver systems the purpose, namely the multiple tasks that a designed receiver system needs to execute, determines which antenna will be used [1] as part of the RF front end system. This desired propagation intent, in part, is the reason for a single or multiple antenna implementation of various ES systems. The requirements stipulating the type of antenna to be used are determined by numerous variables

Table 9.1 Typically used antenna performance parameters. Taken from [1]

Term	Description
Gain	The increase in signal strength (commonly stated in dB) as the signal is converted by the antenna from EM radiation to a voltage signal $(G = \frac{4\pi A_{eff}}{\lambda^2})$
Frequency	The coverage or range of frequency over which the antenna can receive or transmit signals, whilst providing the required parametric performance
Bandwidth	The frequency range of the antenna in units of frequency. Often stated in terms of percentage bandwidth [$100\% \times (\text{maximum frequency} - \text{minimum frequency})/\text{average frequency}$]
Polarization	and the orientation of the E and H waves transmitted/received. Mainly vertical, horizontal, or right- or left-hand circular
Beamwidth	The angular coverage of the antenna, usually in degrees, depicted by spatial radiation pattern plots in terms of degree (deg) and decibels (dB) related to azimuth and elevation
Efficiency	The percentage of signal power transmitted or received compared to the theoretical power from the proportion of a sphere covered by the antenna's beam

known as antenna performance parameters, detailed in Table 9.1, which are consulted when selecting an antenna. Performance requirements of antennas are extensive and continually developing in the antenna design literature [14, 95, 181].

Most antennas, regardless of the application, can be categorized according to the directivity of receiving or transmitting signal [37], therefore an antenna is either defined as omnidirectional or directional. Omnidirectional antenna have equal gain in a spherical/donut radiation pattern allowing for equal receiving and/or transmitting signal-strength from all angles [2]. Similarly directional antenna, as the name suggests, directs EM propagation in a specific direction for a required bearing, based on the design of the antenna. This directionality allows for higher gain along the bore-sight direction² (See Fig. 9.2.).

Varying types of antennas have been developed as part of the proliferation of application and technology. Figure 9.3 details typical antenna used for ED and ES systems. Although numerous types of antenna exist, as suggested earlier, the application dictates the choice of the antenna. From an application perspective with respect to ES tasks such as direction finding (DF) and interception, RF receivers mostly make use of omnidirectional antenna with high gains.

²Bore-sight describes the direction at which the antenna is pointing.

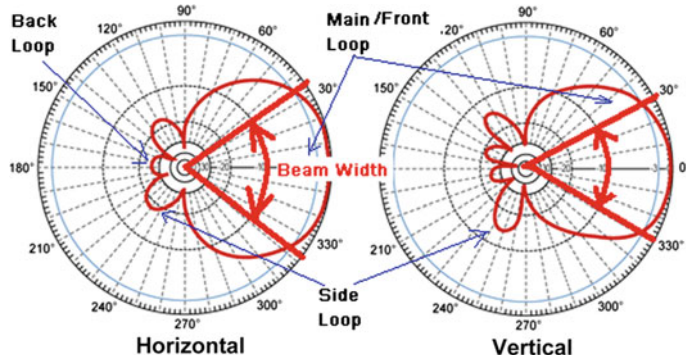


Figure 1.3 Antenna Radiation Pattern

Fig. 9.2 Common radiation pattern, in azimuth (*Horizontal*) and elevation (*Vertical*) planes. Sourced from [24]

When given a specific operating frequency range for a ES system, namely the VHF-UHF bands for our application, the choice of antenna becomes simple. The only antenna that meets this requirement are dipole, whip, loop, biconical or swastika antennas [1, 156] with the dipole, whip, and loop having narrow bandwidth coverage and the biconical and Swastika having large bandwidths (refer Fig. 9.3). The former antennas are more suited to direction finding tasks of narrow band signals and the latter more suited to wideband spectrum sensing for ES application.

Dipole antennas are preferred for DF-ES systems [60] due to their compact size, omnidirectional nature, narrow bandwidth and relatively high gain (refer Fig. 9.4). Hybrid omnidirectional wide bandwidth antennas (like biconical) are used as wide-band antennas for tasks such as spectrum sensing/monitoring. However, when a system requires more gain or directivity, a range of log periodic dipole arrays (LPDAs) are sometimes added [142].

9.2.2 RF Front-End Systems

In radio frequency circuitry the term ascribed to the analog components between the antenna and digital baseband systems (intermediate frequency - IF) are known as the RF front end [39]. The RF front end is standard with the first stage of most RF receiver systems, with exception to direct sampling systems that do not down-convert the signal [5] to IF. When the receiver chain of an ES RF front end system is designed, the typical system blocks used in the process can be accurately described by components common to the super-heterodyne architecture (SHA) (as shown in Fig. 9.5).

Numerous advances have been made in the domain of RF design and processing in the recent years, for example, the advent of software defined radio (SDR) and

Antenna Type	Pattern	Typical Specifications
Dipole	EI  Az 	Polarization: Vertical Beamwidth: 80° x 360° Gain: 2 dB Bandwidth: 10% Frequency Range: zero through μ w
Whip	EI  Az 	Polarization: Vertical Beamwidth: 45° x 360° Gain: 0 dB Bandwidth: 10% Frequency Range: HF through UHF
Loop	EI  Az 	Polarization: Horizontal Beamwidth: 80° x 360° Gain: -2 dB Bandwidth: 10% Frequency Range: HF through UHF
Normal Mode Helix	EI  Az 	Polarization: Horizontal Beamwidth: 45° x 360° Gain: 0 dB Bandwidth: 10% Frequency Range: HF through UHF
Axial Mode Helix	Az & EI 	Polarization: Circular Beamwidth: 50° x 50° Gain: 10 dB Bandwidth: 70% Frequency Range: UHF through low mmw
Biconical	EI  Az 	Polarization: Vertical Beamwidth: 20° x 100° x 360° Gain: 0 to 4 dB Bandwidth: 4 to 1 Frequency Range: UHF through mmw
Lindenblad	EI  Az 	Polarization: Circular Beamwidth: 80° x 360° Gain: -1 dB Bandwidth: 2 to 1 Frequency Range: UHF through μ w
Swastika	EI  Az 	Polarization: Horizontal/ Vertical Beamwidth: 80° x 360° Gain: -1 dB Bandwidth: 2 to 1 Frequency Range: UHF through μ w
Yagi	EI  Az 	Polarization: Horizontal/ Vertical Beamwidth: 90° x 50° Gain: 5 to 15 dB Bandwidth: 5% Frequency Range: VHF through UHF
Log Periodic	EI  Az 	Polarization: Vertical or Horizontal Beamwidth: 80° x 60° Gain: 6 to 8 dB Bandwidth: 10 to 1 Frequency Range: HF through μ w

Antenna Type	Pattern	Typical Specifications
Cavity Backed Spiral	Az & EI 	Polarization: R & L Horizontal Beamwidth: 60° x 60° Gain: -15 dB (min freq) +3 dB (max freq) Bandwidth: 9 to 1 Frequency Range: μ w
Conical Spiral	Az & EI 	Polarization: Circular Beamwidth: 60° x 60° Gain: 5 to 8 dB Bandwidth: 4 to 1 Frequency Range: UHF through μ w
4 Arm Conical Spiral	EI  Az 	Polarization: Circular Beamwidth: 50° x 360° Gain: 0 dB Bandwidth: 4 to 1 Frequency Range: UHF through μ w
Horn	EI  Az 	Polarization: Linear Beamwidth: 40° x 40° Gain: 5 to 10 dB Bandwidth: 4 to 1 Frequency Range: VHF through mmw
Horn with Polarizer	EI  Az 	Polarization: Circular Beamwidth: 40° x 40° Gain: 4 to 10 dB Bandwidth: 3 to 1 Frequency Range: mmw
Parabolic Dish	Az & EI 	Polarization: Depends on Feed Beamwidth: 0.5° x 30° Gain: 10 to 55 dB Bandwidth: Depends on Feed Frequency Range: UHF to μ w
Phased Array	EI  Az 	Polarization: Depends on Elements Beamwidth: 0.5° x 30° Gain: 10 to 40 dB Bandwidth: Depends on Elements Frequency Range: VHF to μ w

Fig. 9.3 Different types of antenna and their respective characteristics in EW applications. (Taken from [1].)

Fig. 9.4 A typical tactical direction finding antenna that spans a frequency range of 20 MHz–3.6 GHz. Taken from [142]

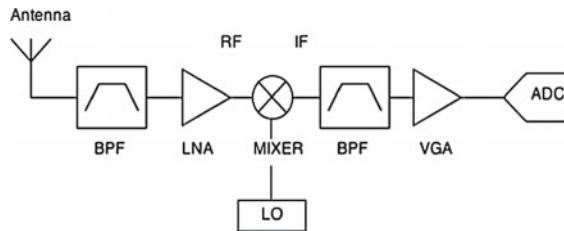


software radio (SWR) [177]. These systems still depend on a modified version of a super-heterodyne architecture to acquire/quantize RF signals. In addition most SWR applications are still not realizable due to limitations on ADCs. This limitation shows how crucial RF front end systems are and suggests that RF front end systems are inseparable for most current technologies (Table 9.2).

The super-heterodyne receiver (SHR) architecture, as seen in Fig. 9.5, is a common model of the front end system. It describes all the individual system blocks that form part of virtually all RF receiver front end systems. Different hybrid forms of RF front end systems, stemming from SHR architecture, exist due to the proliferation of microwave and circuit advances [157]. Such hybrid systems implement multi-stage mixing, filter, amplification stages [80], channelizers, and filter banks [58, 97, 125, 178]. Most of these modifications are done in an attempt to improve RF reception and processing of signal and nowadays manufactured as standard on-chip packages [157].

9.2.2.1 Filter

Filter stages applicable for ES in RF front end systems perform the task of rejection of unwanted frequencies bands, attenuating undesired mixing frequency artefacts (see Sect. 9.2.2.3) and setting the IF bandwidth of the receiver [157]. Filters can be described as two-port networks used to maintain and control the frequency response in RF systems by only allowing transmission of frequencies within the passband [143]. As Fig. 9.6 shows the characteristics that define the filter frequency response can be categorized into three figures of merit, namely the passband, transition-band, and stop-band.



BPF - Band pass filter

LNA - Low Noise Amplifier

Mixer - Using a tunable local oscillator (LO)

IF - Intermediate Frequency

VGA - Variable Gain Amplifier

ADC - Analog-to-Digital Converter

Fig. 9.5 Illustrates the typical RF front end sub-systems shown in block diagram form which constitute a theoretical RF receiver

Table 9.2 Describing the most important system blocks that comprise the RF front end

System block	Description
Antenna	Form the crucial step of converting EM energy into electrical voltage
Amplifiers	Apply a gain (dB) to low strength received signal artefacts to the required power levels to be processed for system tasks (i.e. identifications, transformation, detection)
Filters	Perform the necessary filtering by biasing certain bandwidths of interest
Mixers	Due to the high frequency that RF signals propagate at, it is necessary to convert down convert the signals to manageable frequencies to digitize for digital processing. This is done by mixing stages

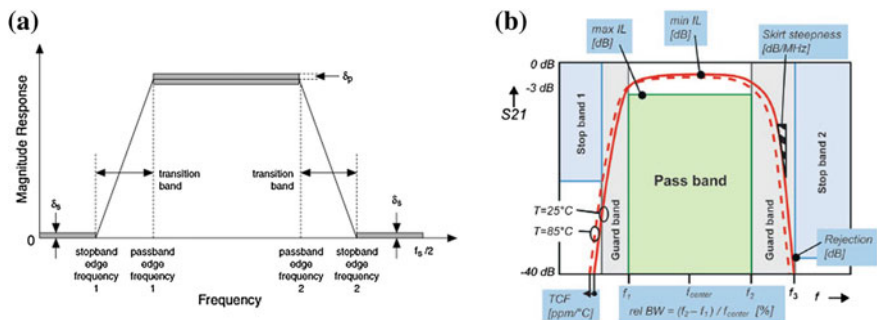


Fig. 9.6 A typical frequency response for a bandpass filter, shown as part of the design process, indicating the respective bands. The ripple effects in (a) are denoted by δ_p & δ_s . Taken from [74]

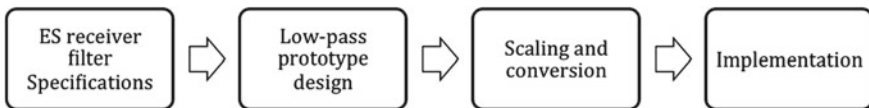


Fig. 9.7 Shows the process system blocks used for filter design by the insertion loss method. (Taken from [143].)

Filters comprise of discrete resistive, inductive and capacitive networks that operate to form the desired frequency response needed by the filter specifications. The use of new material, novel filter design, and manufacturing processes are vast and detailed within the open literature. However, our concern involve operational parameters of filters that need to comply with the requirements of RF receiver in ES systems. These parameters involve the attenuation, ripple strength, phase characteristics and transition band roll off [157]. Furthermore the design process commonly used in designing such filters are known as the insertion loss method detailed in [143, 151] and shown by means of systems blocks in Fig. 9.7.

9.2.2.2 Amplifiers

Amplifiers in an RF front end, performs the pivotal task of applying gain to the signal of interest (SOI) before it reaches the digital domain for further signal processing. Both the design and implementation advances of these systems have come a long way from the initial beginnings in the mid 1900s [92].

Currently, most amplifiers use three-terminal solid-state devices which include; silicon or silicon-germanium bipolar junction transistors (BJT), field effect transistors (FET), complimentary metal oxide semiconductors (CMOS) and high electron mobility transistors (HEMTs) [66, 80, 181]. These devices have resulted in improved gains, dynamic range, and bandwidth performance with amplifiers operating at frequencies up to 100 GHz [157].

Both the RF and IF stage amplifiers sometimes comprise of multiple amplification stages [143] which work in unison to improve gain linearity across the frequency band of interest [181]. The RF amplifiers (i.e. low noise amplifiers- LNAs) increase the power of weak received signal after the filter stage, as mentioned earlier in Sect. 9.2.3, in order to increase dynamic range of the transmitted signal relative to noise which compensates for loss due to the signal propagation. As is the case for most interception tasks, the signal to noise ratio (SNR) is relatively low (e.g. <-5 dB) [156] due to noise levels overpowering the signal content. Different amplifier designs are used to improve the SNR to result in a signal level that is sufficient for operations like detection, identification and classification to be performed with high confidence levels.

In the design stage of an amplifier there are certain operational parameters that need to be consulted to ensure the required performance of an amplifier refer to Table 9.3.

Table 9.3 Describing the important system blocks that comprise the RF front end

Term	Description
Noise figure	The measure of degradation due to noise effects by RF components on the actual signal noise. Mostly caused by device thermal noise and measured in dB using the input and output SNR ratio
Gain	The measure in dB of the amplification added to the input signal. Typically measured by the input and output power figures
Bandwidth	The frequency band at which the amplifier is operational, centered at the operational frequency. Typically, amplifiers have a limited bandwidth wherein they are able to provide the designed gain. This bandwidth is determined by the stability of the system, which is calculated using stability circles and smith charts, as in [143]

Typical the amplifier stage³ in an ES receiver need to have a gain ≤ 60 dB and a bandwidth > 60 MHz [156] to deal with sensitivity and range requirements, which are detailed in Sect. 9.4.1.

9.2.2.3 Mixing

Mixers are used in receiver system as frequency converters, modelled as a 3-port-device and intentionally taking advantage of non-linear characteristics of diodes or transistors to enable frequency conversion [181]. Even though it might not seem obvious initially, frequency conversion is necessary due to the sampling rate limitation of ADC technology not matching the RF frequencies. In fact, to sample RF signal directly without the use of mixing would require double the sampling rate to match the highest frequency present in the received signal [128]. However, recent advances in techniques such as direct sampling have been shown to be effective for frequencies up to 2–5 GHz [167], removing the need for mixers.

Traditionally mixer technologies depended on diodes to implement signal mixing, however nowadays mixers are predominantly dependant on more effective and reliable solid state devices such as field effect transistors (FETs) [66].

A mixer, as shown in terms of the symbol and functional blocks in Fig. 9.8, receives the RF signal (f_{RF}) and convolves a local oscillating frequency (f_{LO}) signal which

³Most amplifiers are manufactured as on-chip integrated circuits (IC's) [77]. This places the emphasis on the task of choice of components rather than design. The design process, serves to arrive at the required system specifications.

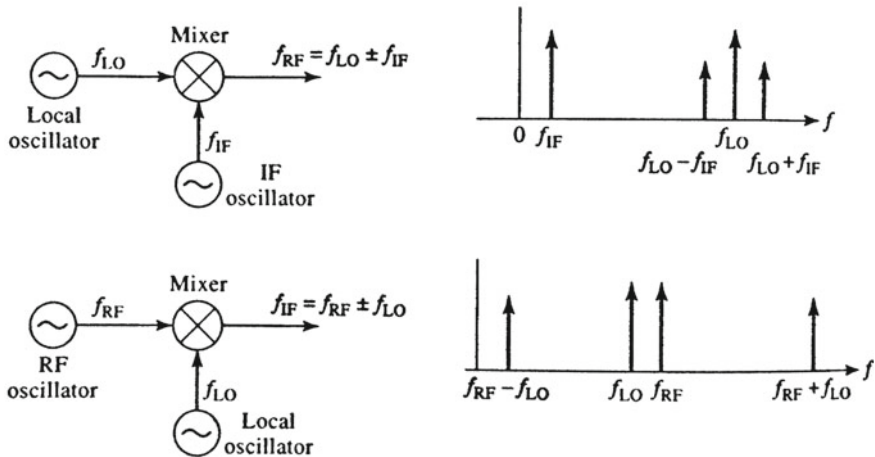


Fig. 9.8 The final outputs in terms of frequency plots of up conversion and down conversion implemented by a mixer. Sourced from [143]

produces an output signal (f_{IF}) usually known as the intermediate frequency (IF) signal which comprise the sum and difference of the input frequencies.

Mixers can be utilized for up conversion and down conversion of a signal dependent on the desired tasks. Following the notation as specified before, the determination from first principles follows. Consider the case when the received signal is down-converted. The input RF signal is

$$x_{RF}(t) = A \cos(2\pi f_{RFT}), \quad (9.5)$$

and it is modulated with the local oscillator at a specific frequency using the mixer

$$x_{LO}(t) = B \cos(2\pi f_{LOT}). \quad (9.6)$$

The output signal produced is the intermediate frequency output in terms of the sum and the difference of the respective input signals (in frequency domain). Conversely, the same holds true for frequency up conversion, however as it is predominantly used for transmitting purposes it is not used in the receiver chain.

Time Domain The time domain mathematical representation of down conversion mixing shown below.

$$x_{IF}(t) = C \cos(2\pi f_{RFT}) \times \cos(2\pi f_{LOT}) \quad (9.7)$$

$$= \frac{C}{2} [\cos(2\pi(f_{RF} + f_{LO})t) + \cos(2\pi(f_{RF} - f_{LO})t)] \quad (9.8)$$

Frequency Domain The frequency domain mathematical representation of down conversion mixing shown below.

$$X_{IF}(\omega) = K\pi\delta[(\omega - \omega_{RF}) + (\omega + \omega_{RF})] * [\pi\delta[(\omega - \omega_{IF}) + (\omega + \omega_{IF})]] \quad (9.9)$$

The effect of down conversion in the frequency domain is shown in Fig. 9.8 and detailed mathematically in Eq. (9.9). This frequency domain mixing can be represented, in terms of frequency, as the sum and difference of the inputs, $f_{IF} = f_{RF} \pm f_{LO}$. Here the sum is better known as the upper side band (USB) and the difference, the lower side band (LSB). When down conversion is applied it is important to note that the spectrum of the LSB and USB are conserved whereas in up conversion the LSB is inverted [157].

For consideration, in an ES receiver, the desired IF output would be determined by the difference $f_{IF} = f_{RF} - f_{LO}$ which can be extracted using an appropriate low pass filter (LPF).

The derivation denoted above holds true for an ideal case. In real systems mixers will generate more artefacts due to non-linearity associated with individual components (e.g. voltage controlled oscillators VCOs), inducing unwanted harmonics and their effects [143]. Some of the effects on signal degradation involve image frequency, conversion loss, increase in noise figure, intermodulation distortion, and isolation.

All these factors account for system loss, frequency drift and spectral anomalies that can adversely affect the effectiveness of a receiver if not accounted for properly. Hence, mitigation of mixer effects form a crucial system consideration with respect to later signal processing stages.

9.2.3 Radio Frequency Propagation Operations

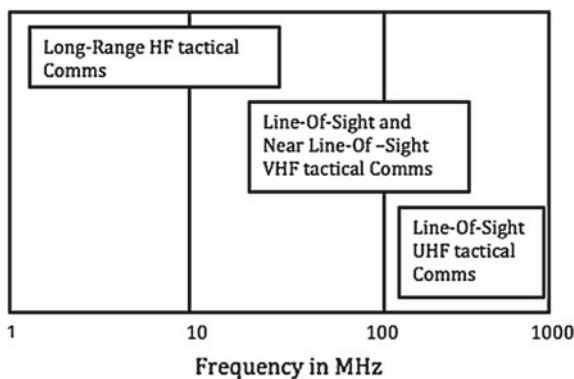
RF communication, for the most part, used for ES activities are restricted to frequency bands lower than 300 GHz, Table 9.4 indicates the current designation of bands as defined for ED purposes. It is important to note that most tactical communication operations primarily take place in the HF, VHF, and UHF and nowadays as communication bandwidths increase, in the SHF bands as well. Figure 9.9 details the typical communication link, tactical communications bands, and propagations modes used for ES communications.

It is well known that for different frequency bands, used for communication, different propagation properties apply [143]. The higher frequency bands (i.e. >100 MHz) rely on clear line of sight between the transmitter and receiver, whereas lower communication bands (i.e. HF) can leverage on propagation phenomena such as surface waves, reflected waves, and ducting [139] which do not rely on line of site (but do introduce reception complexities). Although higher frequency bands have a restriction of line-of-site for communication, they allow for higher bandwidth based communications and hence higher data transfer rates.

Table 9.4 RF band designation as defined in the ED domain [156]. These bands are defined differently depending on the domain

Frequency bands	Wavelength	Name	Designation
3–30 KHz	100–10 km	Very low frequency	VLF
30–300 KHz	10–1 km	Low frequency	LF
0.3–3 MHz	1 km–100 m	Medium frequency	MF
3–30 MHz	100–10 m	High frequency	HF
30–300 MHz	10–1 m	Very high frequency	VHF
0.3–3 GHz	1–0.1 m	Ultra high frequency	UHF
3–30 GHz	0.1–0.01 m	Super high frequency	SHF
30–300 GHz	0.01–0.001 m	Extra high frequency	EHF

Fig. 9.9 Illustrating the range of ED tactical communication conducted in the HF, VHF and UHF bands. Sourced from [2]



VHF and UHF bands have the advantage of being more predictable, and hence can be described more accurately by analytical expressions [2] which can be modelled to analyse the effects of propagation. Such propagation effects, for communication purposes above 100 MHz, include:

- Reflection (Due to ground and/or large objects) — Two-way propagation model,
- Diffraction (Due to edges and corners of EM conductive environment) — Knife-Edge propagation model,
- Scattering (Due to foliage or small objects) — Free Space propagation model, and
- Attenuation (Due to atmospheric events, i.e. different forms of precipitation) — Experimental Environment model.

Our focus, concerns communication that takes place in the higher frequency bands, namely VHF/UHF communications. Understanding the propagation phenomenon (i.e. power requirements, losses measured, and modes of propagation) in these bands are utmost. The review of lower communication bands (i.e. HF) propagation dynamics are excluded in this work due to the majority of communication signals of interest, for ES, operate at higher communication bands.

9.2.3.1 VHF/UHF Modes of Propagation

Propagation theory involves the means of modelling the environment through which a communication link is established. A communication link is set up between a transmitter (XMTR) and a receiver (RCVR), assuming a line-of-sight (LOS) link under good weather condition, as shown in Fig. 9.10. The signal strength, shown in dBm (typical notation for ED applications), leaves the transmitter at a specific dBm level which gets either amplified by the antenna or simply propagates from the antenna at unity gain (0 dBm), known as the emitted radiated power (ERP).

The EM signal propagates through the channel where it attenuates due to spreading losses and atmospheric losses associated with the link. Although this is a simple evaluation of the link losses, it adequately explains the general losses associated with propagation, other more complex forms of attenuation are considered later. Once the signal is received at the receiver antenna it is once again amplified and then processed at a dBm level proportional to the distance from the transmitter.

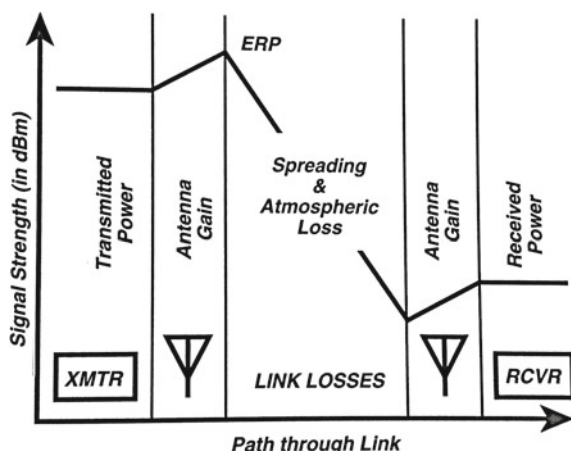
Free Space Propagation

Is the case where spreading loss is the only propagation loss considered in the model and reflection paths are minimal [2]. This loss usually applies to high altitude communication, high frequencies, and narrow beam-width antennas [80]. The typical equation associated with free space propagation determining the link losses, also known as the link equation is shown below in both normal and log form as well.

$$L = (4\pi)^2 d^2 / \lambda^2, \quad (9.10)$$

$$L = 32.44 + 20 \log(f) + 20 \log(d). \quad (9.11)$$

Fig. 9.10 Illustrating the propagation losses involved over a communication link....include db figures



Where

L	is the loss to the system in dB
d	is the distance between the transmitter and receiver
λ	is the wavelength, calculated from the frequency $\lambda = c/f$
32.44	in Eq. 9.11 equates to $20 \log(4\pi)$ which in realistic terms equates to a loss proportional to $1/R^2$ when considering free space propagation losses.

Two-Way Propagation

Is the case where significant reflective objects are in the vicinity of the communication link, usually ground reflections accounting for most of these losses [1]. When this is the case the two-way propagation model is commonly used to model the losses/gains correctly by using Eq. 9.12. The losses associated with this model occur when both the transmitter and the receiver are closer to earth's surface, which exclude most cases of air-to-air and air-to-ground links [156]. Moreover, the generic term describing most of these reflections, in the communication domain, are known as multipath [143]. The losses are detailed below in both forms, namely normal (9.12) and logarithmic (9.13). Overall propagation losses in approximate terms equate to a loss proportional to $1/R^4$ when dealing with ground reflection losses (i.e. multipath) [143].

$$L = (d)^4/h_t^2 h_r^2, \quad (9.12)$$

$$L = 120 + 40 \log(d) - 20 \log(h_t) - 20 \log(h_r), \quad (9.13)$$

where,

L	is the loss to the system in dB
d	is the distance between the transmitter and receiver
λ	is the wavelength, calculated from the frequency $\lambda = c/f$
h_t	is the height of the transmitter
h_r	is the height of the receiver
120	equates to a common dB amount associated to the transmit power (P_t), transmit antenna gain (G_t) and the receive antenna gain (G_r) - $\log(P_t G_t G_r)$.

In a typical ED scenario it is preferable to determine which propagation model must be used for the reception/interception of signals, which is commonly done by

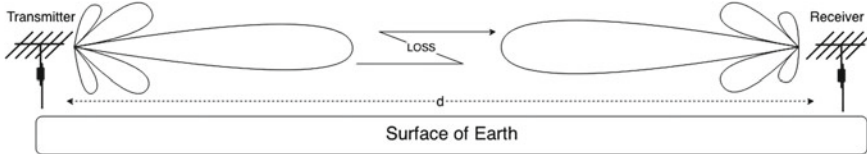


Fig. 9.11 Illustrates the propagation losses associated with the free space model, note that the height of the transmitter and receiver must be a significant height from the earth's surface for this model to be used [65]

calculating the Fresnel zone.⁴ If the communication link is within this zone, free space propagation losses are considered. If it is outside this boundary, two-way propagation losses are used [1].

ES propagation systems are typically designed for dynamic scenarios involving a vast number of established and potential interception links. Thus, the propagation models used are either free space, two-way, or knife edge propagation with the latter model involving a special case of defraction not pertinent to our focus for communication link propagation, and consequently only mentioned herein (Figs. 9.11 and 9.12).

9.2.3.2 Attenuation/Propagation Loss

Attenuation, as defined by [181] in terms of RF design principles, is the propagation losses experienced by a signal in the propagation path which cause signal power to decrease. Causes that contribute to such losses are attributed to atmospheric phenomenon, precipitation and man made structures [2, 143] with the former, commonly playing a major role in the design for ED systems utilizing higher frequencies for example, air-to-ground systems (satellite communication) and radar warning systems (RWR) [178].

Shown in Fig. 9.13 is the typical atmospheric attenuation to propagation per km for different frequencies, where operational frequencies below 10 GHz the propagation losses are negligible.

Due to our focus on VHF-UHF communication bands, the effect of man made structures add more of a significant propagation loss than atmospheric attenuation, which is known as fading.

⁴The Fresnel zone provides a means of calculating when reflected EM waves will arrive at the receiver, either in phase or out of phase, which consequently affects the loss or gain of the signal. The first Fresnel zone is where path-length phase shifts by 0–180° and in the second Fresnel zone path-length phase shifts 180–360° which can be calculated using the equation $F_n = \sqrt{\frac{n\lambda d_1 d_2}{d_1 + d_2}}$.

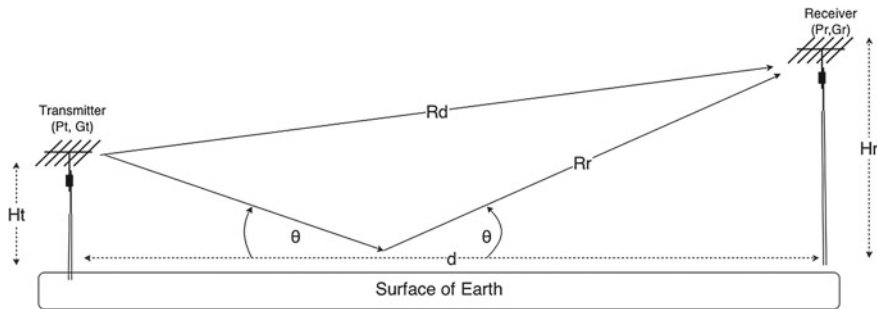


Fig. 9.12 Illustrating the propagation losses involved for the two-way model. Where $P_R = |v|^2/z_0 = P_t G_t G_r \frac{h_t^2 h_r^2}{R_d^4} e^{-j k_0 R_d}$ and $v \approx 2 c k_0 h_t h_r \frac{e^{-j k_0 R_d}}{R_d^2}$. Typically H_t and H_r are multiples of the propagation wavelength

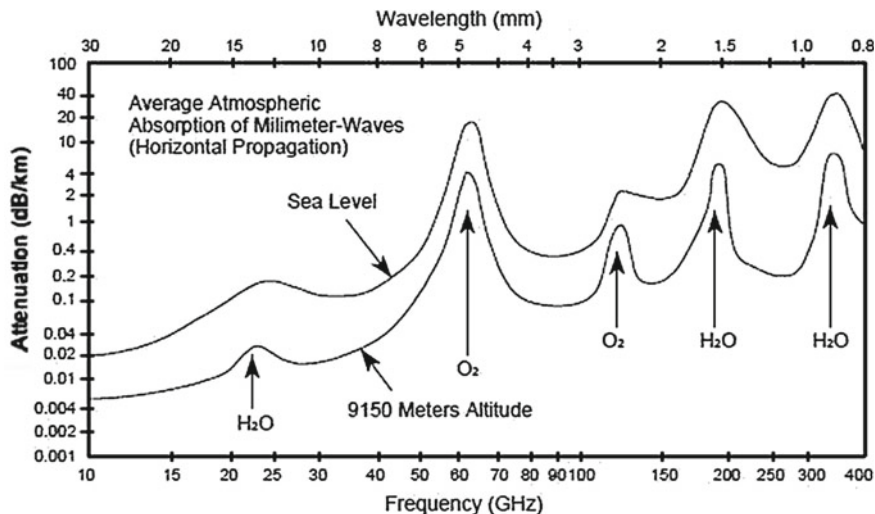


Fig. 9.13 Shows the propagation losses per km in dB for different frequency bands (horizontal polarization), sourced from [151]

9.2.3.3 Fading

Most mobile and land communication scenario aggregate around populated areas involving manmade structures (i.e. buildings, houses, cars etc.). This proximity to man made structures allow for multiple scattering, reflection, and diffraction to take place between the communication transmitter and receiver, causing fading [67].

Fading, is defined [36] as the phenomenon of small-scale variation to the magnitude and phase of the transmitted signal due to a line-of-sight (LOS) not being established. The result of fading causes the propagation of EM waves to rely solely

on reflection and defraction to arrive at the intended receiver point for communication.

The most widely used and accurate model in describing the statistical basis for radio signal propagation with no LOS, is the Rayleigh fading model [67]. This model allows for a possible ES system to compensate for the losses where mobile radio links, mobile phones, and tactical VHF bands exist. The Rayleigh fading model is used for ES systems for the following situations (sourced largely from [67]).

- Urban defence communication monitoring and direction finding as well as RCIED (Radio controlled improvised explosive devices)
- Tactical air to ground links i.e. where a airborne platform (helicopter) is at a low altitude.
- The receiver antenna is embedded in radio clutter,⁵ caused by close proximity to the ground.

The statistical model given in Eqs. (9.14) and (9.15) describe the fading distribution involved where, of the two, the CDF is more important as it relates the likelihood of a given value to be exceeded (Fig. 9.14).

The probability density function (PDF)

$$P(x) = \frac{x}{\sigma^2} e(-\frac{x^2}{2\sigma^2}) \quad (9.14)$$

The cumulative density function (CDF)

$$F(x) = 1 - e(-\frac{x^2}{2\sigma^2}) \quad (9.15)$$

As mentioned, the variation of a propagating signal (see Fig. 9.15) is quantified in terms of its standard deviation σ . In other words, using the Rayleigh model we can relate the probability of exceeding a needed signal strength value to the standard deviation of that signal strength in terms of dB. For our purposes—in ES—the typical value is 10 dB.

For a given scenario where a minimum of -80 dBm signal strength is required by a receiver (sensitivity level—see Sect. 9.4.1.2) and the propagation model indicates a short sector of -70 dBm, creating a 10 dBm margin and an availability of 0.9 probability at the reception point.

Considering the effects of attenuation and fading within the context of an ES receiver it should be noted, even though attenuation affects propagation losses, fading

⁵Radio clutter is a term attributed to structures that influence radio propagation creating spurious scattering signal.

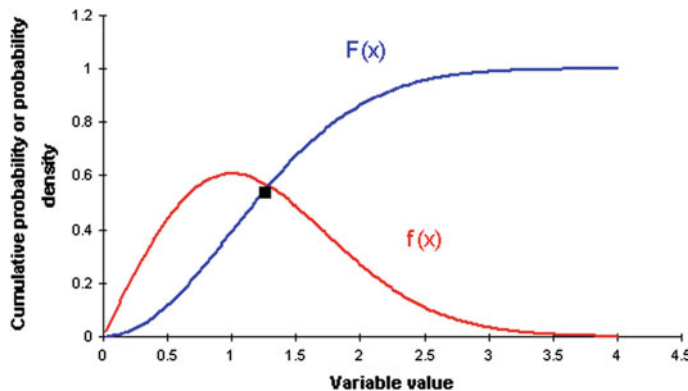
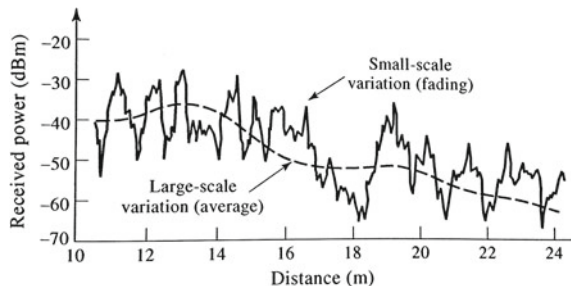


Fig. 9.14 The Rayleigh probability density function $f(x)$ and cumulative density function $F(x)$ with $\sigma = 1$. (Sourced and adapted from [65].)

Fig. 9.15 Received power of a typical receiver versus distance from the transmitter, showing the small-scale fading effects and the large scale variations, sourced from [143]



is more prevalent for interception techniques in ES due to its application in the communication bands which operate at less than 2 GHz, where there is less than 0.02 dB/km propagation losses. Multipath and Rayleigh fading cause variations in phase and magnitude that have the means of deteriorating tasks for ES receivers such as detection and direction finding.

Typical fading effects on ES receiver tasks can be summarized as follows:

- The effects of fading causes an increase in bit error rate for modulation schemes,
- The phase ambiguities caused by multipath, scattering, reflection, and defraction due to no line-of-sight reduce the ability of an ES system to determine the direction of a RF transmission source [149].

9.3 Typical ED System Configuration

A typical ED system does not exist as a stand alone system which can be standardized across all implementations of ED system application. Instead, an ED system's objective determines what is necessary and what will be deemed as redundant. In other

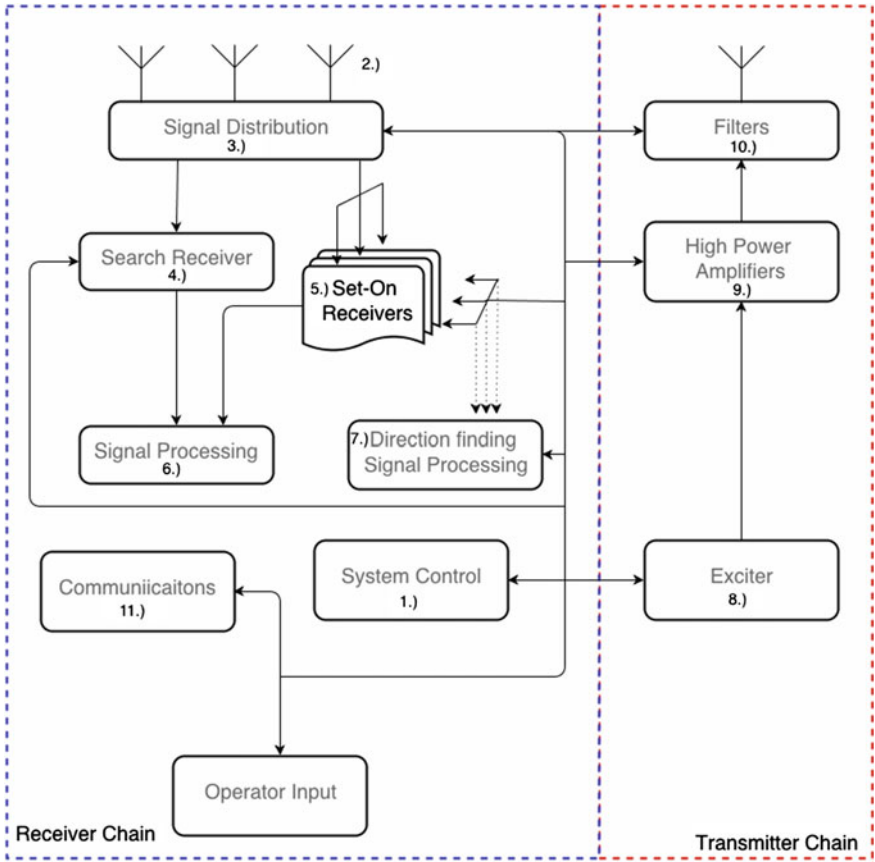


Fig. 9.16 Illustrates the differentiation, in terms of blocks, of operational functions within the implementation of a typical ED system. The *blue* block indicates the receiver components, while the *red* indicates the transmitter components. (Sourced from [3] and modified by the authors.)

words, if the only objective is to intercept a communication transmission, the receiver block of the ED system will be included and a transmitter block removed, due to its redundancy. However, from an overview perspective, the fundamental system blocks are illustrated here to describe the entire ED system chain not for a specific use only.

An ED system chain is illustrated in Fig. 9.16 and will be used throughout this discussion to draw attention to specific components and their purpose in ED, especially ES intercept systems for communication signal purposes. The blue dotted block indicates the systems pertaining to this body of work. A discussion of the individual system blocks are detailed below.

1. **System Control:** Deployment of such systems need a central hub that ensures that all sub-systems are coherent and synchronized to perform operational tasks [157]. Moreover, operations of control systems are typically performed using one

and/or several computers. These computers are either stand alone or distributed which communicate via a network.

2. **Antenna:** From the theory of Electromagnetism⁶ we empirically know that an antenna is an electrically conductive resonant material that extracts and facilitates propagation of electromagnetic energy through an unbounded medium [81] by converting EM energy to electrical signals that can be processed and interpreted. For the purposes of ED antennas enable transmission of signal via a propagation medium (i.e. air, free space), which enables tasks such as interception, direction finding and jamming (using high gain antennas) to be achieved. See Sect. 9.2.1 for further detail.
3. **Signal Distribution:** Regardless of the size of an ED system, it is imperative to have a splitting element to allow signal distribution to several receivers. Signal splitters are placed between the antenna and receiver system, with a typical impedance of 50Ω , requiring closely calibrated impedance matching [181]. This matching is done to reduce distortions between split signal channels and ensure different receivers receive the same signal with respect to gain, magnitude, and phase at the respective receiver systems.
4. **Search Receiver:** This system block, although generic and somewhat common, is crucial to spectral intelligence gathering in the ED receiver chain, specifically used to search the RF spectrum and characterize and classify sources of EM-RF energy [48]. Systems that form a crucial part of this block and add to the reception of the signal include LNAs, Analog Filters, and Mixers. Further discussion of these receivers and subsystems are detailed in Sect. 9.4.
5. **Set-On Receiver:** These systems are used, sometimes in conjunction with search receiver output data, for long-term analysis of the signal which includes measuring parameters of signal for analytical use to the operator. In fact, these receivers often comprise a channelized filter bank, using the search receiver RF front end, in order to pre-select frequency bands of interest that will be passed on to the operator.
6. **Signal Processing:** Realistically and within a modern context, this is where most of the computationally intensive tasks take place. As covered in detail in Sect. 2.2.3, the first task for ED use is to extract usable information of frequency and bandwidth, energy of the signal, modulation type, and the baud rate of digital communication signal. Then secondly, the information is used to detect, identify and classify signal accordingly. Techniques used within this block includes high speed analog-to-digital (ADC) conversion, digital-filtering, DSP-blocks, and signal transformation (i.e. Fast Fourier Transform—FFT, Walsh Hadamard Transform—WHT etc.).
7. **Direction Finding (DF) Signal Processing:** Direction finding systems operate on the principle that every electromagnetic wave propagates from a radiating source in a specific direction through a medium which can be received at another point [60]. Using multiple antennas, with the correct orientation, a DF receiver

⁶Foundational work was done by J.C Maxwell [111]. The field equations relating to this work can be found in the appendix.

- system could, by means of estimation algorithms [176], estimate the angle-of-arrival of that signal.
- 8. **Excitepr:** An excitepr is simply an RF signal generator that has the capability of modulating a generated signal. These systems are generally used for purposes in EA, as detailed earlier, where objective of the RF system is to jam communication systems. Jamming is typically achieved by generating and emitting random noise over an RF channel—effective against most communication signal—or tone jamming which is effective against modulation types such as frequency shift keying (FSK) [3].
 - 9. **Power Amplifier:** Although amplifiers are used as part of the receiver system for ES purpose (the blue block in Fig. 9.16) when it comes to EA tasks these power amplifiers convert the relatively weak signals (typically 0 dBm) into signal with greater energy for transmission. For jamming EA tasks the signal converted up and transmitted via the antenna can reach an order of several kilowatts (typically 1 kW). Issues with this system include, conversion efficiencies, frequency coverage, spectral purity, and leakage [3].
 - 10. **Filters:** Filters are used in most tasks relating to ED. For ES systems filters operate on the input signal to define the bandwidth of interest or used to scan a large bandwidth with a bandpass filter for interception tasks. For EA tasks filters are placed before the antenna as a precautionary step in order to reduce the likelihood of RF damage to friendly receiver systems due to the spurious nature of power amplifiers [1].
 - 11. **Communications:** This subsystem can be disseminated into two main operative tasks, which are to send external data to the receiver and to deliver a report of the data received to a operator [3]. Typically these tasks do not impose on the performance of the overall system, however it does play an important role in directing (i.e. command and control) the objectives of an ED system from a remote location.

9.4 Electronic Support Receiver Systems

Reception and processing of communication signals in context of ED tasks are predominantly handled by means of an ES receiver [178]. However, these receivers are able to support other types of signal reception and processing besides communication signals.

The current demand from ES receiver systems to be effective for intercepting communications, requires a level of sophistication beyond a single conventional system [42]. Modern day ES receivers need to incorporate many closely integrated subsystems which perform different tasks and have high data rate throughput [178]. A typical ES receiver architecture—shown in Fig. 9.17—highlights the number of subsystems (i.e. DF tasks, spectrum monitoring, frequency measurement) that comprise an ES receiver.

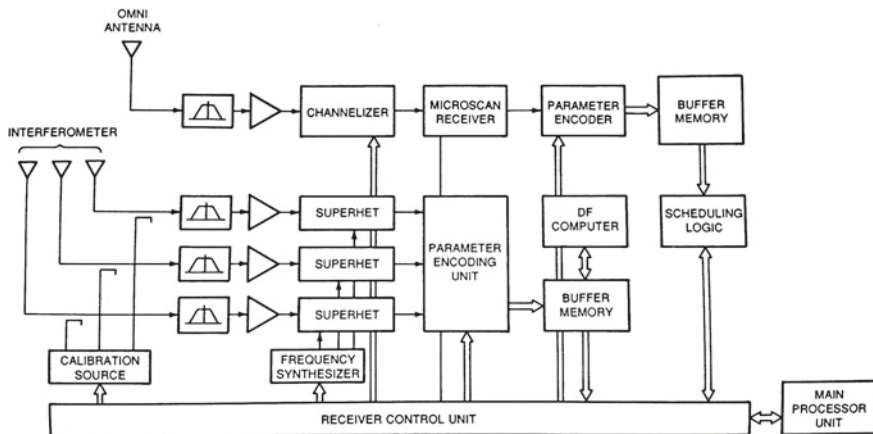


Fig. 9.17 Illustrating a typical ES receiver architecture. Taken from [178]

The performance of such a receiver is an important consideration when developing techniques to be implemented using ES receiver architecture. Although the current literature on ES receiver component/system design, implementation, and use are comprehensive,⁷ for our purpose a review of the operating parameters will be the focus.

9.4.1 ES Receiver Characteristics

When characterising a receiver to operate within an environment, the dynamic range, sensitivity levels and signal-to-noise ratio (SNR) values are key parameters to be considered when designing for signal processing technique to be implemented for detection capability of desired signals [178]. These parameters provide insight into operational capabilities and provide the means to design/select receivers to intercept/receive weak signals with improved probability of detection (Fig. 9.18).

9.4.1.1 Dynamic Range

In simple terms, dynamic range refers to the received input signal range, also explained as the difference between the strongest and the weakest amplitude of a signal that can be processed in real time (instantaneously) [107]. Yet, in practice, the dynamic range remains a parameter that needs to be measured rather than estimated based on theoretical calculations.

⁷The literature that encompass ES receiver design and technical specification, are detailed in much greater depth in the following works [39, 48, 178, 181].

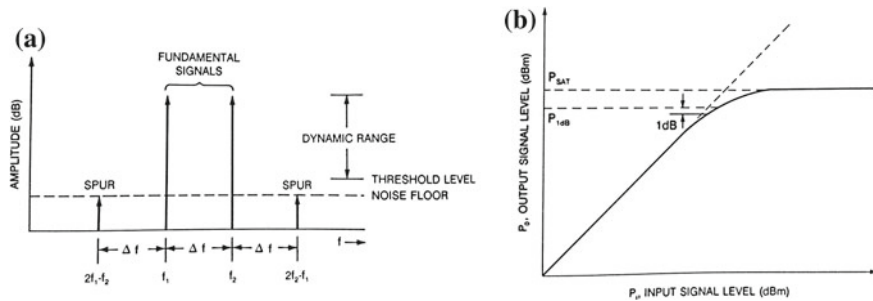


Fig. 9.18 In **a** the dynamic range with regards to amplitude in frequency domain is depicted, whereas **b** denotes the 1 dB compression point. (Taken from [174].)

The dynamic range—in an ES receiver—is predominantly determined by the operation of the amplifiers in the system, with exception to some components like ADC dynamic range. However, taking note of this dependence the dynamic range is commonly defined with respect to the output power levels. The lower limit of the dynamic range is specified by the sensitivity levels (the smallest that can be processed) and the upper limit by the 1—dB compression point [178] (the point where the amplifiers start following non-linear characteristics). Typical values of ES receivers range between 50–90 dB depending on the type of receiver [37].⁸

9.4.1.2 Sensitivity Levels

Receiver sensitivity is defined as the minimum signal power that is required at the receiver input to detect and/or process a desired signal [178]. This requirement provides insight into a receiver's ability to distinguish a signal of interest from accompanying noise under weak signal conditions. However, the required sensitivity is a loose term that does not apply to generic RF scenarios, for example when dealing with modulated signals larger SNR values are required with regard to the carrier frequency.

In the domain of ED it is seen as good practice to define where in the system chain the receiver sensitivity is defined. These sensitivity levels are illustrated by Fig. 9.19 with two different definitions of sensitivities, with the correct value ascribed by the sensitivity at the input of the receiver after the losses associated with cables, coupling, and amplifiers have been included. However, there does exist special instances when sensitivity can be defined differently, in terms of electric intensity ($\mu V/m$) instead of log (dB) due to a complex relationship between the antenna and receiver [139]. Direction finding tasks are one of these exceptions which typically requires a conversion from $\mu V/m$ to dB, expressed in terms of P = signal strength (dB); E = electric intensity ($\mu V/m$); F = frequency (MHz) as below.

⁸Refer Sect. 9.4.3 for further detail on receiver types.

$$P = -77 + 20 \log(E) - 20 \log(F) \quad (9.16)$$

The components that determine receiver sensitivity, which has been eluded to by means of system loss, are attributed to thermal noise, noise figure, and signal to noise ratio and defined as follows:

1. **kTB**—is defined as the thermal noise power level of an ideal receiver [156] which is typically specified at 290 °K with a constant receiver bandwidth (i.e. MHz) nominally denoted in dBm/ MHz , where a common value $kTB = -114$ dBm/MHz and the following values hold:

- k —Boltzmann's constant (1.38×10^{-23} J/°K)
- T —operating temperature, in °K
- B —the effective bandwidth of the receiver.

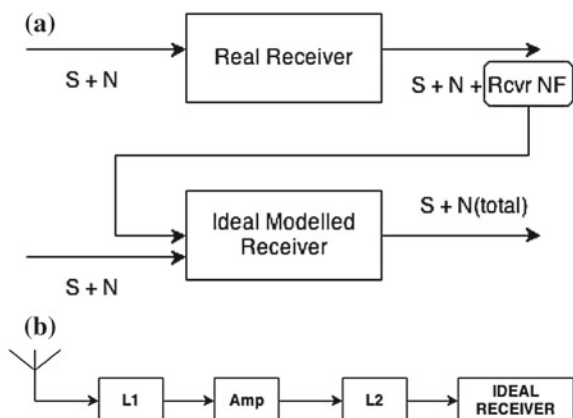
Consider a receiver with an effective bandwidth of 10 MHz, the correct thermal noise would correspond to $kTB = -114$ dBm/MHz + 10 dB = -104 dBm

2. **Noise figure (NF)**—defined by [1] as the ratio of the noise per kTB of actual noise that would have to be added to an ideal, noiseless receiver in order to produce the actual noise that is present at the output. In other words, it is the thermal noise that the receiver adds to the received signal with regards to the receiver input.

Each component in the receiver system comes with its own specified noise figure as determined by the manufacturer. However, when determining a receiver system parameter specifications, it is imperative to include and model the NF of the entire system, since the sensitivity levels rely on the whole system (i.e. antenna, lossy cable, amplifiers and distribution network), not simply the receiver sensitivity level. When determining the entire NF of the system the value calculated is can be expressed accordingly,

$$NF = L_1 + N_p + D. \quad (9.17)$$

Fig. 9.19 **a** Showing the different definitions associated with sensitivity and **b** the losses before the sensitivity of the ideal receiver is considered. Taken from [1]



Where D is determined from the graph in Fig. 9.20 and L_1 encompass all the pre-amplifier losses and N_p is the pre-amplifier noise figure. In non dB form the noise figure can also be expressed as

$$F_0 = \left[\frac{S_{in}/N_{in}}{S_{out}/N_{out}} \right]. \quad (9.18)$$

Typical values for receiver system noise figures are between 8 and 10 dB [2].

3. **Signal to noise ratio (SNR)**—SNR is the most important value to consider, more so than kTB and/or NF, when determining and defining the sensitivity. In ED sensitivity signal processing scenario the SNR is defined as

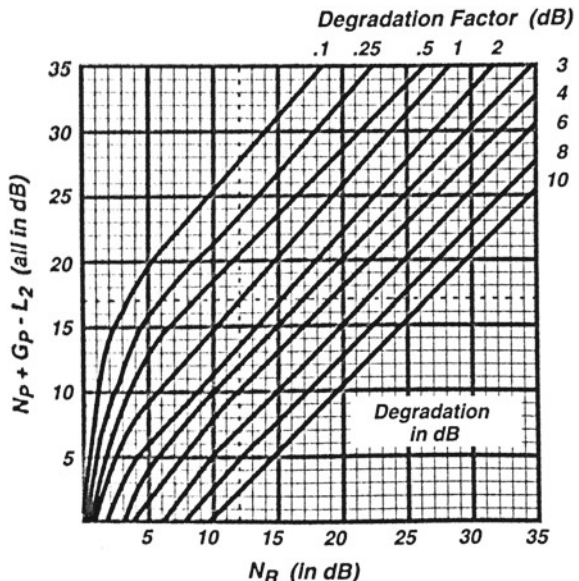
$$SNR = 10 \log \left(\frac{S_{output}}{N_{output}} \right)_{min}, \quad (9.19)$$

which is indicative of the minimum SNR that a receiver can still operate while performing detection with high probability. Subsequently, in such a case, the sensitivity (minimum detectable signal) can be calculated, in standard form according to,

$$S_{min} = Sensitivity = kT B F_0 \left(\frac{S_o}{N_o} \right)_{min}. \quad (9.20)$$

Take for example a scenario with the given parameter for calculating sensitivity, then the system sensitivity can be expressed in dB form in the following way,

Fig. 9.20 Chart used to determine the system degradation, labelled as D in Eq. 9.17. The intersection of where the calculated value of the sum of the preamp NF (N_p), the preamp Gain (G_p) and the loss before the receiver (L_2), with the receiver NF (N_R) determines the degradation value and enables system noise figure to be calculated. Taken from [1]



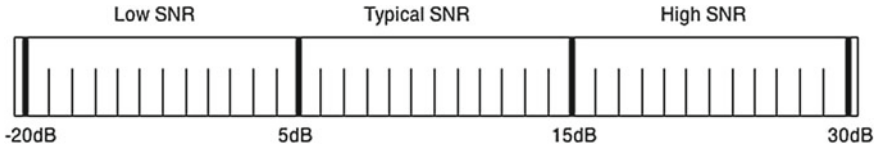


Fig. 9.21 Showing the spectrum of SNR values that are considered for ED scenario's and typical values associated with categorizing signals [151]

$$kTB + NF + \text{required SNR} \quad (9.21)$$

$$= (-114 \text{ dBm} + 10 \text{ dB}) + 10 \text{ dB} + 20 \text{ dB} = -74 \text{ dBm}. \quad (9.22)$$

It is important to note that the minimum SNR required by a receiver is highly dependant on the task that needs to be performed. In the case where information is modulated on to the received signal higher SNR values are required. This form of SNR is known as the pre-detection SNR, called the RF SNR or the carrier-to-noise ratio (CNR) [107]. In most cases the SNR of the signal is relatively higher than the RF SNR.

Where frequency modulation (FM) is considered the receiver sensitivity is determined by the received power levels as well as the modulation characteristics. Therefore, when determining the SNR of frequency-modulated signal, there are two things to consider. First, the RF SNR which tends to be approximately 12 dB [1] in most ED systems and second, if the RF SNR is above this threshold a FM improvement factor holds. This improvement factor equates to IF_{FM} (in dB) = $5 + 20 \log_{10} \beta$ where β is the modulation index. Hence the SNR for FM signals can be expressed as,

$$SNR = RF \text{ SNR} + IF_{FM}. \quad (9.23)$$

With the above mentioned sensitivity parameters, it is prudent to know the common operating sensitivities that are associated with most ES receivers. These sensitivity values are typically dependant on the type of receiver used (see Sect. 9.4.3), which vary from -50 to -90 dBm with the ideal sensitivity preferably higher than 70 dB for tasks such as direction finding [37] (Fig. 9.21).

9.4.2 Sensitivity Conversion

The conversion from dBm to $\mu V/m$ can be expressed as (taken from [1]):

$$E = 10^{(P+77+20 \log[F])/20} \quad (9.24)$$

and conversely as:

$$P = -77 + 20 \log(E) - 20 \log(F) \quad (9.25)$$

These equations are based on power transmitted and antenna gain at the point of reception, which are:

$$P = \frac{E^2 A}{Z_0} \quad (9.26)$$

$$A = \frac{G c^2}{4\pi F^2} \quad (9.27)$$

Where:

P = signal strength (in W)

A = Antenna area (in m^2)

G = Antenna gain (= 1 for isotropic antenna)

F = Frequency (in Hz)

E = Electric intensity (in V/m)

Z_0 = impedance of free space (120π (Ω))

c = speed of light (3×10^8)

9.4.2.1 Effective Range

Considering the definition of sensitivity, it is imperative to determine the effective range of a receiver in order to gauge at what physical distances a receiver is able to operate for interception tasks.

Various parameters are considered in specifying ES receivers to calculate the effective range within a certain margin, which include propagation loss (L_s), sensitivity (equivalent to power received P_R , but referred to as S_R), transmit power (P_T), transmission gain (G_T), receive gain (G_R), and spreading loss (L_s).⁹ In short the effective range can be determined by solving the following expression (written here in dB form),

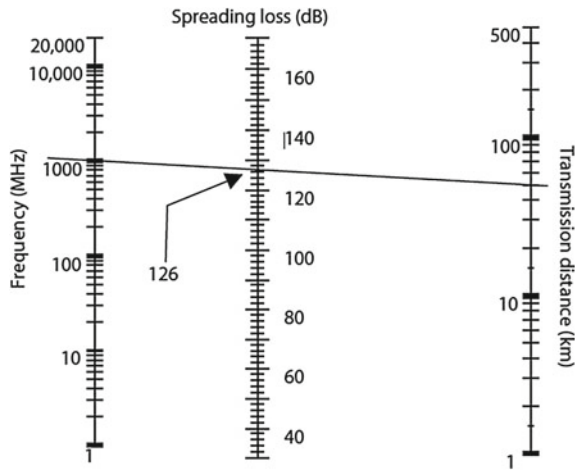
$$S_R = P_T + G_T - L_s + G_R, \quad (9.28)$$

$$\text{where : } L_s = -32.4 - 20 \log(F) - 20 \log(d). \quad (9.29)$$

As a means to describe the effect receiver parameters in real world operations, consider two scenarios that are pertinent to this body of work. Given that an ES receiver has two different sensitivity levels, namely -75 and -80 dBm.

⁹Spreading loss can be determined from the nomograph in Fig. 9.22 or calculated using Eq. 9.11 equating to L_s above.

Fig. 9.22 Illustrates the use of a nomograph to determine the propagation loss for a frequency of 1000 MHz for a given distance. Courtesy of [2]



Scenario 1: Determine the effective range of intercepting a GSM signal from a downlink tower transmission at 1800 MHz, and

Scenario 2: Determine the effective range of intercepting a GSM signal from the uplink transmission of a handset 900 MHz.

Listed below are the effective ranges according to the above expression in Eq. 9.28.

Calculation steps scenario 1:

Description	Symbol	Value	Reference
Power transmitted	P_T	15 W	[154]
Gain transmitted	P_T	10 dB	[37]
Frequency of transmission	F	1800 MHz	[143]
Gain received (omnidirectional antenna)	G_R	0 dBi	[142]
Sensitivity	L_S	-75; -80 dBm	[37]
Effective range (distance)	d	in km	

Sensitivity = -75 dBm:

$$20 \log d = P_T + G_T - 32.4 - 20 \log(F) + G_R - L_S \quad (9.30)$$

$$20 \log d = 10 \log(15000) + 10 - 32.4 - 20 \log(1800) + 0 - (-75) \quad (9.31)$$

$$d = 10^{\left(\frac{29.25}{20}\right)} = 29.02 \text{ km} \quad (9.32)$$

Sensitivity = -80 dBm:

$$20 \log d = P_T + G_T - 32.4 - 20 \log(F) + G_R - L_S \quad (9.33)$$

$$20 \log d = 10 \log(15000) + 10 - 32.4 - 20 \log(1800) + 0 - (-80) \quad (9.34)$$

$$d = 10^{\left(\frac{34.25}{20}\right)} = 51.61 \text{ km} \quad (9.35)$$

Calculation steps scenario 2:

Description	Symbol	Value	Reference
Power transmitted	P_T	2 W	[154]
Gain transmitted	G_T	0 dB	[37]
Frequency of transmission	F	900 MHz	[143]
Gain received (omnidirectional antenna)	G_R	0 dBi	[142]
Sensitivity	L_S	-75; -80 dBm	[37]
Effective range (distance)	d	in km	

Sensitivity = -75 dBm:

$$20 \log d = P_T + G_T - 32.4 - 20 \log(F) + G_R - L_S \quad (9.36)$$

$$20 \log d = 10 \log(2000) + 10 - 32.4 - 20 \log(900) + 0 - (-75) \quad (9.37)$$

$$d = 10^{\left(\frac{29.25}{20}\right)} = 6.7 \text{ km} \quad (9.38)$$

Sensitivity = -80 dBm:

$$20 \log d = P_T + G_T - 32.4 - 20 \log(F) + G_R - L_S \quad (9.39)$$

$$20 \log d = 10 \log(2000) + 0 - 32.4 - 20 \log(900) + 0 - (-80) \quad (9.40)$$

$$d = 10^{\left(\frac{34.25}{20}\right)} = 12 \text{ km} \quad (9.41)$$

Table 9.5 A summary of the typical range of values associated with the important system characteristics of ES receivers. This is valuable when considering signal processing tasks to be implemented on such architectures. (Sourced from [116] and modified by the authors.)

Characteristic	Typical range
Maximum instantaneous analysis bandwidth (GHz)	0.05–2
RF range (GHz)	0.01–60
Dynamic range (dB)	40–90
Sensitivity (dBm)	−70 – −90
Frequency resolution (MHz)	0.5–500
Minimum power (W)	60–200

These values provide an approximate range wherein the ES receiver has the potential to intercept such signals, as well as insights into the relationship that sensitivity parameters hold on the capability of interception.

9.4.3 Types of ES Receivers

By way of introduction, with exception to receiver characteristics, the capability of any receiver is highly dependant on the type of receiver, especially in the case of ES receivers for electronic defence purposes [37]. ES receivers, by design, must make system trade-offs due to several conflicting requirements as there are too many scenarios to execute all ES tasks simultaneously with optimal performance when using a single receiver architecture. Hence, the need for specialized equipment, technologies, and techniques which result in the existence of a wide variety of ES receivers today (Table 9.5).

The review of different ES receiver types are of paramount importance. Each of the receiver's capabilities, provide an insight, as to the approach of implementing new/novel DSP techniques (i.e. Compressive Sensing etc.) on different receiver platforms. The implementation parameters are summarized as follows:

- Receiver flexibility (Reconfigurability),
- Computational performance,
- Frequency resolution,
- Data rate,
- Ease of integration,
- Cost involved with each receiver.

All these parameters are considered in an attempt to determine the most appropriate receiver type to utilize and/or consider for the purposes of this body of work. As

Table 9.6 Typical characteristics associated with different types of ES receivers. Taken from [1]

Receiver type	General characteristics
Wideband crystal video	Wideband instantaneous coverage; low sensitivity and no selectivity; mainly for pulsed signals
Tuned RF crystal video	Similar to crystal video, however. Provides frequency isolation and better sensitivity
IFM	Coverage, sensitivity, and selectivity likened to crystal video; measures frequency of received signals
Superheterodyne wideband	Most common type of receiver; good selectivity and sensitivity
Superheterodyne narrowband	Good selectivity and sensitivity; dedicated to one signal
Channelized	Combines selectivity and sensitivity with wideband coverage
Microscan/Compressive	Provides frequency isolation; measures frequency; does not demodulate
Digital	High flexibility; can deal with signals with unknown parameters

a consequence such determination is leveraged by the characterization of the various receivers in Tables 9.6 and 9.7.

In this section, a brief comparison of the various receiver types—that are typically used for ES purposes—are reviewed. Below is a summarized table of the general characteristics of some common ES receivers and Table 9.6 provides a summary of the qualitative capabilities of each receiver type. Moreover, for the purpose of the reader, a comprehensive table of the qualitative capabilities are detailed at the end of this section in Table 9.7.

9.4.3.1 Crystal Video Receiver

This receiver type provides a simple yet cost effective means of doing instantaneous detection whilst using inexpensive techniques. The receiver consists of a bandpass filter and pre-amplifier circuit, then a crystal (diode) detector followed by a video amplifier that has, as an output, the video band signal.

The diode detector circuit operates at low enough power, which is in the square law¹⁰ region [2]. Benefits associated with this receiver are the simplicity in the technology which incurs less expense, instantaneous detection, and high probability of interception (POI) in wide frequency range [178]. Whereas the drawbacks include, no frequency resolution, poor sensitivity, and poor simultaneous signal performance

¹⁰The output is a function is dependant on the input power rather than the signal voltage.

Table 9.7 Showing the summarized details of the qualitative capabilities of the various receivers

Receiver type	Receiver qualitative capabilities						POI	Cost
	Measures frequency	Selectivity	Sensitivity	Dynamic range	Multiple signals	Frequency coverage		
Crystal video	N	P	P	G	N	G	G	Y
TRF	Y	M	P	G	Y	G	P	Y
IFM	Y	P	P	M	N	G	G	L/M
Superheterodyne wideband	Y	G	G	G	Y	G	P	N
Superheterodyne narrowband	Y	G	G	G	Y	P	Y	M/H
Channelized	Y	G	G	G	Y	P	Y	M/H
Microscan	Y	G	G	G	Y	G	G	N
Digital	Y	G	G	G	Y	G	M	M/H
<i>KEY</i>		M = Good	H = Moderate	P = Poor	H = High	L = Low	Y = Yes	N = No

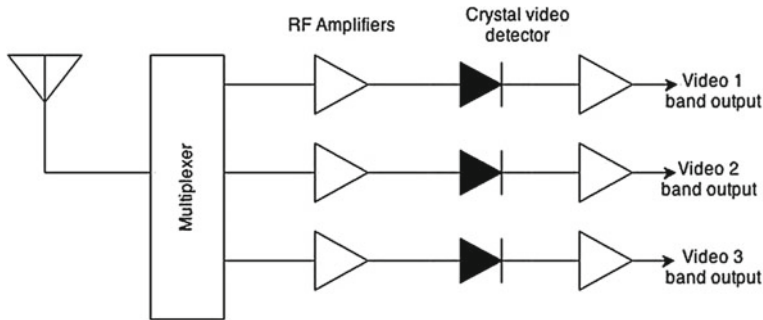


Fig. 9.23 Showing the typical topology of a crystal video receiver

[37]. These receiver are typically used in radar warning receivers (RWRs), consequently, ruling such a receiver type inadequate for our purposes. See Fig. 9.23.

9.4.3.2 Tuned RF Receiver

Tuned RF receiver type share a similar architecture as the wideband crustal video receiver, mentioned previously, however in the earlier days of RF this receiver utilized a YIG filter and oscillator to isolate the signal of interest at a specific frequency. Thus increasing sensitivity but still suffering from slow response time and poor POI [178]. Due to advances in receiver technology this type of receiver has largely been replaced by Superheterodyne receivers [1]. Tuned RF receivers nowadays are optionally used for RWR and frequency measurements in hybrid scenarios [37].

9.4.3.3 Instantaneous Frequency Measurement (IFM) Receiver

As the name suggests, an IFM receiver measures the frequency of a received signal. The received signal is split into two signal paths by means of a delay line, see Fig. 9.24. One of the signal paths have a constant delay time τ which produces a frequency dependant phase difference θ [178] whereas the other signal path remains unchanged.

An IFM receiver takes advantage of this relationship, by measuring the phase difference between the two signals, whereby the frequency can then be inferred by using the expression $\theta = 2\pi f_0 \tau$. Lastly, this frequency inference is digitized and passed on to produce a direct digital frequency reading.

The preamplified IFM receiver exhibits the same sensitivity as the crystal video receiver but less dynamic range. Benefits of an IFM receiver are that they are relatively simple and compact with improved frequency resolution and high instantaneous POI. Associate disadvantages include insufficient sensitivity for some ED scenarios and therefore cannot be used in dense signal environments [37, 139, 178]. However some

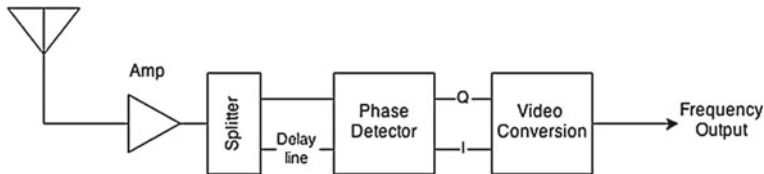


Fig. 9.24 A diagram of a common IFM receiver. Sourced from [37]

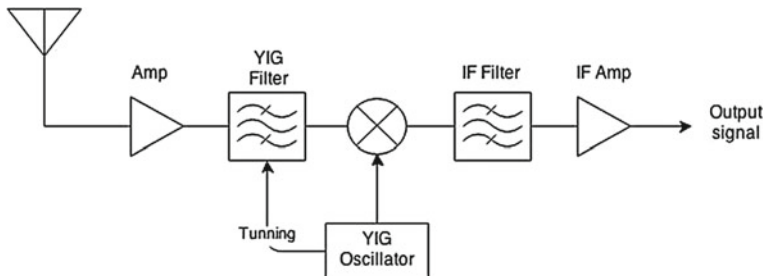


Fig. 9.25 A diagram of a narrow band superheterodyne receiver layout. Sourced from [116]

scenarios/environment exist where IFM receiver are used in shipboard ES, Jammer power management, and SIGINT equipment [37].

9.4.3.4 Superheterodyne: Wideband and Narrowband

Superheterodyne receivers are one of the most versatile receivers in use today [143]. The name super (i.e. higher) and heterodyne (i.e. linear shifts) join to describe the operation of this receiver. It linearly shifts the received signal to an intermediate frequency (IF) by means of a fixed and/or tuneable oscillator, this techniques is known as mixing, see Sect. 9.2.2.3. Furthermore the isolation of other frequency aliasing is done by means of bandpass filters, see Fig. 9.6, where the block diagram illustrates the construction of such a receiver.

These receivers are utilize either a wideband bandpass filter to enable surveillance and search tasks of a wide bandwidth of the RF spectrum, or a narrowband bandpass filter that only isolates a small portion of the spectrum to be analysed with higher frequency resolution and sensitivity. The usefulness of this approach, stems from enabling the flexibility and control of the local oscillator which is varied in a sawtooth-like fashion [178] to provide scanning ability of the frequency spectrum at a cost to response time (Figs. 9.24, 9.25 and 9.26).

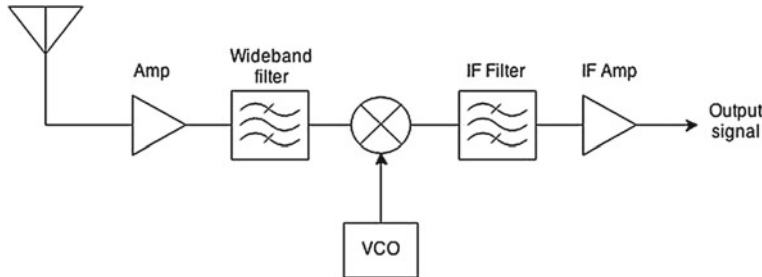


Fig. 9.26 A diagram of a wide band superheterodyne receiver layout. Sourced from [116]

Wideband superheterodyne

Advantages	Improved response time to threats and probability of interception
Disadvantages	Higher probability of spurious signal generation and less sensitivity than its narrowband counterpart

Narrowband superheterodyne

Advantages	High sensitivity, improved frequency resolution and no interference of simultaneous signals
Disadvantages	Slow response time, inadequate POI and suffers with signals that are frequency agile

Both types of superheterodyne receivers are used in SIGINT equipment, Air (i.e. Tactical air warning), shipboard ES, and the analysis system of a hybrid receiver systems.

9.4.3.5 Channelized Receiver

Channelized receivers are widely considered as one of the ideal receiver types in use for ES tasks. The technique behind its wide range adoption is the large number of contiguous bandpass filters [178] for each channel, and as the name suggests, channelizes (i.e. divides) the RF bandwidth by means of a power divider/multiplexer into respective subbands whereby the signal from each channel is amplified, filtered, and digitized further by means of a fixed tuned receiver (FTR), see Fig. 9.27. These FTRs were classically comprised of surface acoustic wave (SAW) devices [107], however in recent years rather use narrowband superheterodyne receivers and other miniaturization technologies [1]. Typical implementation of a Channelized receiver utilizes 10 to 20 TRF channels to cover 10 to 20 % of the RF range, coupled with computer controlled switchable frequency translators allowing 100 % coverage of the entire needed EW RF spectrum [2].

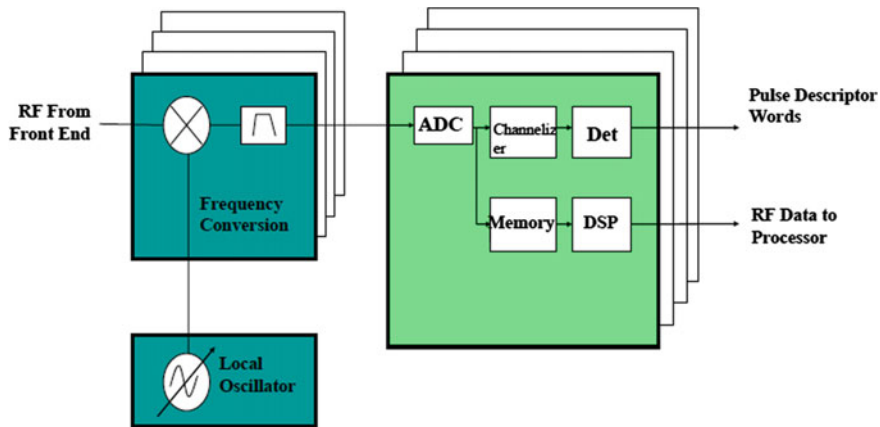


Fig. 9.27 A diagram of a channelized receiver layout

Advantages	Wider RF bandwidth coverage, nearly instantaneous frequency readings as well as moderate frequency resolution due to the limitation on the number of realistic channels, improved sensitivity, and higher selectivity [37]
Disadvantages	With higher performance system, comes at a cost and channelized receivers are no different. These receivers require higher complexity, cost, and provide lower reliability with limited sensitivity
Usage/application	SIGINT equipment and jammer power management

9.4.3.6 Microscan/Compressive Receiver

A Microscan receiver or Compressive receiver for ED tasks are essentially the same receiver, with emphasis on describing the basic operation of the receiver in different ways. Microscan receiver refers to the receivers ability to fast-sweep its local oscillator, subsequently mixing (see Sect. 9.2.2.3) the RF input signal to produce a chirped frequency modulated (FM) signal [178]. Whereas Compressive receiver refers to the compression of the output FM signal by the dispersive delay line (DDL) implemented via SAW filters which are an integral component of this receiver architecture¹¹ [178].

The concept of the compressive receiver was seminal in White's work [186] which allowed for a wide-band receiver to achieve fine-frequency resolution with an output of narrow pulses that held a linear relationship between their position in time and frequency of the RF input signal. The receiver operates by taking an input RF signal—with frequency f_0 —which is mixed with a linear sweeping LO signal, changing at a rate inversely proportional to the frequency-time gradient of the DDL and then passed through a video detector, see Fig. 9.28 for illustration of the process. The DDL must match the bandwidth of the sweeping LO which is defined by the

¹¹ A detailed discussion of the mathematical work needed to design such a receiver is beyond the scope of this work. We refer the reader to the work done in [178, 186] for further detail on this topic.

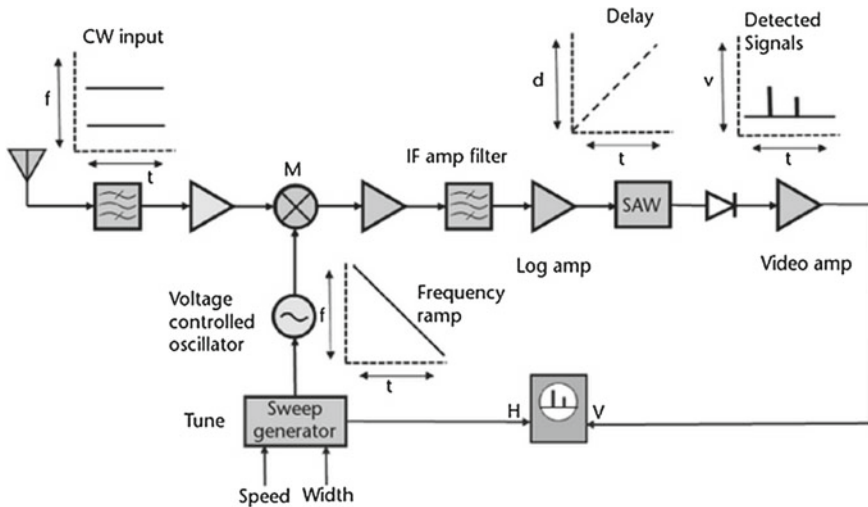


Fig. 9.28 A diagram of a microscan/compressive receiver. Courtesy of [49]

signals that are within the spectrum that are of interest.

Advantages	Near instantaneous processing of frequency, good resolution, dynamic range, and improved simultaneous signal capability
Disadvantages	Implementation of such a system is more complex. It is limited by bandwidth with no pulse modulation information. Moreover, the alignment of the saw filters are critical, if not manufactured correctly can make a system ineffective
Usage/Application	Typically used for SIGINT scenarios due to the large RF spectrum needed to be surveyed. Sometimes used for applications needing fine frequency analysis over a wide frequency range [37]

9.4.3.7 Digital Receivers

A digital receiver in some respects approximate an ideal receiver, where a received signal is directly sampled at twice its highest frequency (i.e. Nyquist criteria) and the digitized signal is made available to a dedicated DSP and/or processor unit where digital filtering, demodulation, and other techniques are applied by means of computation.

This ideal receiver, unfortunately, is not yet fully realizable for the entire RF spectrum that EW occupies, using current technology. The success of such a system is dependant on the acquisition rates of current ADC's (i.e. fastest commercially avail-

able ADC is $2.7 - 3.6 \text{ GSPS}$ [76]), data throughput, processing power, and memory requirements.

In current digital receivers this barrier of digitizing signals is circumvented by applying a technique known as bandpass sampling [179]. We refer the reader to Sect. 9.6.3.1 for a detailed discussion on the topic.

Functionally, as the name suggests, bandpass sampling samples at a lower rate (which is attainable with current technologies) but within a specific bandwidth which allows higher frequencies to alias or down convert to a zero IF where it is then digitized. The performance and accuracy of quantizing the RF signal and removing spurious signals are aided by filters and novel signal techniques in order to cover a RF range of up to 20 GHz. An example of such a system can be found in [167].

Advantages	Good simultaneous signal capability, good POI, improved selectivity and dynamic range
Disadvantages	A system such as this is highly complex and very expensive. It has lower resolution than conventional receivers
Usage/application	Land, sea, air ES, and SIGINT scenarios

9.5 Compressive Sensing Mathematical Fundamentals

Herein we discuss the fundamental building blocks—relating to 1-D time and frequency domain signals - necessary for implementing CS theory. The notation followed throughout this section is derived from work¹² in [44, 53, 150]. Moreover, in this section we will focus on the mathematical concepts that are associated with CS theory and used for explanatory purposes rather than a literature comparison of CS techniques. The review of implementing CS on digital systems are detailed in Sect. 3.4.

9.5.1 Vector Space

As a prerequisite for CS theory, a signal must be sparse in order to be exactly recovered [50], thus to recover such signals an understanding of vector spaces, bases, and frames are required as a fundamental building block for recovery.

¹²We advise the reader to the aforementioned literature for further comprehensive study of CS and to provide insight relating CS to other signal processing applications, particularly in image processing.

For signal processing purposes we model input signals as vectors (i.e. of length N) that exist in a discrete, finite domain known as a vector space, a N -dimensional Euclidean space denoted by \mathbb{R}^N . A function frequently used for vector spaces in CS is the ℓ_p norm defined for $p \in [1, \infty)$ and given as:

$$\|x\|_p = \left(\sum_{i=1}^N |x_i|^p \right)^{1/p}, \quad p \in [1, \infty). \quad (9.42)$$

For application to signal approximation, a common technique is the *norm* as it measures signal strength and/or signal error which is minimized to obtain the best estimate of the true signal in a particular vector space (Fig. 9.29).

As an example, consider a vector $x \in R^2$ that exists in an affine space that needs to be approximated by a point \hat{x} , with $\hat{x} \in A$ where A is an arbitrary subspace; then the following definition holds, by taking the approximation error using an ℓ_p norm,

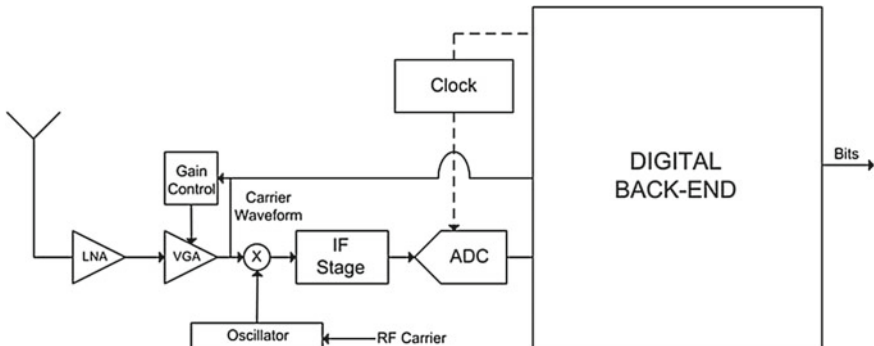


Fig. 9.29 A diagram of a typical digital receiver, however, not representing the ideal receiver but a current realization of given todays technology limits. Courtesy of [176]

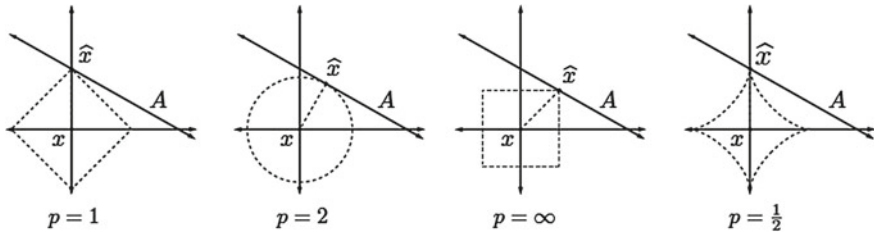


Fig. 9.30 Illustrates the different approximations of ℓ_p norms, $p = 1, 2, \infty$ and the quasi-norm with $p = \frac{1}{2}$, approximating a point in \mathbb{R}^2 by means \hat{x} , for the ℓ_p norm onto A . Where A is a denotes a low dimension subspace that is approximated by expanding the norm conditioned to x . Sourced from [53]

with the objective to minimize $\|x - \hat{x}\|_p$ subject to the vector space A for different norms, the approximation of $\hat{x} \in A$ can diverge to x with a measurable error based on the ℓ_p norm chosen.

In Fig. 9.30 this approximation is shown for different ℓ_p norms. An observation of the figure suggests that the approximations for different norms give rise to varied approximation errors, with $p > 1$ error more evenly distributed or spread, whereas $p = 1$ and the quasi-norm case error tends to be unevenly distributed or sparse [18]. The approximation error is the fundamental basis for sparse signals and their use for CS recovery as it applies to higher dimensional signals and affine vector spaces.

9.5.2 Sets, Bases and Frames

Based on the fundamentals from linear algebra [112] sampled signals can represented as a discrete vector in a finite-dimensional vector space V , where $V \in \mathbb{R}^N$ and $K = \{1, 2, \dots, N\}$, which is the vector space that comprise bases that span V . Take for example a set $\Psi = \{\psi_1, \psi_2, \dots, \psi_K\}$ that is linearly independent and spans V . Then Ψ can be defined as a *basis* for the vector space V .

Bases are vital in describing signals of similar origin or application which can be represented by a linear combination of the vectors of the same basis, with varied coefficients for each signal [53]. In some cases a basis is referred to as a dictionary in CS literature.

In discrete mathematical terms, a signal can be decomposed into a linear set of coefficients (a_i) and a basis (ψ_i) , such that the discrete signal $x \in \mathbb{R}^N$ can be expressed as:

$$x[n] = \sum_{i \in K} a_i \tilde{\psi}_i, \quad (9.43)$$

where $\tilde{\Psi}$ is the dual basis or in matrix terms the inverse used to construct the original signal. Sometimes it is useful, especially for signal reconstruction, to use a dual basis in generating an orthonormal basis where a set of linearly independent vectors $\Phi = \{\mu_1, \dots, \mu_N\}$ that span V would constitute an orthonormal basis, if the following condition holds:

$$\mu_i \cdot \mu_j = \begin{cases} 0 & \text{if } i \neq j \\ 1 & \text{if } i = j. \end{cases} \quad (9.44)$$

Given a basis that is not orthonormal, using the set of vectors that comprise the basis, an orthonormal basis can be generated following the Gram-Schmidt method [112]. A crucial motivation for using orthonormal bases relates to the properties associated with it, that is, its dual is equal to the hermitian adjoint (i.e. transpose) such that $\Psi = \tilde{\Psi}^T$. Furthermore, it is useful to define the frame of a basis as it sometimes provides a more developed representation of a signal due to the inherent redundancies.

A frame is defined as a set of vectors $(\Psi_i)_{i=1}^n$ in \mathbb{R}^d where $d < n$, can be represented as a matrix $\Psi \in \mathbb{R}^{d \times n}$, such that for all the vectors $x \in \mathbb{R}^d$

$$A\|x\|_2^2 \leq \|\Psi^T x\|_2^2 \leq B\|x\|_2^2, \quad (9.45)$$

where $0 < A \leq B < \infty$.¹³ In particular, a frame extends the definition of a basis to include sets that are possibly linearly dependent, giving rise to infinitely many coefficients α for an input signal x and frame Ψ such that $x = \alpha\Psi$. In the case where Ψ is a $d \times N$ matrix, the values of A and B correspond to the eigenvalues of $\Psi\Psi^T$ [150].

The infinitely many coefficients, attributed to the inclusive linear dependency of the frame, provides a choice for coefficient vector when the dual frame is considered, as the frame operated on by the signal is responsible in determining the coefficient vector. Importantly, any dual frame $\tilde{\Psi}$ that satisfies

$$\Psi\tilde{\Psi}^T = \tilde{\Psi}\Psi = I, \quad (9.46)$$

is considered an alternative dual frame, with $\tilde{\Psi} = (\Psi\tilde{\Psi}^T)^{-1}\Psi$ enabling the dual frame to be well-defined due to $\Psi\Psi^T$ being invertible based on the inequality that $A < 0$ requires Ψ to have linear independent rows. Therefore, a means to obtain a feasible coefficient vector β of a signal x , is by applying the following operation

$$\beta = \Psi^T(\Psi\tilde{\Psi}^T)^{-1}x. \quad (9.47)$$

¹³The condition imposed on $A > 0$ implies that the rows of Ψ must be linearly independent. When A is chosen to be the largest and B the least valued of the possible inequalities, it is known as the optimal frame bound. When $A = B$ the frame is known as A -tight. Finally, if $A = B = 1$ then Ψ is a Parseval frame.

This coefficient vector in many CS recovery steps forms the first step of the algorithm, see Sect. 3.4.

9.5.3 Matrix Construction for CS Sensing

A comprehensive study of constructing CS basis compliant matrices exists in the open literature [25, 43]. Nonetheless, we provide an overview of the criteria and the associated proofs required for compliance of possible matrices that match, and subsequently can be used as a sensing matrix for CS. A large majority of the material for this section is sourced from [105, 150] and we refer the reader to these for further insight into CS.

First, let us assume a sensing matrix Φ , with size $M \times N$, operates on a K-sparse input vector x , with size $N \times 1$ (see Fig. 3.5), which produces the output vector y with size $M \times 1$ as

$$y = \Phi x. \quad (9.48)$$

If we desire to recover all sparse signals from x using the measurements y via the matrix Φ , as seen above, it can quickly be deduced that any pair of different vectors $x, \hat{x} \in \sum_K = \{x : ||x||_0 \leq K\}$ must result in $\Phi x \neq \Phi \hat{x}$. Otherwise, it is impossible to distinguish between x and \hat{x} based on the measurement vector y as there will be infinitely many solutions [18].

More formally, Φ represents all $x \in \sum_K$ only if the Null space of Ψ contains no vectors in \sum_{2K} . The Null space of Φ is defined as $\mathcal{N}(\Phi) = \{z : \Phi z = 0\}$. One of the typical ways to characterise this property, and serves as the guarantee for unambiguous recovery, is by means of the spark [46].

Spark

Definition 9.1 *The spark of a given matrix Φ is the smallest number of columns of Φ that are linearly dependent [105].*

This definition yields the following guarantee based on Corollary 1 of [46].

Theorem 9.1 *For any vector $y \in \mathbb{R}^M$, there exists at most one signal $x \in \sum_K$ such that $y = \Phi x$ if and only if $\text{spark}(\Phi) > 2K$ [150].*

Thus, the guarantee holds, based on the spark for the recovery of exactly sparse signals [18], but does not extend to approximately sparse signals, which is dealt with by the null space property (NSP).

9.5.4 Null Space Property

The null space property (NSP) can be considered as a condition that places an even higher restriction on the null space of Φ —denoted as $\mathcal{N}(\Phi)$ —to distinguish between

approximately sparse signals [46]. In other words, the $\mathcal{N}(\Phi)$ must be kept free of any vectors that are too compressible as well as from those that are sparse [150]. Subsequently, this enables the NSP to express, empirically, that the null space of Φ should be spread, and not be congruent on a small subset of indices [166].

The result of NSP provides a guarantee that a matrix of order $2K$ is adequate in establishing exact recovery, subject to the condition in Eq. 9.49. In order to define the operation of the NSP conditional check, we adopt the following notation based on [150]. Let Γ be a subset of indices ($\Gamma \subset \{1, 2, \dots, N\}$) and its correspondent $\Gamma^c = \{1, 2, \dots, N\}/\Gamma$. When referring to a vector x_Γ it designates the length N vector by setting the values of x indexed by Γ^c to zero. Applying the same logic, for a matrix Φ^c with size $M \times N$, results in a matrix with columns of Φ indexed by Γ^c to zero.

Definition 9.2 (Definition 3.2 of [150]) *A matrix satisfies the NSP of order K if there exists a constant $C > 0$ such that*

$$\|h_\Gamma\|_2 \leq C \frac{\|h_{\Gamma^c}\|_1}{\sqrt{K}} \quad (9.49)$$

holds for all $h \in \mathcal{N}(\Phi)$ and for all Γ such that $|\Gamma| \leq K$.

Theorem 9.2 [35] *Let $\Phi : \mathbb{R}^N \rightarrow \mathbb{R}^M$ denote a sensing matrix and $\Delta : \mathbb{R}^N \rightarrow \mathbb{R}^M$ denote an arbitrary recovery algorithm. If the pair (Φ, Δ) satisfies 9.50 then Φ satisfies the NSP of order $2K$.*

Therefore, if a given matrix meets the criteria of NSP, then the only K -sparse vector in its null space is $h = 0$. Although the recovery of the CS measurement vectors will be detailed later, let us consider the example where we let the recovery algorithm be denoted by Δ , then using the NSP inequality of 9.49, a guarantee can be established such that,

$$\|\Delta(\Phi x) - x\|_2 \leq C \frac{\sigma_k(x)_1}{\sqrt{K}} \quad (9.50)$$

for all x , where x is given as

$$\sigma_k(x)_p = \min_p \|x - \hat{x}\|_p \text{ where } x \in \sum_K. \quad (9.51)$$

Although the means of recovery will be covered in Sect. 3.4, the above equation provides a guarantee for exact recovery for all K -sparse vectors, and suggests a high likelihood for non-sparse signal recovery by some other K -sparse vector is possible [105].

9.5.5 Restricted Isometry Property

The restricted isometry property (RIP) is a vital development that extends beyond NSP conditions, allowing a guarantee for recovery where measurements are corrupted by some form of error or noise. The guarantee, formalized by [29], places a more strict condition on matrix Φ , namely the isometry condition, which is ubiquitous with compressive sensing.

Although the proof of the RIP is somewhat involved (see [17] for proof), in simple terms if the RIP condition of order $2K$ holds for a matrix, say Φ , then based on Eq. 9.52 ϕ preserves the Euclidean distance between any pair of K-sparse vectors.

Definition 9.3 (Definition 3.3 of [150]) *A matrix satisfies the restricted isometry property of order K if there exists a $\delta_k \in (0, 1)$ such that*

$$\alpha \|x\|_2^2 \leq \|\Phi x\|_2^2 \leq \beta \|x\|_2^2 \text{ with } \alpha = (1 - \delta_k) \text{ and } \beta = (1 + \delta_k) \quad (9.52)$$

holds for all $x \in \sum_K = \{x : \|x\|_0 \leq K\}$,

where $0 < \alpha \leq \beta < \infty$ and $\delta = (\beta - \alpha)/(\beta + \alpha)$ with Φ multiplied with $\sqrt{2}/(\beta + \alpha)$ provides a matrix that still satisfies the RIP, however, with a scaled matrix version with symmetry about one in accordance with Eq. 9.52.

Stability is of critical concern for recovery of noisy measured sparse signals when dealing with the RIP condition, especially what lower bound must be chosen. In other words, if stable recovery of a signal is needed the RIP of the matrix must meet the lower bound of Eq. 9.53. This lower bound criteria is denoted below, as the condition for a matrix Φ known as C-stable [105].

Definition 9.4 (Definition 3.4 of [150]) *Let $\Phi : \mathbb{R}^N \rightarrow \mathbb{R}^M$ denote a sensing matrix and $\Delta : \mathbb{R}^N \rightarrow \mathbb{R}^M$ denote an arbitrary recovery algorithm. We say that the pair (Δ, Φ) is C-stable if for any $x \in \sum_K$ and any $e \in \mathbb{R}^M$ we have that*

$$\|\Delta(\Phi x + e)\|_2 \leq C \|e\|. \quad (9.53)$$

The above definition dictates that if a small amount of noise is added to the measurement of Φx , the result on the recovery of the signal is not to be unpredictable [150]. Moreover, Theorem 3.3 of [150] shows that by letting $C \rightarrow 1$ forces Φ to satisfy the RIP (9.52) lower bound with $\delta_K = 1 - 1/C^2 \rightarrow 0$. Hence, if we wish to reduce the influence of noise on the signal recovery, Φ must be adjusted to satisfy the RIP lower bound with a smaller constant.

The measurement bounds of a potential sensing matrix (i.e. Φ), based on [17] by the Theorem 3.4 in [150], has to result in a lower bound for the number of measurements needed to achieve the RIP, with a high confidence level in terms of (N , M , and K) by ignoring the impact of δ temporarily. This is given as,

Theorem 9.3 (Theorem 3.4 of [150]) Let Φ be an $M \times N$ matrix that satisfies the RIP of order $2K$ with constant $\delta \in \left(0, \frac{1}{2}\right]$. Then

$$M \geq CK \log\left(\frac{N}{K}\right) \quad (9.54)$$

where $C = 1/2 \log(\sqrt{24} + 1) \approx 0.28$.

Based on the Johnson-Lindenstrauss lemma [41] and related to the RIP, results in a different bound on measurement for Φ when δ is significantly lower. Namely, that for small δ subject to $M \geq \frac{c_0 \log(p)}{\varepsilon^2} = \frac{16c_0 K}{c_1 \delta^2}$ an outcome for measurements of a RIP matrix of order K is proportional to $\frac{K}{\delta^2}$ producing measurement bound of $K \log(N/K)$ instead.

Finally, as shown in [105], a convenient result of the RIP condition surfaces, that if a matrix Φ satisfies the RIP then it also satisfies the NSP (see [105]). This relieves the dependence on multiple checks of a matrix, providing a more efficient way to test for compliance of a sensing matrix for use in CS recovery.

9.5.6 Compliant RIP Matrices

A pivotal technique is needed when generating a matrix that is potentially RIP compliant; it is one thing to test for the RIP of a matrix and another problem entirely to generate one. We follow the approach described in [17] whereby choosing entries ϕ_{ij} from a probability distribution with two strict conditions on the distribution, ensures that a matrix Φ is RIP complaint. Firstly, the distribution must be norm-preserving which leads to a variance of $1/M$ conditioned to

$$E(\phi_{ij}^2) = \frac{1}{M}. \quad (9.55)$$

Secondly, the distribution must be sub-Gaussian¹⁴ stipulating that there exists a constant $c > 0$ such that

$$E(e^{\phi_{ij} t}) \leq e^{-c^2 t^2/2} \text{ for all } t \in \mathbb{R}. \quad (9.56)$$

The theorem that supports this result is given below.

Theorem 9.4 (Theorem 3.6 in [150]) Fix $\delta \in (0, 1)$. Let Φ be an $M \times N$ random matrix whose entries ϕ_{ij} are independent identically distributed (i.i.d) with ϕ_{ij} drawn

¹⁴Sub-Gaussian refers to the decay rate of the tail of the distribution that must be similar to that of a Gaussian distribution. Distributions that fit this definition is the Gaussian, Bernoulli with $\pm 1/\sqrt{M}$ [150].

according to a strictly sub-Gaussian distribution with $c^2 = 1/M$. If

$$M \geq k_1 K \log \left(\frac{N}{K} \right), \quad (9.57)$$

then Φ satisfies the RIP of order K with the prescribed δ with probability exceeding $1 - 2e^{-k_2 M}$, where k_1 is arbitrary and $k_2 = \delta_2 / 2k^* - \log(42e/\delta)/k_1$.

Although a sub-Gaussian random matrix Φ can be chosen as a sensing matrix for noisy measurements, in practice most signals that we are interested in, are not naturally sparse but in some other basis Ψ . With this being the case, we then desire that the product of the two matrices $\Phi\Psi$ satisfy the RIP. Fortunately, based on the findings in [105], if Ψ is an orthonormal basis it can be shown that its product with the sub-Gaussian matrix Φ is also Gaussian distributed. Provided that M is sufficiently large, then $\Phi\Psi$ will satisfy the RIP with a high confidence level. This result is crucial, as it provides the means to construct numerous RIP compliant matrices using a conventional transform basis.

9.5.7 Incoherence

The coherence of a given matrix, say Φ given in Eq. 9.58 provides an easier check for a unique recovery of a sparse signal, closely related to the spark, NSP and RIP. As shown by Theorem 2 of [56] (see below) and work in [150] together with the Welch Bound, provides an upper bound on the sparsity of a signal that guarantees a unique estimate on recovery given that the coherence is of order $K = O(\sqrt{M})$.

Theorem 9.5 (Theorem 2 in [56]) *The eigenvalues of an $N \times N$ matrix M with entries m_{ij} , $1 \leq i, j \leq N$, lie in the union of N discs $d_i = d_i(c_i, r_i)$, $1 \leq i \leq N$, centred at $c_i = m_{ii}$ and with the radius $r_i = \sum_{j \neq i} |m_{ij}|$.*

Additionally, the coherence of a matrix is given as

$$\mu(\Phi) = \max_{1 \leq i < j \leq N} \frac{|\langle \phi_i, \phi_j \rangle|}{\|\phi_i\|_2 \|\phi_j\|_2} \quad (9.58)$$

with $\mu(\Phi)$ the largest absolute inner product¹⁵ between any two columns ϕ_i, ϕ_j of Φ . In [105] it is given that if $M \ll N$ then the lower bound for coherence is approximately $\mu(\Phi) \geq 1/\sqrt{M}$, also known as the Welch bound.

In essence, by means of [105], if Φ has a low coherence $\mu(\Phi)$ and spectral norm $\|\Phi\|_2$, and if $K = O(\mu^{-2}(\Phi) \log N)$, then using CS measurement $y = \Phi x$ the input signal x can be recovered with a high confidence level [150]. Moreover, if the Welch bound is used in the definition of K , it gives $K = O(M \log N)$ which results in a

¹⁵The inner product is denoted here on out as $\langle \beta, \alpha \rangle$, with \aleph and \beth denoting any variable.

linear dependence of sparsity and measurement, much like the condition imposed by RIP [17].

9.6 Sampling Techniques

9.6.1 Sampling Theory

The system block used to mimic an ideal ADC, shown in Fig. 9.31, is the ideal continuous-to-discrete-time (C/D) converter which will be used for explanatory purposes. Given a analog continuous bandlimited input signal, the C/D gives as an output the discrete time signal. Consider an input $x_c(t)$, sampled periodically with period $T_s = \frac{1}{f_s}$ at the sampling frequency f_s gives a discrete-time signal $x[n]$ as an output, where $x[n] = x_c(nT)$. see Fig. 9.31. Another way to look at the sampling process, is by means of mixing (see Appendix 9.2.2.3) $x_c(t)$ to $x_s(t)$ by means of a periodic impulse response train.

$$h(t) = \sum_{n=-\infty}^{\infty} \delta(t - nT) \quad (9.59)$$

Mixed with the input signal $x_c(t)$ gives:

$$x_s(t) = x_c(t) \times h(t) = x_c(t) \sum_{n=-\infty}^{\infty} \delta(t - nT) \quad (9.60)$$

$$= \sum_{n=-\infty}^{\infty} x_c(nT) \delta(t - nT) \quad (9.61)$$

Consequently, the Fourier transform of the continuous-time signals, $x_c(t) \Rightarrow X_c(j\omega)$: $h(t) \Rightarrow H(j\omega)$ is representative of a convolution in the frequency domain resulting in:

$$X_s(j\omega) = \frac{1}{2\pi} X_c(j\omega) * H(j\omega) = \frac{1}{T} \sum_{k=-\infty}^{\infty} X_c(j(\omega - k\omega_s)) \quad (9.62)$$

Which in reality consists of copies of $X_c(j\omega)$ shifted by integer multiples of the sampling frequency ω_s and then superimposed [131]. As shown in Fig. 9.31, if the bandlimited input signal is limited to half of the sampling frequency, then the original signal can be recovered by means of a low pass filter (LPF). Otherwise, aliasing will occur and the signal will be degraded significantly. As mentioned earlier, this frequency is known as the Nyquist frequency, which is expressed as.

$$\omega_s > \omega_N \quad (9.63)$$

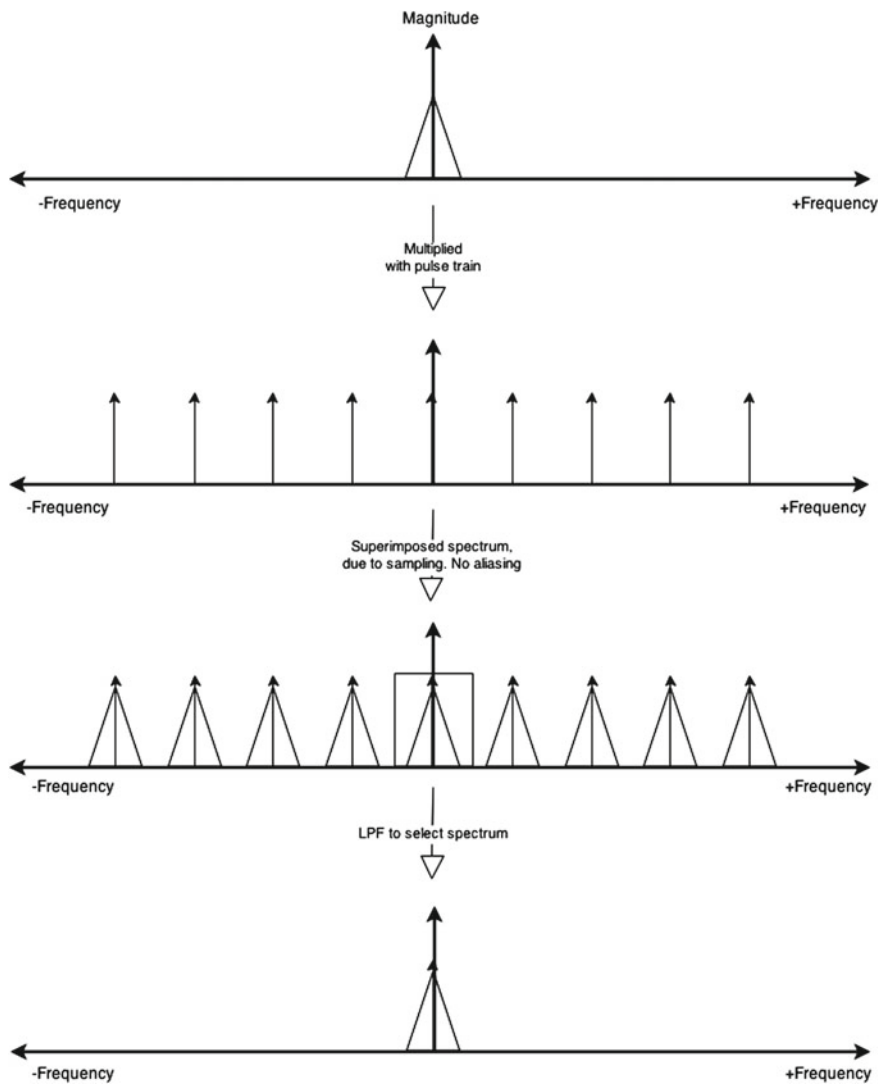


Fig. 9.31 An illustration of sampling a bandlimited signal, using an impulse train superimposed and consequently filtered via a LPF to produce a non-aliased signal

The Nyquist frequency is given as ω_N , and to recover the entire bandlimited signal the frequency Nyquist rate is equal to $2\omega_N$.

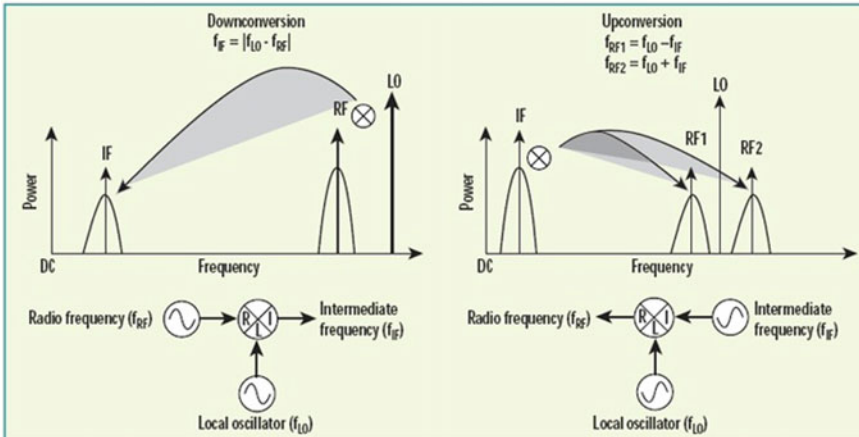


Fig. 9.32 Illustrates the effect mixing has on a bandlimited signal, where down-conversion and up-conversion are shown, respectively. Taken from [106]

9.6.2 Conventional Sampling Mixing-Acquisition

Conventional sampling scheme, utilizing an ADC for quantization, have a limited bandwidth that can be exactly sampled without aliasing taking place due to limitations on the ADC sampling rate as it related to the Nyquist criteria [128]. Two common scenarios arise in any RF sampling system where either a limited bandwidth must be sampled at a carrier frequency that exceed the limitations for current ADCs, or the bandwidth itself is too wide requiring a different approach entirely.

For the first case, the typical approach makes use of a mixer and filter stage (which can be done in the analog or digital domain) to down convert the bandwidth to an appropriate sampling rate matched to the capability of the ADC, known as the intermediate frequency (IF). Figure 9.32 shows how this applies in the frequency domain. Although sampling at IF is the typically technique used for RF purposes (i.e. SH receiver) [39], the inherent frequency ambiguities caused by mixer deviations and drift are a source of concern, as errors occur and reduce the correct representation of the acquired signal. Sampling at IF method is well established, cost effective, and due to the reduced complexity of implementation is a preferred technique [39]. Moreover, for application in RF communications, this is typically the first method for consideration in any system design.

For the second case, where an extensive bandwidth is required to be sampled, most RF systems either use a sweeping technique as detailed in Sect. 2.2.2, employing a variable VCO to sweep across a wide bandwidth with a fixed sampling band. Otherwise, a bank of samplers are used with each branch specific to a predetermined sampled bandwidth that covers the entire spectrum of interest, as in a digital receivers..

9.6.3 Under Sampling Techniques

9.6.3.1 Bandpass Sampling

It has long been known that discrete sampling of a bandlimited analog signal $x(t)$ —by taking advantage of aliasing—can result in high frequency signals being folded down in frequency to an IF that can be recovered in the digital domain [179]. The feasibility of this approach depends on a few factors that allow for coherent sampling of the desired bandlimited signal at a specific carrier frequency. The method relies on the assumption that modulated signals, which are unconverted for transmission at a carrier frequency, still maintain the information embedded in the signal at a lower oscillating frequency due to modulation. This lower information related modulation is within a realistic bandwidth that can be under-sampled at a rate relative to the modulation, instead of the Nyquist frequency dependent on the highest frequency in the bandwidth. The sampling is conditioned on number of critical variables, namely the carrier frequency (f_c), upper frequency of the band (f_u), lower frequency of the band (f_l), the sampling frequency (f_s) and the bandwidth is given as $B = f_u - f_l$. In order to sample the signal at zero IF without ambiguities, two crucial criteria must hold. But first, it is necessary to define the band position which is measured from the bandwidth origin to the lower band edge (f_l) and is usually a fraction of the bandwidth.

The criterion to ensure uniform sampling, with the sampling frequency at $f_s = 2B$, dictates that the lower band edge must be an integer multiple of bandwidth B i.e. $f_l = c(f_u - f_l)$ with $c = 0, \pm 1, \pm 2 \dots \pm N$, known as *integer band positioning* [179]. Another case where uniform sampling will result for band sampling, when the lower band edge is a half-integer multiple, conditioned to $f_l = \frac{(2c + 1)}{2}(f_u - f_l)$, is known as the *half-integer positioning*. Moreover, for uniform sampling one must ensure that the sampling frequency f_s obeys

$$\frac{2f_u}{k} \leq f_s \leq \frac{2f_l}{k-1} \quad (9.64)$$

so that aliasing of positive and negative edges do not overlap. Where k is some integer multiple conditioned by $1 \leq k \leq f_u/B$.

The simplest and most effective sampling is to configure the band to be integer positioned [184]. In the sampling process the degradation of the signal due to noise aliasing is unavoidable. However, by conditioning the sampling frequency to quadrature sampling gives the least distortion ratio of the signal (see [179]). We refer the reader to [184, 179] for further practical related issues when implementing this method.

Bandpass sampling precedes other methods that resemble any sub-sampling or sub-Nyquist qualities, allowing a system to operate with a lower ADC sampling rate and still achieve adequate quantization of signals [4, 134]. Although bandpass sampling has been used for a variety of applications (i.e. radar, communications,

astronomy etc.) the application still depends on the signal being bandlimited at a high operating frequency, low noise environment to limit noise distortion, as well as minimal adjacent spectral occupation (due to the “folding” of the bands) [184]. Bandpassing imposes an inherent limit for multi-band signals and wideband signals, hence for circumstances such as spectrum monitoring/sensing bandpass sampling is not preferred.

9.6.3.2 Periodic Non-uniform Sampling (PNS)

PNS follows the same approach of bandpass sampling, by under-sampling an input signal $x(t)$. However, instead of the under-sampling rate being conditioned to a single bandwidth, PNS adopts a sampling rate relative to the frequency support in the spectrum for multiband signals that tend to be spectrally sparse [116].

As suggested by [90], a lower bound for the sampling rate can be achieved for an input multiband signal with known frequency support relative to the number of active bands in the spectrum N , with individual bandwidths, B . The lower bound results from the product of these values i.e. $B \times N$.

In particular, the PNS allows for under-sampling with suitable recovery of the signal by approximating this bound (BN) without the need for complex circuitry [116]. For practical implementation, PNS simply needs a set of time-delay elements prior to the ADC, realizable by a time-interleaving ADC¹⁶.

PNS consists of m under-sampling branches with related time-shifts $y[n] = x(nT_s + \phi_i)$, $1 \leq m \leq$ where m/T_s is less than the Nyquist frequency f_{NQ} with a final processing step to recover the input signal $x(t)$. In [86] it was demonstrated that a bandpass signal could be exactly recovered using a PNS scheme at a sampling rate of $2B$ samples/s, followed by [94] extending the approach to multiband signals.

Although PNS is a candidate for sub-Nyquist sampling, the practicality of the approach is hampered by a reliance on Nyquist sampling track and hold circuits for each branch in the interleaving ADC [89]. Also, due to imperfect time-delay production in the separate sampling branches, requires a compensation for time skewing causing frequency mismatch and harmonics [89] for correlative recovery. Combined with a necessity for a priori knowledge of the multiband signal spectral support impedes the effectiveness of PNS for generic and dynamic frequency scenarios.

9.6.4 Direct Sampling

In theory, as with ideal software radios [177], direct sampling would be capable of sampling rates that could sample all communication signals (i.e. <30 GHz) in

¹⁶A time interleaving ADC uses m ADCs with a sample rate equal to $1/m$ of the overall sampling rate f_{NQ} in parallel with one another. Each branch has a time delay imposed and the selection of each branch is controlled by a MUX conditioned to the system clock.

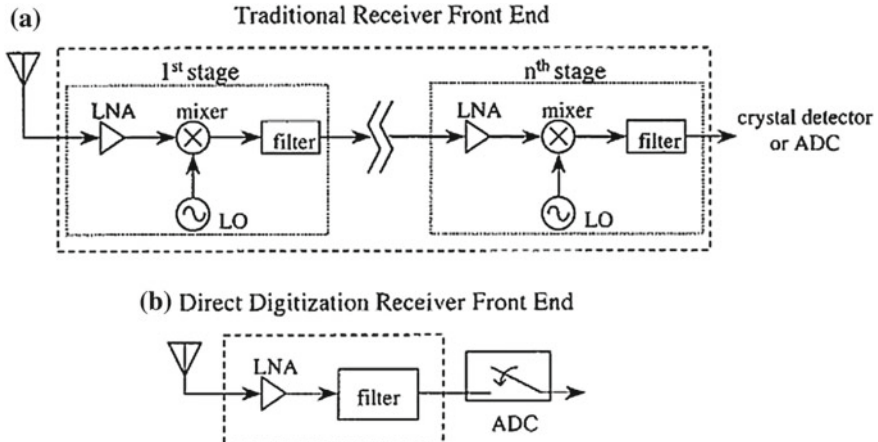


Fig. 9.33 Illustrates the difference between traditional **a** and direct **b** sampling schemes. Taken from [4]

order to remove the need of RF analog components (see Fig. 9.33). However, based on current technologies the upper bound sampling rates restricts the acquisition to a bandwidth of 1.75 GHz using direct sampling which has an associated monetary cost.

Nevertheless, just as it is with most technological trends, current direct sampling systems combine fast ADCs, bandpass sampling techniques, novel digital filtering, and a bank of samplers to enable a large bandwidth to be sampled instantaneously, mimicking the ideal case when an ADC will be available to directly sample a wide bandwidth directly. Such a system can be found in [167] capable of sampling up to 20 GHz instantaneously.

Although the practical implementation of direct sampling have a large associate monetary cost,¹⁷ it does carry benefits that comprise no frequency drift due to mixing, digital processing where lossless processing is capable instead of analog processing (i.e. filter, mixing, amplification), and instantaneous coverage of a wide bandwidth.

9.7 Wideband CS Sampling Techniques

9.7.1 Multi-rate Asynchronous Sub-nyquist Sampling (MASS)

The MASS scheme is a unique approach to sampling, based on a multi channel sampling scheme with sub-Nyquist ADCs that are prime multiples less than twice that

¹⁷A system as shown in [167] will typically be in excess of R 2 million.

of the Nyquist frequency (f_{NYQ}). First proposed by [168] with the intended purpose for wideband spectrum monitoring used in cognitive radio (CR). In Fig. 9.34 the proposed architecture depicts the system block diagram of MASS using a wideband filter and parallel prime numbered sampling rate ADC channels with their respective FFT block.

The subsequent frequency magnitude outputs from each branch is fed into a CS recovery block utilizing a joint sparsity recovery technique [51], similar to that of CMUX, in order to recover the spectrum magnitude plots. The reason behind the prime numbered ADC branches stem from bandpass sampling theory [4] and the effect of Nyquist folding of high frequency signals to baseband. However, instead of a single ADC subject to bandpass sampling conditions (see Sect. 9.6.3.1), MASS uses parallel prime numbered sampling rates as a bases to circumvent the effects of bandpass aliasing, allowing for multiple band signal recovery over multiple wideband signals (see [168] for further detail).

No further work, in the open literature, has yet been done as far as practical implementation of this method, however the theory of MASS remains as one of the most promising CS dependant wideband sampling techniques. The simulation results in [168] suggests an application up to 20 GHz with detection capability in medium to low SNR environments (see Fig. 9.35). Furthermore, as a sampling technique, MASS exhibits one of the highest compression ratios as compared to similar multi-channel sampling schemes [114, 162, 190] relative to the mean squared error (MSE) in recovery of the spectrum.

Even though the implementation complexity of the system is relatively uncomplicated [168], the recovery for MASS is non-trivial and has a large requirement for computation and memory load, but less than other CS based sampling schemes for similar signal inputs. As a spectrum sensing technique MASS does not retain any phase information after FFT processing, which is a drawback, but in reality CS recovery phase information is mostly lost due to the inherent non-sparsity of phase.

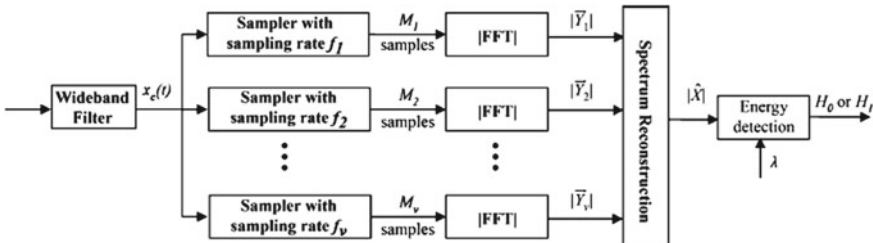


Fig. 9.34 System block depicting the implementation of the MASS sampling scheme. Courtesy of [168]

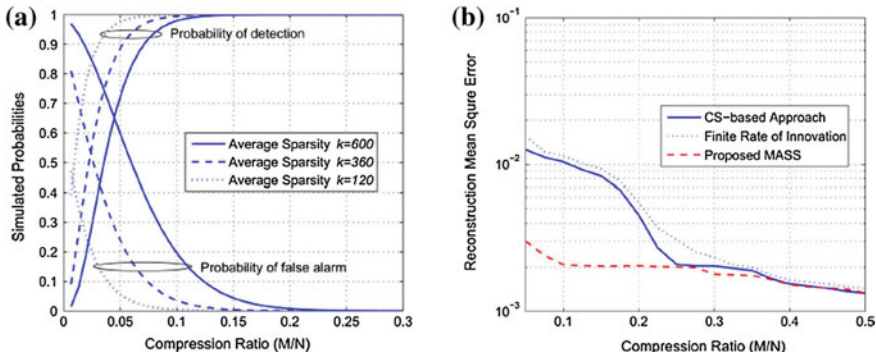


Fig. 9.35 **a** Illustrates the effect of sparsity and the compression ratio on the detection performance of MASS, with received signals exposed to separate AWGN channels with average SNR = 10 dB. **b** Illustrates the comparison between the proposed system and the existing approaches when the compression ratio varies. Courtesy of [168]

9.7.2 Xampling-ADC and Modulated Wideband Converter (MWC)

The application of Xampling technique relates to wideband scenarios with the built-in assumption of a multiband input signal. In other words, the input signal constitutes a finite number of bandlimited signals that are adequately spaced in frequency and do not overlap, as shown in Fig. 9.36b.

The practical implemented modulated wideband converter (MWC) [115], which follows the principles of Xampling [54, 117], leverage analog pre-processing techniques via demodulation of the input signal to reduce sampling rates. However, for MWC a multi-channel approach is adopted where all individual branches are modulated down to baseband, sampled by a low-rate ADC, and then provide a final subset of digital outputs $y_i[n]$, see the illustration of the MWC in Fig. 9.36.

The outputs from the MWC serves as the digital signal used by the continuous-to-finite (CTF) block as shown in Fig. 9.37, used to infer the locations of the respective bands and occupancy, and must be updated every time the band structure changes. The output of the CTF is used for purposes of recovering the spectrum during the final recovery stage.

A Hardware efficient realization of the MWC was implemented in [118] for a multiband signal B_N , with $N = 6$ bandlimited signals and adequate spacing, each having a bandwidth $B = 19$ MHz. The set up follows the scenario of receiving three concurrent transmissions with the Nyquist rate stated as $f_{NYQ} = 2.075$ GHz. Adequate results were taken, which proved the feasibility of such a sampling scheme for sub-Nyquist sampling using CS recovery techniques. However, the MWC flexibility in handling non-multiband signals and frequency sparse signals were hampered as the processing block struggle to group such signals in the contiguous block [182].

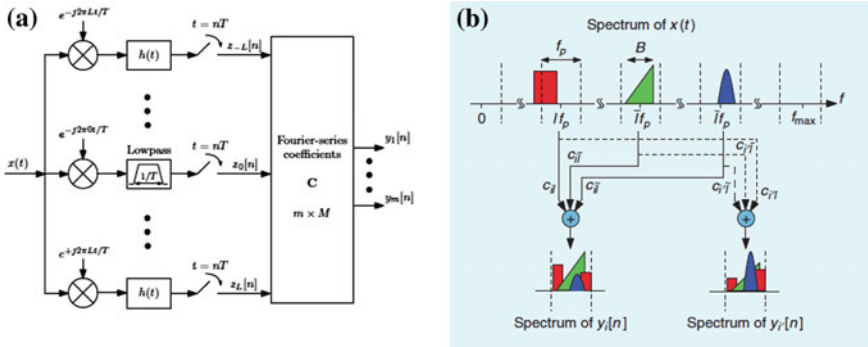


Fig. 9.36 **a** Shows the system block diagram of the modulated wideband converter, and **b** the spectrum of the output digital signals summed into a union subspace that is resolved via the CTF and used by CS methods as inputs. Courtesy of [116, 118]

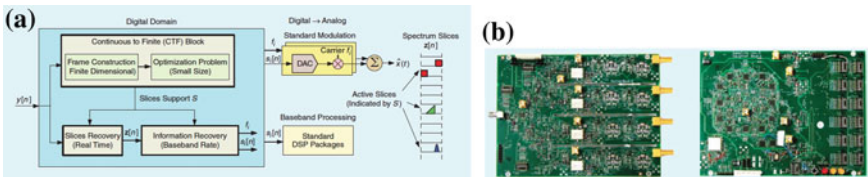


Fig. 9.37 **a** Showing the system block diagram of the CTF and **b** the hardware MWC boards developed in [118]. Courtesy of [116]

The cost due to multiple ADCs and multichannel analog RF front end serves as an impediment for adoption, as well as the limitation to finite multiband signals (i.e. 6–10). In realistic terms, a MWC cannot adequately recover a wideband spectrum for use in spectrum monitoring applications (i.e. CR & Electronic Support) [182]. Furthermore, the case could be made that the MWC implementation of Xampling can be likened to a filter-bank [58] design for wideband applications as the RF front ends are similar in design.

References

1. Adamy, D.L.: EW 101 A First Course in Electronic Warfare. Artech House (2000). ISBN 9781580531696
2. Adamy, D.L.: EW 102 a Second Course in Electronic Warfare. Artech House (2004). ISBN 9781580536867
3. Adamy, D.L.: Introduction to Electronic Warfare Modeling and Simulation. Artech House (2008). ISBN 1580534953
4. Akos, D.M., Stockmaster, M., Tsui, J.B.Y., Caschera, J.: Direct bandpass sampling of multiple distinct RF signals. *IEEE Trans. Commun.* **47**(7), 983–988 (1999a)
5. Alonso, M.T., López-Dekker, P., Mallorqui, J.J.: A novel strategy for radar imaging based on compressive sensing. *IEEE Trans. Geosci. Remote Sens.* **48**(12), 4285–4295 (2010)
6. Antoniadis, I., Glossiotis, G.: Cyclostationary analysis of rolling-element bearing vibration signals. *J. Sound Vib.* **248**(5), 829–845 (2001)
7. Ardoino, R., Megna, A.: LPI radar detection: SNR performances for a dual channel cross-correlation based ESM receiver. In: Radar Conference, 2009. EuRAD 2009. European, pp. 113–116. IEEE (2009)
8. Asif, M.S., Romberg, J.: Sparse recovery of streaming signals using 11-homotopy (2013). [arXiv:1306.3331](https://arxiv.org/abs/1306.3331)
9. Assaleh, K., Farrell, K., Mammone, R.J.: A new method of modulation classification for digitally modulated signals. In: Military Communications Conference, 1992. MILCOM'92, Conference Record. Communications-Fusing Command, Control and Intelligence., IEEE, pp. 712–716. IEEE (1992)
10. Axell, E., Leus, G., Larsson, E.G., Poor, H.V.: Spectrum sensing for cognitive radio: State-of-the-art and recent advances. *IEEE Signal Process. Mag.* **29**(3), 101–116 (2012a)
11. Axell, E., Leus, G., Larsson, E.G., Poor, H.V.: Spectrum sensing for cognitive radio: state-of-the-art and recent advances. *IEEE Signal Process. Mag.* **29**(3), 101–116 (2012b)
12. Azzouz, E.: Automatic Modulation Recognition of Communication Signals. Springer (1996)
13. Balanis, C.A.: Antenna Theory: Analysis and Design. Wiley (2012)
14. Balogh, L., Kollar, I.: Angle of arrival estimation based on interferometer principle. In: 2003 IEEE International Symposium on Intelligent Signal Processing, pp. 219–223. IEEE (2003)
15. Baraniuk, R.G., Cevher, V., Duarte, M.F., Hegde, C.: Model-based compressive sensing. *IEEE Trans. Inf. Theor.* **56**, 1982–2001 (2010)
16. Baraniuk, R., Steeghs, P.: Compressive radar imaging. In: 2007 IEEE Radar Conference, pp. 128–133. IEEE (2007)

17. Baraniuk, R.G.: Compressive sensing (lecture notes). *IEEE Signal Process. Mag.* **24**(4), 118–121 (2007)
18. Baraniuk, R., Davenport, M., DeVore, R., Wakin, M.: A simple proof of the restricted isometry property for random matrices. *Constr. Approx.* **28**(3), 253–263 (2008)
19. Baron, D., Sarvotham, S., Baraniuk, R.G.: Bayesian compressive sensing via belief propagation. *IEEE Trans. Signal Process.* **58**(1), 269–280 (2010)
20. Barrick, D.E., Lipa, B.J.: Radar angle determination with music direction finding, 23 Nov 1999. US Patent 5,990,834
21. Beck, A., Teboulle, M.: A fast iterative shrinkage-thresholding algorithm for linear inverse problems. *SIAM J. Imaging Sci.* **2**(1), 183–202 (2009)
22. Boyd, S., Vandenberghe, L.: Convex optimization, October, 2013. http://www.stanford.edu/~boyd/cvxbook/bv_cvxbook.pdf
23. Broto, D.: Antenna basic theory (2013). <http://denmasbroto.com/article-13-antenna-basic-theory.html>
24. Calderbank, R., Howard, S., Jafarpour, S.: Construction of a large class of deterministic sensing matrices that satisfy a statistical isometry property. *IEEE J. Sel. Topics Signal Process.* **4**(2), 358–374 (2010)
25. Candes, E.J., Romberg, J.K., Tao, T.: Stable signal recovery from incomplete and inaccurate measurements. *Commun. Pure Appl. Math.* **59**(8), 1207–1223 (2006)
26. Candes, E., Romberg, J.: ℓ_1 -magic, Feb 2013. <http://users.ece.gatech.edu/~justin/l1magic/#code>
27. Candes, E., Romberg, J.: l1-magic: recovery of sparse signals via convex programming (2005). www.acm.caltech.edu/l1magic/downloads/l1magic.pdf
28. Candès, E.J.: Compressive sampling. In: Proceedings of the International Congress of Mathematicians: Madrid, August 22–30, 2006: Invited Lectures, pp. 1433–1452 (2006)
29. Carlin, M., Rocca, P., Oliveri, G., Viani, F., Massa, A.: Directions-of-arrival estimation through bayesian compressive sensing strategies. *IEEE Trans. Antennas Propag.* **61**(7), 3828–3838 (2013)
30. Chan, Y.T., Plews, J.W., Ho, K.C.: Symbol rate estimation by the wavelet transform. In: Proceedings of 1997 IEEE International Symposium on Circuits and Systems, 1997, ISCAS'97, vol. 1, pp. 177–180. IEEE (1997)
31. Chen, S.S., Donoho, D.L., Saunders, M.A.: Atomic decomposition by basis pursuit. *SIAM J. Sci. Comput.* **20**(1), 33–61 (1998)
32. Cloete, C.: International ew trends and strategic influences, May, 2013. <http://www.aardvarkaoc.co.za/Proceedings/201305>
33. Cohen, A., Dahmen, W., DeVore, R.: Compressed sensing and best k-term approximation. *J. Am. Math. Soc.* **22**(1), 211–231 (2009)
34. Collin, R.E.: *Antennas and Radiowave Propagation*, vol. 108. McGraw-Hill, New York (1985)
35. Cormode, G., Muthukrishnan, S.: Combinatorial algorithms for compressed sensing. In: Structural Information and Communication Complexity, pp. 280–294. Springer (2006)
36. Cripps, S.C.: *RF Power Amplifiers for Wireless Communications*, (Artech House Microwave Library). Artech House, Inc. (2006)
37. Croisier, A., Esteban, D., Galand, C.: The diffraction of light by high frequency sound waves: Part 1. In: Proceedings of the International Symposium on Information Circuis and Systems (1976)
38. Dasgupta, Sanjoy: Gupta, Anupam: An elementary proof of the johnson-lindenstrauss lemma, 99–006. International Computer Science Institute, Technical report (1999)
39. Davenport, M., Duarte, M., Eldar, Y., Kutyniok, G.: Theory and Application. Compressed sensing, Cambridge University Press (2012)
40. De Martino, A.: Introduction to EW systems. Artech House, Norwood (2012)
41. DeVore, R.A.: Deterministic constructions of compressed sensing matrices. *J. Complex.* **23**(4), 918–925 (2007)
42. Donoho, D.L.: Compressed sensing. *IEEE Trans. Inf. Theor.* **52**(4), 1289–1306 (2006a)

43. Donoho, D.L.: For most large underdetermined systems of linear equations the minimal ℓ_1 -norm solution is also the sparsest solution. *Commun. Pure Appl. Math.* **59**(6), 797–829 (2006b)
44. Donoho, D.L., Elad, M.: Optimally sparse representation in general (nonorthogonal) dictionaries via ℓ_1 minimization. *Proc. Natl. Acad. Sci.* **100**(5), 2197–2202 (2003)
45. Drentea, C.: Modern Communications Receiver Design and Technology. Artech House (2010a)
46. Duarte, M.F., Baraniuk, R.G.: Spectral compressive sensing. *Appl. Comput. Harmonic Anal.* (2012)
47. Duarte, M.F., Davenport, M.A., Takhar, D., Laska, J.N., Sun, T., Kelly, K.F., Baraniuk, R.G.: Single pixel imaging via compressive sampling. *IEEE Signal Process. Mag.* **25**(2), 83–91 (2008)
48. Duarte, M.F., Sarvotham, S., Baron, D., Wakin, M.B., Baraniuk, R.G.: Distributed compressed sensing of jointly sparse signals. In: Asilomar Conference on Signals, System, Computation, pp. 1537–1541 (2005)
49. Eldar, Y.C., Kutyniok, G.: Compressed Sensing: Theory and Applications. Cambridge University Press (2012)
50. Eldar, Y.C., Mishali, M.: Block sparsity and sampling over a union of subspaces. In: 2009 16th International Conference on Digital Signal Processing, pp. 1–8. IEEE (2009)
51. Emmanuel J Candès and Terence Tao. Decoding by linear programming. *IEEE Trans. Inf. Theor.* **51**(12), 4203–4215 (2005)
52. Ender, J.H.G.: On compressive sensing applied to radar. *Signal Process.* **90**(5), 1402–1414 (2010)
53. Falk, I.S.: Iterative einschließung der kleinsten (größten) eigenwerte eines hermiteschen matrizenpaars, ii. *Acta Mech.* **49**(1–2), 111–131 (1983)
54. Fannjiang, A., Liao, W.: Compressed sensing phase retrieval. In: 2011 Conference Record of the Forty Fifth Asilomar Conference on Signals, Systems and Computers (ASILOMAR), pp. 735–738. IEEE (2011)
55. Farhang-Boroujeny, B.: Filter bank spectrum sensing for cognitive radios. *IEEE Trans. Signal Process.* **56**(5), 1801–1811 (2008)
56. Fernandez, M.R.: High performance computing—nodes, sockets and flops (2014). <http://en.community.dell.com/techcenter/high-performance-computing/w/wiki/2329>
57. Figueiredo, M.A.T., Nowak, R.D., Wright, S.J.: Gradient projection for sparse reconstruction: application to compressed sensing and other inverse problems. *IEEE J. Sel. Top. Signal Process.* **1**(4), 586–597 (2007)
58. Finne, M.: Methods for Direction-Finding of Direct-Sequence Spread-Spectrum Signals. DIANE Publishing (1996)
59. Fuller, K.L.: To see and not be seen. In: IEE Proceedings F (Radar and Signal Processing), pp. 1–9. IET (1990)
60. Gabriel, W.F.: Spectral analysis and adaptive array superresolution techniques. *Proc. IEEE* **68**(6), 654–666 (1980)
61. Gardner, W.A.: The spectral correlation theory of cyclostationary time-series. *Signal Process.* **11**(1), 13–36 (1986)
62. Gilbert, A.C., Strauss, M.J., Tropp, J.A., Vershynin, R.: One sketch for all: fast algorithms for compressed sensing. In: Proceedings of the Thirty-Ninth Annual ACM Symposium on Theory of Computing, pp. 237–246. ACM (2007)
63. Golub, G.H., Hansen, P.C., O’Leary, D.P.: Tikhonov regularization and total least squares. *SIAM J. Matrix Anal. Appl.* **21**(1), 185–194 (1999)
64. Gonzalez, G.: Microwave Transistor Amplifiers: Analysis and Design, vol. 2. Prentice Hall, New Jersey (1997)
65. Graham, A.: Communications, Radar and Electronic Warfare. Wiley.com (2011)
66. Grout, I.: Digital Systems Design with FPGAs and CPLDs. Newnes (2011)
67. Guruz, A.C., McClellan, J.H., Scott, W.R.: A compressive sensing data acquisition and imaging method for stepped frequency GPRs. *IEEE Trans. Signal Process.* **57**(7), 2640–2650 (2009)

68. Hale, E.T., Yin, W., Zhang, Y.: A fixed-point continuation method for l1-regularized minimization with applications to compressed sensing. CAAM TR07-07, Rice University (2007)
69. Haupt, J., Bajwa, W.U., Rabbat, M., Nowak, R.: Compressed sensing for networked data. *IEEE Signal Process. Mag.* **25**(2), 92–101 (2008)
70. Haupt, J., Castro, R., Nowak, R., Fudge, G., Yeh, A.: Compressive sampling for signal classification. In: Fortieth Asilomar Conference on Signals, Systems and Computers, 2006. ACSSC'06, pp. 1430–1434. IEEE (2006)
71. Hong, L., Ho, K.C.: Identification of digital modulation types using the wavelet transform. In: Military Communications Conference Proceedings, 1999. MILCOM 1999. IEEE, vol. 1, pp. 427–431. IEEE (1999)
72. Jacques, Laurent: Vanderghenst, Pierre: Compressed sensing: when sparsity meets sampling. Chapter **23**, 507–527 (2010)
73. Ji, S., Xue, Y., Carin, L.: Bayesian compressive sensing. *IEEE Trans. Signal Process.* **56**(6), 2346–2356 (2008)
74. Johnk, C.T.A.: Engineering Electromagnetic Fields and Waves, 667 p. John Wiley, New York (1975)
75. Johnson, R.C., Jasik, H.: Antenna Engineering Handbook, 1356 p. McGraw-Hill Book Company, New York (1984). No individual items are abstracted in this volume 1, 1984
76. Jorge, O.: Estimation, detection, and identification (2014). <http://isr.ist.utl.pt/~pjcro/courses/def0910/docs/EFI3CRLB.pdf>
77. Kay, S.M.: Fundamentals of Statistical Signal Processing, Volume III: Practical Algorithm Development, vol. 3. Pearson Education (2013)
78. Kim, S., Koh, K., Lustig, M., Boyd, S., Gorinevsky, D.: An interior-point method for large-scale ℓ_1 -regularized least squares. *IEEE J. Sel. Top. Signal Process.* **1**(4), 606–617 (2007)
79. Kirolos, S., Laska, J., Wakin, M., Duarte, M., Baron, D., Ragheb, T., Massoud, Y., Baraniuk, R.: Analog-to-information conversion via random demodulation. In: 2006 IEEE Dallas/CAS Workshop on Design, Applications, Integration and Software, pp. 71–74. IEEE (2006)
80. Kohlenberg, A.: Exact interpolation of band-limited functions. *J. Appl. Phys.* **24**(12), 1432–1436 (1953)
81. Kotelnikov, V.: On the carrying capacity of the ether and wire in telecommunications. Izd. Red. Upr. Svyazi RKKA (1993)
82. Kozminchuk, B., Elsaesser, D.: Advanced communication esm system design considerations (2013). <http://www.dtic.mil/cgi/tr/fulltext/u2/a259014.pdf>
83. Kuang, Y., Shi, Q., Chen, Q., Yun, L., Long, K.: A simple way to deinterleave repetitive pulse sequences. In: 7th WSEAS International Conference on Mathematical Methods and Computational Techniques in Electrical Engineering, Sofia, pp. 218–222 (2005)
84. Kurosawa, N., Kobayashi, H., Maruyama, K., Sugawara, H., Kobayashi, K.: Explicit analysis of channel mismatch effects in time-interleaved adc systems. *IEEE Trans. Circ. Syst. I Fundam. Theor. Appl.* **48**(3), 261–271 (2001)
85. Landau, H.J.: Necessary density conditions for sampling and interpolation of certain entire functions. *Acta Math.* **117**(1), 37–52 (1967)
86. Laska, J., Kirolos, S., Massoud, Y., Baraniuk, R., Gilbert, A., Iwen, M., Strauss, M.: Random sampling for analog-to-information conversion of wideband signals. In: 2006 IEEE Dallas/CAS Workshop on Design, Applications, Integration and Software. pp. 119–122. IEEE (2006)
87. Levy, R., Cohn, S.B.: A history of microwave filter research, design, and development. *IEEE Trans. Microw. Theor. Tech.* **32**(9), 1055–1067 (1984)
88. Liang, Y.-C., Chen, K.-C., Li, G.Y., Mahonen, P.: Cognitive radio networking and communications: an overview. *IEEE Trans. Veh. Technol.* **60**, 3386–3407 (2011)
89. Lin, Y.-P., Vaidyanathan, P.P.: Periodically nonuniform sampling of bandpass signals. *IEEE Trans. Circ. Syst. II: Anal. Digit. Signal Process.* **45**(3), 340–351 (1998)
90. Liu, D., Pfeiffer, U., Grzyb, J., Gaucher, B.: Advanced Millimeter-Wave Technologies: Antennas. Wiley, Packaging and Circuits (2009)

91. Looney, M.: Advanced digital post-processing techniques enhance performance in time-interleaved adc systems, October, 2013. http://www.analog.com/library/analogdialogue/archives/37-08/post_processing.html
92. Lopez-Risueno, G., Grajal, J., Sanz-Osorio, A.: Digital channelized receiver based on time-frequency analysis for signal interception. *IEEE Trans. Aerosp. Electron. Syst.* **41**(3), 879–898 (2005)
93. Loris, I.: On the performance of algorithms for the minimization of ℓ_1 -penalized functionals. *Inverse Probl.* **25**(3), 035008 (2009)
94. Louis, E.K.: Electromagnetic spectrum, September, 2013. <http://www.unwittingvictim.com/Electromagnetic-Spectrum-3H.PNG>
95. Lu, W., Vaswani, N.: Modified basis pursuit denoising (modified-bpdn) for noisy compressive sensing with partially known support. In: 2010 IEEE International Conference on Acoustics Speech and Signal Processing (ICASSP), pp. 3926–3929. IEEE (2010)
96. Lustig, M., Donoho, D., Pauly, J.M.: Sparse mri: the application of compressed sensing for rapid mr imaging. *Magn. Reson. Med.* **58**(6), 1182–1195 (2007)
97. Ma, S.: Alternating direction method of multipliers for sparse principal component analysis. *J. Oper. Res. Soc. China* 1–22 (2011)
98. Mallat, S.G., Zhang, Z.: Matching pursuits with time-frequency dictionaries. *IEEE Trans. Sig. Process.* **41**(12), 3397–3415 (1993)
99. Marchesini, S.: Ab initio compressive phase retrieval (2008). arXiv preprint <arXiv:0809.2006>
100. Marki, F., Marki, C.: Taking measure of microwave mixers (2013). <http://mwrf.com/components/taking-measure-microwave-mixers>
101. Matuszewski, J., Paradowski, L.: The knowledge based approach for emitter identification. In: 12th International Conference on Microwaves and Radar, 1998. MIKON'98, vol. 3, pp. 810–814. IEEE (1998)
102. Matuszewski, J.: Specific emitter identification. In: Radar Symposium, 2008 International, pp. 1–4. IEEE (2008)
103. Maurer, D.E., Chamlou, R., Genovese, K.O.: Signal processing algorithms for electronic combat receiver applications. *Johns Hopkins APL Tech. Digest* **18**(1), 69 (1997)
104. Maxwell, J.C.: A dynamical theory of the electromagnetic field. *Philos. Trans. R. Soc. Lond.* **155**, 459–512 (1865)
105. Meyer, C.: Matrix analysis and applied linear algebra book and solutions manual. SIAM, **2** (2000)
106. Milojević, D.J., Popović, B.M.: Improved algorithm for the deinterleaving of radar pulses. In: IEE Proceedings F (Radar and Signal Processing), vol. 139, pp. 98–104. IET (1992)
107. Mishali, M., Eldar, Y.C., Dounaevsky, O., Shoshan, E.: Xampling: analog to digital at sub-nyquist rates. *IET Circ. Dev. Syst.* **5**(1), 8–20 (2011)
108. Mishali, M., Eldar, Y.C., Dounaevsky, O., Shoshan, E.: Xampling: analog to digital at sub-nyquist rates. *IET Circ. Dev. Syst.* **5**(1), 8–20 (2011)
109. Mishali, M., Eldar, Y.C., Elron, A.: Xampling—part 1: Practice. Arxiv preprint (2009)
110. Mishali, M., Eldar, Y.C.: Blind multiband signal reconstruction: Compressed sensing for analog signals. *IEEE Trans. Sig. Process.* **57**(3), 993–1009 (2009)
111. Mishali, M., Eldar, Y.C.: Sub-nyquist sampling. *IEEE Sig. Process. Mag.* **28**(6), 98–124 (2011)
112. Mishali, M., Eldar, Y.C.: Wideband spectrum sensing at sub-nyquist rates. *IEEE Sig. Process. Mag.* **28**(4), 102–135 (2011)
113. Moravec, M., Romberg, J., Baraniuk, R.: Compressed sensing phase retrieval. *SPIE, Wavelets XII* **6701**, 91 (2007)
114. Nandi, A.K., Azzouz, E.E.: Algorithms for automatic modulation recognition of communication signals. *IEEE Trans. Commun.* **46**(4), 431–436 (1998)
115. National Instruments. Filter specifications (2013). http://zone.ni.com/reference/en-XX/help/371325F-01/lvdfdtconcepts/dfd_filter_spec/
116. Naval Air Systems Command. Electronic warfare and radar systems engineering handbook, January, 2013. <http://www.microwaves101.com/encyclopedia/navy>

117. Needell, D., Tropp, J.A.: Cosamp: iterative signal recovery from incomplete and inaccurate samples. *Appl. Comput. Harmon. Anal.* **26**(3), 301–321 (2009)
118. Needell, D., Tropp, J.A.: Cosamp: iterative signal recovery from incomplete and inaccurate samples. *Commun. ACM* **53**(12), 93–100 (2010)
119. Needell, D., Vershynin, R.: Signal recovery from incomplete and inaccurate measurements via regularized orthogonal matching pursuit. *IEEE J. Sel. Top. Sig. Process.* **4**(2), 310–316 (2010)
120. Neri, F.: Introduction to Electronic Defense Systems. SciTech Publishing (2005)
121. Neri, F.: Introduction to Electronic Defense Systems. Artech House, Norwood (1991)
122. Nesterov, Y., Nemirovskii, A.S., Ye, Y.: Interior-point polynomial algorithms in convex programming. *SIAM* **13** (1994)
123. Nyquist, H.: Certain topics in telegraph transmission theory. *Trans. AIEE* **47**, 617–644 (1928)
124. Ohlsson, H., Yang, A.Y., Dong, R., Sastry, S.S.: Compressive phase retrieval from squared output measurements via semidefinite programming (2011). arXiv preprint [arXiv:1111.6323](https://arxiv.org/abs/1111.6323)
125. Oppenheim, A.V., Schafer, R.W., Buck, J.R., et al.: *Discrete-Time Signal Processing*, vol. 5. Prentice Hall, Upper Saddle River (1999)
126. Paige, C.C., Saunders, M.A.: Lsqr: an algorithm for sparse linear equations and sparse least squares. *ACM Trans. Math. Softw. (TOMS)* **8**(1), 43–71 (1982)
127. Parisi, C.: Sensors smart sensors and sensor control electronics (2013). http://www.eeweb.com/blog/carmen_pariisi/P10
128. Patel, M., Darwazeh, I., O'Reilly, J.J.: Bandpass sampling for software radio receivers, and the effect of oversampling on aperture jitter. In: IEEE 55th Vehicular Technology Conference, 2002. VTC Spring 2002, vol. 4, pp. 1901–1905. IEEE (2002)
129. Pati, Y.C., Rezaifar, R., Krishnaprasad, P.S.: Orthogonal matching pursuit: recursive function approximation with applications to wavelet decomposition. In: 1993 Conference Record of The Twenty-Seventh Asilomar Conference on Signals, Systems and Computers, 1993, pp. 40–44. IEEE (1993)
130. Peleg, S., Porat, B.: The cramer-rao lower bound for signals with constant amplitude and polynomial phase. *IEEE Trans. Sig. Process.* **39**(3), 749–752 (1991)
131. Pesavento, M., Gershman, A.B., Haardt, M.: Unitary root-music with a real-valued eigendecomposition: a theoretical and experimental performance study. *IEEE Trans. Sig. Process.* **48**(5), 1306–1314 (2000)
132. Po, K., Takada, J.-I.: Signal detection based on cyclic spectrum estimation for cognitive radio in ieee 802.22 wran system. The Institute of Electronics, Information and Communication Engineers, Technical Report of IEICE (2007)
133. Poisel, R.A.: *Introduction to communication electronic warfare systems*. Artech House (2008). ISBN 1580533442
134. Polo, Y.L., Wang, Y., Pandharipande, A., Leus, G.: Compressive wide-band spectrum sensing. In: IEEE International Conference on Acoustics, Speech and Signal Processing, 2009. ICASSP 2009, pp. 2337–2340. IEEE (2009)
135. Polydoros, A., Kim, K.: On the detection and classification of quadrature digital modulations in broad-band noise. *IEEE Trans. Commun.* **38**(8), 1199–1211 (1990)
136. Poynting defence. Tactical direction finding antenna (2013). <http://www.poyntingdefence.com/index.php?q=cataloguelproductinfo,39,Tactical-Direction-Finding-Antenna>
137. Pozar, D.M.: *Microwave and RF Design of Wireless Systems*. Wiley (2000)
138. Quinn, D.: An fpga implementation feasibility study of the correlative interferometer direction finding algorithm—part 2: in depth. Technical report, NUTAQ (2013). <http://nutaq.com/en/blog/fpga>
139. Quiroga, R.Q., Nadasdy, Z., Ben-Shaul, Y.: Unsupervised spike detection and sorting with wavelets and superparamagnetic clustering. *Neural Comput.* **16**(8), 1661–1687 (2004)
140. Ragheb, T., Laska, J.N., Nejati, H., Kirolos, S., Baraniuk, R.G., Massoud, Y.: A prototype hardware for random demodulation based compressive analog-to-digital conversion. In: 51st Midwest Symposium on Circuits and Systems, 2008. MWSCAS 2008, pp. 37–40. IEEE (2008)

141. Rahman, Arifur: *FPGA Based Design and Applications*. Springer (2008)
142. Ren, Q.S., Willis, A.J.: Fast root music algorithm. *Electron. Lett.* **33**(6), 450–451 (1997)
143. Rice, D.W.: Hf direction finding by wave front testing in a fading signal environment. *Radio Sci.* **17**(4), 827–836 (1982). ISSN 1944-799X. doi:[10.1029/RS017i004p00827](https://doi.org/10.1029/RS017i004p00827)
144. Richard, B., Mark, D., Marco, D., Chinmay, H., Jason, L., Mona, S., Wotao, Y.: *An Introduction to Compressive Sensing* (2012). <http://cnx.org/content/col11133/1.5/>
145. Rohde, U.L., Rudolph, M.: RF/microwave circuit design for wireless applications. Wiley.com (2013)
146. Romberg, J.: Imaging via compressive sampling. *IEEE Signal Process. Mag.* **25**(2), 14–20 (2008)
147. Roy, R., Kailath, T.: Esprit-estimation of signal parameters via rotational invariance techniques. *IEEE Trans. Acoust. Speech Signal Process.* **37**(7), 984–995 (1989)
148. Saeid, S.H.: Study of the cell towers radiation levels in residential areas. In: *Communication Systems*, p. 87 (2013)
149. Schaller, R.R.: Moore's law: past, present and future. *IEEE Spect.* **34**(6), 52–59 (1997)
150. Schleher, D.C.: *Electronic Warfare in the Information Age*, 1st edn. Artech House Inc, Norwood, MA, USA (1999). ISBN 0890065268
151. Schleher, D.C.: *Introduction to Electronic Warfare*. Artech House, Norwood, MA (1994)
152. Schmidt, R.: Multiple emitter location and signal parameter estimation. *IEEE Trans. Antennas Propag.* **34**(3), 276–280 (1986)
153. Shan, T.-J., Kailath, T.: Adaptive beamforming for coherent signals and interference. *IEEE Trans. Acoust. Speech Signal Process.* **33**(3), 527–536 (1985)
154. Shannon, C.: Communication in the presence of noise. *Proc. Inst. Radio Eng.* **37**(1), 108211:21 (1949)
155. Sills, J.A.: Maximum-likelihood modulation classification for psk/qam. In: *Military Communications Conference Proceedings*, 1999. MILCOM 1999. IEEE, vol. 1, pp. 217–220. IEEE (1999)
156. Slavinsky, J.P., Laska, J.N., Davenport, M.A., Baraniuk, R.G.: The compressive multiplexer for multi-channel compressive sensing. In: *2011 IEEE International Conference on Acoustics, Speech and Signal Processing (ICASSP)*, pp. 3980–3983. IEEE (2011)
157. Soliman, S.S., Hsue, S.-Z.: Signal classification using statistical moments. *IEEE Trans. Commun.* **40**(5), 908–916 (1992)
158. Stearns, S.D., Hush, D.R.: *Digital Signal Processing with Examples in MATLAB*. CRC Press (2012)
159. Stephens, J.P.: Advances in signal processing technology for electronic warfare. *IEEE Aerosp. Electron. Syst. Mag.* **11**(11), 31–38 (1996)
160. Stojnic, M., Xu, W., Hassibi, B.: Compressed sensing-probabilistic analysis of a null-space characterization. In: *IEEE International Conference on Acoustics, Speech and Signal Processing*, 2008. ICASSP 2008, pp. 3377–3380. IEEE (2008)
161. Strmbck, P., Schultz, H.: Direct sampled wide band digital receivers in rwr/esm applications, October 2013. http://www.aardvarkaoc.co.za/index_files/Page5847.htm
162. Sun, H., Nallanathan, A., Wang, C.-X., Chen, Y.: Wideband spectrum sensing for cognitive radio networks: a survey. *IEEE Wirel. Commun.* **20**, 74–81 (2013)
163. Texas Instruments. Data converters, October 2013a. <http://www.ti.com/lscs/ti/data-converters/high-speed-adc-greater-than-1gspss-rf-sampling.page>
164. Texas Instruments. Digital signal processors (2014). <http://www.ti.com/lscs/ti/dsp/overview.page>
165. Texas Instruments. Low noise amplifiers, October 2013b. <http://www.ti.com/lscs/ti/amplifiers-linear>
166. Tian, Z., Giannakis, G.B.: Compressed sensing for wideband cognitive radios. In: *IEEE International Conference on Acoustics, Speech and Signal Processing*, 2007. ICASSP 2007, vol. 4, pp. IV-1357. IEEE (2007)
167. Tropp, J.A., Gilbert, A.C.: Signal recovery from random measurements via orthogonal matching pursuit. *IEEE Trans. Inf. Theor.* **53**(12), 4655–4666 (2007a)

168. Tropp, J.A., Laska, J.N., Duarte, M.F., Romberg, J.K., Baraniuk, R.G.: Beyond nyquist: efficient sampling of sparse band limited signals. *IEEE Trans. Inf. Theor.* **56**(1), 520–544 (2010)
169. Tsai, Y., Donoho, D.L.: Extensions of compressed sensing. *Signal Process.* **86**(3), 549–571 (2006)
170. Tsui, J.: *Digital Techniques for Wideband Receivers*. SciTech Publishing (2004)
171. Tuncer, T.E., Friedlander, B.: *Classical and Modern Direction-of-Arrival Estimation*. Access Online via Elsevier (2009)
172. Tuttlebee, W.H.W.: *Software defined radio: origins, drivers, and international perspectives*. John Wiley (2002)
173. University of Berkley: Software (2013). <http://www.eecs.berkeley.edu/~yang/software/softwarepage.html>
174. Vaccaro, D.D.: *Electronic Warfare Receiving Systems*. Artech House (1993)
175. Vaughan, R.G., Scott, N.L., White, D.R.: The theory of bandpass sampling. *IEEE Trans. Signal Process.* **39**(9), 1973–1984 (1991)
176. Venosa, E.: Eeweb electrical engineering home, how to specify an adc for a digital communications receiver, February, 2013. http://www.eeweb.com/blog/elettra_venosa
177. Vizmuller, P.: *Radio Frequency Design Guide*. Artech House (1995)
178. Wakin, M., Becker, S., Nakamura, E., Grant, M., Soviero, E., Ching, D., Yoo, J., Romberg, J., Emami-Neyestanak, A., Candes, E.: A nonuniform sampler for wideband spectrally-sparse environments. *IEEE J. Emerg. Sel. Top. Circ. Syst.* **2**(3), 516–529 (2012)
179. Walden, R.H.: Analog-to-digital converter survey and analysis. *IEEE J. Sel. Areas Commun.* **17**(4), 539–550 (1999)
180. Waters, W.M., Jarrett, B.R.: Bandpass signal sampling and coherent detection. *IEEE Trans. Aerosp. Electron. Syst.* **1**(6), 731–736 (1982)
181. Wepman, J.A.: Analog-to-digital converters and their applications in radio receivers. *IEEE Commun. Mag.* **33**(5), 39–45 (1995)
182. White Paper Altera. Radar proveressing: Fpgas or gpus (2014). https://www.altera.com/en_US/pdfs/literature/wp/wp-01197-radar-fpga-or-gpu.pdf
183. White, W.D.: Frequency domain conversion, September 27 1960. US Patent 2,954,465
184. Whittaker, E.: On the function which are represented by the expansions of interpolation theory. *Proc. Roy. Soc. Edinburgh, Sect. A* **35**, 1818211;194 (1915)
185. Wright, S.J., Nowak, R.D., Figueiredo, M.A.T.: Sparse reconstruction by separable approximation. *IEEE Trans. Signal Process.* **57**(7), 2479–2493 (2009)
186. Yang, A.Y., Sastry, S.S., Ganesh, A., Ma, Y.: Fast ℓ_1 -minimization algorithms and an application in robust face recognition: a review. In: 2010 17th IEEE International Conference on Image Processing (ICIP), pp. 1849–1852. IEEE (2010)
187. Yoo, J., Becker, S., Monge, M., Loh, M., Candes, E., Emami-Neyestanak, A.: Design and implementation of a fully integrated compressed-sensing signal acquisition system. In: 2012 IEEE International Conference on Acoustics, Speech and Signal Processing (ICASSP), pp. 5325–5328. IEEE (2012)
188. Ziskind, I., Wax, M.: Maximum likelihood localization of multiple sources by alternating projection. *IEEE Trans. Acoust. Speech Signal Process.* **36**(10), 1553–1560 (1988)